UNIVERSIDAD COMPLUTENSE DE MADRID

FACULTAD DE CIENCIAS BIOLÓGICAS

TESIS DOCTORAL

Relaciones estructura-función de la proteína del surfactante pulmonar SP-B: participación en complejos proteicos y en la homeostasis alveolar

Structure-function relationships of pulmonary surfactant protein SP-B: participation in protein complexes and in alveolar homeostasis

MEMORIA PARA OPTAR AL GRADO DE DOCTORA

PRESENTADA POR

Marta Martínez Calle

Directores

Bárbara Olmeda Lozano
Jesús Pérez Gil

Madrid
Ed. electrónica 2019

UNIVERSIDAD COMPLUTENSE DE MADRID

FACULTAD DE CIENCIAS BIOLÓGICAS

Departamento de Bioquímica y Biología Molecular

RELACIONES ESTRUCTURA-FUNCIÓN DE LA PROTEÍNA DEL SURFACTANTE PULMONAR SP-B: PARTICIPACIÓN EN COMPLEJOS PROTEICOS Y EN LA HOMEOSTASIS ALVEOLAR

STRUCTURE-FUNCTION RELATIONSHIPS OF PULMONARY SURFACTANT PROTEIN SP-B: PARTICIPATION IN PROTEIN COMPLEXES AND IN ALVEOLAR HOMEOSTASIS

MEMORIA PARA OPTAR AL GRADO DE DOCTOR

PRESENTADA POR

Marta Martínez Calle

DIRECTORES

Bárbara Olmeda Lozano

Jesús Pérez Gil

Madrid, 2018

The research included in this Thesis has been conducted in the Department of Biochemistry and Molecular Biology of Complutense University of Madrid under the supervision of Prof. Jesús Pérez Gil, Ph.D. and Bárbara Olmeda Lozano, Ph.D. Part of the experimental work was performed in collaboration with Prof. Paul Dietl, Ph.D. from Ulm University (Germany), Prof. Manuel Prieto from Center for Molecular Chemistry and Physics (Lisbon University, Portugal). Funding for short-term stays was provided by the Spanish Ministry of Economy and Competitiveness (EEBB-I-2015-10363) and by an EMBO short-term fellowship (7343)

The financial support to complete this Thesis was provided by the Spanish Ministry of Economy and Competitiveness (BES-2013-066972) and research grants from Spanish Ministry of Economy and Competitiveness (BIO2012-30733, BIO2015-67930-R) and the Regional Government of Madrid (S2013/MlT-2807).

Agradecimientos

En primer lugar, quisiera agradecer a mis directores, Jesús y Bárbara, por haberme dado la gran oportunidad de comenzar mi carrera investigadora con ellos, por transmitirme su entusiasmo por la ciencia y por enseñarme a reflexionar.

Gracias también a Antonio, Mer y Bego por su disposición a ayudarme en todo momento y por todas esas charlas sobre fructíferas sobre proteínas y membranas.

Gracias a todos mis compañeros, pasados y presentes, Nuria, Raquel, Alberto, José Carlos, Álex, Alicia, Alejandro, Elena, Sonia, Carolina, Miriam, Barri. Ha sido un verdadero placer haber trabajado junto a vosotros. Gracias a todos por vuestra apoyo, risas y cervezas.

Gracias al Pr. Paul Dietl y a todo su equipo en la Universidad de Ulm por recibirme con los brazos abiertos y hacer posible que esa estancia fuera muy fructífera.

Gracias al Pr. Manuel Prieto y el Dr. Luis Loura por transmitirme su pasión hacia la espectroscopía de fluorescencia. Gracias a todos los miembros del Centro de Quimica-Fisica Molecular por la gran acogida, la ayuda y las salidas fuera del laboratorio.

Por último, gracias a mis padres. Esta Tesis es tanto mía como vuestra. He llegado hasta aquí gracias a los valores que me habéis transmitido y todo el apoyo recibido.

INDEX

LIST OF ABBREVIATIONS

AFM: atomic force microscopy

ATI cell: alveolar type I cell

ATII cell: alveolar type II cell

AUC: analytical ultracentrifugation

BN-PAGE: Blue native-polyacrylamide gel electrophoresis

BODIPY/SP-B or BODIPY FL/SP-B: SP-B protein derivatized with BODIPY FL probe

BODIPY: boron dipyrromethene; 4,4-difluoro-4-bora-3a, 4adiaza-*s*-indacene

BODIPY-PC or BODIPY 500/510 C_{12}-HPC: phosphatidylcholine derivatized with BODIPY 500/510 probe

BS(PEG)$_9$: PEGylated bis(sulfosuccinimidyl)suberate

BS^3: bis(sulfosuccinimidyl)suberate

CBS: captive bubble surfactometer

DPPC: 1,2-dipalmitoyl-*sn*-glycero-3-phosphocholine

DPPG: 1,2-dipalmitoyl-*sn*-glycero-3-phospho-(1'-*rac*-glycerol)

DSP: dithiobis(succinimidyl propionate)

FITC-dextran: dextran labelled with fluorescein isothiocyanate

FM1-43: N-(3-triethylammoniumpropyl)-4-(4-(dibutylamino)styryl)pyrinidium dibromide

FRET: Förster resonance energy transfer

Fura-2 or Fura-2 AM: Fura-2 acetoxymethyl ester

IEC: ion exchange chromatography

IP3R: inositol trisphosphate receptor

k_p: partition coefficient

LB: lamellar body

LUVs: large unilamellar vesicles

MLVs: multilamellar vesicles

MSP: membrane scaffolding protein

ORB: octadecyl rhodamine B chloride (R18)

PG: phosphatidylglycerol

POPC: 1-palmitoyl-2-oleoyl-*sn*-glycero-3-phosphocholine

POPG: 1-palmitoyl-2-oleoyl-*sn*-glycero-3-phospho-(1'-*rac*-glycerol)

PS: pulmonary surfactant

SDS-PAGE: sodium dodecyl sulfate-polyacrylamide gel electrophoresis

SEC: size exclusion chromatography

SMALPs: styrene maleic anhydride lipid particles

SUVs: small unilamellar vesicles

TEM: transmission electron microscopy

TM: tubular myelin

RESUMEN

ABSTRACT

RESUMEN

El sistema respiratorio es imprescindible para la obtención del oxígeno necesario para los procesos metabólicos. El intercambio gaseoso tiene lugar a través de la barrera alveolo-capilar, donde el oxígeno y el dióxido de carbono difunden entre el espacio aéreo en los alveolos y los eritrocitos en el torrente sanguíneo. El epitelio respiratorio representa la superficie más extensa del organismo expuesta a la atmósfera y se compone de dos tipos celulares, las células alveolares tipo I (ATI) y las células alveolares tipo II (ATII). Las células ATI constituyen la mayor superficie epitelial destinada a intercambio gaseoso en los alveolos, mientras que la principal función de las células ATII es la síntesis y el ensamblaje de los componentes del surfactante pulmonar en forma de ensamblados de membranas altamente empaquetadas en el interior de organelas ácidas, denominadas cuerpos lamelares. El principal estímulo fisiológico para la secreción de surfactante es el estiramiento del epitelio alveolar durante la inspiración, el cual provoca un incremento en la concentración de calcio citoplasmático que, a su vez, desencadena la fusión de los cuerpos lamelares con la membrana plasmática de las células ATII y finalmente, la liberación de surfactante al espacio alveolar. Una vez secretado, el surfactante pulmonar se adsorbe y se extiende a lo largo de la interfase aire-líquido alveolar, donde el surfactante estabiliza la superficie respiratoria durante los sucesivos ciclos de inspiración-espiración al reducir la tensión superficial. Además de esta función principal, el surfactante pulmonar también participa en la defensa pulmonar contra infecciones provocadas por virus, bacterias y hongos, ejerciendo actividades microbicidas directas u opsonizando patógenos y modulando las respuestas celulares inflamatorias.

El surfactante pulmonar se compone de aproximadamente un 90% de lípidos y un 10% de proteínas específicas, en masa. La dipalmitoilfosfatidilcolina (DPPC) es el fosfolípido más abundante, constituyendo alrededor de un 41% de la masa total de surfactante. Entre otros fosfolípidos, las especies de fosfatidilglicerol (PG), cargadas negativamente, comprenden aproximadamente un 9% de la masa de surfactante. En lo que respecta a la fracción proteica del surfactante, las proteínas hidrofílicas SP-A y SP-D participan en la defensa inmune del pulmón, mientras que las proteínas hidrofóbicas SP-B y SP-C están involucradas en la función biofísica del surfactante pulmonar.

La función tensioactiva del surfactante pulmonar comprende tres propiedades fundamentales: 1) rápida adsorción de los complejos de surfactante, 2) máxima compresión de la película interfacial, logrando muy bajas tensiones superficiales al final de la espiración y 3) eficiente re-extensión a lo largo de la nueva superficie expuesta durante la inspiración. DPPC, SP-B y SP-C poseen papeles esenciales en el surfactante que aseguran una actividad interfacial óptima del surfactante pulmonar. En el caso de la DPPC, sus cadenas acilo saturadas permiten un alto grado de empaquetamiento de estas

moléculas fosfolipídicas en monocapas interfaciales sometidas a compresión lateral. Por su parte, las proteínas SP-B y SP-C ejercen una amplia variedad de efectos sobre bicapas y monocapas lipídicas que promueven profundas reorganizaciones en los lípidos estrechamente relacionadas con la función tensioactiva del surfactante pulmonar en la interfase alveolar.

SP-B es la proteína más importante para el mantenimiento de la función respiratoria, ya que la ausencia de su expresión conlleva fallo respiratorio en el momento del nacimiento. Además de su participación en la función tensioactiva del surfactante, la SP-B está involucrada en otros procesos de la homeostasis del surfactante, incluyendo su participación en el procesamiento post-traduccional de la SP-C y en la biogénesis de los cuerpos lamelares, así como en la formación de formas extracelulares del surfactante, como la mielina tubular, una estructura en forma de red compuesta por lípidos del surfactante y las proteínas SP-A y SP-B. Aunque la estructura terciaria de la proteína SP-B no se conoce en su totalidad, su purificación a partir de surfactante pulmonar porcino solubilizado en detergente reveló la existencia de complejos nativos de SP-B que adoptan una estructura en forma de anillos de 10 nm de diámetro. De acuerdo con un modelo de la estructura tridimensional de la SP-B basada en la estructura de la Saposina B, la organización supramolecular nativa de la SP-B consistiría en 5 o 6 dímeros covalentes ensamblados en forma de anillo, que se dispondrían de manera paralela a la superficie de bicapas lipídicas a través la interacción de los segmentos helicoidales amino- y carboxilo-terminales con las cabezas polares de los fosfolípidos.

OBJETIVOS

El principal objetivo de esta Tesis es contribuir al conocimiento de las estructuras y funciones de los complejos proteicos nativos presentes en el surfactante pulmonar, con un foco especial en aquellos constituidos por SP-B. Así, se han abordado cinco objetivos específicos en este trabajo:

1. La realización de análisis composicionales y estructurales de complejos proteicos procedentes de surfactante solubilizado en detergente o de nanodiscos de surfactante. Además, se utilizó la técnica del entrecruzamiento de proteínas para intentar clarificar las interacciones entre SP-B y SP-C en ambientes lipídicos cuasi-nativos.

2. El estudio del efecto de los complejos proteicos del surfactante en la permeabilidad y la dinámica interfacial de las membranas del surfactante pulmonar, para proponer un potencial mecanismo para la acción dual de la SP-B en ambas actividades del surfactante.

3. El abordaje de una caracterización más profunda de los oligómeros nativos de SP-B, principalmente en ambientes lipídicos, tratando de generar muestras con una calidad apropiada para una posterior caracterización estructural de los complejos a alta resolución.

4. El estudio de características estructurales de la SP-B aplicando metodologías de espectroscopía de fluorescencia, incluyendo la determinación de la estequiometria de los oligómeros nativos de SP-B en membranas y un estudio cuantitativo de los cambios topológicos inducidos por SP-B en estructuras multilamelares.

5. El estudio del efecto de la SP-B en la secreción del surfactante en células ATII. Esclarecimiento de los mecanismos de señalización que conectan la SP-B con la exocitosis de cuerpos lamelares en células ATII.

RESULTADOS PRINCIPALES Y CONCLUSIONES

El presente trabajo revela características estructurales y funcionales de la SP-B a través de tres procesos inducidos por la proteína: la agregación de membranas que conduce a la reorganización de estructuras del surfactante, la permeabilidad de membranas a través de la formación de poros, que permiten el flujo de lípidos y moléculas polares, y la estimulación de la secreción de surfactante en células ATII.

A lo largo de esta Tesis, ha quedado probado de manera reiterada la existencia de una organización supramolecular de la SP-B en el surfactante pulmonar. Además de los complejos nativos de SP-B purificados a partir de membranas de surfactante solubilizadas en detergente, los dímeros de SP-B procedentes del extracto orgánico completo del surfactante pulmonar o de la proteína aislada en solvente orgánico son capaces de auto-ensamblarse en presencia de lípidos, dando lugar a la estructura en forma de anillo del oligómero de SP-B, que se dispone sobre las cabezas polares de los fosfolípidos en bicapas y monocapas.

Se sabe que la SP-B induce la formación de estructuras multicapa altamente cohesivas asociadas a la monocapa interfacial, que parece constituir un reservorio de surfactante que asegura la estabilidad de la película tensioactiva contra el estrés mecánico producido por los continuos ciclos alveolares de compresión-expansión durante la respiración. Los experimentos de transferencia de energía por resonancia Förster resuelta en el tiempo (Time-resolved FRET) realizados en este trabajo aportan información cuantitativa sobre la topología de los agregados SP-B/membrana, demostrando que la conexión entre dos membranas está mediada por la interacción de dos oligómeros de SP-B en forma de anillos. Estas interacciones SP-B/SP-B serán responsables del papel de la SP-B en la función biofísica del surfactante pulmonar en la interfase alveolar, pero también podrían

estar participando en el empaquetamiento de membranas durante la biogénesis de los cuerpos lamelares en las células ATII.

Sobre el estudio de la permeabilidad de membranas del surfactante, el bloqueo selectivo de la SP-B con anticuerpos demuestra que los oligómeros de SP-B en forma de anillo son responsables de la generación de poros en membranas del surfactante, que permiten el flujo de moléculas polares y la transferencia de lípidos a través de membranas interconectadas del reservorio de surfactante y entre estas y la monocapa interfacial. De acuerdo con los resultados obtenidos del estudio de FRET, dos oligómeros de SP-B constituirían la maquinaria de transferencia de lípidos que aseguraría la función tensioactiva óptima del surfactante pulmonar. Además, la presencia de estas estructuras formadoras de poros en las membranas del surfactante facilitaría la difusión de iones, gases, como el oxígeno, y pequeñas moléculas polares, como péptidos implicados en la defensa innata del pulmón, asegurando un equilibrio iónico adecuado en la fina capa de fluido que recubre el epitelio alveolar y una rápida difusión de oxígenos desde el espacio aéreo a través de las membranas del surfactante.

El presente trabajo revela que la SP-B extracelular asociada a membranas induce de manera eficiente la secreción de surfactante pulmonar en células ATII. La SP-B activa la ruta de señalización purinérgica $P2Y_2$ que produce un incremento en Ca^{2+} citoplasmático, el cual en última instancia desencadena la exocitosis de cuerpos lamelares. Nuestros datos sugieren que la SP-B promueve la secreción de surfactante via liberación de ATP mediada por canales desde las células ATII. La SP-B induciría la exocitosis de surfactante en células ATII. SP-B induciría la exocitosis de surfactante en células ATII para reponer el espacio alveolar con surfactante recién secretado, asegurando el establecimiento de una red con una densidad apropiada de membranas de surfactante en la interfase alveolar.

Finalmente, esta Tesis muestra recurrentes evidencias de la relevancia de las interacciones nativas para la función óptima del surfactante pulmonar. Las interacciones de la proteína SP-B con otros componentes del surfactante ha demostrado ser importante para la actividad de la proteína. Nuestros resultados muestran que la presencia de PG es necesaria para asegurar la función adecuada de la SP-B con respecto a dos procesos: la permeabilidad de membranas y la estimulación de la secreción de surfactante en células ATII. Respecto a las interacciones de SP-B con otras proteínas del surfactante, nuestros resultados sugieren la presencia de complejos nativos constituidos por SP-B junto con SP-A o SP-C en surfactante solubilizado en detergentes. También se han sugerido posibles interacciones entre SP-B y SP-C por el bloqueo selectivo de estas proteínas con anticuerpos que acarrea una disfunción de la secreción de surfactante inducida por SP-B y altera la permeabilidad de las membranas del surfactante. Además, la SP-C parece modular la estructura de los poros formados por la SP-B en las membranas, manteniendo

una adecuada permeabilidad del surfactante nativo. La interacción entre SP-B y SP-C sería crucial para la modulación espacial y temporal de sus actividades, necesarias para la función óptima del surfactante pulmonar.

Para concluir, la presente Tesis confirma que la SP-B es una pieza clave del surfactante pulmonar, al ejercer papeles fundamentales en cada etapa del ciclo del surfactante. En primer lugar, la SP-B es necesaria para lograr la función tensioactiva óptima del surfactante pulmonar en la interfase alveolar. En segundo lugar, la SP-B participa en la biogénesis de los cuerpos lamelares en células ATII. Y, por último, el presente trabajo demuestra por primera vez que la SP-B estimula la secreción de surfactante en células ATII, asegurando la disponibilidad de complejos de surfactante recién secretados en la interfase alveolar.

ABSTRACT

The respiratory system is necessary to obtain the oxygen required for metabolic processes. Gas exchange takes place through the alveolar-capillary barrier, where oxygen and carbon dioxide diffuse between air space in alveoli and erythrocytes in the bloodstream. The respiratory epithelium represents the largest surface in the organism exposed to the atmosphere and comprises two cell types, alveolar type I (ATI) and alveolar type II (ATII) cells. ATI cells constitute the major gas exchange surface in the alveoli, whereas the main function of ATII cells is the synthesis and assembly of the components of pulmonary surfactant in the form of tightly packed membrane arrays inside acidic organelles, called lamellar bodies. The primary physiological stimulus for surfactant secretion is the mechanical stretching of alveolar epithelium during inspiration, which leads to a rise in the cytoplasmic calcium concentration that triggers the fusion of lamellar bodies with the plasma membrane of ATII cells and finally, surfactant release. Once secreted, pulmonary surfactant is adsorbed and spread along the alveolar air-liquid interface, where surfactant stabilizes the respiratory surface during successive inspiration-exhalation cycles by reducing the surface tension. Besides this main role, pulmonary surfactant also participates in lung defense against infection caused by virus, bacteria and fungi, exerting direct microbicidal activities or opsonization of pathogens and modulating the inflammatory cellular responses.

Pulmonary surfactant is composed of approximately 90% of lipids and 10% of specific surfactant proteins, by mass. Dipalmitoylphosphatidylcholine (DPPC) is the most abundant phospholipid, constituting about 41% of total mass of surfactant. Among other phospholipids, negatively charged phospatidylglycerol (PG) species comprise of approximately 9% of surfactant mass. Regarding the protein fraction of pulmonary surfactant, hydrophilic proteins SP-A and SP-D play roles in the lung immune defense, whereas hydrophobic proteins SP-B and SP-C are involved in the biophysical function of pulmonary surfactant.

Surface function of pulmonary surfactant involves three relevant properties: 1) fast interfacial adsorption of surfactant assemblies, 2) maximal compression of the interfacial film, achieving very low surface tension at the end of exhalation and 3) efficient film re-spreading along the new exposed surface area during inhalation. DPPC, SP-B and SP-C plays essential roles in surfactant that ensure an optimal surface activity of the pulmonary surfactant. In the case of DPPC, its saturated acyl chains allow a highly packing state of these phospholipid species in interfacial monolayers upon lateral compression. Concerning the proteins SP-B and SP-C, they exert a wide variety of effects on lipid bilayers and monolayers that lead to deep lipid rearrangements closely related to the surface active function of pulmonary surfactant at the alveolar interface.

SP-B is the most important protein for maintenance the respiratory function, since its lack of expression leads to respiratory failure at birth. Besides its participation in the interfacial function of surfactant, SP-B is involved in other processes of the surfactant homeostasis, including its participation in the post-translational processing of SP-C and in biogenesis of lamellar bodies, as well as the formation of extracellular surfactant forms, such as tubular myelin, a net-like structure formed by surfactant lipids and the proteins SP-A and SP-B. Although the tertiary structure of the protein SP-B is not yet well-known, its purification from detergent-solubilized porcine pulmonary surfactant revealed the existence of native SP-B complexes that adopt a ring-shaped structure of 10 nm of diameter. According to a proposed model of tridimensional structure of SP-B based on the structure Saposin B, the native supramolecular organization of SP-B would consist of 5 or 6 covalent dimers assembled in a ring-shaped structure, which would locate parallel to the surface of lipid bilayers through the interaction of N-terminal and C-terminal helical segments of the protein with the polar head groups of phospholipids.

OBJECTIVES

The main objective of this Thesis is to contribute to the understanding of the structures and functions of the native protein complexes present in pulmonary surfactant, with a particular focus on those constituted by SP-B. In this way, five specific objectives have been addressed in the present work:

1. To perform a compositional and structural analysis of protein complexes derived from detergent-solubilized surfactant or surfactant nanodiscs. Besides, protein crosslinking is applied to attempt the clarification of the interactions between proteins SP-B and SP-C in quasi-native lipid environments.

2. To study the effect of surfactant protein complexes on the permeability and interfacial dynamics of pulmonary surfactant membranes, in order to propose a potential mechanism for the dual action of SP-B on both surfactant activities.

3. To address a deeper structural characterization of native SP-B oligomers, mainly in lipid environments, attempting the generation of samples with a proper quality, in order to approach further high-resolution structural characterization of the complexes.

4. To study the structural features of SP-B applying fluorescence spectroscopy methodologies, including the determination of the stoichiometry of native SP-B oligomers in membranes and a quantitative study of the topological changes induced by SP-B in multilamellar structures.

5. To study the effect of SP-B on surfactant secretion by ATII cells. Elucidation of the signaling mechanisms connecting SP-B with lamellar body exocytosis in ATII cells.

MAIN RESULTS AND CONCLUSIONS

The present work reveals structural and functional features of SP-B through the study of three processes induced by the protein: membrane aggregation that lead to rearrangement of surfactant structures, membrane permeability trough the formation of pores, which allow the flow of lipids and polar molecules, and stimulation of surfactant secretion by ATII cells.

The existence of a supramolecular organization of SP-B in pulmonary surfactant has been repeatedly proven throughout this Thesis. In addition to native SP-B complexes purified from detergent-solubilized surfactant membranes, SP-B dimers from both the whole organic extract of pulmonary surfactant or the protein isolated in organic solvent are able to self-assemble in the presence of lipids, yielding the ring-shaped structure of the SP-B oligomer that locates over the polar head groups of phospholipids in bilayers and monolayers.

It is known that SP-B induces the formation of highly cohesive multilayered structures associated to the interfacial monolayer, which seems to constitute a surfactant reservoir that ensures the stability of the surface active film against mechanical stress induced by continuous alveolar compression-expansion cycles during breathing. Time-resolved Förster Resonance Energy Transfer (FRET) experiments performed in the present work provide quantitative information about the topology of SP-B/membrane aggregates, demonstrating that the connection between two membranes is mediated by the interaction of two SP-B ring-shaped oligomers. These SP-B/SP-B interactions would be responsible for the role of SP-B on the biophysical function of pulmonary surfactant at the alveolar interface, but also might be involved in the membrane packing during lamellar body biogenesis in ATII cells.

Regarding the study of surfactant membranes permeability, the selective blockage of SP-B with antibodies demonstrates that SP-B ring shaped oligomers are responsible for the generation of pores in surfactant membranes, that allow the flow of polar molecules and the lipid transfer across the interconnected membranes of the surfactant reservoir and between these and the interfacial monolayer. According to the results obtained from FRET study, two SP-B oligomers would constitute the lipid transfer machinery that would ensure the optimal interfacial function of pulmonary surfactant. Moreover, the presence of such pore-forming structures in surfactant membranes would facilitate the diffusion of ions, gases, such as oxygen, and small polar molecules, such as peptides involved in lung innate defense, ensuring a proper ion equilibrium in the alveolar fluid and a rapid oxygen diffusion from air space through surfactant membranes.

The present work reveals that extracellular membrane-associated SP-B efficiently induces secretion of pulmonary surfactant by ATII cells. SP-B activates the $P2Y_2$ purinergic signaling pathway that leads to an increase in cytoplasmic Ca^{2+}, which ultimately triggers exocytosis of lamellar bodies. Our data suggest that SP-B prompts surfactant secretion via channel-mediated ATP release from ATII cells. SP-B would induce surfactant exocytosis by ATII cells to replenish the alveolar space with newly secreted surfactant, ensuring the establishment of a network with a proper density of surfactant membranes at the alveolar interface.

Finally, this Thesis showed recurring evidences of the relevance of native interactions for the optimal function of pulmonary surfactant. SP-B interactions with other surfactant components have been shown to be important for the protein activity. Our results show that the presence of PG is required to ensure the proper function of SP-B with respect two features: membrane permeability and stimulation of surfactant secretion by ATII cells. Regarding SP-B interactions with other surfactant proteins, our results suggest the presence of native complexes constituted by SP-B together with SP-A or SP-C in surfactant solubilized by detergents. Possible interactions between SP-B and SP-C have been also suggested by the selective blockage of these proteins with antibodies that lead to an impairment of SP-B-induced surfactant secretion and alters the surfactant membrane permeability. Furthermore, SP-C seems to modulate the structure of SP-B-generated pores, maintaining the proper native surfactant permeability. The interaction between SP-B and SP-C would be crucial for the spatial and temporal modulation of their activities, required for the optimal function of the pulmonary surfactant.

To conclude, the present Thesis confirms that SP-B is a key element of pulmonary surfactant, playing essential roles at every stage of the surfactant cycle. Firstly, SP-B is required to achieve the optimal surface function of pulmonary surfactant at the alveolar interface. Secondly, SP-B is involved in the biogenesis of lamellar bodies in the alveolar type II cells. And lastly, the present work demonstrates for the first time that SP-B stimulates the surfactant secretion by alveolar type II cells, ensuring the availability of newly secreted surfactant complexes at the alveolar interface.

INTRODUCTION

1. INTRODUCTION

1.1. THE LUNG: RESPIRATORY PHYSIOLOGY

Respiration is the essential physiological process for life where organisms obtain oxygen, required for multiple metabolic processes. Throughout the evolution and due to habitat expansion, different respiratory systems have been developed to facilitate the exchange of gas with the environment, as skin, tracheae, gills, and lungs, as well as their intermediate stages, which coexist within the same species either temporally separated (like gills in larvae and lungs in adult stage) or simultaneously (such as skin, gills and lungs in some salamanders). Lungs have evolved as specialized organs for handling gas exchange between bloodstream and the atmosphere, where the air is ventilated through internal sack-like structures that regularly inflate and deflate. In mammals, the bronchoalveolar lung is a branching organ composed of a set of tubes that progressively subdivide up to reach alveoli, the functional units of the lung. This architecture maximizes the surface area engaged in the gas exchange with the atmosphere. Human lungs present around 480 million alveoli with an average diameter of 200 µm (Ochs *et al.*, 2004), which yields a respiratory surface area of about 70 m^2 (Daniels and Orgeig, 2003).

Gas exchange is ultimately a passive diffusion process that takes place through the alveolar-capillary barrier. From alveoli to hemoglobin in the erythrocytes, the oxygen would pass through the alveolar lining fluid (or hypophase), alveolar epithelium, interstitial layer, capillary endothelial cells and membranes of erythrocytes.

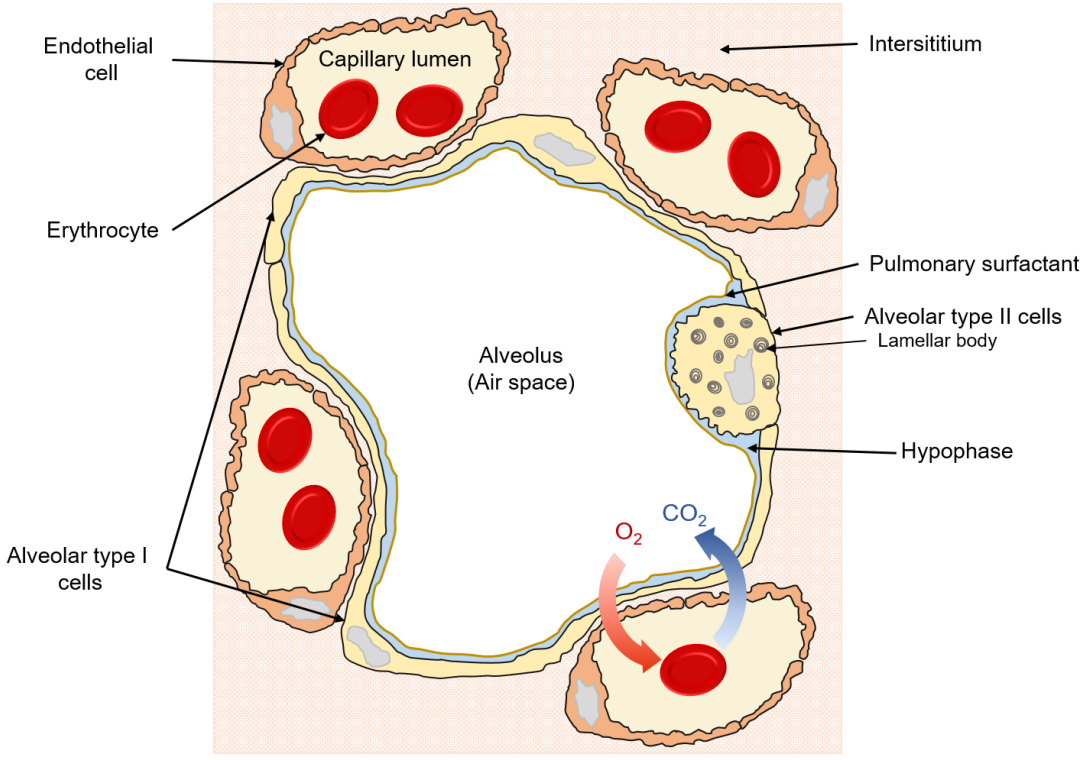

Figure 1.1. Schematic representation of the alveolar-capillary barrier.

The alveolar epithelium is composed by two cellular types: alveolar type I (ATI) cells and alveolar type II (ATII) cells. Thin and flattened ATI cells comprise the major gas exchange surface of the alveolus (about 93% surface area) (Crapo *et al.*, 1983), and also participate in the maintenance of the alveolar fluid. ATII cells are cuboidal and polarized cells that only represent about 7% of the alveolar surface (Crapo *et al.*, 1983). ATII cells perform multiple essential functions, including production of pulmonary surfactant, maintenance of the alveolar fluid and production of molecules involved in inflammation and repair processes of the lung tissue (Mason, 2006). Besides, a third cellular type can be also found in a healthy alveolus, the alveolar macrophages, which constitute the first line defense against pathogens, but also participate in the alveolar homeostasis (Divangahi, King and Pernet, 2015).

ATII cells are the only cells able to synthesize all the components of pulmonary surfactant to assemble them in acidic organelles, called lamellar bodies (Weaver, Na and Stahlman, 2002). Upon secretion, pulmonary surfactant adsorbs and spreads along the air-liquid interface to form a surface-active film, accomplishing its main function: the stabilization of the respiratory surface by minimizing surface tension during inhalation-exhalation cycles (Parra and Perez-Gil, 2015).

1.2. THE PULMONARY SURFACTANT AT THE ALVEOLAR INTERFACE

The alveolar epithelium is covered by a lining fluid, establishing the air-liquid interface. Molecules in the bulk of a liquid and molecules at the interface are subjected to different interaction forces. Molecules deep into the liquid phase establish polar interactions with other surrounding molecules that are spatially balanced. However, molecules at the interface scarcely establish interactions with the molecules of the gas phase (air), resulting in a net attractive force towards the liquid phase and a high state of energy. To minimize this energy, the system decreases the area exposed to the interfacial film by reducing the number of molecules at the interface, generating the surface tension. In the mammalian alveolar interface, as an interface subjected to compression-expansion cycles, the continuous changes in the interfacial area would require extra input of energy to increase the respiratory surface against surface tension during inhalation (Hills, 1999).

Alveoli are quasi-spherical sacks of a variety of sizes, from 3.3 to $4.8 \cdot 10^6$ μm^3 in human lung (Ochs *et al.*, 2004). According to Young-Laplace's law, the pressure inside a spheric chamber (like a bubble) is directly proportional to surface tension and inversely proportional to radius ($\Delta P = 2\,\gamma / r$). Pulmonary alveoli can be considered as interconnected bubbles of different sizes, at constant surface tension the smaller ones would be subjected to higher pressures and would tend to collapse toward those of larger size during inhalation, resulting in the progressive collapse of the lung.

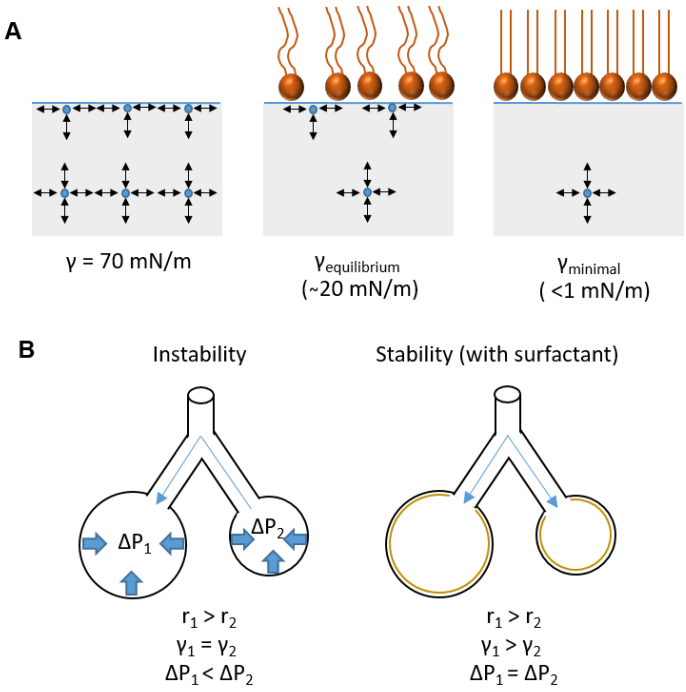

Figure 1.2. Surface tension at the alveolar interface and the function of pulmonary surfactant. A) Molecules at the air-liquid interface experience a net force toward the bulk of the fluid, which leads to minimize the exposed area to the air. When pulmonary surfactant is present, water molecules are excluded from the interface and surface tension is reduced. Once surfactant phospholipids saturate the interface, the equilibrium surface tension is reached. Upon lateral compression of surfactant film, the highly packing of phospholipids restricts the exposure of water molecules to the interface almost entirely, reaching minimal surface tension < 1 mN/m. B) Schematic representation of the Young-Laplace's law for two ideal spherical alveoli of different radii. In the absent of surfactant, a gradient of pressures is established between the two interconnected alveoli, which leads to the collapse of the alveolus with shorter radius. When surfactant is present, the system is stabilized.

Pulmonary surfactant has evolved to stabilize the alveolar interface by reducing surface tension. This main function is primarily accomplished by surfactant phospholipids, which are intercalated between water molecules at the alveolar surface, reducing the surface tension at the alveolar air-liquid interface. Once the phospholipid molecules are stably packed at the interface, the surface tension at equilibrium is reached. For an air-water interface the surface tension at 37 °C is about 70 mN/m, whereas in the presence of surfactant the surface tension decreases down to 20 mN/m at equilibrium. However, the mammalian alveolar interface is a dynamic surface since it is subjected to continuous compression-expansion processes during breathing. Thus, to prevent the alveolar collapse at the end of exhalation, pulmonary surfactant is able to reach very low surface tensions, < 1 mN/m (Hills, 1999).

1.3. PULMONARY SURFACTANT: COMPONENTS AND FUNCTION

As explained, the major function of pulmonary surfactant is the stabilization of the respiratory surface, minimizing the surface tension at the alveolar air-liquid interface. The composition of this system has been optimized along the evolution to accomplish this role efficiently.

In most mammals, pulmonary surfactant is constituted by approximately 90% lipids (by mass), from which phosphatidylcholine (PC, around 60-70%) and phosphatidylglycerol (PG, about 9%) are predominant. Besides, surfactant also contains neutral lipids, such as cholesterol (up to 8%) and other minor species (monoacylglycerol, diacylglycerol, triacylglycerol and free fatty acids) (Goerke, 1998). In contrast, the protein fraction constitutes about 10% by mass of the pulmonary surfactant. They include four specific proteins associated to surfactant SP-A, SP-B, SP-C and SP-D, which are essential for both the biophysical function of surfactant and the innate immune defense at the alveolar surface (Perez-Gil and Weaver, 2010).

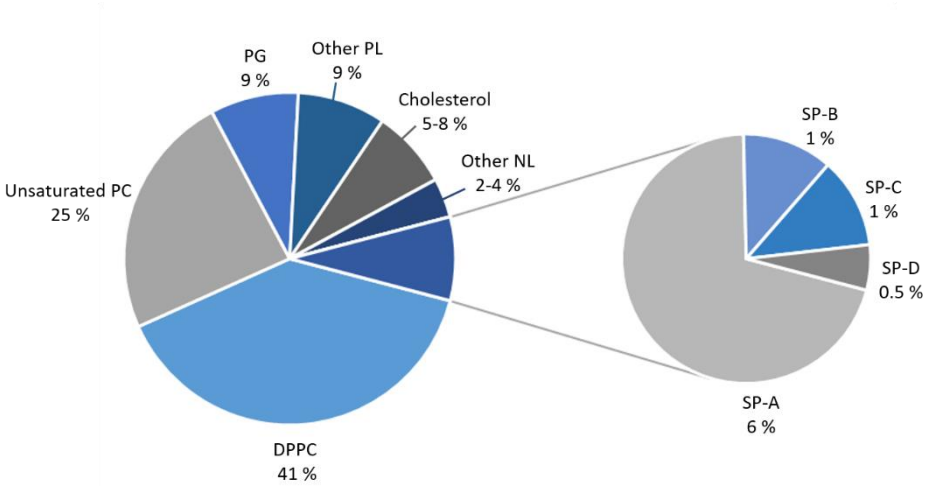

Figure 1.3. Composition of pulmonary surfactant. Pulmonary surfactant obtained from bronchoalveolar lavages of mammalian lungs comprises around 90% of lipids and 10% of proteins. DPPC: dipalmitoylphosphatidylcholine, PC: phosphatidylcholine, PG: phosphatidylglycerol, PL: phospholipids, NL: neutral lipids and SPs: surfactant proteins (SP-A, -B, -C and -D).

LIPID FRACTION

Phospholipids represent the most abundant component in pulmonary surfactant. Their structure consists in a polar headgroup and a hydrophobic region comprised by two hydrocarbon chains. Surfactant mainly contains glycerophospholipids, constituted by a glycerol molecule sterified by two hydrocarbon chains and a negatively-charged phosphate group bound to a polar variable group. Phospholipids can be classified by the charge of the polar group, which includes zwitterionic (null net charge at physiologic pH), such as phosphatidylcholine (PC) and phosphatidylethanolamine (PE), and anionic phospholipids (negatively charged), as phosphatidylglycerol (PG), phosphatidylinositol

(PI) and phosphatidylserine (PS). The two hydrocarbon chains also define relevant properties of the phospholipids depending on their chain length, unsaturation degree and the position of these unsaturations.

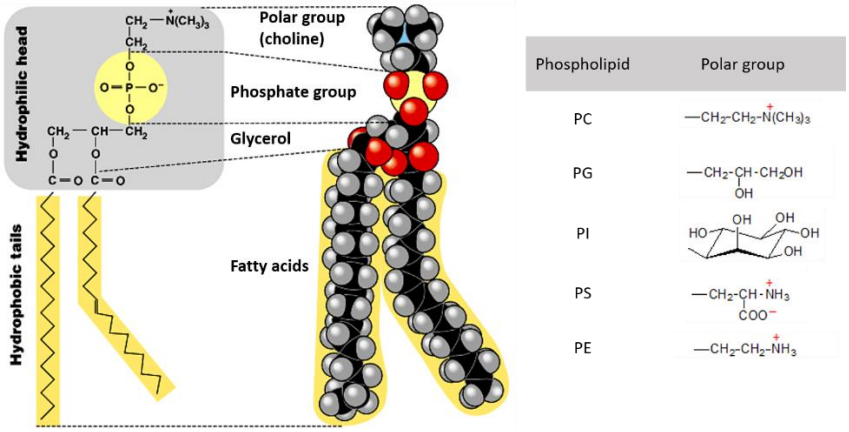

Figure 1.4. Structure of glycerophospholipids. Representation of the molecular structure of dipalmitoylphosphatidylcholine, including the hydrophobic region and the polar region. Most common polar groups of phospholipids present in pulmonary surfactant, choline (PC), glycerol (PG), inositol (PI), serine (PS) and ethanolamine (PE). Adapted from (Campbell, Reece and Mitchell, 1999; Kelly and Jacobs, 2011).

The phospholipid fraction, and especially the most abundant species, dipalmitoylphosphatidylcholine (DPPC), are the main responsible for the surface active function of pulmonary surfactant. Due to its amphipathic structure, phospholipid adopts an energetic favorable orientation at the air-liquid interface, with the polar heads interacting with the liquid phase and the hydrophobic chains oriented towards the air, displacing water molecules from the surface and decreasing surface tension. The lack of unsaturations in the acyl chains of DPPC makes this phospholipid particularly favorable to form a tightly and stable film at the interface, yielding very low surface tensions upon film compression (near 0 mN/m). PCs with unsaturated fatty acids show larger average molecular sizes and cannot be packed as tight as DPPC molecules, displaying higher surface tension values (Possmayer *et al.*, 2001).

Lipids dispersed in water have the ability to self-assemble into different supramolecular organizations due to the hydrophobic effect. They adopt preferential geometrical shapes depending on the lipid structure, leading to the so-called lipid polymorphism. Most phospholipids, as PC, are considered to have a cylindrical shape, since the cross-sectional areas of the headgroup and the acyl chains are similar. This molecular structure favors the generation by self-assembly of flat bilayer structures, also termed lamellar phases, whose curvature is virtually 0. In contrast, those lipid species with a cross-sectional area of polar headgroup smaller than the acyl chains, such as phosphatidylethanolamine (PE), generates negatively-curved structures, termed hexagonal type II phase and cubic phase. In the case of amphipathic molecules with a larger cross-sectional area of the headgroup, as lysophospholipids or detergents, they give

rise to positively-curved structures such as micelles or type I phases. Apart from the lipid chemical structure, many other factors, like temperature, pH, lateral pressure and hydration, influence the overall organization of lipid structures. Furthermore, the incorporation of membrane proteins can modulate the curvature of these lipid assemblies (Goñi, 2014).

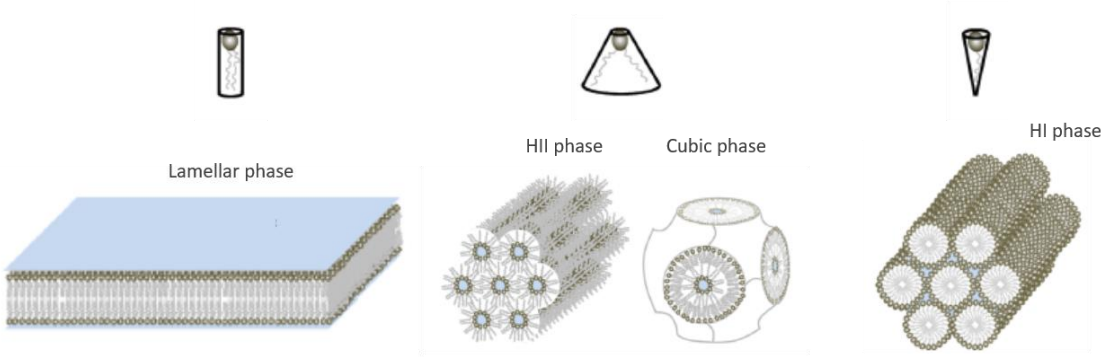

Figure 1.5. Structures of lipid phases according to their molecular structure. Cylindrical-shaped lipids, as phosphatidylcholines (PC), preferentially assemble into lamellar phases. Conical lipids like phosphatidylethanolamine (PE) or dyacilglycerol (DAG) tend to form negatively-curved structures (hexagonal phase HII or cubic phase). Inverted conical lipids, such as detergents or lysophospholipids, arrange as positively-curved structures (hexagonal phase HI). Adapted from (Jouhet, 2013).

In membranes, phospholipids adopt different levels of molecular ordering and mobility as a function of the temperature. An increase in temperature would take the membrane from an ordered state, the gel (L_β) phase, with a high packing degree and little rotational mobility of the phospholipids, to a more disordered state, the liquid crystalline (L_α) phase. This phase transition occurs at the melting temperature (T_m), where both phases ordered and disordered coexist in equilibrium. The T_m of a given phospholipid depends on the number of unsaturations and the length of its acyl chains, where long, saturated phospholipids undergo the phase transition at higher temperatures than short, unsaturated ones. The melting temperature of DPPC is 41 °C. Thus, a pure DPPC film would be in a gel phase at 37 °C, the physiological temperature of most homeothermic mammals. Pulmonary surfactant exhibits a fine balance between the proportion of saturated and unsaturated phospholipids, which allows the coexistence of ordered and disordered phases at a wide range of temperatures, including the physiological values (De La Serna *et al.*, 2004). In interfacial monolayers, phospholipids also organize into ordered and disordered phases depending on its lipid composition, temperature and compression state. Lipids with a high lateral mobility constitute the liquid-expanded (L_e) phase, which would correspond to a L_α phase in bilayers. However, upon lateral compression of the interfacial film, the area is reduced and the interactions between molecules increase, causing the shift to a more ordered phase, the liquid-condensed (L_c) state, whose high packing state is comparable to L_β phase in bilayers (Parra and Perez-Gil, 2015).

With respect to lipid phase segregation, cholesterol also displays an important role modulating the thermodynamic properties and lipid packing of membranes. The incorporation of this small amphipathic molecule into phospholipid monolayers and bilayers gives rise to two distinct liquid phases: liquid-ordered (L_o) and liquid-disordered (L_d) (Veatch and Keller, 2002). When cholesterol partitions into L_d phases, the translational mobility and diffusion of phospholipids is restricted. However, in L_o phases, the interactions of cholesterol with phospholipids lead to phase fluidization. Cholesterol present in pulmonary surfactant has been shown to influence the lateral organization of its membranes (De La Serna *et al.*, 2004).

In pulmonary surfactant, the coexistence of ordered and disordered phases at different temperatures and lateral pressures manifests in a high stability of surfactant layers at high compression sustained by saturated molecules, mainly DPPC, and enough fluidity and dynamics, favored by unsaturated species. Moreover, proteins SP-B and SP-C show a preferential partition into disordered domains (Nag *et al.*, 1997; De La Serna *et al.*, 2004). Thus, the lipid composition together with surfactant proteins provides surfactant membranes with the optimal structure and dynamics to respond to physiological demands.

PROTEIN FRACTION

Besides lipids, pulmonary surfactant is composed by four specific proteins: SP-A, SP-B, SP-C and SP-D, which are essential for surfactant activity at alveoli. They can be classified in two groups depending on both nature and function: hydrophilic proteins, SP-A and SP-D, participate in innate immune defense at the alveolar surface, while hydrophobic proteins, SP-B and SP-C, are involved in the biophysical function of surfactant.

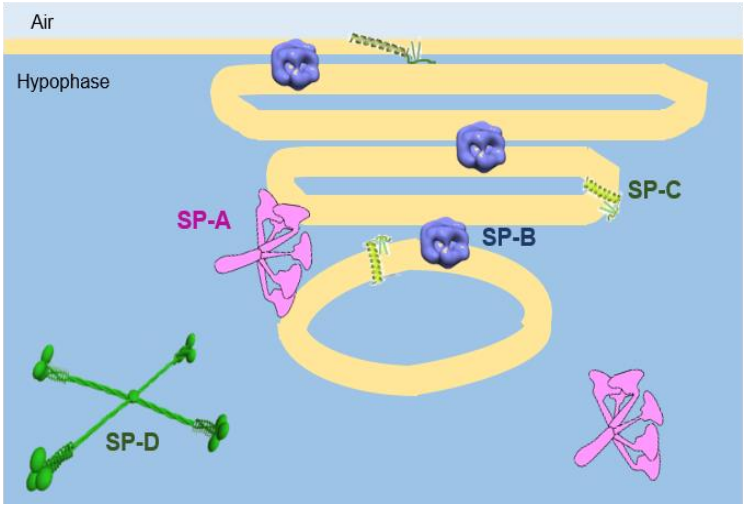

Figure 1.6. Surfactant proteins in the context of the alveolar hypophase. SP-B and SP-C are proteins permanently integrated into surfactant membranes, from which they modulate the surface activity of the pulmonary surfactant, while SP-A and SP-D are soluble proteins mainly involved in host defense. In the case of SP-A, it can also participate in the biophysical function of pulmonary surfactant by mediating contacts between bilayers and between these and the monolayer at the near-interface environment.

Hydrophylic proteins SP-A and SP-D

SP-A and SP-D are components of the innate immune defense system in the alveolar epithelium. SP-A is the most abundant protein in pulmonary surfactant, constituting 5-6 % in mass of surfactant as obtained from the bronchoalveolar fluid, in contrast to only 0.5% of SP-D (Serrano and Perez-Gil, 2006). Oligomerization of SP-A and SP-D is required to constitute biologically active proteins. Monomers of SP-A (28-37 KDa) are assembled into a structure constituted by 6 trimers (630 KDa) (Crouch and Wright, 2001), whereas SP-D (monomers of 43 KDa) associates in trimers that can further oligomerize forming dodecamers (520 KDa) and even higher order oligomers (Arroyo *et al.*, 2018). These hydrophilic proteins belong to a family of mammalian C-type lectins containing collagen regions, termed collectins. They share structural features particularly optimized for their function in the host innate defense, including a N-terminal containing cysteines responsible of the oligomerization via disulfide bonds, a triple helical collagen region, an α-helical coiled coil neck segment (involved in the trimerization of the protein) and a C-terminal globular lectin domain (Kishore *et al.*, 2006). SP-A and SP-D recognize carbohydrate epitopes in the outer surface of virus, bacteria and fungi through their lectin domains or CRD (carbohydrate recognition domains). Upon binding, they opsonize and aggregate pathogens, enhancing their phagocytosis by macrophages, monocytes, neutrophils and dendritic cells (Wright, 2005). Lung collectins also display a direct microbicidal activity by increasing the permeability of bacterial membranes and inducing leakage (Wu *et al.*, 2003). Additionally, SP-A and SP-D modulate the inflammatory cellular response by binding to membrane receptors of various immune cells (Wright, 2005).

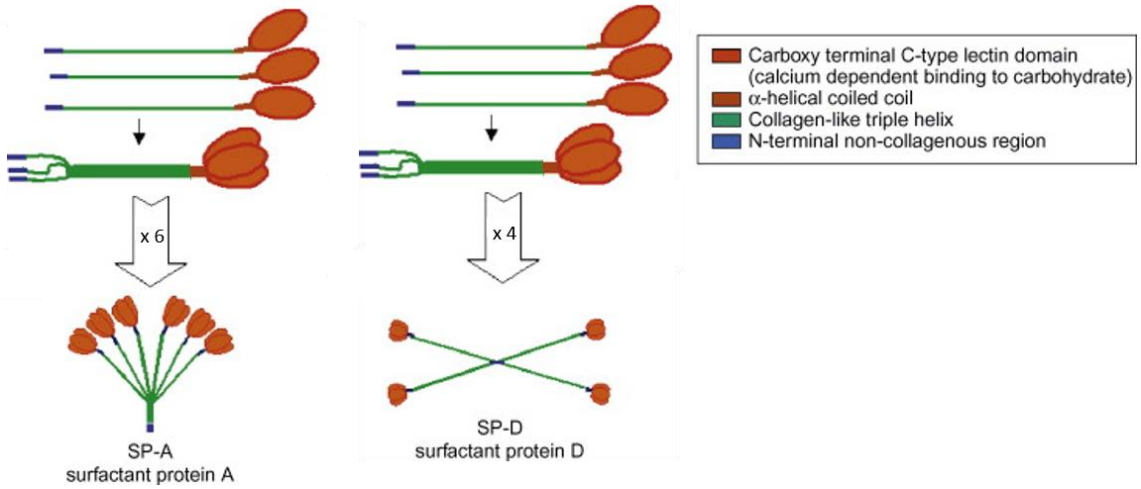

Figure 1.7. Schematic representation of SP-A and SP-D structures. As members of the collectin family, SP-A and SP-D show structural common features as C-type lectin domain, also termed carbohydrate recognition domain (CRD). SP-A quaternary structure consists of a hexamer of trimers, while SP-D assembles into tetramers of trimers. Adapted from (Thursz and Khamri, 2010).

Regarding their membrane-interacting properties, SP-A binds preferentially to DPPC via the CRD domain in a Ca^{2+} dependent manner (Kuroki and Akino, 1991; Casals, Miguel and Perez-Gil, 1993; Palaniyar *et al.*, 1998; Yu and Possmayer, 1998) and can promote lipid vesicle aggregation. SP-A is essential for the formation of tubular myelin (Palaniyar *et al.*, 1999) and contributes to the surface activity of surfactant, enhancing the interfacial adsorption of phospholipids and generating a highly cohesive multilayer film with optimal biophysical properties (Lopez-Rodriguez *et al.*, 2016). On the contrary, SP-D is not usually associated to surfactant membranes, being 75% of total amount of SP-D in the aqueous fraction of the bronchoalveolar lavage (Kishore *et al.*, 2006). However, SP-D is able to interact with PI and glucosylceramide, both minor lipids in pulmonary surfactant that contain sugar groups (Kuroki *et al.*, 1992; Ogasawara, Kuroki and Akino, 1992). Both proteins are involved in the homeostasis and recycling of surfactant (Hawgood and Poulain, 2001). SP-A inhibits surfactant secretion and enhances the lipid uptake by alveolar type II cells (Dobbs *et al.*, 1987; Rice *et al.*, 1987; Wright *et al.*, 1987). In the case of SP-D, *in vivo* experiments demonstrate the relevance of SP-D in the modulation of the surfactant lipid pool by yielding structural conversion of surfactant membranes (Korfhagen *et al.*, 1998; Ikegami *et al.*, 2009).

Hydrophobic proteins SP-B and SP-C

SP-B and SP-C account each for about 1% in mass of the total content of pulmonary surfactant. However, with a molecular weight of 3.7 KDa, SP-C is more abundant than SP-B in molar terms.

SP-B

SP-B is a 79-residue polypeptide with a molecular weight of 8.7 KDa. It presents a highly hydrophobic content (approximately 40%) and mainly adopts an α-helical secondary structure (Johansson and Curstedt, 1997). SP-B contains 6 cysteines in a highly conserved position that establish 3 intramolecular disulfide bridges (Cys8-Cys77, Cys 11-Cys71, Cys 35-Cys46) and an additional cysteine (Cys 48) responsible for the formation of the intermolecular disulfide bridge of the covalent homodimer of 18 KDa. Besides, SP-B exhibits positive net charge of +7, which yields a preferential interaction with anionic phospholipids (Perez-Gil, Casals and Marsh, 1995; Cabré *et al.*, 2012).

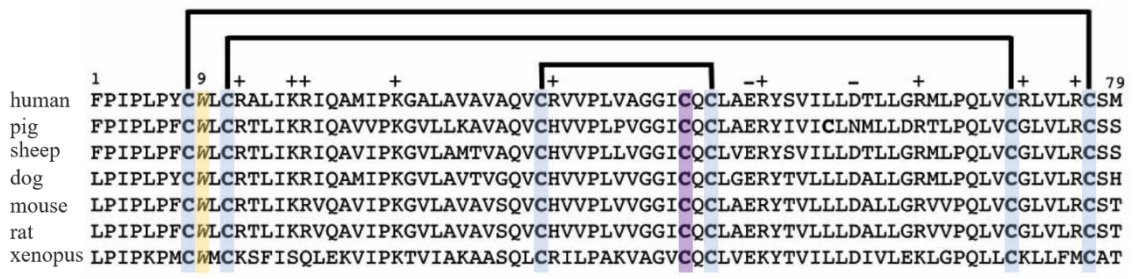

Figure 1.8. Protein sequence alignment of SP-B from different species. Cysteines involved in intramolecular disulfide bonds (represented by connecting lines) are colored blue, while cysteine responsible for the interdimer disulfide bond is colored purple. The unique and highly conserved tryptophan residue is in yellow. Positive and negatively charged residues are marked with plus and minus symbols. Adapted from (Mingarro *et al.*, 2008).

The amphipathic character of SP-B and the presence of charged residues suggest that the protein establishes a superficial interaction with bilayers and monolayers. Hydrophobic regions of its amphipathical segments would interact with the acyl chains of phospholipids, while basic amino acid residues establish electrostatic interactions with polar head groups of anionic phospholipids. This superficial interaction of SP-B with membranes has been supported by fluorescence anisotropy (Baatz, Elledge and Whitsett, 1990), nuclear magnetic resonance (Morrow *et al.*, 1993) and time-resolved Förster resonance energy transfer (Cabré *et al.*, 2012). However, a deeper insertion of the protein with the membrane has been suggested by differential scanning calorimetry (Shiffer *et al.*, 1993) and electron spin resonance (Perez-Gil, Casals and Marsh, 1995).

SP-B belongs to the saposin-like protein (SAPLIP) family. SAPLIP are small proteins that contain 4 or 5 amphipathic α-helices and 6 highly conserved cysteines involved in the formation of 3 disulfide bonds, responsible for the so called saposin fold. This family includes membrane-interacting proteins with diverse functions, such as saposins, involved in the degradation of sphingolipids as co-lipases, and several antimicrobial proteins, like NK-lysin and granulysin. However, SP-B is the only member of the family which is permanently associated to lipids due to its high hydrophobicity. Since the three dimensional structure of SP-B is still unkown, several structural models of the protein has been developed based on other SAPLIPs.

Sequence alignment of the sequence of SP-B and NK-lysin, a monomeric antimicrobial and antitumor protein, predicted the existence of 4 amphipathic α-helices which are associated by pairs, 1-4 and 2-3, through disulfide bonds, with Cys 48 being located at the hydrophilic face of helix 3 (Andersson *et al.*, 1995). Based on this model, the interaction of SP-B dimer with membranes could imply the connection between two bilayers, where each SP-B monomer would locate in one of them (Johansson and Curstedt, 1997) (Figure 1.9 A).

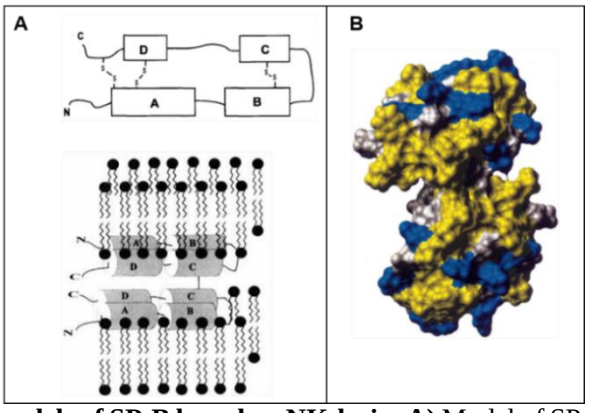

Figure 1.9. Structural models of SP-B based on NK-lysin. A) Model of SP-B based on the sequence of NK-lysin developed by (Andersson *et al.*, 1995). Up: schematic representation of a SP-B monomer where the amphipathic helices (shown as rectangles) are aligned and intramolecular disulfide bonds are highlighted. Down: possible structure of a SP-B dimer in membranes, where the two monomers are located in different phospholipid bilayers. Taken from (Johansson and Curstedt, 1997). **B)** SP-B model based on the quaternary structure of NK-Lysin, according to (Zaltash *et al.*, 2000). Representation of the globular SP-B dimer where charged residues are colored blue, hydrophobic residues in yellow and other residues in white.

On the other hand, a model for the three-dimensional structure of SP-B dimer was generated from the structure of NK-lysin obtained by nuclear magnetic resonance (NMR) (Zaltash *et al.*, 2000). According to this model, SP-B monomer would be constituted by 5 amphipathic α-helices, where the hydrophobic regions are buried towards the inner of the protein. SP-B dimer is a globular fold stabilized by the interdisulfide bond between Cys 48, which aligned the highly conserved and charged residues Glu 51 and Arg 52 of both monomers allowing the establishment of two saline bonds (Figure 1.9 B). It has been proposed that the existence of these non-covalent bonds could still sustain the dimerization of the mutated form of SP-B Cys48Ser (Zaltash *et al.*, 2001), which supports the evidence that the interdisulfide bond C48-C48 is not crucial for SP-B activity (Ikegami, Takabatake and Weaver, 2002). This proposed globular structure may unfold at the air-liquid interface upon surface tension increases, extending its structure and exposing the hydrophobic region towards the air, and folding again upon monolayer compression (Fullagar *et al.*, 2003).

Recently, an oligomeric structural model of SP-B was generated from the three-dimensional structure of saposin B. In this model, SP-B monomers with 5 amphipathic α-helixes (6-18, 25-35, 43-53, 56-62, 69-74) show two structural variants that differ on the presence of a kink between helices 3 and 4, as in saposin B monomers (Figure 1.10 A). From these modelled SP-B monomers, open and closed conformations of SP-B dimers were generated (Figure 1.10 B). These non-covalent dimers would be formed by the interactions between helices 1 and N-terminal segments through an antiparallel coiled coil. Cys 48, involved in the covalent dimerization of SP-B, and residues involved in the salt bond, Glu 51 and Arg 52, would locate into the external face of the dimer. Modeled structures satisfying disulfide bond and salt bridges predict the existence of a high-order

oligomer formed by 5 or 6 dimers (Figure 1.10 C-D). This model implies a superficial SP-B-membrane interaction defined by the contact of helices 1 and 5 with polar headgroups of phospholipids, while Trp 9 residues and the N-terminal segment might insert deep into the bilayer. The hydrophobic residues of each non-covalent dimer are shielded in the inner of the dimer, forming a hydrophobic cavity that could accomodate a phospholipid molecule, like saposin B dimer. The concerted opening of all dimers in the oligomer would induce the pivoting of the whole structure toward the inner of the membrane, eventually exposing the SP-B hydrophobic cavities to the phospholipid acyl chains and the eventual loading of the complex. This feature of the oligomeric model is in agreement with experimental evidences suggesting that SP-B mediates lipid transfer between membranes (Poulain *et al.*, 1992; Poulain, Nir and Hawgood, 1996).

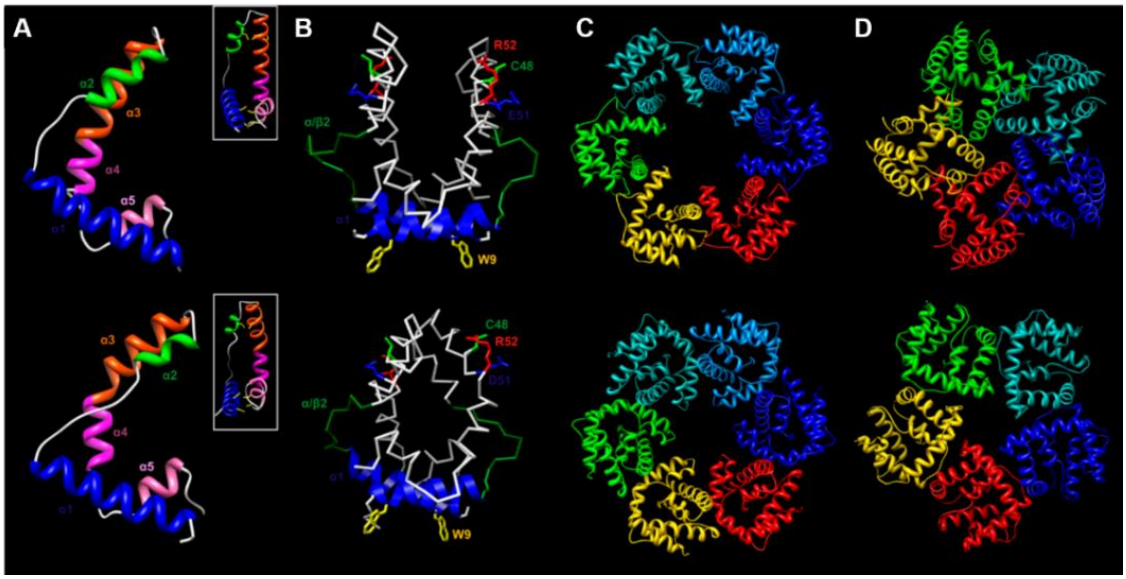

Figure 1.10. Oligomeric model of SP-B structure based on saposin B. A) SP-B monomers generated using the two structural variants of saposin B. B) SP-B dimers modeled from the open (up) and closed (down) dimers of saposin B. C and D) Models of hexamers and pentamers of open (up) and closed (down) SP-B dimers. Model developed by (Olmeda *et al.*, 2015).

The oligomerization model of SP-B has been confirmed by the presence of native SP-B complexes in detergent-solubilized pulmonary surfactant (Olmeda *et al.*, 2015). As determined by transmission electron microscopy, these fully-functional SP-B complexes purified in detergent are ring-shaped particles with a diameter of ~10 nm, which could be formed by the vertical apposition of two rings. Each SP-B ring would be constituted by 5 or 6 SP-B dimers. It has been proposed that the docking of SP-B oligomers between different membranes could be required for the optimal activity of pulmonary surfactant at the air-liquid interface at two stages: 1) enhancement of interfacial adsorption through lipid transfer between surfactant structures and 2) maximizing the mechanical stability of the interfacial monolayer by formation of multilayered structures.

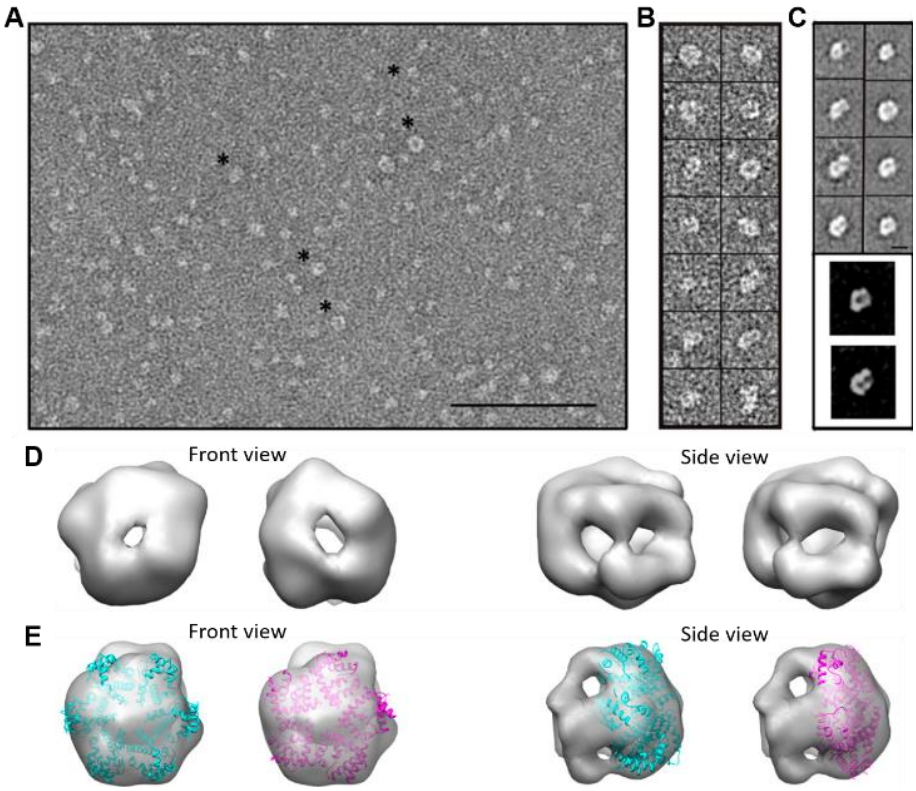

Figure 1.11. Supramolecular structure of SP-B complexes obtained from surfactant membranes solubilized with CHAPS. A) Representative trasnsmission electron micrograph of negative-stained SP-B complexes. Scale bar, 100 nm. B) Selection of representative single particles. C) Selection of representative 2-dimensional averages obtained from the oligomeric SP-B complexes. Scale bar, 30 nm. D) Front and side views of the 3-dimensional model built from oligomeric SP-B complexes, obtained by angular refinement. E) Front and side views of the 3-dimensional model of oligomeric SP-B complex (transparent gray density), showing the atomic structure theoretical model of a hexamer (blue) and pentamer (pink) of SP-B dimers fitting into the electron microscopy density. Taken from (Olmeda *et al.*, 2015).

Regarding SP-B functions, it has been described that SP-B induces membrane rearrangements leading to aggregation, fusion and lysis of vesicles (Ryan *et al.*, 2005). These membrane perturbing activities seem to lie underneath the ability of SP-B to form multilayered aggregates attached to a monolayer film (Krol *et al.*, 2000; Diemel *et al.*, 2002; Cruz *et al.*, 2004; Cabre *et al.*, 2009), as well as promoting lipid transfer from vesicles to a preformed interfacial monolayer (Oosterlaken-Dijksterhuis *et al.*, 1991a, 1991b) or directly to the clean air-liquid interface (Cruz *et al.*, 2000; Schurch *et al.*, 2010), which entails the reduction of surface tension at the alveolar surface. An extensive study for the identification of the functional determinants of the SP-B described that helices 1 and 2 are responsible for aggregation, lipid mixing and fusion of membranes, while N-terminal domain (residues 1-9) is critical for the surface tension reducing property of SP-B (Ryan *et al.*, 2005). In addition, SP-B, together with SP-C, induces membrane permeabilization (Parra *et al.*, 2011, 2013).

SP-B is the most relevant protein for the maintenance of the respiratory surface, since the absence of its expression leads to lethal respiratory failure at birth (Nogee *et al.*, 1993;

Clark *et al.*, 1995). Besides its participation in the biophysical function of surfactant, SP-B is involved in many functions throughout the metabolic cycle of surfactant. SP-B participates in the post-translational processing of SP-C (Vorbroker *et al.*, 1995) and promotes the lipid packing to generate lamellar bodies (Stahlman *et al.*, 2000). Moreover, it is required, together with SP-A, to convert tightly associated membrane arrays inside lamellar bodies into net-like structures, termed tubular myelin, once surfactant is secreted towards the alveolar hypophase (Williams, 1977). These functions of SP-B are explained in detail in the context of surfactant homeostasis in section 1.4.

Finally, given the presence of the common structural framework of saposins, SP-B exhibits a limited antimicrobial activity by inducing membrane permeabilization in Gram positive and Gram negative bacteria, as well as a likely function of bacterial opsonization, which is related to its ability to aggregate membranes (Ryan *et al.*, 2006).

SP-C

SP-C is the only surfactant protein exclusively present in the lungs. It is a 35 amino acid transmembrane protein (4.3 KDa), which adopts an α-helical structure between residues 9 and 34, rich in aliphatic residues, mostly valine (Guy Vandenbussche *et al.*, 1992; Johansson *et al.*, 1994). The N-terminal segment of SP-C (residues 1-8) exhibits an amphipathic character with a positive net charge, yielding a preferential interaction with anionic phospholipids (Perez-Gil, Casals and Marsh, 1995). Furthermore, the N-terminal segment is double palmitoylated at cysteines 5 and 6.

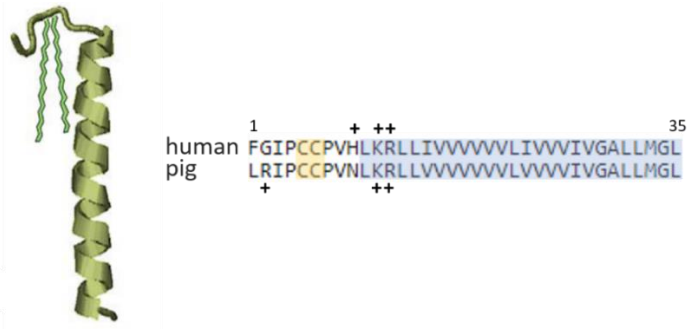

Figure 1.12. Surfactant protein SP-C. A) Molecular model of the SP-C monomer based on the structure obtained by NMR of the protein in organic solvent (Johansson *et al.*, 1994). B) Amino acid sequences of human and porcine SP-C. The α-helical segment is colored blue and cysteines subjected to palmitoylation colored yellow. Positively charged residues are marked with plus and minor symbols.

Regarding its function, SP-C alters lipid packing in membranes and monolayers, affecting the lateral organization of lipids (Pérez-Gil *et al.*, 1992; Dico *et al.*, 1997). SP-C also promotes interfacial adsorption and lipid exchange between bilayers and between bilayers and monolayers (Possmayer *et al.*, 2001; Wang *et al.*, 2005). It has been suggested that the N-terminal segment would have the potential to perturb lipids of the

adjacent bilayer or monolayer, inducing packing defects in interfacial monolayers (Plasencia, Keough and Perez-Gil, 2005) and bilayers, leading to vesicle aggregation and leakage (Plasencia *et al.*, 2004). The double palmitoylation contributes to reach and maintain the lowest surface tensions at high compression rates, in the presence of SP-B and cholesterol, although it is not required for interfacial lipid adsorption (Baumgart *et al.*, 2010). It has been proposed that palmitoylation is important for SP-C to induce the generation of interdigitated phases (Plasencia *et al.*, 2008; Roldan, Pérez-Gil, *et al.*, 2017), which would potentially take part of bilayer-bilayer and bilayer-monolayer transitions, especially at high compression pressures. Moreover, these SP-C-induced interdigitated phases appear to maximize the segregation of lipid phases (Roldan, Pérez-Gil, *et al.*, 2017). Additionally, SP-C would have a potential role in cholesterol mobilization and pulmonary homeostasis at the alveolar interfaces, since SP-C has the ability to fragment lipid bilayers into small highly curved vesicles where cholesterol accumulates (Roldan *et al.*, 2016). Some evidences have been found about a likely dimerization of SP-C through a specific motif in its C-terminal segment (Kairys, Gilson and Luy, 2004). In this way, SP-C/SP-C interactions have been recently confirmed in membranes by time-resolved fluorescence spectroscopy (Cabre *et al.*, 2018).

Lack or dysfunction of SP-C expression is not as critical as SP-B, since animals can breathe and survive (Nogee, 2004). However, deficiencies in SP-C are related to chronic severe respiratory pathologies associated with emphysema and pulmonary fibrosis (Glasser *et al.*, 2003). Thus, SP-C may be essential for an efficient stabilization of the respiratory epithelium at long term.

SP-B and SP-C: role at the surfactant film

SP-B and SP-C display essential functions for an optimal interfacial activity of pulmonary surfactant, which involves three relevant properties, in all of which SP-B and SP-C participate (Figure 1.13):

- Fast adsorption into the interface. Surfactant proteolipid assemblies accumulated near the interface are transferred into and spread along the interface. The interfacial adsorption of phospholipids is not energetically favorable because transfer of phospholipids entails transient exposure of acyl chains to polar environments, making this process slow. Both SP-B and SP-C enhance the insertion of phospholipids into the interface, increasing the rate of lipid adsorption (on the scale of seconds), although SP-B is specially effective in this process (Schurch *et al.*, 2010). It has been proposed that upon touching the interface, SP-B and SP-C, in a concerted way, would unravel the newly-secreted surfactant membranes and catalyze the lipid insertion into the

interface (Hobi *et al.*, 2016). The proteins would somehow form structures conducting surface active lipid species without allowing their exposure to water.

- Maximal compression of the interfacial film. As surfactant film is subjected to successive compression-expansion cycles, this system has to be very dynamic with fast lipid reorganization processes to maintain the stability of the respiratory surface. During exhalation, the reduction of the alveolar surface is stabilized by a deep decrease in surface tension, to near 0 mN/m. To achieve this extremely low surface tension, the maximal compaction of the material at the surface film is required. As mentioned before, saturated acyl chains of DPPC achieve a high degree of packing, leading to very low surface tension. Thus, upon compression of the film, this becomes enriched in DPPC molecules, while the unsaturated phospholipids and other lipids result excluded from the monolayer and form multilayered structures attached to the interface. This process has been called "squeeze-out" and it has been proposed to be driven by the hydrophobic protein fraction of surfactant (Keating *et al.*, 2012). Although excluded from the monolayer upon compression, SP-B promotes film stability, likely by facilitating the formation of highly cohesive multillamelar arrays (Taneva and Keough, 1994b; Diemel *et al.*, 2002; Cruz *et al.*, 2004; Cabre *et al.*, 2009; Schurch *et al.*, 2010; Bernardino de la Serna *et al.*, 2013). It has been proposed that a continuous network of membrane multilayers are established by the apposition of SP-B oligomers between membranes, so that a pair of connected oligomers would form a hydrophobic pore through which lipids could be transferred (Olmeda *et al.*, 2015). This assumption is supported by experimental evidences that reveal that SP-B induces the formation of multilayered structures through SP-B/SP-B interactions (Cabre *et al.*, 2009). On the other hand, SP-C is excluded from the interface under high compression pressures, but the palmitoylated N-terminal segment of SP-C is entitled to maintain the association with the highly packed interfacial film, which would be especially relevant at the end of exhalation (Taneva and Keough, 1994c; Plasencia *et al.*, 2008).

- Efficient film re-spreading is essential for maintaining the equilibrium surface tension (around 20 mN/m) during inhalation. This re-adsorption process entails the lipid transfer from the interconnected multilamellar arrays into the interfacial monolayer. This process is also enhanced by both hydrophobic proteins, although SP-B appears to be more efficient promoting re-spreading of the film (Taneva and Keough, 1994a; Serrano and Perez-Gil, 2006), most likely because of the specialized structure of SP-B pores.

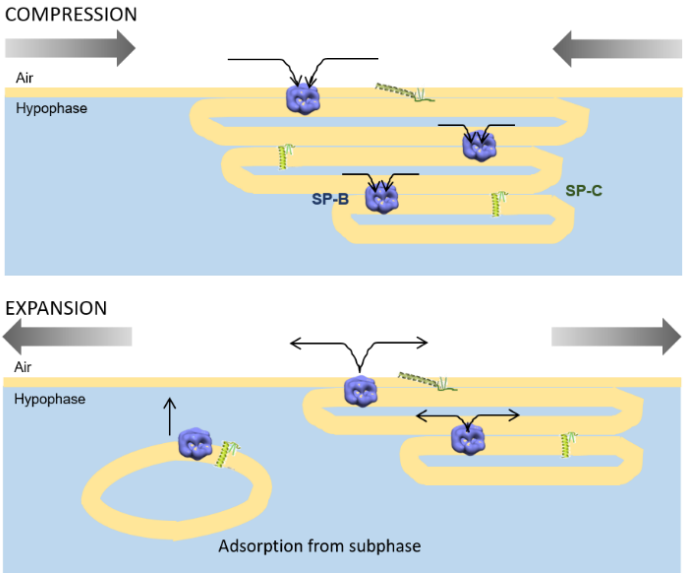

Figure 1.13. Participation of SP-B and SP-C in surfactant dynamics during compression-expansion cycles. Up: monolayer and membrane reservoir connected by both hydrophobic proteins showing the exclusion of material from the interface that occurs during compression (exhalation). Down: re-spreading of the interfacial film and adsorption of new material during expansion (inhalation).

1.4. PULMONARY SURFACTANT HOMEOSTASIS

SYNTHESIS OF SURFACTANT COMPONENTS

Although a fraction of pulmonary surfactant is recycled, *de novo* synthesis of surfactant components is continuously required to satisfy the demand of surface active material. These surfactant components are produced by alveolar type II cells. Synthesis of lipids and most of the surfactant proteins undergo different pathways that converge during the assembly of surfactant complexes into the lamellar bodies.

LIPID SYNTHESIS

Surfactant phospholipids are produced in ATII cells by novo synthesis in the endoplasmic reticulum (ER) or by remodeling from extracellular surfactant (Olmeda, Martinez-Calle and Perez-Gil, 2017). In the case of the major lipid component of surfactant, 45 % of DPPC comes from *de novo* synthesis (via the Kennedy pathway), whereas the remodeling pathway contributes with 55-75% of DPPC (Batenburg, 1992). Both pathways intersect at the enzyme LPCAT1, which regulates the PC synthesis to demand for surfactant (Butler and Mallampalli, 2010).

PROTEIN SYNTHESIS

Both SP-A and SP-D are synthesized as propeptides that undergo post-translational modifications, such as glycosylations and hydroxilations, and oligomerization processes during trafficking via endoplasmic reticulum and Golgi in alveolar type II cells (Weaver and Whitsett, 1991; Crouch, 1998). The secretion of SP-D to the alveolar space seems to be regulated by a constitutive route of secretion that is independent of lamellar body secretion. In contrast, whether the newly-synthesized SP-A secretion occurs either as a regulated process via lamellar bodies or as constitutive release by an alternative pathway is still a matter of controversy. Some studies proposed that SP-A is exocytosed to the alveolar space not associated to lamellar bodies, corresponding the fraction of SP-A present in lamellar bodies to the previously endocytosed protein (Osanai, Mason and Voelker, 1998; Ochs *et al.*, 2002; Schmiedl *et al.*, 2005). Alternatively, it has been described that the alveolar uptake is not the major source of SP-A in lamellar bodies, suggesting that newly-synthesized SP-A would be primarily secreted via this organelle (Fisher, Dodia and Chander, 1994).

Hydrophobic proteins SP-B and SP-C are synthesized as much larger precursors that suffer multiple proteolytic cleavage steps before reaching their mature forms and being assembled into LBs (lamellar bodies). Both proteins follow parallel pathways of endosomal processing from ER (endoplasmic reticulum) to LBs, involving the sequential enzymatic activities of several proteases and a progressive decrease in the pH gradient down to 5.5 in LBs.

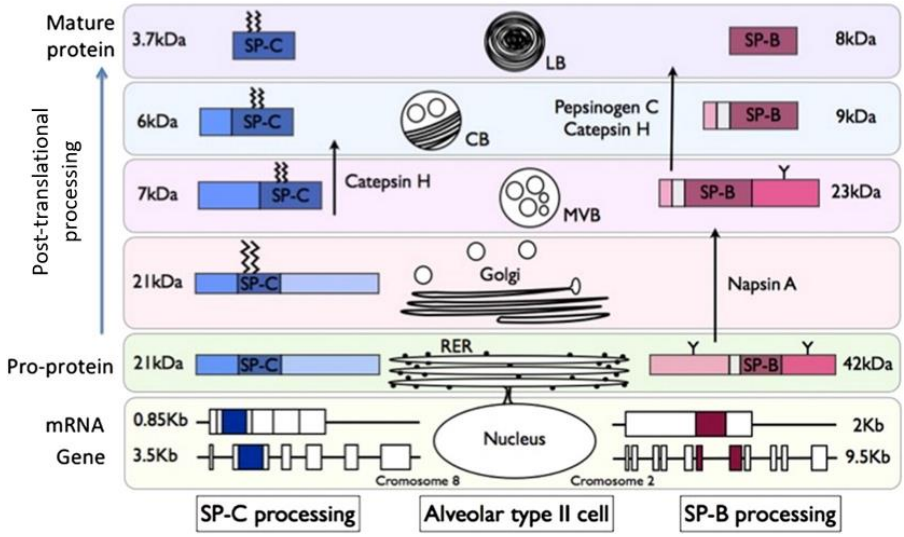

Figure 1.14. Synthesis and processing of SP-B and SP-C in alveolar type II cells. Both proSP-B and proSP-C are sequentially cleaved along the endosomal pathway (RER: rough endoplasmic reticulum, Golgi, MVB: multivesicular bodies, CB: composite bodies, LB: lamellar bodies) until they are assembled into lamellar bodies for its exocytosis. Taken from (Lopez-Rodriguez and Perez-Gil, 2014).

The gene encoding SP-B is located in the chromosome 2 and its expression is regulated by TTF1 (thyroid transcription factor 1) (Lopez-Rodriguez and Perez-Gil, 2014). Human SP-B mRNA is translated into to a preprotein consisting of 381 amino acids. This preprotein is translocated to the ER to initiate its post-translational processing. SP-B precursor (proSP-B) of 42 KDa consists of 3 saposin-like domains: the mature SP-B sequence and the glycosilated N-terminal and C-terminal propeptides. Both propeptides would protect the highly hydrophobic mature peptide from the exposure to the aqueous environment. In particular, the N-terminal domain act as a chaperone involved in the pH-regulated proteolytic processing of the mature SP-B (Serrano, Cabre and Perez-Gil, 2007). Processing of the 42 KDa precursor to the 8 KDa mature SP-B takes place in multivesicular bodies, intermediate composite bodies and lamellar bodies and involves at least the sequential participation of Cathepsin H, Napsin A and Pepsinogen C proteases (Brasch *et al.*, 2003; Guttentag *et al.*, 2003; Gerson *et al.*, 2008), whose activities are largely dependent on the pH gradient along the endosomal pathway (Serrano, Cabre and Perez-Gil, 2007; Banares-Hidalgo, Perez-Gil and Estrada, 2014). Together with mature SP-B, the free N-terminal fragment is also transported to LBs and further secreted to the alveolar hypophase, where it exhibits a microbicidal activity related to its saposin-like domain (Brasch *et al.*, 2004; Yang *et al.*, 2010). As the mature SP-B, the C-terminal propeptide might somehow also participate in modulating lamellar body biogenesis, as transgenic mice expressing a SP-B precursor lacking the C-terminal propeptide exhibited an increased tissue surfactant pool size and dramatically enlarged lamellar bodies (Akinbi *et al.*, 1997). Moreover, and given that the C-terminal propeptide contains another saposin domain, it has been proposed that this peptide might display a further antimicrobial-protecting role (Perez-Gil and Weaver, 2010)

SP-C is synthesized as a proprotein of 197 amino acids and a molecular weight of 21 KDa, which consists of a N-terminal propeptide, the mature sequence of SP-C and a C-terminal propeptide. ProSP-C is inserted in the ER through the transmembrane segment of the mature SP-C, with the C-terminal region facing the ER lumen and the N-terminal segment exposed to the cytoplasm (Beers and Mulugeta, 2005). After its insertion in the ER, proSP-C is palmitoylated in Cys 5 and 6 (corresponding positions in the mature SP-C sequence). This palmitoylated precursor initiates its sequential proteolytic processing towards the final generation of the 4 KDa mature SP-C in the lamellar bodies.

SP-B is required for the proper processing of proSP-C (Vorbroker *et al.*, 1995). Although the mechanism by which SPB modulates the cleavage of SP-C is still unclear, it has been proposed that membrane fusion and lysis promoted by the mature form of SP-B would cause the orientation of the N-terminal domain of the proSP-C towards the lumen of multivesicular bodies, and its exposure to the specific proteases that release the N-terminal domain from the mature SP-C (Weaver and Conkright, 2001). Alternatively,

since a direct molecular interaction between SP-B and SP-C has been determined (Cabre *et al.,* 2018), one could speculate about a possible interaction between SP-B and SP-C precursors that might facilitate the processing cleavage of SP-C, although this is something that needs to be further clarified.

ASSEMBLY OF SURFACTANT INTO LAMELLAR BODIES

Lamellar bodies (LBs) are the specialized acidic organelles in ATII cells where surfactant is stored in a highly packed stated. After synthesis, surfactant components must be transferred to LBs. Newly synthesized SP-B and SP-C are incorporated to the lamellar bodies via multivesicular bodies, as well as lipids derived from the remodeling pathways. In contrast, the transport of newly synthesized lipids to LBs is not completely understood, although it is likely that they bypass these organelles (Olmeda, Martinez-Calle and Perez-Gil, 2017). A non-vesicular vesicular transport of PC from the ER to LBs has been proposed based on the experimental evidence that the disruption of Golgi by brefeldin A does not affect surfactant secretion (Agassandian and Mallampalli, 2013). This non-vesicular transport of PC in ATII cells seems to be mediated by the phospholipid transport protein StarD10 (Lin *et al.,* 2015).

Lipid and protein assembly into tightly-packed structures of LBs requires the action of the protein ABCA3 (ATP-binding cassette transporter A3), which belongs to the family of membrane transporters that pump lipids across membranes coupled to ATP hydrolysis. ABCA3 is localized at the limiting membrane of the LBs and is responsible for the transfer of lipids into the lumen of these organelles (Ban *et al.*, 2007; Cheong *et al.*, 2007). The energy provided by the hydrolysis of ATP during the continuous lipid transfer towards the inner of LB could be used to form highly packed lipid-protein structures, with a highly dehydrated state and the likely generation of non-lamellar phases (Cerrada *et al.*, 2015; Malacrida *et al.*, 2016). Once LBs are secreted and unpacked in contact with the alveolar interface, the accumulated energy would lead to a rapid and highly efficient interfacial adsorption. This hypothesis is supported by experimental data which demonstrated that lamellar body-like particles (LBPs or secreted LBs) obtained from ATII cell cultures showed faster interfacial adsorption kinetics than surfactant membranes purified from bronchoalveolar fluid, which are already unpacked by pre-exposure to air (Ravasio *et al.,* 2010).

Besides ABCA3, SP-B is also necessary for proper LB biogenesis, as SP-B deficiency entails the formation of immature LBs with loosely packed membranes that once secreted, fail to form functional films (Stahlman *et al.,* 2000). SP-B would allow the packing and organization of surfactant membranes in LBs, due to its ability to promote membrane-membrane interactions.

SECRETION OF LAMELLAR BODIES

The primary physiological stimulus for surfactant secretion is the mechanical stretching of alveoli during inspiration, which leads to an elevation of the cytoplasmic calcium (Nicholas, Power and Barr, 1982). Although *in vitro* studies have demonstrated that stretching of ATII cells promotes surfactant secretion (Wirtz and Dobbs, 1990; Frick *et al.*, 2004), ATI cells are the primary sensors of lung inflation that in turn modulate ATII cell secretion of surfactant. The mechanical stretching of ATI cells triggers oscillations in calcium concentration that propagate to ATII cells through gap junctions (Ashino *et al.*, 2000). Additionally, the response of ATI cells to stretching promotes ATP release to the extracellular fluid, which induces surfactant secretion in ATII cells (Patel *et al.*, 2005). Moreover, different lines of evidence have shown that exposure of ATII cells to air also prompts surfactant secretion (Ramsingh et al., 2011; Ravasio et al., 2011). During lung inflation, alveolar surface extension leads to a reduction in thickness of the hypophase covering the alveolar epithelium, and subsequently, the surface tension increases. It has been suggested that the thinning of the hypophase and the elevation in surface tension exert forces onto the apical side of ATII cells that, in turn, trigger surfactant secretion by an increase in cytoplasmic calcium concentration (Ravasio *et al.*, 2011).

Surfactant secretion, as a vital process, is highly regulated by different signaling pathways. Several physiological agents, such as β-adrenergic and purinergic agonists (ATP and UTP) stimulate surfactant secretion through activation of signaling mediators, such as protein kinase A (PKA), protein kinase C (PKC), phospholipase C (PLC) and Ca^{2+}/calmodulin-dependent protein kinase (CaMK) (Rooney 2001). On the contrary, SP-A can inhibit surfactant exocytosis (Dobbs, Wright et al. 1987, Rice, Ross et al. 1987), although the mechanism is still unclear.

Ca^{2+} is the major second messenger, responsible for triggering the fusion of LB with the ATII plasma membrane. Mechanical stretch-induced Ca^{2+} signal in ATII cells is supplied by both Ca^{2+} release from intracellular stores and Ca^{2+} entry from extracellular space through TRPV2 channel, the latter being the main contributor to increase cytoplasmic calcium concentration ($[Ca^{2+}]_c$) (Frick *et al.*, 2004; Fois *et al.*, 2012). Ca^{2+} induced-LB fusion is determined not only by the amplitude of the calcium concentration peak but also by the integrated $[Ca^{2+}]_c$ value over time (=dose) (Frick *et al.*, 2001). Upon stimulation of ATII cells, a transient elevation of $[Ca^{2+}]_c$ above the threshold of 320 nM Ca^{2+} activates several cytoskeletal elements that are involved in the trafficking and docking of the LB to the plasma membrane (Figure 1.15). The LB fusion machinery is integrated by annexins-2 and -7, some SNARE proteins (syntaxin-2 and SNAP23/25 in

the plasma membrane and VAMP-2, located in the limiting membrane of LB), as well as some regulatory proteins, as Rab14 and Rab3D.

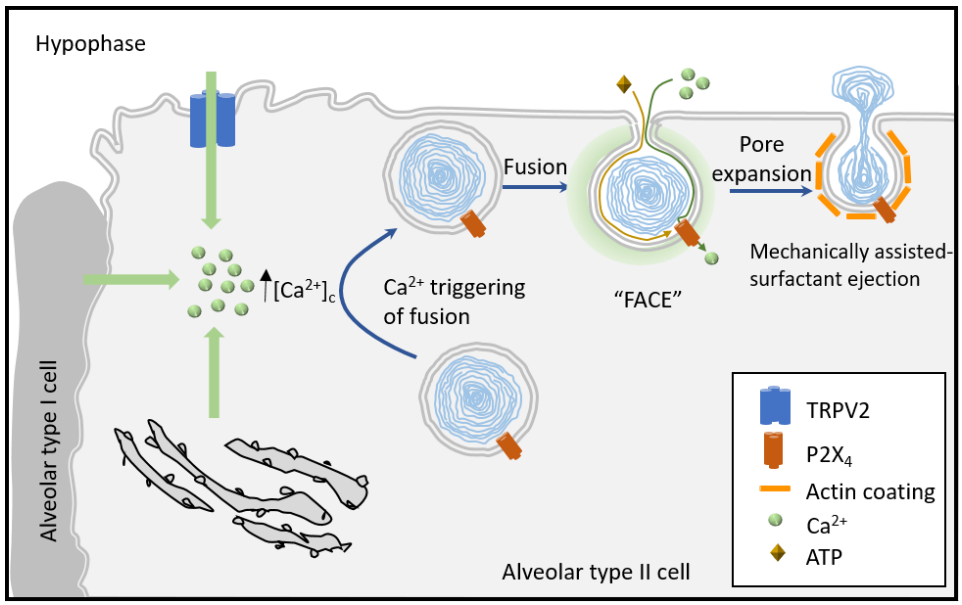

Figure 1.15. Secretion of lamellar bodies. Mechanical stretch of alveoli elicits oscillations in $[Ca^{2+}]_c$ in alveolar type II cells, originated from extracellular Ca^{2+} entry, Ca^{2+} release from intracellular Ca^{2+} stores as well as paracrine signaling from alveolar type I cells. This $[Ca^{2+}]$ signal triggers LB fusion with the plasma membrane. Upon LB fusion, extracellular Ca^{2+} gets access to $P2X_4$ channel in the outer limiting membrane of the fused lamellar body. ATP-mediated Ca^{2+} pumping prompts additional local rise in $[Ca^{2+}]$, termed "fusion activated Ca^{2+} entry" (FACE), which leads to the fusion pore dilation and facilitates surfactant release. During the post fusion stage, an actin coat together with actin-associated proteins surround the fused vesicle. Actin coat contraction results in the compression of the whole vesicle that leads to the final surfactant release.

Once LB is fused with the plasma membrane, the surfactant release to the alveolar lining fluid is delayed minutes and even hours not only because of the high hydrophobicity of the tightly packed membranes, which impedes its rapid diffusion in aqueous solution, but also because of the mere existence of the fusion pore that constitutes a mechanical barrier for surfactant release (Haller *et al.*, 2001; Singer *et al.*, 2003). The final surfactant release is a step-wise regulated process, which includes the fusion pore dilation and the compression of the fused vesicle to favor surfactant release. The expansion of the fusion pore is a Ca^{2+} dependent process. After a single LB fusion event, an elevation in cytoplasmic calcium takes place at the site of vesicle fusion (Miklavc *et al.*, 2009, 2010). This Ca^{2+} entry mechanism associated with the LB fusion process is called "fusion-activated Ca^{2+} entry" (FACE). FACE is mediated via activation of the purinergic cation channel $P2X_4$, located in the limiting membrane of LBs (Miklavc *et al.*, 2011). Upon LB fusion, this channel becomes immediately part of the apical membrane. Activation of $P2X_4$ by extracellular ATP results in a localized transient Ca^{2+} entry surrounding the fused LB, which then accelerates the fusion pore expansion and subsequent surfactant release. However, the molecular mechanisms that transduce this Ca^{2+} signal into forces that facilitate the fusion pore opening are not completely

understood. It has been proposed that Synaptotagmin-7, expressed in LBs, might be the molecular linker between FACE and fusion pore dilation (Neuland, Sharma and Frick, 2014).

Besides regulatory mechanisms for the fusion pore opening, surfactant release requires the involvement of an active extrusion machinery, constituted by actin and actin-associated proteins (Miklavc *et al.*, 2009, 2012, 2015; Kittelberger *et al.*, 2016). Upon LB fusion, actin molecules polymerize surrounding the fused vesicle. This actin coat compresses the whole vesicle, resulting in collapse of the vesicle into the plasma membrane and surfactant release.

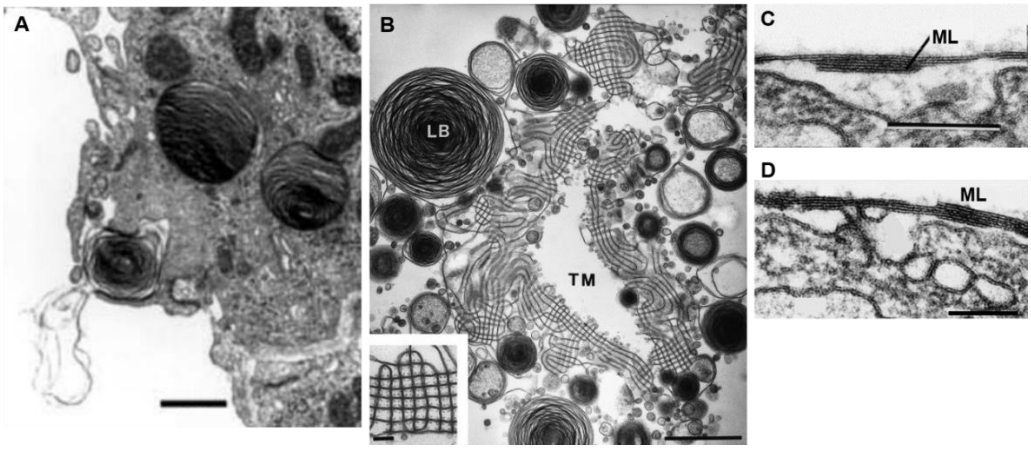

Figure 1.16. Transmission electron micrographs of extracellular and intracellular surfactant forms. A) Lamellar body exocytosis by alveolar type II cell in a rat lung (scale bar, 1 µm), taken from (Perez-Gil, 2008). B) Alveolar subphase in a section of an adult rat lung, where secreted lamellar bodies (LB) and tubular myelin (TM) are visualized (scale bar, 1 µm); taken from (Goerke, 1998). C and D) Alveolar surface film from a guinea pig lung showing multilamellar structures (ML) associated to the interfacial monolayer (scale bars, (C) 0.6 µm and (D) 0.1 µm); taken from (Schurch, Green and Bachofen, 1998).

After secretion of lamellar bodies, they mostly retain their densely packed organization, as lamellar body-like particles (Haller *et al.*, 2004). Upon contact with the air-liquid interface, these structures unravel in a cooperative and efficient way forming an interfacial film thanks to the coordinated action of SP-B and SP-C (Hobi *et al.*, 2016). Moreover, some unpacked surfactant membranes have been found rearranged in a lattice-like structure, termed tubular myelin. Tubular myelin was initially considered as an intermediate form between LBs and functional surfactant membranes attached to the interface (Sanderson and Vatter, 1977; Williams, 1977). However, the need of tubular myelin as a precursor of surface films has not been well-established and is a matter of controversy, as several *in vitro* and *in vivo* studies have reported that the presence of tubular myelin is not essential for surfactant biophysical activity (Massaro, Clerch and Massaro, 1981; Ikegami *et al.*, 1998; Sato and Kishikawa, 2001) . DPPC, PG, SP-A, SP-B and Ca^{2+} are the essential components to reconstitute *in vitro* the structure of tubular myelin (Suzuki, Fujita and Kogishi, 1989). Although the way these components interact

is scarcely understood, it has been proposed that SP-A octadecamers may interact with LB membranes by its CRD domains, generating corrugated membrane assemblies. Protein-protein interactions of SP-A established by its N-terminal segment would promote the apposition of corrugated membranes, leading to the formation of lattice-structures. Furthermore, according to this model, the presence of SP-B/SP-B interactions would be relevant in the tubular myelin structure by favoring membrane-membrane interactions (Palaniyar *et al.*, 2001; Perez-Gil, 2008). Although the specific function of the tubular myelin is still unclear, it has been proposed that it could work as an antimicrobial network, where SP-A and other molecules of the host defense would be located (McCormack and Whitsett, 2002).

Finally, besides LBPs and tubular myelin, large lipid vesicles can also be formed by the unpacking of secreted LBs. All these extracellular complex lipid-protein assemblies would constitute a surfactant pool in the hypophase to satisfy its demand at the interface.

DEGRADATION AND RECYCLING

Once surfactant reaches the interface and forms the functional film that stabilizes the respiratory surface, it is subjected to successive compression-expansion cycles that lead to compositional and structural reorganizations of surfactant components coupled to a progressive loss of "spent" material (Gunther *et al.*, 1999). Maintenance of a functional surfactant film continuously requires its refinement through clearance of its components and the replacement with newly-secreted surfactant. The "spent" surfactant is released from the interfacial film in the form of small aggregates and driven towards alveolar type II cells and alveolar macrophages for clearance.

Surfactant lipids can be recycled by ATII cells through a process mediated by SP-A. SP-A binds to small aggregates and upon its interaction with a specific receptor in ATII cell, probably P63 (Bates, 2010), both SP-A and lipids are internalized by a clathrin-dependent pathway. Lipids are transferred to lamellar bodies from early endosomes in a calmodulin-dependent mechanism (Wissel *et al.*, 2001). Alternatively, lipids can also be uptaken by alveolar type II cells in an actin-dependent process, although this pathway contributes in a lesser extent to surfactant recycling (Bates *et al.*, 2008).

A fraction of proteins and lipids might be altered as a consequence of their exposure to an oxidizing environment or at the presence of external harmful agents in the respiratory airways. Thus, degradation of these not-fully active components is essential for a proper turnover of the surfactant pool and it mainly occurs in alveolar macrophages, although ATII cells can also participate in surfactant lipid catabolism (Olmeda, Martinez-

Calle and Perez-Gil, 2017). Lipid degradation in both cells mainly occurs through the action of PLA2.

SP-C and SP-D modulate the uptake of phospholipids and thus, accomplish essential roles in maintaining the homeostasis of surfactant. SP-D appears to participate in the conversion of large aggregates of surfactant into small aggregates, probably through binding to PI, although the mechanism remains unclear (Ikegami *et al.*, 2009). In the case of SP-C, this protein induces membrane fragmentation that leads to the formation of small lipoprotein vesicles enriched in cholesterol (Roldan *et al.*, 2016). Recently, it has been described that SP-C and cholesterol increase lipid uptake by alveolar macrophages. After the engulfment process, lipids are accumulated intracellularly in the form of lipid droplets, while SP-C is located at defined regions in the plasma membrane (Roldán López *et al.*, 2017).

1.5. METHODS FOR MEMBRANE PROTEIN PURIFICATION

DETERGENTS

Over the past decades, the use of detergents has made a clear impact on the progress of membrane protein research. Detergents serve as tools to solubilize, isolate and manipulate membrane proteins for subsequent structural and functional characterization. They are surface-active molecules that self-associate in aqueous solutions forming globular structures, termed as micelles, where polar head groups form an envelope in contact with water while hydrophobic tails are sequestered from water in the inner of the micelle. Thus, detergent micelles provide an amphipathic environment that can somehow mimic lipid bilayers and solubilize membrane proteins by interaction with hydrophobic regions of the protein, preventing their exposure to water and maintaining protein stability (Garavito and Ferguson-Miller, 2001).

The general properties of detergents that are pertinent as membrane protein tools are the critical micelle concentration (cmc) and the aggregation number. At low concentrations, detergent molecules exist as monomers in aqueous solution. As detergent concentration increases above the cmc, detergent monomers start to self-associate into micelles. The cmc of a given detergent varies with temperature, pH, ionic strength, as well as the presence of proteins, lipids and other detergents (Seddon, Curnow and Booth, 2004). The aggregation number is the number of monomers contained in a micelle, so that the size of the micelle can be described by the aggregation number (Garavito and Ferguson-Miller, 2001).

Detergents can be classified according to the type of polar head group (Garavito and Ferguson-Miller, 2001; Seddon, Curnow and Booth, 2004):

- Ionic detergents contain a hydrophilic head group with a net charge that can be either cationic or anionic. The cmc of an ionic detergent is determined by the combined effect of the repulsive interactions between headgroups and the hydrophobic interactions of the tails. Ionic detergents, such as sodium dodecyl sulfate (SDS), are very effective in membrane solubilization, but they usually cause protein denaturation.
- Nonionic detergents contain an uncharged head group, such as *n*-dodecyl-β-maltoside (DDM). They are milder than ionic detergents, as they break lipid-lipid and protein-lipid associations, rather than protein-protein interactions. Thus, nonionic detergents solubilize membrane proteins maintaining their structure.
- Zwitterionic detergents have charged hydrophilic head group with a zero net charge. They combine properties of the other two types of detergents. They are harsher than nonionic detergents. CHAPS (3-[(3-Cholamidopropyl) dimethylammonio]-1-propanesulfonate) is a known member of this group, which has a high cmc that decreases with increasing of ionic strength (Chattopadhyay and Harikumar, 1996).

The optimal choice of the detergent is key to ensure the solubilization of the membrane protein of interest into a functional, active form comparable to that in their native membranes. Besides, this choice has to take into account the type of techniques that will be used for the study of the solubilized membrane protein. Therefore, the process of solubilization of a membrane protein requires a detailed previous analysis to determine the best detergent and its optimal concentration.

Membrane protein solubilization by detergents strongly depends on detergent/lipid/protein ratios. The solubilization process of membrane proteins goes through several stages as the detergent to lipid ratio increases (Silvius, 1992; le Maire, Champeil and Møller, 2000). At low detergent concentration, detergent monomers insert into the bilayers with minimal membrane perturbation. As the concentration of detergent increases, the membrane bilayer is disrupted, giving rise to the start of membrane solubilization. At this stage, lipid/protein/detergent mixed micelles coexist with intact membranes. Further detergent addition leads to the formation of mixed lipid/detergent micelles and membrane proteins surrounded by micellar detergent. A steady increase of solubilized lipid and protein fractions occurs by addition of detergent until their complete solubilization. However, such a high detergent concentration is not recommended as this could lead to the inactivation or aggregation of the protein (Silvius, 1992). Besides, the presence of remaining lipids in protein solubilized complexes would be an evidence of the importance of this lipid-protein interaction in the structure and function of the membrane protein (Catoire, Warnet and Warschawski, 2014).

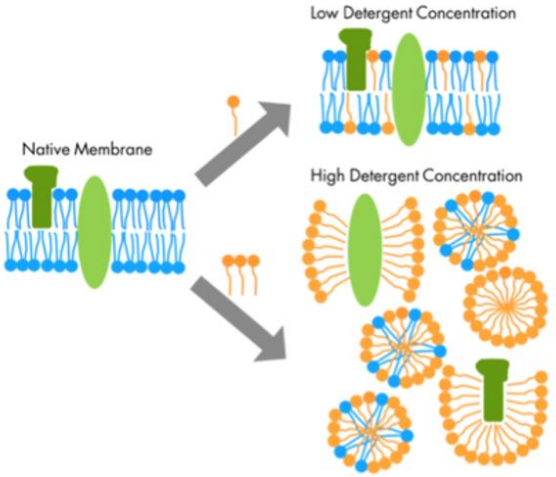

Figure 1.17. Solubilization of membrane proteins using detergents. Taken from Jena Bioscience GmbH's website.

Once the membrane protein is solubilized and eventually purified, it can be reconstituted into alternative lipid membranes for further study in a desired lipid environment. Two common approaches can be used to form proteoliposomes with a protein purified in detergent. The first one is based on diluting the detergent/protein mixture into the liposome suspension. When the detergent is below its cmc, micelles becomes unstable, disaggregating in monomeric detergents, and the protein transfers into the liposomes. In a second approach, the concentration of detergent used is enough to destabilize the membranes of the vesicles, favoring the incorporation of the protein into the liposomes, after which an additional step to remove the excess of detergent becomes essential. Depletion of detergent from a vesicle suspension can be performed by several methods, including size-exclusion chromatography, dialysis and adsorption to hydrophobic beads (Seddon, Curnow and Booth, 2004).

The dissociating properties of detergents have been used to extract membrane proteins from their native membranes. In a solution of membrane protein solubilized in detergent, detergent molecules are in equilibrium with molecules bound to the protein, micelles and monomers. To prevent its desorption from the hydrophobic regions of the protein, the detergent concentration must be close to its cmc. However, under these conditions, detergents tend to destabilize the membrane protein by two main mechanisms: 1) detergent micelles can solubilize hydrophobic cofactors, lipids or subunits, that contributes to the stability of the membrane protein; and 2) detergents can disrupt intramolecular protein-protein interactions, altering the 3D structure of the protein (Breyton, Pucci and Popot, 2010). This problem has been overcome with the development of new alternatives to conventional detergents, such as amphipols, nanodiscs and SMA-lipid nanoparticles.

AMPHIPOLS

Amphipols are amphipathic polymers, composed by numerous hydrophobic groups and many highly polar moieties, which are usually charged. The unique feature of amphipols is their ability to self-assemble into well-defined particles of several KDa. For instance, four molecules of amphipol A8-35 form a 9-10 KDa particle (Popot, 2010; Popot *et al.*, 2011). A8-35, which is by far the most extensively used amphipol, shows a low charge density which seems to favor the stability of membrane proteins. A8-35 has been shown to form a soluble complex with a very wide range of membrane proteins, from < 5KDa to > 1.1 MDa (Popot, 2010).

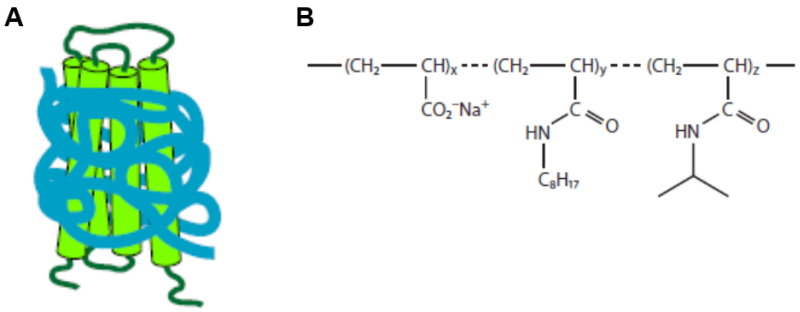

Figure 1.18. Membrane protein stabilized by Amphipols. A) Representative cartoon, amphipols are shown in blue. Modified from (Liang and Tamm, 2018) B) Chemical structure of amphipol A8-35. Modified from (Popot, 2010).

Amphipols show a high affinity for the surface of the protein, so that the equilibrium dissociation constant is small, which means that little amounts of surfactant would be sufficient to surround the hydrophobic regions of the membrane protein. In contrast to detergents, the free surfactant phase vanishes in solution of amphipols-stabilized membrane proteins (Breyton, Pucci and Popot, 2010; Popot, 2010). Besides its stabilizing properties, amphipols are compatible with a wide range of biochemical and biophysical techniques, like size exclusion chromatography, analytical ultracentrifugation, electron microscopy, small-angle X-ray scattering and solution nuclear magnetic resonance.

Generally, amphipols are unable to directly extract membrane proteins from native membranes, because they are poorly dissociating surfactants (Breyton, Pucci and Popot, 2010; Popot *et al.*, 2011). Therefore, a previous solubilization of the target protein by detergents is required before transferring it to the polymer. The incubation of the detergent-solubilized protein with amphipols gives rise to the formation of the ternary complex membrane protein/detergent/amphipol. These complexes can also incorporate lipids that had been solubilized by detergents or lipids added afterwards to enhance the stability and/or activity of the protein. Finally, the detergent is removed usually by adsorption to polystyrene beads or by detergent dilution below its cmc. In the latter case, the detergent remains in the solution as monomers and its concentration surrounding the protein surface declines. The concentration ratio amphipol to membrane protein must be

optimized in each case, because it varies depending on the molecular mass of the protein and the extent of its hydrophobic surface.

NANODISCS

Nanodiscs are soluble self-assembled phospholipid bilayers that constitute a useful tool to reconstitute membrane proteins in a desired lipid environment. They consist of a circular fragment of phospholipid bilayer encapsulated by two molecules of a membrane scaffolding protein (MSP) derived from Apolipoprotein A1. The interactions between phospholipids and MSP molecules are established by the amphipathic α-helices of the protein that shield the acyl chains of the phospholipid bilayer from the aqueous environment (Denisov *et al.*, 2004). Nanodiscs have been extensively used over the last decade, mostly due to the development of new constructs of MSP proteins, including truncated and extended variants of MSP that generate nanodiscs that range in size from ~ 7 to ~17 nm of diameter (Denisov and Sligar, 2017), as the length of the MSP determines the size of nanodisc. Thus, nanodiscs show a defined and stable size which depends on the MSP construct used to yield them. The advantage of nanodiscs over other self-assembled systems, such as micelles, bicelles or liposomes, is that they are more stable and with a better defined structure because of the strong interaction between the scaffold proteins and lipids.

In this Thesis, the membrane scaffolding protein used was MSP1D1 (its sequence is shown in figure 1.19), which yields nanodiscs of about 10 nm of diameter. MSP1D1 shows a polihistidine tag at its N-terminal end, followed by a linker containing a Tobacco Etch Virus (TEV) protease site, to enable tag removal, and the main MSP sequence (Ritchie *et al.*, 2009). The histidine tag allows purification of the generated nanodiscs by immobilized metal affinity chromatography.

The general protocol for the formation of nanodiscs begins with the solubilization of lipids by cholate, followed by the addition of purified MSP (Ritchie *et al.*, 2009). The molar ratio phospholipid to MSP is key to yield nanodiscs efficiently. The number of phospholipid molecules that can be incorporated into the nanodisc depends on the length of the MSP belt. An optimal ratio phospholipid/MSP ensures that there is a complete self-assembly of nanodiscs with a homogeneous size. If the ratio is shifted, the excess of scaffold protein or phospholipid would lead to the formation of aggregates that could be removed by a size-exclusion chromatography or ultracentrifugation. Nanodiscs self-assemble by progressive removal of detergent by adsorption to polystyrene beads or by dialysis.

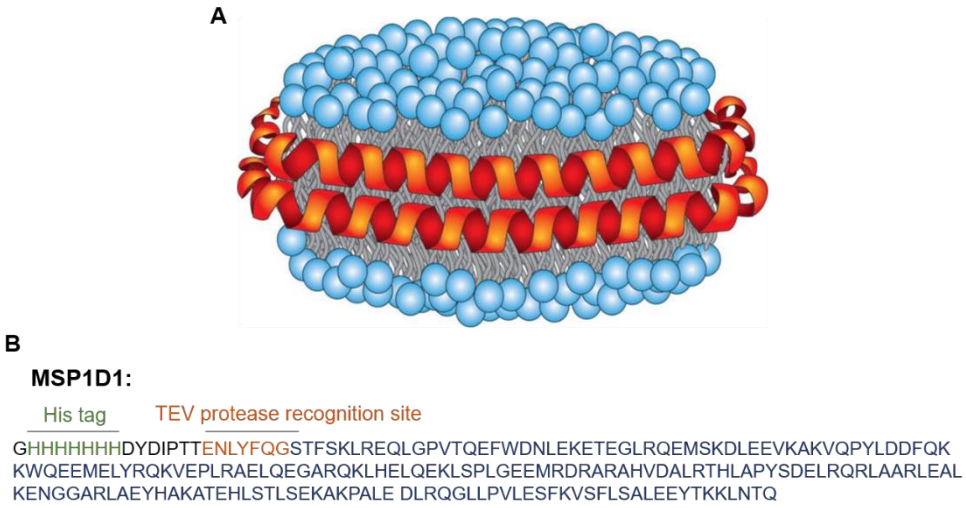

Figure 1.19. Nanodiscs are discoidal lipid bilayers assembled by two molecules of amphipathic helical membrane scaffolding protein (MSP). A) Representative illustration of a nanodisc. Taken from (Denisov and Sligar, 2017). B) Sequence of the scaffolding protein MSP1D1 consisting of histidine tag (green), recognition site for TEV protease (orange) with cleavage in G/S, and the sequence of the MSP (blue).

For the incorporation of a given membrane protein into nanodiscs the protein must be previously solubilized in detergent. This detergent-solubilized protein is mixed together with cholate-solubilized phospholipids and MSP, and finally, detergent is removed by one of the methods previously mentioned. To obtain nanodiscs with the membrane protein, temperature, time of incubation and the molar ratio of scaffold protein, lipids and membrane protein should be optimized. Additionally, the presence of cofactors or substrates that enhance the stability and/or activity of the membrane protein should be considered (Ritchie *et al.*, 2009; Denisov and Sligar, 2017).

Nanodiscs have been successfully assembled with various synthetic lipids and with mixtures of native lipids. Moreover, nanodiscs can be assembled directly from native tissue or cell membranes solubilized by detergent (Marty *et al.*, 2013; Roy *et al.*, 2015; Wilcox *et al.*, 2015). The removal of detergent by common methods ensures the self-assembly of nanodiscs. This experimental approach allows the generation of membrane protein nanodisc libraries, which reflect the protein and lipid interactome of the original membrane.

The potential of the nanodisc technology as a powerful and versatile tool for the study of the structure and function of membrane proteins has been demonstrated by numerous investigations that combined the use of nanodiscs with a wide range of biochemical and biophysical techniques, as X-ray crystallography, electron microscopy, small-angle X-ray scattering (SAXS) and liquid chromatography combined with tandem quadrupole mass spectrometry (LC/MS/MS) (reviewed in (Denisov and Sligar, 2017)).

SMA/lipid nanoparticles

Recently, styrene/maleic acid (SMA) copolymers have been developed to directly extract membrane proteins from natural or artificial membranes without the use of detergents (Knowles *et al.*, 2009; Orwick *et al.*, 2012; Long *et al.*, 2013; Postis *et al.*, 2015). SMA copolymers recruit membrane proteins and associated lipids into SMA/lipid particles (SMALPs) (Dörr *et al.*, 2016). These lipid particles are discoidal nanoscale lipid bilayer systems, similar to MSP nanodiscs, in which acyl chains of the boundary phospholipids are shielded by SMA copolymer, instead of membrane scaffolding proteins.

SMA is produced by the copolymerization of styrene and maleic anhydride. The distribution of the two types of monomers in the resulting polymer depends on their ratio, from a nearly regular distribution with a ratio 1:1 to less regular polymers for ratios 1:2 to 1:4, commonly used in biochemical applications.

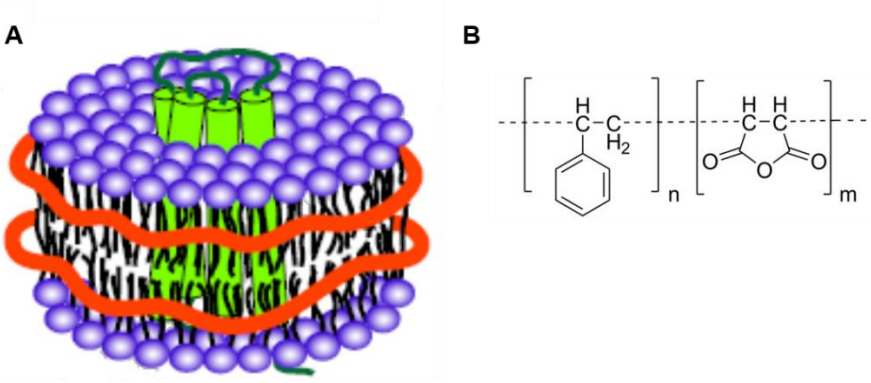

Figure 1.20. Protein stabilization in membrane-mimetic system using SMA polymers. A) Representative illustration of SMA lipid nanoparticles, SMA polymers are shown as orange belts. Modified from (Liang and Tamm, 2018). B) Structure of SMA copolymer, repeating units of styrene (n) and maleic anhydride alternate within the resulting copolymer.

The size range of the particles depends on the styrene/maleic anhydride ratio, as well as the protein and lipids used (Zhang *et al.*, 2015, 2017; Craig *et al.*, 2016; Dörr *et al.*, 2016). Thus, SMALPs emerge as a membrane mimetic tool with different nanoscale sizes, which can be used for the study of a wide range of membrane proteins, even mitochondrial complexes of around 200 KDa (Long *et al.*, 2013). Unlike the length of a particular MSP construct, the polymer length is not exactly fixed, so that the range of particle sizes obtained can be more variable. Thus, to obtain a more homogeneous sample size, the experimental conditions need to be optimized, mainly lipid to protein and lipid to SMA ratios, and combined with a size-exclusion chromatography.

SMALPs have been successfully used for functional and structural studies on membrane proteins in a near-native environment, providing a wide number of biochemical and biophysical applications (reviewed in (Dörr *et al.*, 2016)).

OBJECTIVES

2. OBJECTIVES

Pulmonary surfactant protein SP-B is essential for life. Although its folding and three-dimensional tertiary structure is not yet well-known, the native structure of SP-B seems to be assembled in the form of a ring-shaped oligomer, formed by 5 or 6 covalent SP-B dimers. SP-B, together with SP-C, exerts a wide variety of effects on surfactant lipid bilayers and monolayers that lead to profound rearrangements closely related to the surface active function of pulmonary surfactant at the alveolar interface.

The main objective of the present Thesis is to contribute to the understanding of the structure and function of the native protein complexes present in pulmonary surfactant, with a particular focus on those constituted by SP-B. In this way, five specific objectives have been addressed in the present work:

1. To perform a compositional and structural analysis of protein complexes derived from detergent-solubilized surfactant or surfactant nanodiscs. Besides, protein crosslinking is applied to attempt the clarification of the interactions between proteins SP-B and SP-C in quasi-native environments.

2. To study the effect of surfactant protein complexes on the permeability and interfacial dynamics of pulmonary surfactant membranes, in order to propose a potential mechanism for the dual action of SP-B on both surfactant activities.

3. To address a deeper structural characterization of native SP-B oligomers, mainly in lipid environments, attempting the generation of samples with a proper quality, in order to approach further high-resolution structural characterization of the complexes.

4. To study the structural features of SP-B applying fluorescence spectroscopy methodologies, including the determination of the stoichiometry of native SP-B oligomers in membranes and a quantitative study of the topological changes induced by SP-B in multilamellar structures.

5. To study the effect of SP-B on surfactant secretion by alveolar type II cells. Elucidation of the signaling mechanisms connecting SP-B with lamellar body exocytosis in ATII cells.

MATERIALS AND METHODS

3. MATERIALS AND METHODS

3.1. MATERIALS

Pulmonary surfactant from bronchoalveolar lavages

Pulmonary surfactant was isolated from bronchoalveolar lavage fluid (BALF) of porcine adult lungs, as previously described (Taeusch *et al.*, 2005). Porcine lungs were obtained from industrial slaughterhouse (Matadero Madrid-Norte S.A., San Agustín de Guadalix, Madrid). Lavages were performed with 2.5 L of cold 5 mM Tris pH 7.4, 150 mM NaCl solution per respiratory apparatus. The obtained BALF was filtered through a gauze and centrifuged at 1000 g for 5 minutes at 4 °C to eliminate cells and debris. BALF was stored at -20 °C. Purification of pulmonary surfactant fraction from BALF required a first centrifugation at 100000 g for 1 hour at 4 °C to pellet surfactant membranes and a subsequent density gradient centrifugation that allowed the separation of pulmonary surfactant complexes from other cell membranes. For this last centrifugation, pellets were resuspended in a 16% NaBr, 0.9 % NaCl (w/v) solution and disposed in the appropriate centrifuges tubes. The discontinuous gradient was formed by addition of 13% NaBr, 0.9% NaCl solution, followed by 0.9% NaCl solution. Tubes were centrifuged in a swinging angle rotor at 120000 g for 2 hours at 4 °C. Surfactant membranes were concentrated at a fringe between the 0.9% NaCl solution and the 13% NaBr, 0.9% NaCl solution. After removing the upper solution carefully, surfactant fractions were recovered and homogenized in 0.9% NaCl solution. Pulmonary surfactant was aliquoted, frozen in liquid N_2 and stored at -80 °C.

Organic extract from pulmonary surfactant

Pulmonary surfactant hydrophobic components were obtained by organic extraction (Bligh and Dyer, 1959). One volume of pulmonary surfactant was mixed with two volumes of methanol and one volume of chloroform, followed by thoroughly vortexing of the mixture for 30 seconds. The single-phase solution was then incubated for 30 minutes at 37 °C under continuous shaking to flocculate the water soluble-proteins in the mixture. Next, one volume of distilled water and one additional volume of chloroform were added and the mixture was thoroughly vortexed. After that, it was centrifuged at 600 g for 5 minutes at 4 °C to obtain a biphasic solution. After careful collection of the organic solvent phase, two volumes of chloroform were added to the aqueous phase, followed by centrifugation and organic phase harvesting. This repetitive process improves the yield of the extraction of lipids and hydrophobic proteins. The material recovered at the several organic phases, defined as organic extract from pulmonary surfactant (OE), was preserved at -20 °C.

Obtaining of lipid and hydrophobic protein fractions of pulmonary surfactant

To separate the lipid fraction and the hydrophobic protein fraction of organic extract of PS, a size exclusion chromatography was performed. OE was concentrated using a rotatory evaporator and applied into a gel filtration-packed column (Sephadex LH-20, GE Healthcare) equilibrated with chloroform/methanol 2:1 (v/v). Absorbances at 240 nm and 280 nm were measured in the collected fractions to identify the lipid fraction (LF) and the hydrophobic protein fraction (PF). All fractions were stored at -20 °C.

Purification of SP-B and SP-C from minced lungs

To improve their yielding, surfactant proteins SP-B and SP-C were also isolated from porcine minced lungs (Perez-Gil, Cruz and Casals, 1993). Each respiratory apparatus was minced and lavaged with 1 L of cold 5 mM Tris pH 7.4, 150 mM NaCl. Minced lungs were filtered with a gauze and centrifuged (1000 g, 4 °C, 5 minutes) to remove cells and debris. A second centrifugation (3000 g, 4 °C, 2 hours) allowed the yield of membranes in the pellet. Pellets were harvested and stored at -20 °C. To continue the purification process, pellets of minced lungs were thawed and an organic extraction was performed to obtain SP-B and SP-C together with lipids. The obtained organic solvent solution was subjected to two sequential size exclusion chromatographies. For the first one, a Sephadex LH-20 resin packed-column (GE Healthcare) was used equilibrated with chloroform/methanol (2:1, v/v) as mobile phase. Absorbances at 240 nm and 280 nm were measured to resolve the protein fraction (SP-B and SP-C) from lipids. Protein fraction was carefully concentrated by rotatory evaporation and loaded onto a Sephadex LH-60 column (GE Healthcare), with chloroform/methanol (1:1, v/v), 0.5% 0.1N HCl as eluent. SP-B eluted in the void volume of the chromatrogram, showing absorbance at 240 nm and 280 nm. Meanwhile, SP-C eluted in a second peak, which absorbs only at 240 nm due to the lack of aromatic amino acids. Fractions of SP-B and SP-C were harvested and preserved at -20 °C. Purity was determined by western blot and protein was quantified by amino acid analysis.

Fluorescent labelling of SP-B with BODIPY FL

SP-B was derivatized with BODIPY FL NHS-ester (Thermo Fisher Scientific) as described in (Cabre *et al.*, 2018). The apparent pH of the organic solution containing SP-B was adjusted to 6.6 by adding an appropriate volume of 50 mM Tris in methanol, which allowed the deprotonation of the N-terminal amino group of SP-B. BODIPY FL dissolved in methanol (10 mg/ml) was added to the protein solution in a molar probe/protein proportion of 3:1. Conjugation reaction took place overnight at 4 °C. After that, the

protein/probe solution was reacidified up to an apparent pH of 2 to stop the reaction and the non-conjugated probe was removed by a Sephadex LH-20 chromatography (GE Healthcare) in chloroform/methanol (1:1, v/v), 0.5% 0.1 N HCl. BODIPY FL/SP-B fractions were detected by measuring absorbances at 280 nm and 504 nm. The degree of SP-B labelling was estimated from amino acid analysis and spectroscopic determination of the probe. The molar extinction coefficient used for BODIPY FL in chloroform/methanol (1:1, v/v) was $\varepsilon_{504nm} = 82\times10^3\ M^{-1}cm^{-1}$ (Haugland, 2002). The molar ratio probe/protein determined for BODIPY FL/SP-B was 0.91.

Lipid and protein/lipid sample preparation

Throughout this Thesis, different liposomes or proteoliposomes were extensively used: porcine pulmonary surfactant membranes (PS), multilamellar vesicles (MLVs), which are formed by numerous concentric membranes and are highly polidisperse in size, small unilamellar vesicles (SUVs) with diameters between 20-50 nm, large unilamellar vesicles (LUVs) with diameters around 100 nm and giant unilamellar vesicles (GUVs) in the range of microns. These vesicles contained a variety of components; native pulmonary surfactant and its derivatives (organic extract, lipid fraction, hydrophobic protein fraction and isolated SP-B and SP-C), as well as the following synthetic lipids (purchased from Avanti lipids): 1,2-dipalmitoyl-*sn*-glycero-3-phosphocholine (DPPC), 1,2-dipalmitoyl-*sn*-glycero-3-phospho-(1'-*rac*-glycerol) (DPPG), 1-palmitoyl-2-oleoyl-*sn*-glycero-3-phosphocholine (POPC), and 1-palmitoyl-2-oleoyl-*sn*-glycero-3-phospho-(1'-*rac*-glycerol) (POPG).

Multilamellar vesicles

Multilamellar vesicles were prepared by the evaporation-rehydration method. Proper volumes of the appropriate lipid and protein stock solutions in organic solvent were mixed inside glass tubes. Mixtures were dried under N_2 stream. To remove solvent traces, tubes were kept under a vacuum centrifuge for 2 hours, obtaining dried films at the bottom of the tubes. Membranes were reconstituted by hydration of dried films in 5 mM Tris pH 7.4, 150 mM NaCl. Rehydration process took place for 1 hour with intermittent shaking at 1400 rpm. The incubation temperature, which is key for proper membrane reconstitution, was in all cases higher than the phase transition temperatures of the corresponding phospholipid mixtures. Thus, dried films containing DPPC (T_m= 41 °C), which is the main component of pulmonary surfactant, were rehydrated at 45 °C. Liposomes or proteoliposomes containing only unsaturated lipid species, like POPC and/or POPG (T_m= -2 °C) were reconstituted at 37 °C.

Small unilamellar vesicles

Sonication of MLV suspensions produces small unilamellar vesicles (SUVs) in the range of 15-50 nm. Probe tip sonicator delivers high energy input to the lipid suspension, disrupting membranes. When these membranes reseal, they form vesicles with a high curvature, which makes them very unstable.

Small unilamellar vesicles were formed using a sonicator Hierlcher UP200 equipped with a titanium probe and the following parameter settings: 0.5 s/cycle and 65% of amplitude. MLVs were sonicated for 2 cycles of 2 minutes. SUVs suspensions were used immediately, taking care of keeping them always in ice.

Large unilamellar vesicles

Unilamellar vesicles can also be obtained by extrusion of MLVs suspensions through a polycarbonate filter with defined pore size. As the concentric layers of MLVs deform to be able to pass through the pores, rupture and resealing of membranes occurs. After repeatedly extruding the MLVs suspension, a population of unilamellar vesicles is formed with a mean diameter that reflects the filter pore size. The advantage of the extrusion method in comparison to sonication is that the resulting liposome suspensions show higher homogeneity and stability.

In the present work, MLVs suspensions were extruded using a Mini-Extruder (Avanti Polar Lipids) with 10 mm diameter filter discs and polycarbonate membranes Nucleopore Track-Etch with 100 nm diameter pore (both from Whatman). The extrusion process was performed at 45 °C. MLV suspensions were forced to pass 15 times through the filters, until the turbidity was decreased. At the end, LUV suspensions were obtained with a mean diameter of 100 nm. These suspensions were immediately used or kept at 4 °C to be used in the same day.

Giant unilamellar vesicles

Giant unilamellar vesicles (GUVs) are a well-established membrane model to study physicochemical properties of biological membranes and the activity of associated membrane proteins. Due to their size in the micrometric range, these vesicles can be visualized or manipulated by optical microscopy. A number of methods have been developed in order to get giant unilamellar vesicles with diameters between 1-100 μm (Walde et al. 2010).

In the present work, giant vesicles of diverse complexity in composition were obtained by membrane hydration in the presence of an electric field, the so-called electroformation method (Angelova and Dimitrov 1986). This technique is based on the application of an electric field on a dried lipid film deposited on a conductive glass slide or platinum wires.

In this work, dried films were formed on indium-tin oxide (ITO) coated glass slides, with 70-100 Ω/sq surface resistivity (Sigma Aldrich). GUVs were prepared from two different sources, lipids and proteins dissolved in organic solvent or pulmonary surfactant membranes in aqueous buffer.

For GUVs originated from organic solvent samples, 50 µl of lipid or lipoprotein stocks containing 1 mg/ml of phospholipid (typically labelled with 0.5% molar Rhodamine-DOPE) were spread over two ITO glasses. After drying the films in a vacuum chamber for 2 hours to completely remove organic solvent, the electroformation chamber was assembled: the two film-covered glasses were disposed with the conducting sides face to face and separated by a 2 mm thick Teflon spacer, pre-coated with vacuum grease. The chamber was filled with a sucrose solution (200 mOsm), sealed at both sides with vinyl paste (Critoseal, Leica Biosystems) and connected to a function generator. Electroformation was performed at 45 °C, protected from light, in three different phases: phase I, sine wave with a frequency 8 Hz, peak-to-peak amplitude ramped up from 250 to 1500 mV for 30 minutes; phase II, sine wave at constant 8 Hz frequency and an amplitude of 1500 mV during 2 hours; and phase III, sine wave with ramped down from 6 to 0 Hz and a constant amplitude of 1500 mV for 30 minutes. After electroformation, the suspensions were carefully collected from the chamber and stored at 4 °C.

Some modifications of this protocol were included for GUVs formed from native pulmonary surfactant membranes. Native surfactant at 10 mg/ml of phospholipid was incubated with Rhodamine-DOPE, added in an aliquot of DMSO (4.43 µl at 1 mg/ml), at a final concentration of 0.5% molar for one hour at 37 °C. Labeled native surfactant suspension was diluted at 1mg/ml of phospholipid and drops of the preparation (50 µl) were spread over two ITO glasses, where the film was then gradually dried under a nitrogen stream, and finally surfactant covered glasses were kept in a vacuum chamber for 30 minutes.

Primary ATII cell cultures

ATII cells were isolated from Sprague-Dawley rats according to the procedure of (Dobbs, Gonzalez and Williams, 1986) with minor modifications (Haller *et al.*, 1998). Briefly, lungs were cleared of blood by perfusion and removed from the thorax. After lavage, the lungs were instilled with 0.05 % trypsin and 0.5 % elastase (w/v) solution, incubated at 37 °C, and minced with scissors in the presence of DNase. After stopping the enzymatic digestion by addition of fetal bovine serum (FBS), the cell suspension was sequentially filtered through cotton gauze and three nylon meshes (100-, 20-, and 10-µm mesh size) and centrifuged at 160 g for 8 minutes at room temperature. The cell pellet was resuspended in DMEM and panned on an IgG-coated plastic dish to remove

macrophages. The unattached cells were again centrifuged and then suspended in Mucilair (Epithelix) supplemented with 1% (v/v) gentamicin 10 mg/ml (Thermo Fisher Scientific). Yield and purity of ATII cell isolations were routinely monitored using a combined cell counting and lysotracker staining assay. The average purity of all the ATII isolations used in this Thesis was 85-95%. After isolation, cells were seeded on 8-well chambers (Ibidi) or 96-well plate (Sarstedt) and cultured in 95% humidified air and 5% CO_2 at 37 °C. Experiments were performed 48 hours after isolation.

Isolated plasma membrane from ATII cell cultures

Isolation of plasma membrane of ATII cell cultures was performed based on methods described by (Duck-Chong, 1978; Gupta *et al.*, 2006). Pellets from $16 \cdot 10^6$ ATII cells were thawed and then incubated for 30 minutes at 4 °C with lysis buffer containing 20 mM Tris pH 7.4, 150 mM NaCl, 2 mM EDTA, 1% triton X-100 (v/v) and a protease inhibitor cocktail (Sigma Aldrich). Following, cell suspensions were sonicated (4 cycles of 15 seconds, 10% amplitude) and centrifuged (16000 g, 4 °C, 20 minutes) to pellet membranes. After that, pellets were resuspended in 5 mM Tris pH 7.4, 0.32 M sucrose. Isolation of ATII plasma membrane was performed through a sucrose density-gradient ultracentrifugation in a swinging angle rotor (100000 g, 4 °C, 1 hour). The discontinuous gradient was formed with 5 mM Tris pH 7.4 solutions containing 1.2, 0.9, 0.7 and 0.5 M sucrose. At the top of the centrifuge tube, ATII membranes solubilized in 5 mM Tris, 0.32 M sucrose were added. Upon ultracentrifugation, plasma membranes were located at the bottom of the tube, forming a pellet. Finally, plasma membrane pellet was resuspended in 5 mM Tris pH 7.4, 150 mM NaCl, 0.1% Triton X-100 (v/v). Isolated ATII plasma membrane suspension was stored at 4 °C until the following day for co-immunoprecipitation assay (detailed in section 3.2 Analytical techniques).

3.2. ANALYTICAL TECNIQUES

Phospholipid quantification

Phospholipid concentration was determined by phosphorus quantification (Rouser, Siakotos and Fleischer, 1966). Samples were dried in glass tubes, and then lipid hydrolysis and phosphorus mineralization was performed by incubation with 0.65 ml of 70% perchloric acid in a sand bath at 260 °C for 30 minutes. Tubes were capped with glass globes to prevent from acid solution evaporation. Next, 3.5 ml of milliQ water, 0.5 ml of 2.5% ammonium molybdate (w/v) and 0.5 ml 10% ascorbic acid (w/v) were added and thoroughly vortexed after each solution addition. The colorimetric reaction was triggered by incubation at 100 °C for 7 minutes, where ascorbic acid reduced phospho-

molybdic complexes, resulting in a blueish sample solution. A calibration curve with known amounts of phosphate were assessed together with samples of interest. Absorbance at 820 nm was measured in samples and calibration standards.

Thin layer chromatography

Lipid composition of pulmonary surfactant reconstituted into MSP nanodiscs was analyzed by thin layer chromatography (TLC). 60 µl of nanodisc preparations were dried under N_2 stream and solubilized in 10 µl of chloroform/methanol 2:1 (v/v). These samples and a set of lipid standards (10 µg) were applied at the bottom of a 20 x 20 cm silica plate (TLC Silica Gel 60, Millipore). Once applied samples were dried, TLC was performed by incubating the silica plate with the mobile phase solution chloroform/methanol/water (65:25:4, v/v/v) at room temperature. Finally, plate was air-dried and stained with iodide vapors for analysis.

Amino acid analysis

The highly hydrophobic character of proteins SP-B and SP-C, the use of organic solvents for their isolation and the lack of aromatic amino acids in SP-C prevented the use of conventional techniques to determine protein concentration, such as spectrophotometry or Bradford assay. Thus, 200-300 µl of purified protein in organic solvent (about 10-20 µg) was dried under N_2 stream and subjected to an acidic hydrolysis under vacuum for 24 hours at 100 ºC. The acid solution contained 6 N HCl, 0.1% phenol (w/v) and a known *nor*-leucine concentration to be used as an internal standard. After hydrolysis, HCl was evaporated under N_2 stream followed by two washing/evaporation steps with milliQ water to ensure the complete removal of HCl. Finally, samples were resuspended in 0.2 N sodium citrate and subjected to ion exchange chromatography and post-column nynhidrin derivatization using a high performance amino acid analyzer (Biochrom 30, Biochrom). From the obtained chormatograms, the amounts of each amino acid species and the known sequence of each protein were used to determine the concentration of each protein.

ATP quantification by luciferase assay

ATP release in non- or SP-B-stimulated ATII cell cultures was quantified by the luciferase assay as follows. 10^6 rat primary ATII cells were seeded into wells of a 96-well plate and maintained in MucilAir medium. 48 hours after seeding, the medium was exchanged with fresh medium containing 100 µM ARL 67156. The cells were then

stimulated with POPC:POPG vesicles containing 12% SP-B (by weight) and supernatants were collected for ATP quantification. ATP release was quantified using ATP Determination kit (Thermo Fisher Scientific). In parallel, extracellular ATP was determined in non-treated ATII cells, following the same procedure.

Electrophoretic analysis of proteins

SDS-PAGE

Hydrophobic surfactant proteins obtained from minced lungs, protein complexes obtained from solubilization of pulmonary surfactant by detergent or from reconstitution into nanodiscs, as well as samples from the SP-B co-immunoprecipitation of plasma membrane proteins from rat ATII cells, were analyzed by electrophoresis in polyacrylamide gels.

Water-soluble samples were prepared in loading buffer containing 10% glycerol, 2% SDS and 0.03% bromophenol blue in the presence or absence of 5% ß-mercaptoethanol, as reducing agent. In the case of samples in organic solvent, they were first evaporated under a nitrogen stream before adding the loading buffer. All samples were boiled for 10 minutes and afterwards, loaded into gels of different polyacrylamide percentages, together with prestained protein standards (Precision Plus Protein Dual Color Standards, Bio-Rad, or HiMark Pre-stained Protein Standard, Thermo Fisher Scientific). Electrophoresis were performed at 110 V.

After SDS-PAGE, gels were stained by silver nitrate or Coomassie Brilliant Blue R-250 or were transferred to the appropriate membranes for protein immunodetection.

BN-PAGE

Blue Native (BN)-PAGE allows to determine native molecular masses and oligomerization states of proteins, as well as identifying protein-protein interactions. This electrophoretic technique makes use of the anionic probe Coomassie Blue G-250 (Sigma) to produce a charge shift of proteins to negative charge, allowing their migration primarily depending on their mass.

Samples were diluted into loading buffer containing 5% Coomassie Blue G-250 and 1 M aminocaproic acid, enhancing the latter the solubilization of membrane proteins. A high molecular weight calibration kit for native electrophoresis (GE Healthcare) was used as protein standards. For BN-PAGE, gradient gels of 4-20% polyacrylamide (Bio-Rad) and two different electrophoresis buffers were used: dark cathode buffer (15 mM BisTris, 15 mM tricine pH 7, 0.02% Blue G-250), light cathode buffer (which differs from the first buffer in the percentage of probe, 0.002% Blue G-250) and anode buffer (50 mM

BisTris pH 7). Electrophoresis were performed at 4 °C in two steps: first, at 100 V in dark cathode buffer until the dye had run one third of the gel, and secondly, dark cathode buffer was replaced by light cathode buffer and the voltage was increased to 220 V.

Finally, gels were stained by silver nitrate staining or transferred to membranes for immunoblotting. In the latter case, membranes were unstained previously to the blocking step by incubation with 8% acetic acid for 15 minutes, followed by a membrane drying step and washing in methanol.

Two-dimensional electrophoresis

Native protein complexes of pulmonary surfactant were studied by BN-PAGE followed by SDS-PAGE. Gel strips from the BN-PAGE were cut and incubated for 2 hours with equilibration buffer containing 50 mM Tris pH 8.8, 30% glycerol (v/v), 2% SDS (v/v), 0.002% bromophenol blue (w/v) and 30 mM DTT. After a quick rinse with running buffer, the gel strip was placed on the top of a separating gel. A one-well plastic comb was also placed over the gel to load the protein standards. A sealing solution containing 0.5% agarose (w/v) and 0.002% bromophenol blue (w/v) was added. After gelation of the agarose, and loading of protein standards, SDS-PAGE was performed at 110 V.

Silver nitrate staining

After electrophoresis, gels were fixed for 30 minutes in a solution containing 40% ethanol and 10% acetic acid and incubated then for 30 minutes in sensitizing solution (30% ethanol, 0.5% glutaraldehyde, 0.8 M sodium acetate and 12.6 mM sodium thiosulphate). Afterwards, gels were washed three times with milliQ water for 5 minutes, and incubated in silver solution (0.6 mM silver nitrate, 0.04% formaldehyde) for 20 minutes. After a quick rinse with milliQ water, bands were developed with a solution containing 0.2 M sodium carbonate and 0.02% formaldehyde. The reaction was stopped with 50 mM EDTA pH 8.

Coomassie staining

Gels were incubated in a solution containing 1 mg/ml Coomassie Brilliant Blue R-250, 50% methanol and 10% acetic acid for 30 minutes. Destaining with 10% acetic acid, 45% methanol solution revealed blue stained bands.

Western blot

Proteins in gel were transferred to a PVDF (polyvinylidene fluoride) membrane (Bio-Rad) using a wet transfer system at 300 mA for 1 hour at room temperature. For gradient polyacrylamide gels, transfer settings were 400 mA for 90 minutes at 4 °C. Membrane was then blocked in PBS containing 0.05% Tween-20 and 5% milk for 2 hours. The

primary antibody, diluted in blocking solution, was added for overnight incubation at 4 °C. After consecutive washing with PBS-Tween, membrane was incubated with the HRP-labeled secondary antibody in blocking solution for 1 hour at room temperature, followed by extensive washing with PBS-Tween to eliminate unbound antibody. Finally, membrane was developed in Millipore Immobilon Western Chemiluminiscent HRP Substrate. Images were recorded in Image Quant LAS500 (GE Healthcare).

The primary antibody dilutions used were rabbit polyclonal anti human SP-A antibody 1:10000 (kindly supplied by Dr. J. Floros, from Penn State University, USA), rabbit polyclonal anti human SP-B antibody 1:5000 and rabbit polyclonal anti human SP-C antibody 1:1500, both from Seven Hills Bioreagents, and, lastly, mouse monoclonal α-His_6 Peroxidase IgG_1 (Sigma). As HRP-conjugated secondary antibody, polyclonal swain α-rabbit Ig 1:2000 (Dako) was used.

Protein crosslinking

In order to study protein-protein interactions between SP-B and SP-C, a number of crosslinking reactions were performed by using dithiobis(succinimidyl propionate) (DSP), BS^3 (bis(sulfosuccinimidyl)suberate) and (PEGylated bis(sulfosuccinimidyl) suberate) $BS(PEG)_9$ (purchased from Thermo Fisher Scientific). These are homobifunctional crosslinking reagents with NHS-ester groups at both ends, which specifically crosslink primary amines, although they differ in their structure, providing them with different water-solubility, membrane permeation abilities and range of crosslinking chain length.

First, the hydrophobic protein fraction of surfactant (PF), a mixture of isolated SP-B and SP-C, or SP-B alone were reconstituted into vesicles made of the lipid fraction (LF) of pulmonary surfactant or synthetic lipid mixtures DPPC:POPC:POPG (5:2.5:1.5, w:w:w) or POPC:POPG (7:3, w:w). Proteoliposome suspensions were prepared at a phospholipid concentration of 100 μg/ml in 15 mM MOPS pH 7.4, 50 mM NaCl or 20 mM HEPES pH7, 150 mM NaCl. Protein:lipid ratio used in each case is indicated in the text in Chapter 1. Multilamellar preparations were sonicated to form small unilamellar vesicles or extruded using polycarbonate filter membranes with pore size of 100 nm to form large unilamellar vesicles.

Next, 12-25 μl of vesicles (1-2.5 μg of total protein) were crosslinked with the appropriate reagent at the desired crosslinker:protein molar ratios. Stocks of crosslinking reagents were prepared as follows: 10 mM DSP in DMSO, 25 mM BS^3 and 2.5 mM $BS(PEG)_9$ in milliQ water. The reaction was performed for 30 minutes at 37 °C (30 seconds vortexing every 5 minutes) or eventually for 2 hours at 4 °C (30 seconds

vortexing every 15 minutes). The crosslinker was quenched by addition of 5 mM Tris pH 7. Samples were concentrated with StrataClean Resin (Agilent Technologies), diluted in loading buffer and loaded into a 4-20% polyacrylamide gel (Bio Rad), to be analyzed by SDS-PAGE and subsequent immunoblotting for SP-B and SP-C detection

In addition to the crosslinking experiments between SP-B dimers or SP-B and SP-C reconstituted into vesicles, SP-B complexes purified in detergent from pulmonary surfactant (15 µg protein) were subjected to crosslinking by $BS(PEG)_9$ following the same protocol detailed above.

Co-immunoprecipitation assay

To identify a putative receptor of SP-B in the plasma membrane (PM) of ATII cells, a co-immunoprecipitation assay was performed. Prior to the immunoprecipitation, rabbit polyclonal α-SP-B antibody (from Seven Hills Bioreagents) was crosslinked to Protein A beaded agarose resin (Santa Cruz Biotechnology) by the crosslinker agent dithiobis succinimidyl propionate (DSP) (from Thermo Fisher Scientific). For this, 100 µl of beads were diluted in 100 µl of blocking solution (PBS, pH7 containing 1 mg/ml BSA). After 15 minutes of incubation at 4 °C, beads were pelleted by centrifugation at 1000 g for 5 minutes, and then incubated with α-SP-B antibody in blocking solution (1 µl of antibody diluted 1/10 in solution) for 1 hour at 4 °C with gentle agitation. Beads were then washed with blocking solution and crosslinked to the antibody with DSP through three consecutive incubations with 2.5 mM DSP, followed by washing in PBS. For crosslinker quenching, conjugated beads were incubated for 30 minutes with 1 M Tris and washed with PBS. Next, free antibody was removed by incubating twice with a solution containing 0.2 M glycine pH 2.8 for 30 minutes, followed by three washing steps with PBS.

Before immunoprecipitation, ATII plasma membrane fraction (234 nmol) was incubated with POPC:POPG (7:3) SUVs containing SP-B (46 nmol SP-B) for 3 hours at room temperature with gentle agitation. Next, sample was solubilized in CHAPS 1% (1 hour with thoroughly agitation) and was then preclarified by incubation with 20 µl of naïve Protein A-agarose beads for 2 hours.

For immunoprecipitation, solubilized and precleared suspension containing SP-B and ATII PM fraction was added to α-SP-B-conjugated Protein A-agarose beads and the mixture was then incubated overnight at 4 °C with gentle shaking. After washing 6 times in PBS, bead-bound proteins were eluted in three consecutive steps: 0.2 M glycine, 2% SDS and SDS-PAGE loading buffer containing 5% ß-mercaptoethanol (boiling the mixture at 99 °C). Eluted fractions were analyzed by SDS-PAGE.

Mass spectrometry

Interaction between SP-B and a putative receptor in plasma membrane of ATII cells was studied by co-immunoprecipitation coupled to mass spectrometry analysis. After, co-immunoprecipitation and SDS-PAGE, the gel was stained by silver nitrate with a modified mass spectrometry-compatible protocol lacking fixing agents. Stained bands of interest were cut and digested by trypsin. Next, samples were subjected to MALDI-TOF/TOF analysis in order to allow protein identification by peptide mass fingerprint and fragmentation. The proteomic analysis was performed in the Proteomics Unit of Complutense University of Madrid.

Furthermore, silver stained bands from the electrophoretic analysis of pulmonary surfactant solubilized by CHAPS were also subjected to mass spectrometry, following the same procedure described above.

Analytical ultracentrifugation

In velocity sedimentation analysis, macromolecules are subjected to a high centrifugal field where centrifugal force is higher than diffusion, promoting a net transport of sample towards the outside of the rotor. This hydrodynamic method splits macromolecular species with different sedimentation coefficient, which depends on the macromolecular mass, density and shape.

SP-B complexes purified by CHAPS, as well as SP-B complexes stabilized with amphipols, were subjected to velocity sedimentation (48000 rpm, at 20 °C, for 4 hour) in a Proteome Lab XL-I ultracentrifuge (Beckman Coulter). These experiments were performed at the Analytical Ultracentrifugation and Light Scattering facilities in Centro de Investigaciones Biológicas (CSIC, Madrid).

3.3. PURIFICATION AND STABILIZATION METHODS OF MEMBRANE PROTEIN COMPLEXES FROM PULMONARY SURFACTANT MEMBRANES

Purification of native SP-B complexes from CHAPS-solubilized pulmonary surfactant

SP-B complexes from PS were purified upon detergent solubilization as previously described (Olmeda *et al.*, 2015). Surfactant was solubilized by CHAPS

(detergent:phospholipid molar ratio of 6:1, purchased from Sigma Aldrich) for 1 hour at 25 °C under vigorous shaking, and loaded onto a 5 ml prepacked ion exchange chromatography Hitrap SP HP column (GE Healthcare). 50 mM phosphate pH 7, 9.8 mM CHAPS and 3 different concentrations of NaCl (0.15, 0.5, and 1 M) were subsequently eluted. Fractions of 1 mL were collected and the absorbance was measured at 280 nm. SP-B was collected at fractions eluted with 1 M NaCl. Sample purity was assessed by western blot and protein was quantified by bicinchoninic acid assay (Thermo Fisher Scientific) or by Lowry assay.

Stabilization of SP-B complexes by GraFix method

GraFix (Gradient Fixation) is a technique that allows stabilization of macromolecular complexes, improving the sample quality for negative-staining EM and cryo-EM (Kastner *et al.*, 2008). During GraFix, macromolecules undergo a weak, intramolecular chemical crosslinking while being purified by density gradient ultracentrifugation. The GraFix procedure combines a glycerol-density gradient ultracentrifugation purification with a mild and progressive increasing exposure of macromolecules to glutaraldehyde, the crosslinking reagent.

SP-B complexes purified from CHAPS-solubilized PS were subjected to GraFix method as an approach to stabilize the macromolecular oligomers. A continuous gradient of 50 mM PBS pH 7, 150 mM NaCl, ranging from 30 % sucrose (w/v) and 45% glutaraldehyde (v/v) to 5% sucrose and 15% glutaraldehyde, was formed by a gradient former. 100 µl of SP-B complexes purified with CHAPS were applied at the top of the density gradient. Glutaraldehyde stock used was a commercial solution specially purified for electron microscopy applications, purchased from Sigma Aldrich. To analyze the impact of crosslinking agent on the macromolecular association of SP-B, a continuous sucrose gradient ultracentrifugation in the absence of glutaraldehyde was performed by following the same procedure. After centrifugation in a swinging angle rotor at 50000 g, 4 °C, for 14 hours, a pasteur pipette connected to a peristaltic pump was introduced at the bottom of the centrifuge tube to collect sample fractions of 180 µl. After harvesting all the solution from the centrifuge tube, non-visible pellet was resuspended in 50 mM PBS pH 7, 150 mM NaCl. Purification profile was obtained by absorbance measurements at 280 nm. Electrophoretic mobility of SP-B in the different fractions was analyzed by SDS-PAGE followed by western blot. For SDS-PAGE, fractions were concentrated by StrataClean resin (Agilent Technologies) and diluted in loading buffer.

Stabilization of SP-B complexes by amphipols

Amphipol A8-35 (Anatrace) was used to stabilize SP-B complexes purified from CHAPS-solubilized pulmonary surfactant. The solution of SP-B complexes contained 50 mM phosphate pH 7, 10 mM CHAPS, 1 M NaCl. A8-35 powder was dissolved in distilled water to obtain a 5 mg/ml stock. In order to optimize the experimental procedure, several protein:A8-35 mass ratios were tested, from 0.25% to 8% (by weight). After incubation for 30 minutes in ice, the detergent was removed from the mixtures by incubation with nonpolar polystyrene adsorbent, Bio-Beads SM-2 Resin (Bio-Rad). Efficiency of the different A8-35 concentrations to "trap" SP-B complexes was analyzed by BN-PAGE in 4-20% polyacrylamide gradient gels. Next, a size exclusion chromatography was performed with the solution containing A8-35 and SP-B at a ratio 1:1 (w/w), after sample concentration using Vivaspin 500 with a molecular weight cut off of 10000 Da (GE Healthcare). Suspension of SP-B/A8-35 was loaded onto a Superdex 200 10/300GL (GE Healthcare) equilibrated in 50 mM phosphate pH 7, 1M NaCl at room temperature at a flow rate of 0.5 ml/minute, monitoring absorbance at 280 nm and collecting fractions of 0.250 ml. The oligomerization state of selected fractions were analyzed by BN-PAGE and sedimentation velocity analytical ultracentrifugation.

Purification of pulmonary surfactant proteins into MSP1D1 nanodiscs

Expression and purification of MSP1D1

The plasmid with the construct His_6tag-MSP1D1 was generously provided by Dr. Germán Rivas (Centro de Investigaciones Biológicas, CSIC, Madrid). This plasmid was cloned into *E. coli* BL21 (DE3) and His_6tag-MSP1D1 expression was induced in LB medium containing kanamicin 1:1000 and 1 mM IPTG.

Bacterial cultures were centrifuged and pellets were collected and stored at -80 °C. The pellets were then lysed by 20 mM phosphate buffer pH 7, containing 1% Triton x-100 (v/v) and PMSF. The suspension was vortexed gently for 30 minutes at 4 °C and then sonicated to facilitate the rupture of bacterial membranes. To obtain the soluble fraction, the bacterial lysate was ultracentrifuged at 30000 g during 30 minutes. Protein purification was performed by an immobilized metal affinity chromatography (5 ml prepacked column HisTrap HP, purchased from GE). The chromatography consisted of several elution steps which involve the use of 40 mM Tris pH 8, containing 300 mM NaCl and the following specific components at each step: 1. 1% Triton x-100 (v/v); 2. 50 mM cholate; 3. 50 mM imidazole; 4. 300 mM imidazole. Total protein content of collected fractions was determined by measuring absorbance at 280 nm. Yield and purity of the purification process was evaluated by SDS-PAGE and subsequent Coomassie staining. HisTag-MSP1D1 eluted with the buffer containing 500 mM imidazole and, subsequently, was dialyzed in 20 mM Tris pH 7.4, 100 mM NaCl, 1 mM EDTA. Protein concentration

was determined spectrophotometrically by using ε_{280} = 21,000 M^{-1} cm^{-1}. Protein aliquots were stored at -80 °C.

SP-B reconstitution into MSP nanodiscs

First, SP-B purified in organic solvent was reconstituted into 8 mM POPC vesicles in 20 mM Tris pH 7.4, 150 mM NaCl. Next, proteoliposome suspensions were solubilized with 4 mM CHAPS during 90 minutes at 25 ºC under vigorous shaking. Then, MSP1D1 was added to the suspensions and the mixture was incubated for 1 hour at 4 °C with gentle shaking. In order to set up the experimental conditions that yielded SP-B nanodiscs, various suspensions with different ratios of POPC, SP-B and MSP1D1 were assessed, as detailed in the table below:

POPC:MSP1D1(mol/mol)	MSP1D1:SP-B (mol/mol)	POPC:SP-B (mol/mol)
40:1	4:1	160:1
50:1	4:1	200:1
60:1	4:1	246:1

Following, the detergent was removed from the mixtures by incubation with Bio-Beads SM-2 Resin, allowing the formation of nanodiscs. Suspensions were centrifuged at 100000 g for 20 min at 4 °C and pellets were collected. After centrifugation, samples were injected onto a Superdex 200 10/300GL equilibrated in reconstitution buffer at room temperature at a flow rate of 0.5 ml/minute, with absorbance monitoring at 280 nm and collection of 0.250 ml fractions. Fractions were analyzed by SDS-PAGE on 16% polyacrylamide gels and Coomassie staining.

Formation of native pulmonary surfactant nanodiscs

Two different concentrations of pulmonary surfactant, 56 and 224 mM of phospholipid, were used to form the nanodiscs. Surfactant suspensions were solubilized by CHAPS or cholate (6:1 or 3.5:1, molar ratio detergent:phospholipid, respectively) for 90 minutes at 37 °C under vigorous shaking. MSP1D1 was then added (molar ratio MSP1D1: phospholipid, 1:100, unless otherwise stated) and the mixtures were incubated for 1 hour at 37 °C with gentle agitation. Next, Bio-Beads SM-2 resin were added to the suspensions to remove detergent. Samples were centrifuged at 100000 g for 20 minutes at 4 °C, discarding supernatants. Nickel affinity chromatography was used to separate nanodiscs assembled by MSP1D1 from free surfactant membranes. Suspensions were loaded onto a HisTrap HP prepacked column (GE Healthcare). For nanodiscs purification, the column was equilibrated using 20 mM Tris pH 7.4, 150 mM NaCl and MSP1D1 nanodiscs were eluted by 500 mM imidazol-supplemented buffer. Fractions of 1 ml were collected and absorbance was measured at 280 nm. Subsequently, nanodiscs were subjected to a size exclusion chromatography using a Superdex 200 10/300GL

column equilibrated in 20 mM Tris pH 7.4, 150 mM NaCl at room temperature at a flow rate of 0.5 ml/minute, with absorbance monitoring at 280 nm and collection of 0.5 ml fraction. Fractions collected from both affinity and size exclusion chromatography were assayed using SDS-PAGE on 16% polyacrylamide gels and immunoblotting detection for MSP1D1, SP-A, SP-B or SP-C.

SP-B reconstitution into SMA lipid nanoparticles

A mixture of POPC:POPG (7:3, by weight) and SP-B in organic solvent (10%, protein:lipid weight ratio) was reconstituted into MLVs in 5 mM pH 7.4, 150 mM NaCl at 37 °C for 1 hour. Styrene:maleic anhydride (SMA) copolymer powder at a ratio 3:1 (purchased from Sigma Aldrich) was dissolved at 10% (w/v) in liposome reconstitution buffer, followed by 1 minute of water-bath sonication to complete solubilization. Lipid nanoparticles were formed with a mass ratio of lipid to polymer of 1:1.5 (w:w) and a final SMA concentration of 5% (w/v) by adding SMA polymers dropwise to the POPC:POPG + SP-B vesicles. Samples were then mixed thoroughly by vortexing and equilibrated through two freeze/sonication cycles. At the same time, SMA lipoparticles containing POPC:POPG (7:3, w/w) were formed following the same protocol. A size exclusion chromatography was performed by injecting nanoparticle samples onto Superdex 200 10/300 GL column equilibrated in liposome reconstitution buffer at room temperature at a flow rate of 0.5 ml/minute with monitoring absorbance at 280 nm. Collected fractions of 0.150 ml were analyzed by BN-PAGE and visualized by transmission electron microscopy and atomic force microscopy.

3.4. FLUORESCENCE SPECTROSCOPY

Luminiscence is the emission of light from any substance and occurs from electronically excited states to ground states. Luminiscence is formally divided into two categories: fluorescence and phosphorescence, which differ from each other in the nature of the excited state. Fluorescence occurs when the electron in the excited orbital has opposite spin than the second electron in the ground state level. In this scenario, the return to the ground state by emission of a photon is spin allowed and, thus, it occurs rapidly. The emission rates of fluorescence are about 10^8 s^{-1}, so that fluorescence lifetimes are typically near 10 ns. The lifetime of a fluorophore (λ) is the average time a fluorophore population spends in the excited state before decaying to the ground state. Several processes occur between adsorption and emission of a photon, as Jablonski diagram illustrates (**Figure 3.4.1**). A fluorophore is usually excited to a higher vibrational level of the excited electronic states (S_1 or S_2), and then the molecule rapidly relaxes to the lowest

level of the excited state S_1 in a radiationless process called internal conversion. It usually occurs within 10^{-12} s, so that it is prior to the photon emission.

In the case of phosphorescence, energy undergoes an intersystem crossing from S_1 excited state to a triplet excited state, where the photon emission comes from. In T_1 state, the excited electron shows the same spin orientation as the ground state electron. Thus, transition to the ground state is a spin forbidden process and the emission rates are slow, 10^3- 10^0 s^{-1}. Phosphorescence lifetimes are typically milliseconds to seconds.

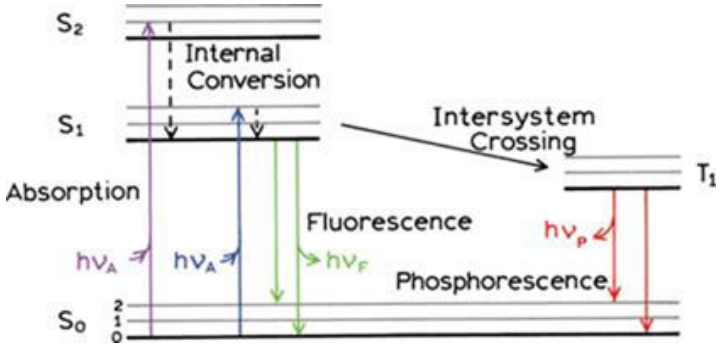

Figure 3.4.1. Jablonski diagram. Illustration from (Lakowicz, 2006).

Steady-state and time-resolved fluorescence spectroscopy

Fluorescence spectroscopy measurements can be performed by two methodologies: steady-state and time-resolved. In steady-state fluorescence the sample is illuminated with a continuous beam of light, and the intensity is recorded. Once the sample is exposed to light, the steady state is reached almost immediately after the sample is exposed to light due to the nanosecond timescale of fluorescence. For the time-resolved fluorescence measurements, the sample is exposed to a pulse of light, whose width is typically shorter than the decay time of the sample. The intensity decay is recorded with a high-speed detection system that allows intensity and anisotropy decay measurements in the range of nanoseconds. On the contrary, the steady-state measurements are the result of the integrstion over time of the time-resolved phenomena over the intensity of the sample. Thus, much of the molecular information is lost during the averaging process and can be only obtained by time-resolved measurements. For instance, the shape of the anisotropy decay contains information about the shape of the macromolecule and its flexibility. Moreover, different conformational states of macromolecules can be detected by different intensity decay times. In the presence of resonance energy transfer, the intensity decays reveal the spatial distribution of acceptors around the donors.

Fluorescence anisotropy

Anisotropy measurements are based on the principle of photoselective excitation of fluorophores by polarized light. All fluorophores show transition moments that occur

along a specific direction in the molecular axis. A fluorophore preferentially absorbs photons whose electric vectors are aligned parallel to the transition moment of the fluorophore. Thus, upon excitation with a polarized light, only those fluorophore molecules whose absorption transition dipole is parallel to the electric vector of excitation reach an excitation state (photoselection). The selectively excited fluorophores emit photons along a fixed axis of the molecule (polarized emission). The anisotropy is determined by the angle between absorption and emission transition moments of the fluorophore.

The measurement of fluorescence anisotropy is illustrated in **figure 3.4.2**, where the excitation light is oriented parallel to the z axis and the emission intensity is measured through a polarizer. When the emission polarizer is oriented parallel to the direction of the polarized excitation light, the emission intensity measured is called $I_{\parallel}$. While, $I_{\perp}$ is the observable emission intensity when the polarizer is perpendicular to the direction of the polarized light. These intensity measurements are used to calculate the anisotropy by the following expression:

$$r = \frac{I_{\parallel} - I_{\perp}}{I_{\parallel} + 2I_{\perp}}$$

The difference between $I_{\parallel}$ and $I_{\perp}$ is normalized by the total measured intensity $I_{\parallel} + 2I_{\perp}$. Thus anisotropy is a dimensionless intensity ratiometric measurement. In the absence of artifacts, anisotropy is independent of the fluorophore concentration.

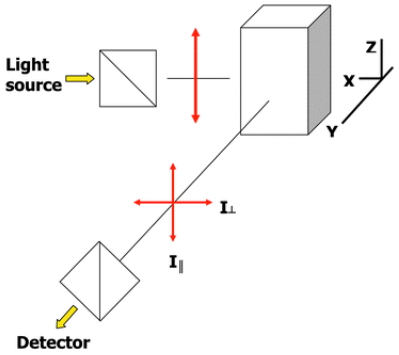

Figure 3.4.2. Schematic diagram for measurement of fluorescence anisotropies. Illustration from (Mann and Krull, 2003).

The maximum r value of a fluorophore, termed as fundamental anisotropy (r_0) corresponds to the emission anisotropy observed in the absence of other depolarizing processes taking place during the excited state lifetime. The r_0 values provide a measurement of the angle between the excitation and emission transition moments of a fluorophore in a dilute highly viscous solution, where rotational diffusion or resonance energy transfer (RET) do not occur. A number of factors can alter the experimental anisotropy, yielding lower values than r_0. Rotational diffusion of fluorophores is a dominant cause of fluorescence depolarization. If a fluorophore can freely rotate between

excitation and emission, the anisotropy detected for that molecule will change. With time, the preferential orientation of excited fluorophores resulting from the action of photoselection with polarized light will be counteracted by random molecular rotations. Fluorophore excitation and its descent to the lowest vibrational energy level of the S_1 excited state occurs on a picosecond time scale. However, molecular rotation of the fluorophore typically is a much slower process, ranging from 10 picoseconds to milliseconds (Korczynski and Włodarczyk, 2009). Thus, the longer a fluorophore remains in the excited state (longer fluorescence lifetime), the higher the probability is that the molecule rotates before emitting a photon. Thus, if molecular rotation occurs, the anisotropy will decay from an initial value (r_0) to lower values. Depolarization by rotational diffusion of a spherical fluorophore is given by the Perrin equation (Perrin, 1926):

$$\frac{r_0}{r} = 1 + \tau/\phi$$

where τ is the fluorescence lifetime and ϕ is the rotational correlation time for the diffusion process. ϕ is related to the rotational diffusion coefficient (D), which is a function of the temperature, the viscosity and the molar volume of the fluorophore.

The steady-state anisotropy of a fluorophore or a macromolecule bound to a fluorophore is given by:

$$r = \frac{r_0}{1 + (\tau/\phi)}$$

Steady-state anisotropy analysis has been extensively applied to the study of protein-protein and protein-lipid interactions induced by proteins in membranes. These anisotropy measurements provide information about the structure and dynamics of the protein (size and shape), and the membrane (fluidity).

Moreover, the rotational motions of a fluorophore can be analyzed from time-resolved anisotropy decay. For a spherical molecule, the anisotropy follows a single-exponential decay:

$$r(t) = r_0\, e^{-t/\phi}$$

According to the formalism, large molecules have longer correlation times and the anisotropy decay will be slower. Only spherical molecules display a single exponential anisotropy decay. A fluorophore bound to a protein in an anisotropic environment would display more complex decays of anisotropy:

$$r(t) = \sum_{i=1}^{n} \beta_i\, e^{\left(-\frac{t}{\phi_i}\right)} + r_\infty$$

where β_i and ϕ_i are the normalized amplitude and the rotational correlation time of the ith decay component of anisotropy, respectively. The residual anisotropy, r_∞, is a constant term that describes r value at time $t \to \infty$, when the rotational motion of the fluorophore is restricted, thus $r_\infty > 0$ (typical case of proteins inserted in membranes). Time-resolved parameters contains precise information about the shape, size, segmental flexibility of the macromolecule, as well as the rigidity of the environment (for instance, a lipid membrane) (Lakowicz, 2006).

Resonance energy transfer

Förster resonance energy transfer (FRET) is a photophysical phenomenon, which occurs between a donor fluorophore in the excited state and an acceptor molecule in the ground state. Energy transfer requires that the emission spectra of the donor overlaps with the absorption spectra of the acceptor. Upon excitation of the donor, the energy is transferred to the acceptor through long-range dipole-dipole interactions between both molecules. Due to the FRET process, the donor fluorophore results quenched and the acceptor turns out excited, followed by a relaxation process to the ground state. In case of the acceptor molecule is a fluorophore, $S_1 \rightarrow S_0$ transition may take place by photon emission.

The rate of energy transfer depends upon the extent of spectral overlap of the emission spectrum of the donor with the absorption spectrum of the acceptor, the quantum yield of the donor, the relative orientation of the donor and acceptor transition dipoles, and the distance between both molecules. The rate of energy transfer from a donor to and acceptor, $k_T(r)$, is:

$$k_T(r) = \frac{1}{\tau_D}\left(\frac{R_0}{r}\right)^6$$

where τ_D is the lifetime of the donor in the absence of acceptor, r is the donor-acceptor distance and R_0 is the Förster distance.

The Förster distance, R_0,is the distance at which the efficiency of FRET is 50%, which typically ranges from 20 to 60 Å. These distances are comparable in size to biological macromolecules. Thus, FRET can be used as a “spectroscopic ruler” to measure, for instance, the distance between a protein and its ligand, between sites of multi-subunits in proteins or to estimate the size of nanodomains in lipid bilayers (Lakowicz, 2006).

The transfer efficiency can be obtained from the decrease of donor fluorescence lifetime in the presence or absence of acceptor:

$$E = 1 - \frac{\tau_{DA}}{\tau_D}$$

For unlinked donors and acceptors, the situation becomes more complex due to the wide range of donor-acceptor distances. In this case, it is important to consider that the acceptor concentration determines the proximity between donor and acceptor, and one donor might be surrounded for more than one acceptor molecule.

There are two general types of FRET reactions, hetero-FRET and homo-FRET, which differ in the spectral overlap. The hetero-FRET occurs in the presence of a donor fluorophore and an acceptor with different absorption and emission spectra. In contrast, when the FRET reaction involves two fluorophores with identical spectra, the transfer is called homo-FRET.

Oligomer stoichiometry of SP-B by fluorescence anisotropy-based homo-FRET measurements

Steady-state and time-resolved fluorescence anisotropy-based homo-FRET experiments were performed to determine the degree of oligomerization of SP-B complexes in membranes.

Sample preparation

For these homo-FRET experiments, a stock of SP-B was fluorescently labeled with BODIPY FL at its amino terminal region, showing a high yield of labeling, with molar ratio probe/protein of 0.91 (the procedure is detailed in 3.1. Materials). Following, vesicles of different proteolipid composition were prepared with mixtures of BODIPY/SP-B and SP-B at different proportions to vary the fractional labeling of the sample. POPC:POPG (7:3, molar ratio) LUVs containing different proportions of BODIPY/SP-B and non-fluorescent SP-B (0.67% total protein/lipid molar ratio) were generated at a final lipid concentration of 0.3 mM. Additionally, mixtures of BODIPY/SP-B and SP-B were reconstituted into LUVs made of surfactant lipids and supplemented with SP-C, at a final lipid concentration of 0.357 mM of phospholipid with SP-B and SP-C concentrations of 0.67% and 0.088% (protein/lipid molar ratios), respectively.

Proteoliposomes were prepared as follows: mixtures of BODIPY/SP-B and SP-B at different molar ratios were dried under a nitrogen stream together with lipids and the dried films were later rehydrated in 5 mM Tris pH 7, 150 mM NaCl at 45 °C. After 5 freeze-thaw cycles, vesicle suspensions were extruded to form LUVs with a diameter of ~100 nm.

Steady-state measurements

For steady-state fluorescence anisotropy measurements, samples were excited at 335 nm or 470 nm, and the polarized emission was detected at 515 nm. For excitation at 335 nm, the bandwidth used was 8 nm, while bandwidths of 4 nm were applied for excitation at 470 nm and emission at 515 nm. Steady-state anisotropy, $\langle r \rangle$, was determined according to (Lakowicz, 2006):

$$\langle r \rangle = \frac{I_{VV} - G \cdot I_{VH}}{I_{VV} + 2G \cdot I_{VH}}$$

Eq. 3.4.1

where the different intensities are the vertical and horizontal components of the fluorescence emission with excitation vertical (I_{VV} and I_{VH}, respectively) and horizontal (I_{HV} and I_{HH}, respectively) to the emission axis. The latter pair of components was used to calculate G factor ($G = I_{HV}/I_{HH}$). The G factor is an instrumental correction factor which takes into account the transmission efficiency of the monochromators to the polarization of the incoming light. Data are shown as average ± standard deviation of 2 independent experiments.

Time-resolved measurements

The fluorescence intensity decay curves, $I(t)$, were described by a sum of discrete exponential terms (Lakowicz, 2006):

$$I(t) = \sum_{i=1}^{n} \alpha_i \; e^{(-t/\tau_i)}$$

Eq. 3.4.2

where α_i and τ_i are, respectively, the amplitude and the lifetime of the ith decay component of fluorescence. Briefly, the fluorescence decay parameters (α_i and τ_i) were obtained by iterative convolution of the fluorescence decay $I(t)$ with the instrumental response function, IRF(t), and fitting to the experimental data, $I_{exp}(t)$. In all cases, two decay times gave the best fit to the fluorescence decays.

Then, the anisotropy decay parameters were obtained by simultaneous iterative convolution of $I_{VV}(t)$ and $I_{VH}(t)$.

$$I_{VV}(t) = \frac{I(t)}{3}\,[1 + 2r(t)]$$

$$I_{VH}(t) = \frac{I(t)}{3}\,[1 - r(t)]$$

Eq. 3.4.3 and 3.4.4

with the IRF and globally fitting to the experimental parallel and perpendicular polarized components of the fluorescence, after fixing the fluorescence decay parameters to the values obtained from the first step.

The fluorescence anisotropy decay curves, $r(t)$, were fitted to a sum of discrete exponential terms:

$$r(t) = \beta_1 e^{(-t/\phi_1)} + \beta_2 e^{(-t/\phi_2)}$$

Eq. 3.4.5

where β and ϕ are the normalized amplitude and the rotational correlation time of the two decay components of the bi-exponential anisotropy decay, respectively. From the obtained anisotropy decay parameters (β and ϕ), the apparent time-zero anisotropy, $r(0)$, was calculated $[r(0) = \beta_1 + \beta_2]$. For this fitting model of bi-exponential anisotropy decay, the second decay component displays a very long lifetime, so that the residual anisotropy is defined by the anisotropy of the long-term component $[r_\infty = \beta_2]$.

Data analysis was carried out using a non-linear least squares iterative convolution method based on the Marquardt algorithm (Marquardt, 1963). A reduced χ_G^2 value < 1.3 and a random distribution of weighted residuals and autocorrelation plots were used to evaluate the goodness of the fitness (Lakowicz, 2006). To confirm the suitability of the fit, the expected steady-state fluorescence anisotropy, $\langle r \rangle_{calc}$, was calculated from the parameters obtained in the time-resolved analysis

$$\langle r \rangle_{calc} = \frac{\int_0^\infty I(t) \cdot r(t) dt}{\int_0^\infty I(t) dt}$$

Eq. 3.4.6

and then, compared to the experimental steady-state anisotropy for each sample.

FRET study of SP-B-induced membrane aggregates

The structure of aggregates formed by SP-B and negatively-charged membranes, POPC:POPG at a molar ratio 7:3, were characterized at the nanoscale using FRET methodologies. FRET experiments were performed between donor and acceptor membrane probes BODIPY(500/510)-PC and ORB, respectively, or between SP-B labeled with BODIPY FL as donor, and ORB as acceptor. SP-B was covalently labeled at its amino terminal segment with BODIPY FL, showing a molar probe/protein ratio of 0.91 (the experimental procedure is described in 3.1 Materials). BODIPY 500/510 C_{12}-HPC and octadecyl rhodamine B chloride (R18), also called ORB, were purchased from Thermo Fisher Scientific (**Figure 3.4.3**). The concentrations of stock probe solutions

were determined spectrophotometrically using the molar absorption coefficient values ε(BODIPY500/510-PC, 509 nm, in EtOH)= 8.6 x 10^4 M^{-1} cm^{-1} (Haugland, 2002) and ε(ORB, 555 nm, in ethanol)= 85 x 10^3 M^{-1} cm^{-1} (Johansson and Niemi, 1987).

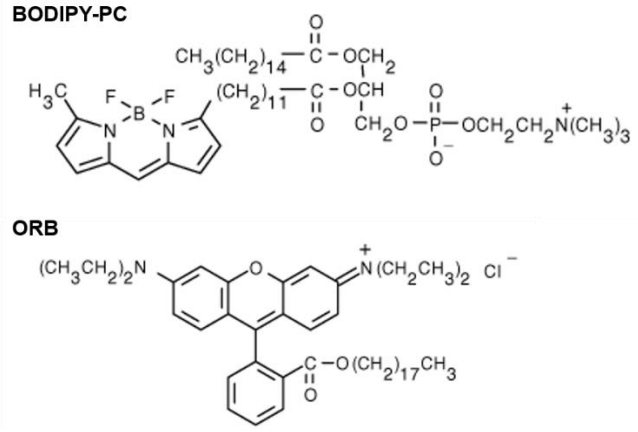

Figure 3.4.3. Chemical structure of BODIPY 500/510 C_{12}-HPC (BODIPY-PC) and octadecyl rhodamine B chloride (R18, ORB). Taken from Thermo Fisher Scientific's catalog.

Sample preparation

For preparation of all liposomes or proteoliposomes, adequate amounts of synthetic lipids, proteins and probes were mixed in chloroform/methanol solutions, dried under nitrogen stream, and rehydrated in 5 mM Tris pH 7, 150 mM NaCl at 45 °C. Multilamellar vesicle suspensions were subjected to 5 freeze-thaw cycles and then extruded to form LUVs with a diameter of ~100 nm.

For FRET experiments, two different procedures of sample preparation were followed. The first one consisted of the reconstitution of the protein (native SP-B or BODIPY/SP-B) together with the lipid mixture POPC:POPG (7:3, mol/mol) labeled with the corresponding membrane probes. Then, vesicle suspension was extruded to form LUVs. By this method, two different vesicle suspensions were prepared:

Mixture 1: POPC:POPG labeled with BODIPY-PC and ORB and containing different amounts of unlabeled SP-B, with final protein concentration that varied between 0 and 5 µM SP-B.

Mixture 2: POPC:POPG labeled with ORB and supplemented with different amounts of SP-B labeled with BODIPY FL (BODIPY/SP-B). The final protein concentration varied between 0 and 4.17 µM BODIPY/SP-B.

The second procedure for sample preparation consisted of the generation of POPC:POPG (7:3, mol/mol) LUVs labeled with the corresponding membrane probes. Then, 5 µl of native SP-B or BODIPY/SP-B in methanolic solution at different protein concentration were added to the vesicle suspension. Due to the high miscibility of methanol in water and the hydrophobic character of these proteins, both native SP-B and

labeled SP-B will be instantaneously incorporated into membranes. To prepare the protein in methanolic solution, the original protein stock in methanol:chloroform solution was transferred to methanol by chloroform evaporation under nitrogen stream, keeping the protein solution at the desired concentration for the assay. Two different vesicle suspensions were prepared following this procedure:

Mixture 3: SP-B in methanolic solution was added onto POPC:POPG LUVs labeled with BODIPY-PC and ORB. FRET experiments were performed at a final protein concentration ranging from 0 to 5 µM SP-B.

Mixture 4: BODIPY/SP-B in methanol was added onto POPC:POPG LUVs labeled with ORB. Final protein concentration in the suspensions varied between 0.4 and 4.44 µM BODIPY/SP-B.

For water/membrane partitioning assay of ORB, POPC:POPG (7:3, mol/mol) at variable phospholipid concentration (0.05 µM - 1mM) were labeled with a fixed concentration of ORB (0.75 µM).

FRET measurements

Time-resolved FRET measurements were obtained by the fluorescence intensity donor decays in the absence and in the presence of acceptors. Thus, in addition to all the samples described above, it was necessary to prepare vesicle suspensions with the same proteolipid composition but in the absence of the acceptor molecule, ORB.

All samples contained POPC:POPG (7:3, molar ratio) LUVs at a final lipid concentration of 0.5 mM. For the FRET pair BODIPY-PC/ORB, the donor/lipid ratio was kept 1:1000, whereas for the FRET pair formed by BODIPY/SP-B and ORB, the donor/lipid ratio was given by the protein content. In all experiments, the ORB/lipid ratio was kept 1:400.

After 1 hour of sample stabilization at room temperature, vesicle suspensions containing donor alone or donor and acceptor probes were subjected to time-resolved donor intensity decay measurements. Data analysis was carried out using a nonlinear least-squares iterative convolution based on the Marquardt algorithm (Marquardt, 1963). The goodness of the fit was determined by global X^2 values and a random distribution of weighted residuals and autocorrelation plots. For each experimental condition, FRET efficiency was obtained. Moreover, donor intensity decays were faced to different models of protein-membrane interactions, using a set of formalisms (see section *7.2.2.2. FRET modelling* in Chapter 4).

Liposome aggregation assay

Protein-induced membrane aggregation was determined from variation in the absorption at 630 nm, which reflects the increase in turbidity of the LUVs suspension containing SP-B or BODIPY/SP-B. Samples containing different protein concentrations were incubated for 1 hour at room temperature and then, absorbances at 630 nm were measured in a spectrophotometer.

Instrumentation

Absorption spectroscopy was performed with a Shimadzu UV-3101PC spectrophotometer (Shimadzu Scientific Instruments). When required, absorption spectra were corrected for turbidity using the method described by (Castanho, Santos and Loura, 1997). Steady-state fluorescence measurements were carried out on a SLM-Aminco 8100 Series 2 spectrofluorimeter (SLM Instruments) in L-format. For anisotropy measurements, the equipment was operated with automated rotating Glan-Thompson polarizers. The light source was a 450-watt Xe arc lamp and the reference was a Rhodamine B quantum counter solution. Correction of emission spectra was performed using the apparatus correction software.

Time-resolved fluorescence intensity decays with picosecond resolution were obtained by the time-correlated single-photon timing system described elsewhere (Loura, Fedorov and Prieto, 1996; de Almeida *et al.*, 2005). The samples were excited at 335 nm by pulses from a frequency doubled, mode-locked Tsunami Ti: sapphire laser (Spectra Physics) pumped by Nd:YVO_4 diode laser (Spectra Physics). The fluorescence was detected by a Hamamatsu R-2809U microchannel plate photomultiplier at the 515 nm that was selected using a Jobin-Yvon HR320 monochromator in combination with an adequate cut-off filter to avoid interference from Rayleigh-scattered light. The instrument response function (IRF) was recorded as excitation light scattered by a Ludox solution (silica, colloidal water solution from Sigma Aldrich). Data were collected using a multichannel analyzer with a time window of 1024 channels, at time scale of 39.1 ps/channel, and up to 50000 and 20000 counts in the peak channel of the IRF and decay curves, respectively. In the case of fluorescence anisotropy decay measurements, the parallel and perpendicular polarized components of the fluorescence to the plane of polarization of the excitation beam were alternatively recorded. For this setup system, the instrumental G factor is expected to be 1 because the polarized fluorescence light components were depolarized before the entrance slit of the monochromator. Quartz cuvettes of 5 x 5 mm were used for all the spectroscopy measurements. In the case of time-resolved measurements, samples were continuously agitated with a magnetic stirring bar.

3.5. IMAGING TECHNIQUES

Epifluorescence microscopy

Fluorescence microscopy allows visualizing fluorescent probes by using a high intensity light source that emits light in a broad range of spectrum, from ultraviolet to visible. In the particular case of an epifluorescence microscope, the optical components are mounted in a way that the specimen is illuminated from above.

Epifluorescence microscopy for the evaluation of membrane permeability

Permeability of pulmonary surfactant membranes to polar molecules was evaluated in giant vesicles by their direct visualization under fluorescence microscopy. Different lipoprotein mixtures labelled with Rhodamine-DOPE (at 1% molar concentration) were used to form giant unilamellar vesicles as described in section 3.1. Materials, 'Lipid and protein-lipid sample preparation'. Giant vesicles prepared in a 200 mOsm sucrose solution were transferred to equiosmolar glucose solutions containing two different types of polar fluorescent probes (from Sigma Aldrich): calcein (at a final concentration of 100 μM) or dextrans of different average sizes (final concentration of 50 μM) labelled with fluorescein isothiocyanate (FITC). The employed FITC-dextrans and their estimated hydrodynamic radii are detailed in table 3.1. Vesicles were incubated in these fluorescent solutions at room temperature in darkness for 3 hours. Then, the preparations were visualized by fluorescence microscope Leica DM-4000B (Leica Microsystems) with L5 and TX2 fluorescence filters and recorded with a digital camera C10600-10B ORCA-R2 (Hamamatsu). The images were processed with FIJI software (Schindelin *et al.*, 2012). Three independent experiments were performed to evaluate the permeability of each kind of surfactant-based GUVs.

FITC-dextrans	
MW (KDa)	Hydrodinamic radius (nm)
4	1.4
10	2.3
20	3.3
40	4.5
70	6
250	8.5

Table 3.5.1. Approximate Stokes' radii of FITC-dextrans. Product data taken from Sigma Aldrich.

For the evaluation of a possible blockage effect by α-SP-B or α-SP-C antibodies on the permeability of pulmonary surfactant-based GUVs, vesicle suspensions were pre-incubated with the specific antibodies for 2 hours at room temperature and then, incubated in FITC-dextrans for 3 hours to evaluate the permeability of vesicles in the presence of

the antibodies. For these experiments, the following polyclonal antibodies were used: anti human SP-B and anti-human SP-C antisera (from Seven Hills Bioreagents), anti-human SP-A antiserum (kindly supplied by Dr. J. Floros, from Penn State University, USA), anti-human tubulin antiserum (Sigma Aldrich) and anti-human SP-B Ig (Millipore). Antibodies concentrations used for each experiment are detailed in Chapter 2, section 5.2.1.2. In the case of antisera, their antibody concentration was determined by the Easy-Titer Mouse IgG Assay Kit (Thermo Fisher Scientific), while the total protein concentration was quantified by Lowry method. Three independent experiments were performed to evaluate the blockage effect of the diverse antibodies on the permeability of each kind of surfactant-based GUVs.

Live-cell real time imaging assay for the study of lamellar body exocytosis in alveolar type II cell cultures

Lamellar body (LB) exocytosis in rat primary alveolar type II cell cultures was real-time monitored by a fluorescent-based method that combines the use of the probe Fura-2 acetoxymethyl ester (AM) and the membrane probe N-(3-triethylammoniumpropyl)-4-(4-(dibutylamino)styryl)pyrinidium dibromide (FM1-43). This water-soluble dye, non-fluorescent in aqueous medium, is able to reversibly partition into membranes, exhibiting a bright fluorescence intensity in lipid environments. In this method, single exocytotic events are detected in ATII cell cultures, as a consequence of FM1-43 in the extracellular medium gaining access to surfactant membranes in fusing LBs through the fusion pore, while changes in cytoplasmic Ca^{2+} concentration are monitored by Fura-2 measurements in stimulated cells.

To evaluate the ability of pulmonary surfactant and its derivatives to stimulate lamellar body exocytosis in ATII cells, a variety of protein-lipid suspensions were employed: POPC or POPC:POPG (7:3) containing organic solvent-isolated SP-B and/or SP-C (12% of either protein, by weight), POPC:POPG supplemented with SP-B purified in detergent (12%) or vesicles formed by organic extract from pulmonary surfactant (with equivalent total protein amount to vesicles containing both proteins). For the concentration-response assay, POPC:POPG vesicles containing different protein:lipid ratios were tested, maintaining lipid content constant while varying the amount of SP-B. All these preparations were bath sonicated for 1 hour to form LUVs before applying them to the ATII cell cultures.

For combined Fura-2 AM and FM1-43 experiments, cells were loaded with 2 μM Fura-2 AM for 30 minutes in MucilAir, washed twice in bath solution (10 mM Hepes pH 7.4, 5 mM glucose, 140 mM NaCl, 5 mM KCl, 1 mM $MgCl_2$, 2 mM $CaCl_2$) and kept in bath solution with 1 μM FM1-43. ATII cells were treated with vesicles containing different

components of pulmonary surfactant in order to evaluate their effects on LB fusion. As a control for efficient induction of LB fusion and surfactant secretion, ATII cells were treated with 100 μM ATP, a known potent agonist for LB fusion. ATP concentration was chosen to induce maximum fusion response. Different chemical agents were used to characterize the mechanism behind the regulatory effect of SP-B towards surfactant secretion. Apyrase (50 U/ml) was applied at the start of the experiment for extracellular ATP depletion. Cells were incubated with 200 nM thapsigargin for 20 minutes in order to deplete intracellular Ca^{2+} stores. To block $P2Y_2$ receptor, the cells were pretreated with 800 μM suramin for 5 minutes. In the experiments with connexin and pannexin inhibitors, cells were incubated with 10 μM carbenoxolone or 100 μM flufenamic acid for 15 minutes.

Images were acquired in an IMIC Digital Microscope (TILL Photonics) using its corresponding control software, Live Acquisition, and a 40x objective lens (Olympus). For Fura-2 AM, dye-loaded cells were illuminated for 100 ms at 50% intensity and at the excitation wavelengths 340 nm and 387 nm, respectively, while for FM 1-43 dye, the used exposure time and intensity were 100 ms and 60%, respectively, and the excitation wavelength was 482 nm. Image analysis was performed by FIJI.

The extent of exocytosis during 15-minute observation time was expressed in two ways. First, as percentage of fusing cells, which refers to the number of cells showing at least one fusion event, per total number of cells. Lamellar body fusion events with plasma membrane were followed by the appearance of FM1-43 fluorescence spots. Alternatively, LB exocytosis was also evaluated as percentage of cells showing Ca^{2+} peak, using data obtained by image analysis of Fura-2 signal.

Samples from three different primary cell isolations were tested in duplicate for each experimental condition.

Citotoxicity assay of alveolar type II cells by propidium iodide uptake

Cells were rinsed and challenged with 8 μM propidium iodide (PI) for 5 minutes to assess integrity of plasma membrane in cells exposed to SP-B. PI is a small fluorescent molecule that can only enter the cells and produce fluorescence upon binding to DNA when the plasma membrane is damaged. Images were acquired in an IMIC Digital microscope, using a 20x objective lens (Olympus, Tokyo, Japan) and an excitation wavelength of 563 nm.

Alternatively, cytotoxicity of the different treatments with secretagogues and inhibitors was detected and quantitatively evaluated from the maintenance of plasma membrane integrity to the permeation of the FM1-43 probe, which only penetrates and labels internal membranes in cells with damaged plasma membrane.

Atomic force microscopy

Atomic force microscopy (AFM) is a technique where a cantilever with a sharp tip is systematically scanned across a sample surface to produce high resolution images by measuring different physical properties of a sample at nanometric scale. This assembly is translated over the sample by a computer-controlled piezo scanner with subnanometer accuracy. Surface topography induces cantilever deflections, which allow to determine the surface contour of the sample. There are two classical imaging operating modes: contact and tapping. In the contact mode, the tip keeps permanent contact with the sample due to the rise and descent of the sample by the scanner to maintain this contact. In the tapping mode, the cantilever oscillates at or slightly below its resonant frequency with a fixed amplitude. During scanning, the tip touches intermittently the sample, contacting the surface at the bottom of its swing. The interaction between tip and sample surface alters the resonance frequency of the cantilever and thus, changes in the amplitude are registered. A feedback loop maintains constant the amplitude of oscillations while this feedback response is used to generate the topographical image. Tapping mode uses lower forces, reducing the potential damage of soft samples, such as biological samples. This operating mode also allows to produce a secondary type of image, the phase image, which detects variations in composition, adhesion, friction and viscoelasticity of the scanned material.

In this Thesis, samples of SP-B purified in detergent or SP-B (either purified in detergent or isolated in organic solvent) incorporated into lipids were characterized by AFM. Two different methods for sample preparation were employed:

- Direct application of the sample onto mica supports. 20 µl of 50 µg/ml POPC:DPPG (7:3, by weight) SUVs containing or not SP-B were placed on a mica square. After 5 minutes of incubation, mica is washed with 3 ml of fresh milliQ water. Mica is placed vertical and the water is carefully added on the top edge of mica, letting it run over the surface. Finally, mica is dried under a N_2 stream.
- Interfacial films transferred to mica. These samples were prepared using a Langmuir balance to prepare the so-called Langmuir-Blodgett films, as detailed in a specific section below.

AFM images were obtained with a Nanoscope IIIa scanning probe microscope (Bruker), operated in tapping mode, using TESP-SS tips (Bruker), in the ICTS Centro Nacional de Microscopía Electrónica (Universidad Complutense de Madrid). Image analysis was performed by NanoScope Analysis software (Bruker).

Transmission electron microscopy

Transmission electron microscopy (TEM) uses an electron beam to be transmitted through a specimen to visualize it with a resolution at angstrom scale. TEM operates as follows. The electron gun generates the electron beam, which is focused onto the object by a set of condenser lens. The beam strikes the specimen and some parts of it are scattered, depending on the sample density. The unscattered electrons hit onto a fluorescent screen, giving rise to an image of the object with its different parts displayed in varied darkness as a consequence of density variation.

In this Thesis, transmission electron microscopy was employed to visualize protein complexes in pulmonary surfactant, as well as SP-B complexes in different environments. Carbon-coated cupper grids (EMS400-Cu, Gilder grids) were subjected to glow discharging. Then, 2-3 µl of sample were applied onto the grid for 2-3 minutes. The excess of liquid was eliminated by drying with filter paper before washing twice with milliQ water and drying again with filter paper. 2% uranyl acetate (w/v) was used as staining agent. After 1 minute of grid incubation with uranyl acetate, the stain excess was eliminated with a filter paper. The grids were imaged in a JEOL JEM-1230 transmission electron microscope operated at 100 kV and recorded at a magnification of 40000x using a TemCam-F416 (TVIPS). TEM images were obtained in the Electron Microscopy Facility at the Centro de Investigaciones Biológicas (CSIC, Madrid).

3.6. INTERFACIAL TECHNIQUES

Captive bubble surfactometry

The captive bubble surfactometer (CBS), designed and developed by Dr. Samuel Schürch and coworkers at the University of Calgary (Canada) (Schurch *et al.*, 1989), has become an essential tool to study the biophysical behavior of films of pulmonary surfactant or clinical surfactant preparations under physiologically meaningful conditions.

The CBS is an experimental setup where the surface activity of pulmonary surfactant can be monitored once adsorbed into the air-water interface of an air bubble confined in a buffer-filled chamber under controlled environmental conditions (**Figure 3.6.1**). The specific software of the equipment calculates surface tension, area and volume of the bubble, from measuring its height and diameter, which is recorded by a video camera (Schoel, Schurch and Goerke, 1994).

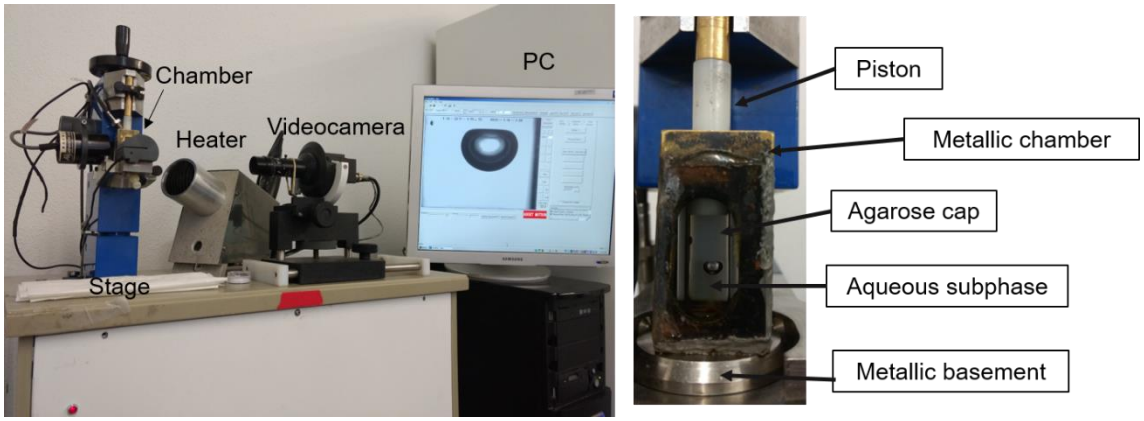

Figure 3.6.1. Overview of the CBS system used in the present Thesis, with a detailed image of the bubble chamber (right).

The chamber consists of a glass cylinder on a metallic base with a small hole (2 mm) through which a bubble of approximately 0.035-0.040 cm^3 can be created, and through which a capillary is inserted for sample injection. The opposite side of the chamber is sealed with an agarose cap, where the created bubble is settled. The cap is adjusted to a piston, which is moved in a controlled way producing the compression and expansion of the space between the agarose cap and the sealed metallic base. The bubble volume changes as pressure inside the chamber varies by the piston movement. As bubble volume is decreased, the surface area is subsequently reduced and, in the presence of surfactant film, the surface tension drops, which results in a bubble flattening. The chamber is filled with 5 mM Tris pH 7.4, 150 mM NaCl, 10% sucrose. The presence of sucrose increases the density of the buffer, helping surfactant to float against the air bubble during injection, preventing its dilution into the subphase. The chamber is thermostatted at 37 °C. Temperature is controlled by enclosing the chamber in a water bath which allows a homogeneous distribution of the heat provided by a heater. Degasification of the subphase buffer is required before starting the experiment. This process is performed by expanding a bubble in the sealed chamber during 10 minutes, allowing the liberation of the dissolved air in the buffer in the form of little air bubbles that join to the main expanded bubble, due to the pressure inside the chamber. Pulmonary surfactant preparations are usually tested at 25 mg/ml phospholipid concetration, although in the experiments performed in this Thesis, a limiting surfactant concentration of 4.7 mg/ml was used with the aim of detecting the potential disfunction of surfactant film in the presence of a polyclonal anti-SP-B IgG.

The evaluation of surface activity of surfactant films in the CBS is performed in 4 stages:

- Initial adsorption kinetics: it simulates the adsorption process of surfactant from the aqueous subphase to the alveolar-liquid interface and allows analysing the ability of surfactant samples to be adsorbed into the interface and form a

surface active film. The sample (~200 nl) is applied with a microcapilar, directly over the bubble surface. Then, changes in bubble shape, and thus in surface tension, are registered during 5 minutes (**Figure 3.6.2 A-B**). Upon native surfactant adsorption into the air-liquid interface, surface tension drops, in a few seconds, from 70 mN/m to an equilibrium surface tension of about 20 mN/m.

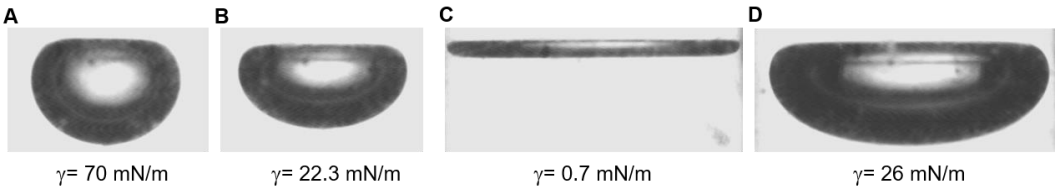

Figure 3.6.2. Surface tension drives changes in bubble shape. In the CBS system, a bubble is created (A) and, after surfactant sample injection, surface tension decreases down to reaching equilibrium, producing flattening of the bubble (B). Upon compression, the surface active film leads to a further drop of surface tension, close to 0 N/m, which causes an extreme flattening of the bubble (C). During expansion, surface tension increases to original values (D).

- Post-expansion adsorption: after sealing the chamber, the bubble is expanded up to a maximum bubble volume of 0.15 cm^3 by the motion of the piston controlled by the software. Then, the surface tension is again registered for 5 minutes. This stage evaluates the ability of re-organization, transferring and spreading of surfactant structures into an expanding surface. Typically, native surfactant films rapidly lead to a surface tension decrease down to ≈ 20 mN/m.
- Quasi-static cycling: it consists of 4 low speed stepwise compression-expansion cycles, in which the bubble volume changes 20% over the volume in the immediately previous step. Maximal bubble volume is set during the post-expansion adsorption stage (0.15 cm^3), whereas minimal bubble volume is set manually at each compression cycle. Upon cycling, an active surfactant film is able to reach minimal surface tension with values near 0 mN/m under compression and, during subsequent expansion, low maximal surface tension is restored to the original state (**Figure 3.6.2 C-D**). At the end of compression, collapse of the bubble can occur, so that the area of the bubble is dramatically reduced without change in surface tension (this can be identified visually as a relaxation of the flattened bubble shape). Data are shown as surface tension-area isotherms, which give information about minimal and maximal surface tension reached by the film and hysteresis of each cycle. Low speed compression-expansion cycles allow analysis of re-organization of the surfactant films and also film stability due to the relaxation process of the film between compression-expansion steps. However, no direct physiological implications can be inferred at this stage, as the speed of compression-expansion cycles during breathing is much faster.
- Dynamic compression-expansion cycling: at this final stage, fast compression-expansion cycles are applied to the bubble at a rate of 20 cycles/min,

which mimic physiological breathing rates. Maximal and minimal bubble volumes are set taking as a reference the limits applied in the 4th quasi-static cycle. Typically, the 1st, 10th and 20th cycles are analyzed as illustrative parts of the cycling dynamics, plotting surface tension-area isotherms.

Langmuir balance

Surface balances constitute a classical method to assess the interfacial activity of pulmonary surfactant preparations. They can evaluate the adsorption of surfactant to an air-liquid interface, its spreading along this interface and even its interfacial behavior under compression/expansion cycles. There are several types of surface balances, although all of them are equipped with a Teflon thermostatted trough that confines the aqueous solution, and a pressure sensor which monitors real-time changes in surface tension or pressure. Surface pressure is defined as the difference between the surface tension in the absence and in the presence of surface active material.

$$\Pi = \gamma_{water} - \gamma_{surfactant}$$

Langmuir balances allow to evaluate the dynamics of the interfacial activity of pulmonary surfactant, as the surface area of the trough can be modified by the computer-controlled movement of a mobile barrier. Upon injection of surfactant on the surface of the aqueous solution, the amphipathic molecules form an interfacial film. Closure of the mobile barrier causes the compression of the interfacial film, increasing lateral pressure and packing density of the molecules (typically phospholipids) in the monolayer. Opening the barrier gives rise to the reorganization of material in an expanded area (**Figure 3.6.3**).

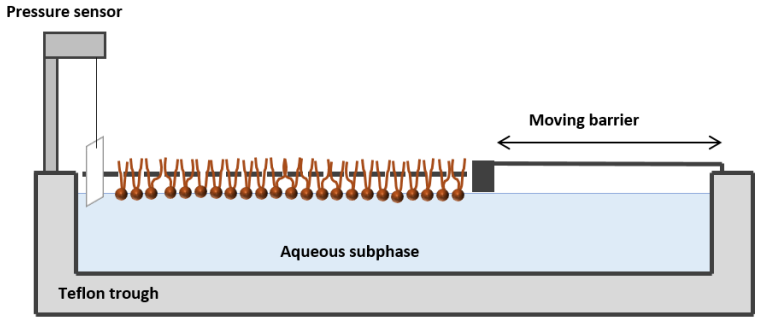

Figure 3.6.3. Schematic illustration of a Langmuir balance.

Compression isotherms register the increase of surface pressure (reduction in surface tension) as surface area diminishes. This allows determination of changes in the molecular organization of interfacial films during compression, which may also reflect the occurrence of lateral phase transitions. The compression isotherm of a DPPC film is commonly used to explain the phase transitions that undergoes a phospholipid interfacial film during compression (**Figure 3.6.4**). At low surface pressure, phospholipid molecules

are in gas-like phase, characterized by extremely high mobility and disorder, where the intermolecular interactions are very scarce. Upon compression, surface area is diminished favoring that phospholipids interact between them by van der Waals attractive forces or headgroup interactions, so that the surface pressure starts rising up to a phase termed as liquid-expanded (LE), where the phospholipids still have a high mobility because of the presence of *trans*-gauche isomerizations at the phospholipid acyl chains. Further film compression generates the orientation of phospholipids perpendicular to the surface plane and the lipid packing, which drives saturated phospholipids into the liquid-condensed (LC) phase. Between the LE and LC phases, a plateau indicates the coexistence of both phases, during which the work of compression is used to complete the lipid packing without increase in surface pressure. If compression still progresses, the interfacial monolayer turns much less compressible and the surface pressure rises up to 70 mN/m. At the highest compression levels, the interfacial film may collapse, generating the conversion of bi-dimensional structures into three-dimensional ones (Takamoto, Aydil, *et al.*, 2001; Wustneck *et al.*, 2005), that may or may not continue associated to the interface.

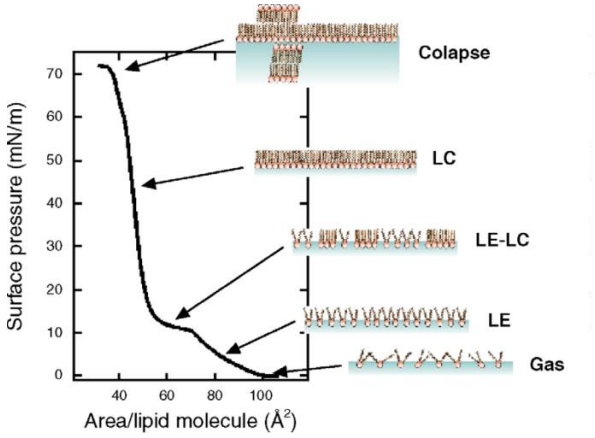

Figure 3.6.4. π/A isotherm of a DPPC monolayer at 24ºC. LE: liquid-expanded phase, LC: liquid-condensed phase, LE–LC: liquid-condensed/liquid-expanded coexistence. Image modified from (Wustneck *et al.*, 2005).

In this Thesis, the interfacial activity of POPC:DPPG films was characterized as a previous step for further structural studies of the effect of SP-B on these mixed monolayers. 33 nmol of the lipid mixture in chloroform/methanol (2:1, v/v) solution was spread onto a buffered subphase (5 mM Tris pH 7.4, 150 mM NaCl) at 25 °C in a surface balance (Nima Technology). After spreading of the monolayer, the organic solvent was allowed to evaporate for 10 minutes. Then, the monolayer was compressed at a rate of 65 cm^2/min.

In addition to measuring the interfacial activity of surfactant material, the Langmuir balance allowed the transference of the interfacial film onto a mica support for further structural characterization by atomic force microscopy (AFM) (**Figure 3.6.5**). A

comparative study of the morphology of POPC:DPPG films containing native SP-B complexes purified from detergent-solubilized PS or SP-B isolated in organic solvent was performed. For this purpose, dried lipid films of POPC:DPPG (7:3, w:w) were rehydrated in the presence of SP-B purified in detergent to form vesicles at a lipid concentration of 5 mg/ml and different SP-B concentrations (10 and 20% w/w, protein/lipid ratio). In parallel, dried lipid films were rehydrated in the presence of buffer with an equivalent amount of detergent than lipoprotein samples. After detergent removal by incubation with Bio-Beads SM-2 Resin, multilamellar suspensions were sonicated to form small unilamellar vesicles (SUVs). On the other hand, organic mixtures of POPC:DPPG (7:3, w:w) containing or not SP-B isolated in organic solvent (20% w/w, protein/lipid ratio) were prepared. Different samples, either in the form of small unilamellar vesicle suspensions or chloroform/methanol solutions, were spread onto the surface of a buffered subphase at 25 °C in a surface balance (Nima Technology). In the case of solvent mixtures, 5 µl containing 33 nmol of phospholipids were applied onto the interface, whereas 30 µl of vesicle suspensions containing SP-B or 100 µl of vesicle suspensions without the protein (200 or 660 nmol of phospholipids, respectively) were directly deposited at the surface. After waiting 10 minutes to allow organic solvent evaporation (in the case of aqueous suspension this step was kept in the procedure), monolayers were compressed to the required pressure at a slow rate of 25 cm^2/min. After 30 minutes of equilibration, monolayers were transferred to the mica support, which was previously immersed in the subphase, to form Langmuir-Blodgett films at a transfer speed of 5 mm/min. Film transferences onto mica supports were performed at 12 °C (subphase temperature was gradually refrigerated during 30 minutes of equilibration), due to it has been suggested that a higher rigidity of the monolayer could be favored the formation of the oligomeric structure of SP-B in the film, as it was previously observed in solvent-spread films of DPPG + SP-B (Olmeda *et al.*, 2015). Lipid monolayers without the protein were also transferred at this low temperature with the aim to be compared with those containing SP-B. Alternatively, interfacial films of native SP-B complexes from detergent-solubilized PS in the absence of lipids were generated. 6 nmol of SP-B purified in detergent at different concentrations of protein (1 and 2 mg/ml of SP-B) were applied and spread onto the surface of the buffered subphase at 12 °C. Interfacial films of SP-B purified in detergent were then transferred to a mica support for AFM analysis.

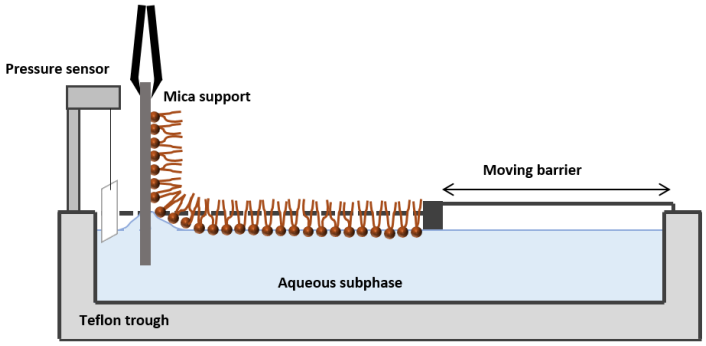

Figure 3.6.5. Schematic illustration of the method used to obtain Langmuir-Blodgett films.

Chapter 1

CHARACTERIZATION OF NATIVE PROTEIN COMPLEXES IN PULMONARY SURFACTANT

4. CHARACTERIZATION OF NATIVE PROTEIN COMPLEXES IN PULMONARY SURFACTANT

4.1. INTRODUCTION

Pulmonary surfactant is a highly dynamic system, which adopts a variety of structural arrangements according to the stage of its biological cycle. Surfactant is assembled by alveolar type II cells into tightly packed membranes stored in specialized acidic organelles, called lamellar bodies (LBs) (Weaver, Na and Stahlman, 2002). Upon secretion, surfactant undergoes structural conversion processes giving rise to different structures, such as lamellar body-like particles, tubular myelin, multilayer assemblies and the interfacial monolayer spread along the respiratory surface (Goerke, 1998). Protein-protein and protein-lipid interactions are behind this dynamic polymorphism of pulmonary surfactant. In particular, SP-B and SP-C have been proposed as the major players for these membrane rearrangements due to their membrane-perturbing activities. Several functional studies have suggested the existence of interactions between SP-B and SP-C as both proteins, though showing partially overlapping interfacial activities, are required acting together in a concerted way for surfactant to achieve its optimal function (Taneva and Keough, 1994d; Schurch *et al.*, 2010; Roldan *et al.*, 2016). Additionally, both of them are necessary for the disassembly of secreted lamellar body-like particles to give rise to the formation of the interfacial monolayer film and its associated multilayer arrays upon touching the air-liquid interface (Hobi *et al.*, 2016). In the case of protein SP-A, interactions with SP-B can be also suspected, as these proteins display a cooperative action enhancing the adsorption of phospholipids to the air-liquid interface (Hawgood *et al.*, 1987), and both of them are required for the formation of tubular myelin (Perez-Gil, 2008).

Direct or indirect interactions among the different proteins of surfactant seem to be important for the proper function of the system. Thus, the scope of this chapter is to elucidate the existence of supramolecular protein complexes in pulmonary surfactant membranes. During the first section of the chapter, pulmonary surfactant or its organic extract were solubilized by the zwitterionic detergent CHAPS in order to get native protein complexes, whose composition and structure were analyzed. Secondly, SP-B and SP-C reconstituted into lipid vesicles were conjugated with a variety of protein crosslinking reagents to attempt the determination of the stoichiometry of potential SP-B oligomers and SP-B/SP-C heterocomplexes. Lastly, a solubilized membrane protein library from pulmonary surfactant was generated using the nanodisc technology in order to get insights of the interactions between different components of the pulmonary surfactant.

1.2. RESULTS

1.2.1. BIOCHEMICAL ANALYSIS OF PROTEIN COMPLEXES IN PULMONARY SURFACTANT

Pulmonary surfactant purified from bronchoalveolar lavages was solubilized by the zwitterionic detergent CHAPS in order to characterize protein complexes by electrophoresis. Silver staining of non-denaturing Blue Native (BN)-PAGE reveals the existence of protein complexes of high molecular weight (**Figure 4.1A**). Several silver-stained bands were subjected to protein identification by mass spectrometry, revealing that immunoglobulins were present at the well-defined band over 669 KDa marker (green arrowhead), while the band over 66 KDa marker contained albumin (red arrowhead). Western blots showed the presence of surfactant proteins in high molecular weight bands. SP-B and SP-C were forming part of high molecular weight complexes, which were not detected as well-defined bands but as smears, likely as a consequence of excessive amount of detergent and lipids. In contrast, SP-A was detected in the upper region of the lane, in agreement with the presence of highly oligomerized SP-A aggregates unable to penetrate through the gel under native conditions.

Next, in order to test the stability of the native supramolecular complexes, electrophoresis in the presence of SDS was performed (**Figure 4.1B**). SP-A aggregates were able to dissociate during the denaturing electrophoresis, showing lower molecular weight bands corresponding to dimers, trimers, hexamers and other higher molecular weight oligomers. In the case of SP-B, complexes were partly split into entities of lower molecular weight, showing a smear from 37 KDa to 250 KDa. Regarding SP-C, this protein seemed to be completely disassembled of high molecular weight complexes in the presence of anionic detergent, showing a smear below 37 KDa.

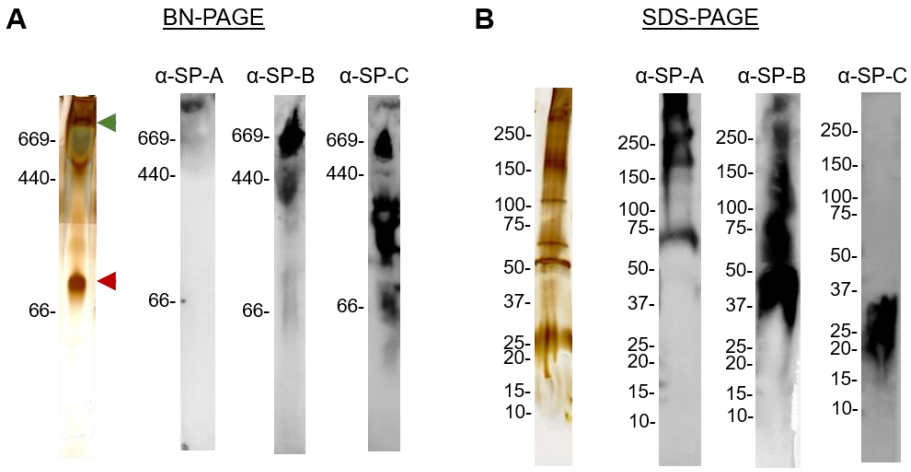

Figure 4.1. Surfactant protein complexes in CHAPS-solubilized pulmonary surfactant. A) Silver staining and western blots from non-denaturing BN-PAGE (A) and from SDS-PAGE under non-reducing conditions (B) on 4-20% polyacrylamide gels. Arrowheads correspond to bands containing proteins identified by mass spectrometry: albumin (red) and immunoglobulin heavy chain (green).

In order to improve the biochemical characterization of pulmonary surfactant complexes solubilized by CHAPS, as no defined bands were mostly observed in western blots of non-denaturing and non-reducing gels, a second SDS-PAGE dimension under reducing conditions was performed from gel strips obtained from Blue Native-PAGE (**Figure 4.2 A**) and SDS-PAGE (**Figure 4.2 B**). In this way, we intended to ensure that smeared bands were in fact made up of surfactant proteins (which would be particularly important due to the presence of endogenous immunoglobulins in surfactant that could generate unspecific binding of secondary antibodies), and determining the size range of the native complexes which they were initially associated to.

Second dimension electrophoresis from BN gel strip caused the dissociation of the high molecular complexes in several bands (silver staining, **Figure 4.2 A**). The upper side of non-denaturing strip was resolved as several bands from 100 to 23 KDa. The band with mobility corresponfing to about 500 KDa in the first dimension split in several spots in the second dimension: 100, 75, 65, 50, 37 and 25 KDa. In the case of the defined band around 100 KDa in the non-denaturing strip, two main bands of about 65 and 50 KDa were revealed in the second dimension. The protein composition of several spots of this bidimensional electrophoresis were analyzed by mass spectrometry, although only few of them could be identified accurately. This is the case of 65 KDa bands from around 500 KDa and 100 KDa in first non-denaturing dimension, which contained albumin (red arrowhead). Besides, transferrin was detected in the 75 KDa band corresponding to the area of around 500 kDa in the first dimension strip (purple arrowhead).

The presence of surfactant proteins in BN gel strips was analyzed by western blots of the second dimension, revealing bands which corresponded to their monomeric forms, as expected in the presence of reducing agent (**Figure 4.2 A**). SP-A was detected in the upper side of the non-denaturing strip, pointing that SP-A under native electrophoresis was associated into complexes heavier than mere octadecamers (~630 KDa), which were not able to penetrate the gel. SP-B was also detected along almost the entire non-denaturing strip, including the very top segment of it, although the major proportion of the protein was distributed between 440 and 140 KDa. On the other hand, SP-C was detected between 669 and over 140 KDa. These results confirmed the existence of SP-A, SP-B and SP-C in native high molecular weight complexes, in agreement with the results obtained by direct western blots of the first dimensions. The co-existence of different surfactant proteins into high molecular weight bands could also suggest possible interactions between SP-A and -B, as well as between SP-B and -C.

Finally, silver staining of the second dimension of the SDS-PAGE gel strip showed a notable lower complexity than the one obtained from BN-PAGE strip (**Figure 4.2 B**). Regarding to immunoblotting analysis for surfactant proteins, SP-A was detected from

the top region to 75 KDa of the denaturing first dimension gel strip. In the case of SP-B, most of the protein in the non-reducing gel was associated into structures of low molecular weights, 30-50 KDa, such as dimers or tetramers of SP-B. However, a minor fraction of SP-B was detected as a smear between 50-150 KDa, forming higher oligomeric structures. In contrast, SP-C was restricted to the region between 37-50 KDa of the first dimension strip. Thus, second dimension electrophoresis confirmed the presence of a variety of macromolecular protein complexes that were partly disrupted in the presence of SDS.

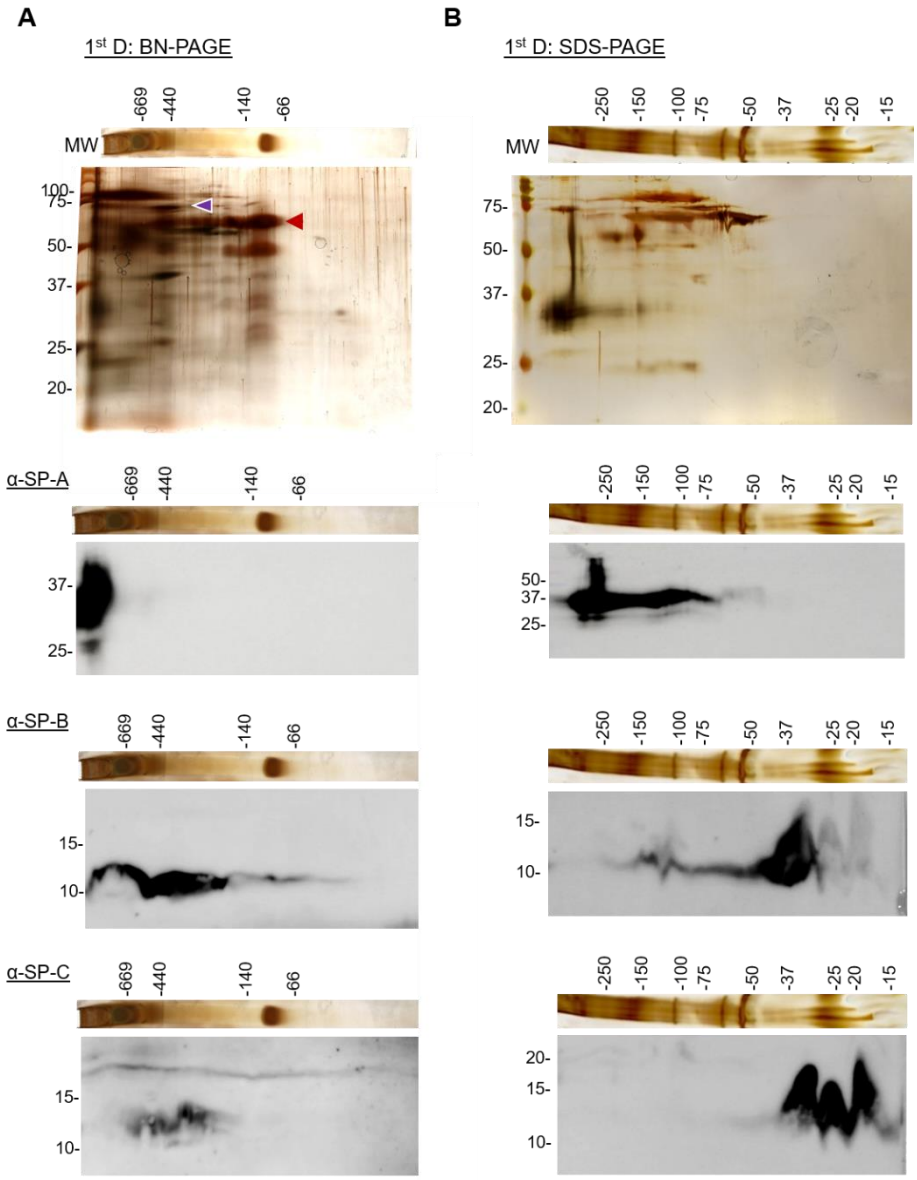

Figure 4.2. Characterization of surfactant protein complexes by two dimensional electrophoresis. Second dimension was performed of a band strip from previous BN-PAGE (A) or SDS-PAGE under non-reducing conditions (B). All second dimension electrophoresis were SDS-PAGE in the presence of reducing agent and gels contained 12% polyacrylamide for silver staining and α-SP-A western blot, and 16% polyacrylamide for α-SP-B and α-SP-C western blots. Arrowheads correspond to bands containing proteins that could be identified by mass spectrometry: transferrin (purple) and albumin (red).

1.2.2. BIOCHEMICAL AND STRUCTURAL ANALYSIS OF SURFACTANT PROTEIN COMPLEXES RECONSTITUTED INTO MEMBRANES

Two-dimensional electrophoresis analysis of detergent-solubilized surfactant suggested the possible presence of SP-B/SP-C complexes. To get deeper insight of these protein heterocomplexes found in PS membranes, vesicles made by its extract (containing SP-B 1% and SP-C 1%, mass protein to lipid ratio) were used. After vesicle solubilization with CHAPS, suspension was subjected to a size-exclusion chromatography (SEC). This chromatography did not allow to resolve complexes of different defined molecular sizes entirely, showing overlapped peaks that contain both SP-B and SP-C **(Figures 4.3 A-B**). To compare the supramolecular organization of SP-B in the organic extract of PS with that of SP-B alone reconstituted into synthetic model membranes, POPC or POPC:POPG vesicles containing SP-B 10% (by weight, protein to lipid) were solubilized with CHAPS and subjected to similar analysis. Size-exclusion chromatograms of both preparations showed two different populations that contain SP-B (**Figures 4.3 A-B**); the first one was comprised by protein complexes from 29 KDa to < 66 KDa, while the other one contained protein entities lower than 12.4 KDa, according to the elution volumes of a set of protein standards of known molecular weight. The peaks eluting first from SP-B vesicles and OE vesicles contained protein aggregates similar in size.

Electrophoretic analysis under native conditions (BN-PAGE) of detergent-solubilized OE suspension showed a major proportion of SP-B forming aggregates higher than 200 KDa, but also SP-B was detected as a smear from 100 KDa to the end of the lane, which might had contained SP-B dimers and low order oligomeric forms (**Figure 4.3 C**). After performing SEC of this sample, SP-B and SP-C were detected as smears with molecular weights higher than 140 KDa in fractions 1 and 2. Thus, size-exclusion chromatography got rid of low molecular weight SP-B oligomers detected in the original suspension of solubilized OE. In the case of fractions from SEC of CHAPS-solubilized POPC:POPG vesicles supplemented with SP-B, this protein was detected in well-defined bands with approximate molecular weights of 200, 232 and 500 KDa. Therefore, SP-B complexes solubilized from vesicles made by either organic extract or POPC:POPG + SP-B show high order oligomerization states. A previous study has revealed the existence of native SP-B oligomers by their purification from pulmonary surfactant solubilized in CHAPS (Olmeda *et al.*, 2015). The native electrophoretic analysis of SP-B purified in detergent showed the presence of high order oligomers ($SP\text{-}B_{det}$ in **figure 4.3 C**), with a similar band profile as solubilized OE or the SP-B-supplemented vesicle suspensions analyzed along this section. Moreover, notice that all immunoblots from BN-PAGE showed in Figure 4.3 C showed very large protein aggregates with molecular weights higher than 669 KDa in the top of the blot. So, samples from SEC of different elution volumes, with estimated molecular weights lower than 66 KDa (according to the column calibration),

showed not only higher molecular weight oligomers but also large protein aggregates in native electrophoresis, meaning that protein mixed micelles could undergo an aggregation process after SEC. SP-B might prompt this process by establishing protein-protein interactions between oligomers, as suggested in (Olmeda *et al.*, 2015).

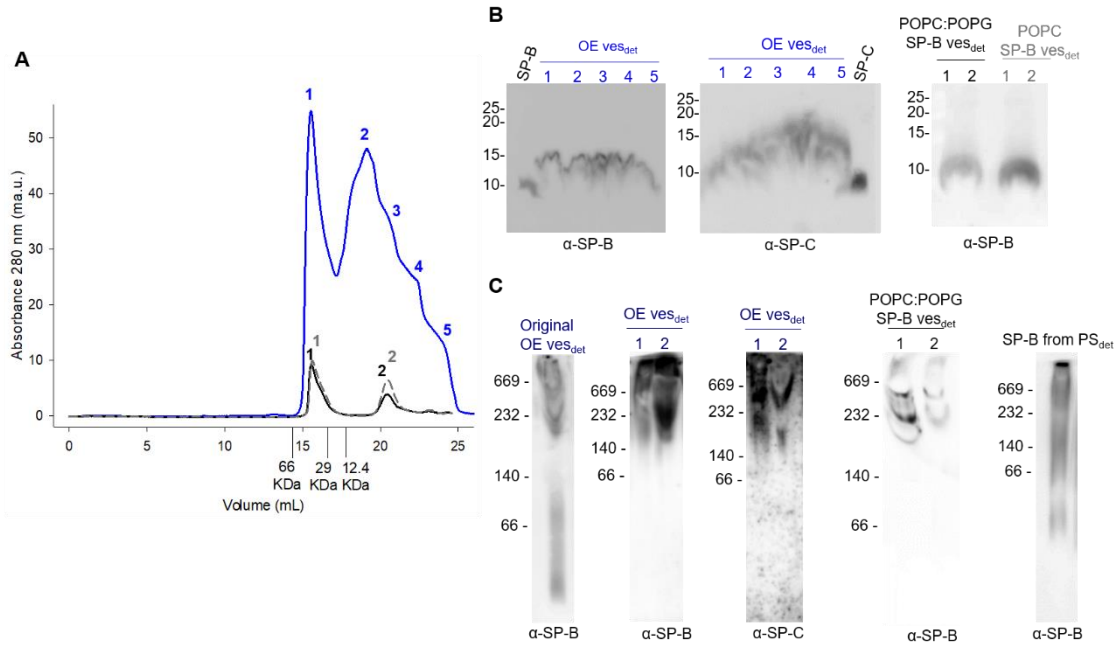

Figure 4.3. Size separation of CHAPS-solubilized surfactant protein complexes. Vesicles made by organic extract from pulmonary surfactant or of POPC or POPC:POPG (7:3) containing SP-B 10% (w/w, protein/lipid) were solubilized by CHAPS (detergent/phospholipid mass ratios of 5:1 and 1.5:1, respectively) . **(A)** Profiles of size-exclusion chromatography in Superdex 200 10/300GL column of detergent-solubilized vesicles made of organic extract (OE ves$_{det}$; blue), POPC + SP-B (POPC SP-B ves$_{det}$, black) and POPC:POPG + SP-B (POPC:POPG SP-B ves$_{det}$; grey dashed line). Several fractions from each chromatogram were chosen for biochemical and structural characterization (numbered from 1 to 5). **(B-C)** α-SPB and α-SP-C western blots from SDS-PAGE under reducing conditions or BN-PAGE. Original OE ves$_{det}$ refers to CHAPS-solubilized vesicles of organic extract before size-exclusion chromatography. SP-B from PS$_{det}$ corresponds to BN-PAGE analysis of SP-B complexes purified from CHAPS-solubilized pulmonary surfactant. SDS-PAGE and BN-PAGE were performed on 16% and 4-20% polyacrylamide gels, respectively.

To structurally characterize the protein complexes observed by native electrophoresis, fractions obtained from SEC were analyzed by TEM (**Figure 4.4**). Fractions 1 and 2 from detergent-solubilized organic extract show surfaces covered by domains likely formed by detergent, lipid and protein, in which ring-shaped particles with a 10 nm of average diameter could be distinguished (labeled with circles). Apart from these flattened surfaces, several vesicle-like arrangements were visualized. In the case of solubilized POPC or POPC:POPG membranes containing 10% SP-B, similar domains in the surface were visualized, although the size of these domains abruptly decreased in late eluted fractions named as 2. Nevertheless, both fractions show ring-shaped structures similar to those observed in solubilized vesicles made by organic solvent mixtures. These particles of 10 nm of diameter are compatible in size and shape to SP-B complexes purified from

pulmonary surfactant visualized by TEM and AFM, which fitted with the tridimensional model of SP-B that predicted SP-B oligomers constituted by 5 or 6 SP-B covalent dimers (Olmeda *et al.*, 2015).

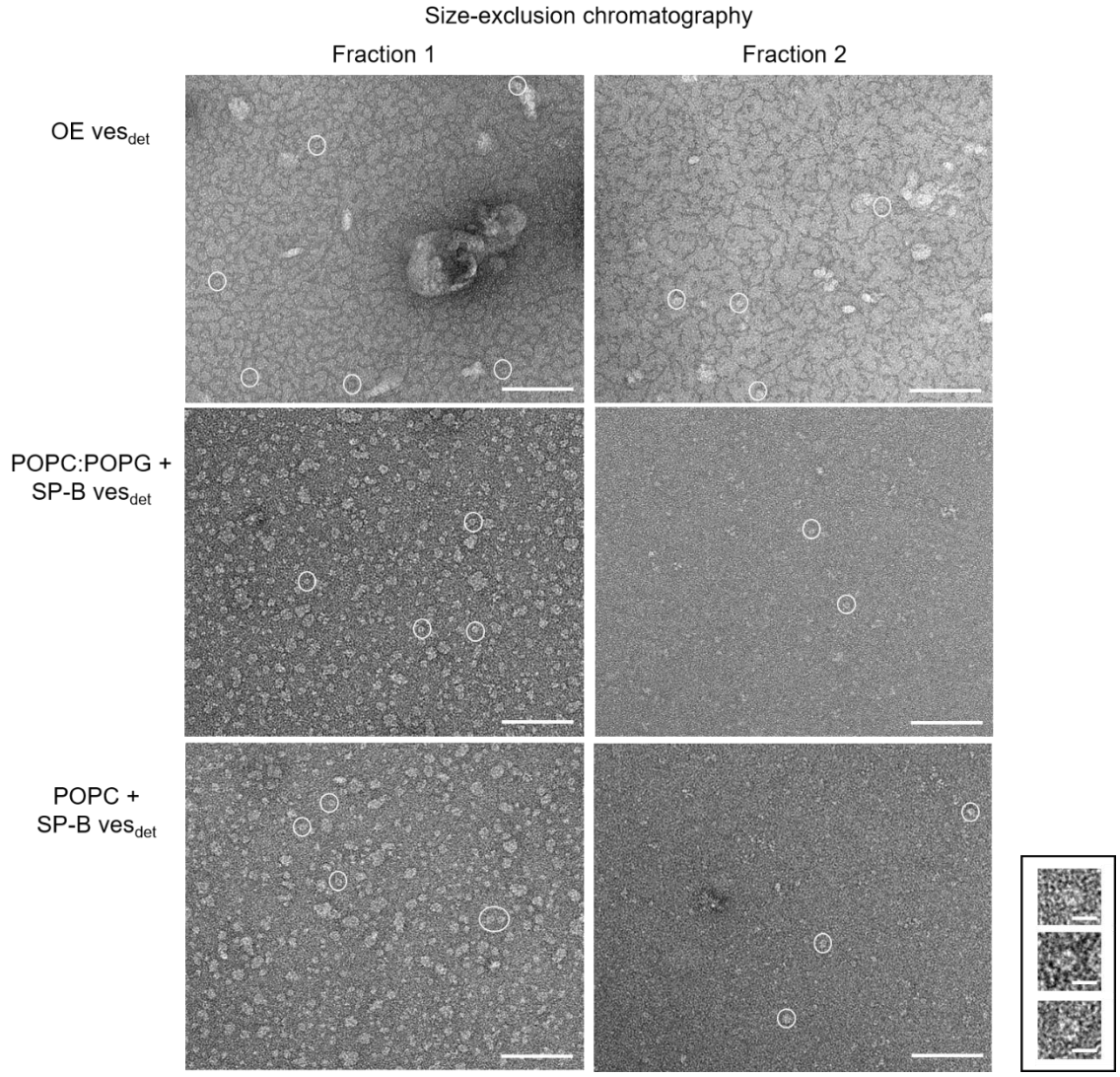

Figure 4.4. Transmission electron micrographs of fractions 1 and 2 obtained from size-exclusion chromatography of the different vesicle preparations solubilized by CHAPS. Samples were negatively stained for TEM. White circles label ring-shaped particles of 10 nm of average diameter. Scale bars, 100 nm. Enlarged views of some ring-shaped particles from the different vesicle suspensions solubilized by CHAPS are shown on the right panel (scale bars, 10 nm).

1.2.3. BIOCHEMICAL ANALYSIS OF SP-B/SP-C INTERACTIONS BY PROTEIN CROSSLINKING

Chemical crosslinking is a widely used method to covalently stabilize protein-protein interactions. In this chapter, a number of crosslinking reactions were performed to characterize possible macromolecular assemblies containing SP-B and SP-C in the pulmonary surfactant system. The results from the previous section suggested that protein macromolecular assemblies of pulmonary surfactant are re-established upon membrane reconstitution of pulmonary surfactant derivatives isolated in organic solvent. To further

investigate the protein interactions involved in the generation of such assemblies, the starting material for these experiments included vesicles made of lipid fraction (LF) of pulmonary surfactant or mixtures of synthetic lipids supplemented with hydrophobic protein fraction (PF) (containing SP-B and SP-C, in their precise native proportion), a mixture of isolated SP-B and SP-C (close to physiological proportion, 1:1 (w/w)) or SP-B alone.

The first approach to crosslink SP-B oligomers themselves and together with SP-C was performed by dithiobis(succinimidyl propionate) (DSP). This agent is an amine-reactive crosslinker with N-hydroxysuccinimide (NHS) ester reactive ends and a cleavable disulfide bond in its 8-carbon spacer arm. Proteins generally contains several primary amines in the N-terminal segment of the protein and in the side chain of lysine reisudes which are targets for NHS-ester group at physiological pH. Particularly, SP-B contains two lysine residues per monomer and each SP-C monomer only have one lysine, as well as their respective amine terminal group. Small unilamellar vesicles (SUVs) containing PF, a mixture of SP-B and SP-C or SP-B at different protein concentrations, were subjected to crosslinking at different molar ratios DSP:protein (**Figure 4.5 A**). None of the conditions tested resulted in an efficient stabilization of SP-B complexes with the expected molecular weight of 87 or 104.4 KDa, depending on whether the structure is formed by the association of 5 or 6 covalent dimers, respectively (Olmeda *et al.*, 2015). However, most of SP-B showed an electrophoretic behavior compatible with the covalent dimer (17.4 KDa) and assemblies of two covalent dimers (34.8 KDa). Smears of protein with higher molecular weights were detected for all conditions tested, although it is worthy to notice that crosslinked SP-B in LF vesicles showed four defined bands of high molecular weights labelled from B1 to B4 in **Figure 4.5 A**: B1 of approximately 200KDa, which could correspond to a decamer of SP-B dimers; B2, with a molecular weight around 75-100 KDa, might contain from pentamers to octamers of SP-B dimers; whereas B3 and B4 might be constituted by tetramers and trimers of SP-B dimers, respectively. On the other hand, no other protein assembly was detected for SP-C but its monomeric form (right panel in **Figure 4.5 A**), with an electrophoretic mobility of 10 KDa (as expected for SP-C in membranes, due to alteration of its electrophoretic behavior by the presence of lipids). Concerning the effect of DSP concentration, a progressive loss of material was detected when molar ratios above 50:1 were tested. This fact might be due to an excessive crosslinker concentration, which could negatively affect protein stability, promoting its aggregation. To increase the detection of possible protein oligomers, higher protein concentrations were assessed. To this end, crosslinking experiments by DSP were performed with POPC:POPG (7:3, w/w) SUVs containing PF 10% (protein to lipid, weight), a mixture of SP-B and SP-C (at its roughly physiological mass proportion 1:1, with a 5% of each protein) or SP-B alone at 10%. Crosslinking reactions were performed

with molar ratios DSP to protein varying from 10:1 to 100:1. **Figure 4.5 B** shows for all reactions that SP-B was detected as a smear with molecular weights lower than 71 KDa. In the case of SUVs with 10% SP-B, a band < 31 KDa can also be distinguished, which would correspond to covalent SP-B dimers.

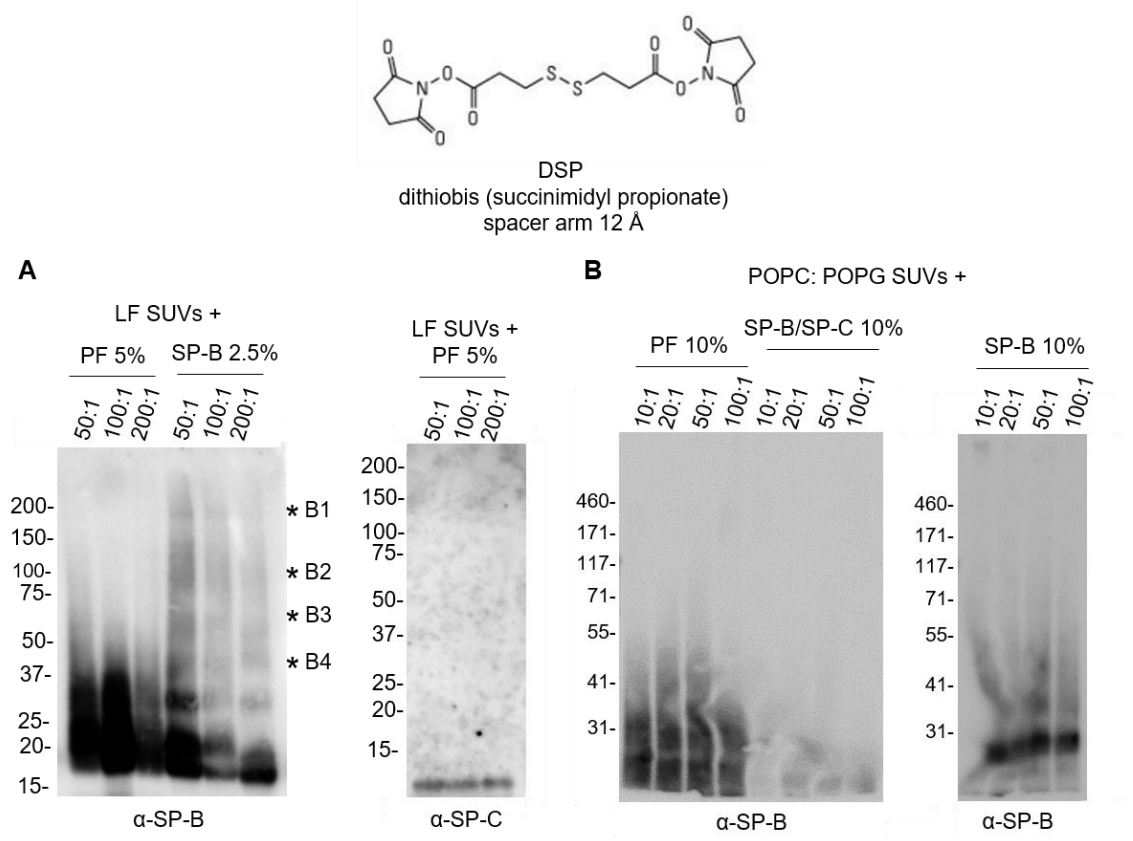

Figure 4.5. SDS-PAGE analysis of surfactant protein complexes after crosslinking by DSP. A) Anti SP-B and anti SP-C western blots of small unilamellar vesicles (SUVs) made by lipid fraction (LF) of pulmonary surfactant containing the hydrophobic protein fraction (PF) 5% (w:w, protein:lipid) or SP-B 2.5% (w/w). **B)** SUVs made by a mixture of POPC:POPG (7:3, w:w) supplemented with PF 10%, a mixture of isolated SP-B and SP-C (5% of each protein, according to its approximate physiological ratio 1:1, in mass) or SP-B 10% (w/w). Crosslinking assays were performed at different crosslinker:protein molar ratios, which are indicated over each line. SDS-PAGE were run into 4-20% polyacrylamide gels.

Although DSP is a membrane permeable crosslinker, which could be in principle favourable for membrane proteins, crosslinking efficiency for SP-B and SP-C oligomers resulted very poor, as previously shown, so next approach involved the use of an alternative sulfonated amine-reactive crosslinker, bis(sulfosuccinimidyl)suberate (BS^3). BS^3 is a water-soluble crosslinker, widely used to crosslink proteins in the external plasma membrane of cells, due to its inability to permeate through membranes. It is important to consider that the presence of SP-B and SP-C imparts to phospholipid membranes a high permeability to a polar molecules (Parra *et al.*, 2011). In this work, a range of molar ratios BS^3:protein was used to crosslink SP-B and SP-C reconstituted in small vesicles with different lipid/protein composition. Again, the SDS-PAGE analysis showed a low yield of crosslinking reactions for all BS^3 concentrations (**Figure 4.6**). Most of SP-B was forming entities of low molecular weight, although weak bands of high molecular weight were detected, which showed similar molecular weights to bands B1 to B4 distinguished in crosslinking of SP-B-supplemented LF vesicles by DSP (**Figures 4.5 A** and **4.6 A-B**).

In the case of SP-C, only SP-C monomers were detected in the suspensions containing PF and a mixture of isolated SP-B and SP-C. Concerning the lipid composition of vesicles, lipid fraction (LF) of pulmonary surfactant and the synthetic mixture POPC:POPG (7:3) showed similar crosslinking yields.

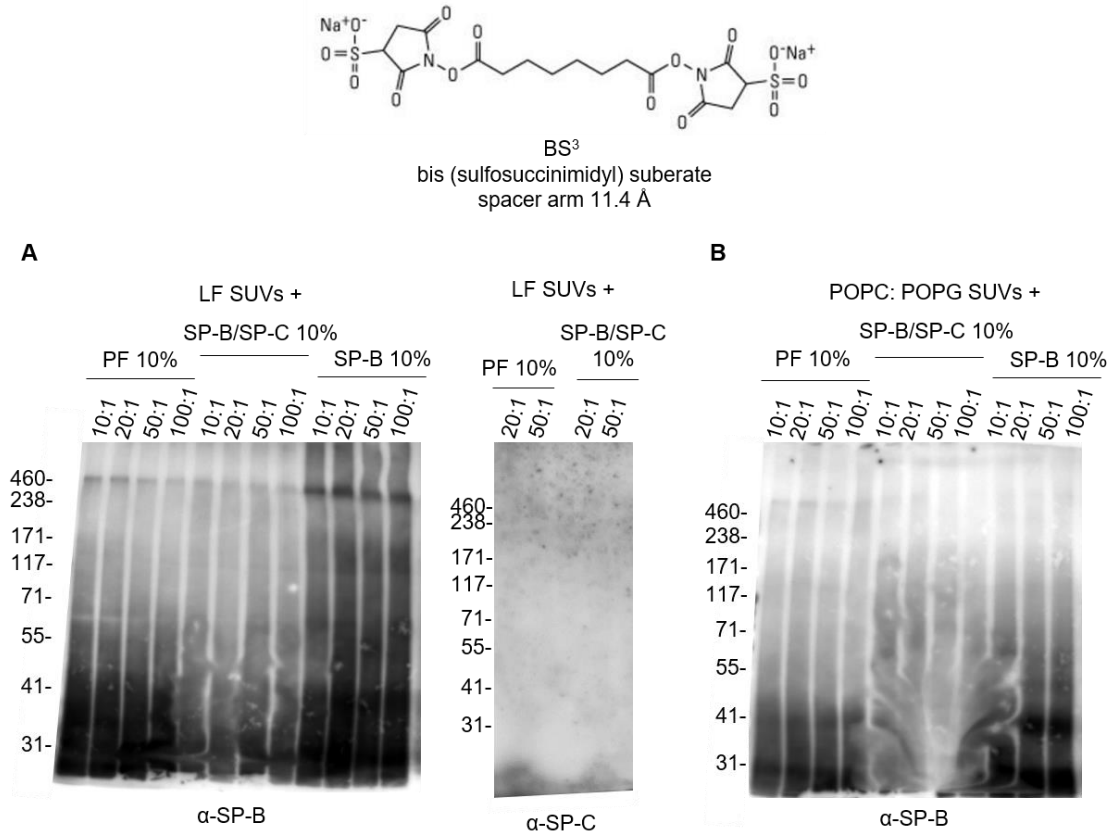

Figure 4.6. SDS-PAGE analysis of surfactant protein complexes upon crosslinking by BS^3. Small unilamellar vesicles (SUVs) were made by lipid fraction (LF) (A) or a mixture of POPC:POPG (7:3,w:w) (B) containing the hydrophobic protein fraction (PF) 10% (w:w, protein:lipid), a mixture of isolated SP-B and SP-C (5% of each protein, according to its physiological ratio 1:1, in mass) or SP-B 10% (w:w). Vesicles were crosslinked by BS^3 at different crosslinker:protein molar ratios, which are indicated over each line. SDS-PAGE was run into 4-20% polyacrylamide gels followed by western blots for SP-B and SP-C detection.

The existence of a tridimensional model structure for SP-B oligomers based on the structure of Saposin B (Olmeda *et al.*, 2015) resulted to be a useful tool to determine expected distances between amine groups of amino acid residues susceptible to conjugation by NHS-ester of bifunctional crosslinking reagents. Distances between primary amine residues of adjacent covalent SP-B dimers were measured using Pymol Software. Thus, the interdimer distances between amine groups of side chain of lysine varied from 10.8 to 31.1 Å, whereas distances varying from 9.7 to 36.5 Å were measured between side chains of lysine and amino group of the N-terminal end of the protein. In case of intradimer distances between amino groups of N-terminal region, measured values increased to 57.3-67.3 Å.

As both amine-reactive crosslinkers DSP and BS3 have spacer arms of 12 and 11.4 Å, respectively, the length of these spacers restrict largely the number of amine group pairs

in SP-B complexes that can be available for the crosslinking reactions. PEGylated bis(sulfosuccinimidyl)suberate [BS(PEG)$_9$] emerged as a reasonable alternative. This is a water-soluble amine-reactive crosslinker with a flexible polyethylene glycol spacer between NHS esters, which result in a spacer arm length of 35.8 Å. A number of crosslinking reactions were performed to target SP-B complexes, varying lipid composition and size of vesicles, as well as temperature and duration of crosslinking reaction. In this set of experiments, SP-B was reconstituted in membranes of two different synthetic lipid mixtures, POPC:POPG (7:3) and DPPC:POPC:DPPG (5:2.5:1.5). The latest one mimics the phospholipid composition of pulmonary surfactant but in the absence of phospholipid with primary amine groups, such as phosphatidylserine (PS) or phosphatidylethanolamine (PE). PS and PE only represents about 8 % in mass of the total phospholipid content of pulmonary surfactant (Blanco and Perez-Gil, 2007), but their presence could interfere to some extent in the protein conjugation with NHS esters of BS(PEG)$_9$. The electrophoretic analysis of crosslinked samples showed that neither the use of a crosslinking agent with a long spacer arm neither the substitution of FL by a mixture of synthetic lipids free of PS and PE enhanced crosslinking efficiency for SP-B complexes (**Figure 4.7 A-B**). Moreover, in an attempt to improve the yield of crosslinking, we performed the experiments with vesicles containing those proteolipid mixtures diminishing the reaction temperature from 37ºC to 25ºC, for 30 min, or to 4ºC during 2 hours. However, decreasing the crosslinking reaction rate did not lead to favor the stabilization of SP-B oligomers (data not shown). Finally, SP-B complexes purified in CHAPS from detergent-solubilized pulmonary surfactant were subjected directly to crosslinking by BS(PEG)$_9$ at different concentrations. However, the subsequent SDS-PAGE analysis showed that SP-B was mostly found as covalent dimers or as assemblies of two covalent dimers (**Figure 4.7 C**). Therefore, BS(PEG)$_9$ was not able to stabilize high molecular weight oligomers of SP-B. To sum up, none of the protein crosslinking experiments in this section allowed to confirm the existence of SP-B oligomers nor SP-B/SP-C interactions.

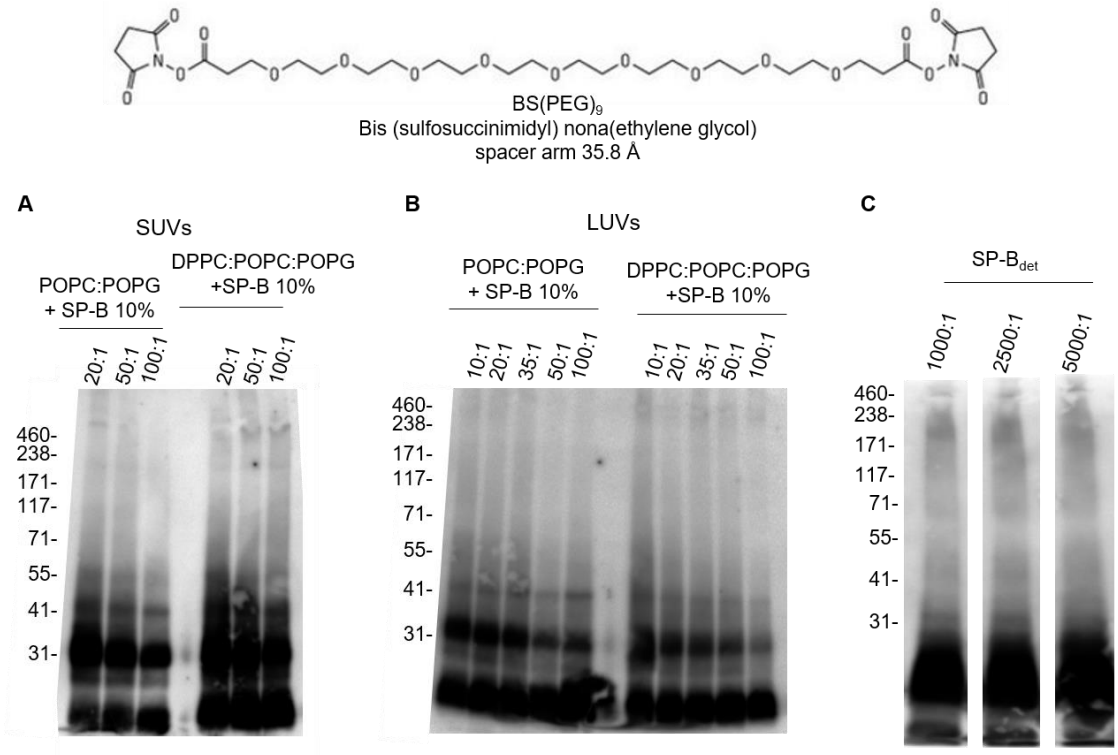

Figure 4.7. SDS-PAGE analysis of SP-B complexes upon crosslinking by BS(PEG)$_9$. Small unilamellar vesicles (SUVs) **(A)** or large unilamellar vesicles (LUVs) **(B)** made by a mixture of POPC:POPG (7:3, in mass) or DPPC:POPC:DPPG (5:2.5:1.5, in mass) containing SP-B 10% (w:w, protein:lipid). **(C)** A sample containing SP-B complexes purified from detergent-solubilized pulmonary surfactant was directly subjected to crosslinking. All suspensions were crosslinked by BS(PEG)$_9$ at different crosslinker:protein molar ratios, which are indicated over each line. SDS-PAGE were run into 4-20% polyacrylamide gels followed by western blots for SP-B detection.

1.2.4. PULMONARY SURFACTANT COMPLEXES INCORPORATED INTO MSP NANODISCS

Pulmonary surfactant membranes were reassembled into MSP1D1 nanodiscs to study surfactant protein-lipid complexes through their compositional analysis. The first step of the nanodiscs formation method is the solubilization of pulmonary surfactant membranes by detergent. Here, PS solubilization was performed by the ionic detergent cholate or by CHAPS, a zwitterionic detergent. Next, cholate-solubilized scaffolding protein MSP1D1 (final molar ratio 100:1, phospholipid to MSP1D1) was added to solubilized PS and by a detergent removal step, nanodiscs were self-assembled containing lipoprotein components of PS. To purify the assembled nanodiscs, an immobilized metal ion affinity chromatography (IMAC) was performed (**Figure 4.8**). Thanks to the His$_6$tag attached to the MSP1D1 N-terminal region, nanodiscs were retained in Ni^{2+}-NTA resin until its elution with imidazole. The electrophoretic analysis showed that nanodiscs formed from cholate-solubilized PS scarcely contain SP-A and SP-B. The vast proportion of these proteins were found in the non-retained fraction of the IMAC. In the case of SP-C, this protein was not detected at any fraction. On the other hand, nanodiscs generated from

CHAPS-solubilized PS included SP-B, SP-C and a little proportion of SP-A. However, most of SP-A and also part of SP-B and SP-C were not incorporated into nanodiscs, being found in the non-retained fraction of the chromatography. These results suggest that CHAPS yields better solubilization of PS membranes than cholate, achieving nanodiscs enriched in surfactant proteins. Therefore, a new purification of nanodiscs was performed with a higher amount of CHAPS-solubilized PS (four times) in order to improve the detection of surfactant components confined into nanodiscs (blue dashed line in IMAC profile, **Figure 4.8**).

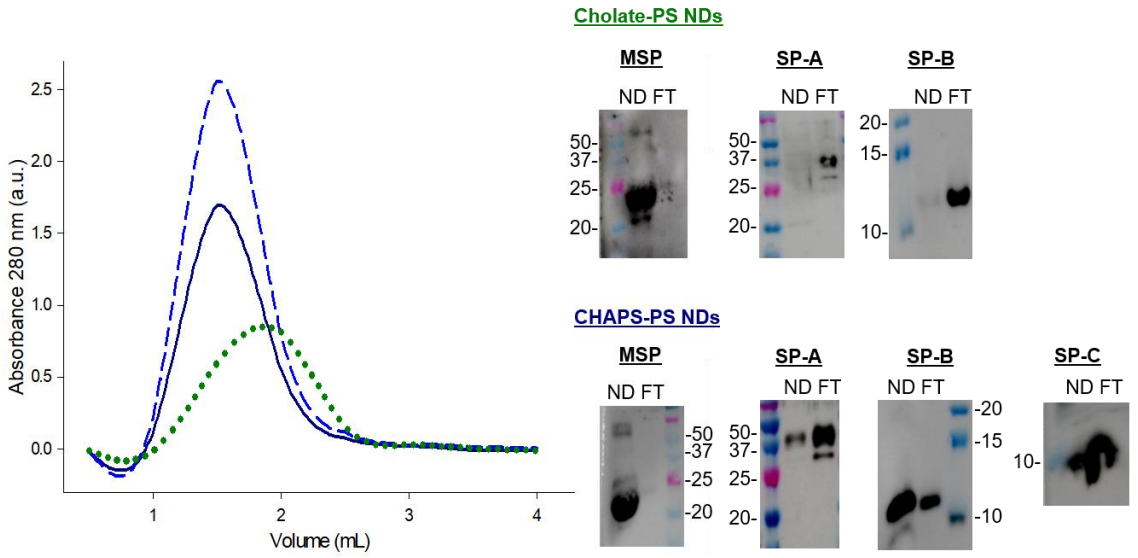

Figure 4.8. Incorporation of pulmonary surfactant complexes into MSP1D1 nanodiscs (molar ratio 100:1, phospholipid to MSP1D1). Immobilized Ni^{2+} affinity chromatography was performed from suspensions containing nanodiscs assembled together with PS solubilized by different detergents: 56 mM of PS solubilized by cholate at a molar ratio detergent:phospholipid of 3.5:1 (dotted green line), PS (56 mM) solubilized by CHAPS at molar ratio 6:1 (dark blue line), CHAPS-solubilized PS (224 mM) at molar ratio 6:1 (light blue dashed line). Left panel shows the chromatography profiles of the different preparations eluted with 500 mM imidazole-supplemented Tris buffer, pH7.4. Right panel: SDS-PAGE analysis under reducing conditions of IMAC eluted fractions (named as nanodisc fraction, ND) and the flow-through (FT) non-retained fractions from nanodiscs of CHAPS-solubilized and cholate-solubilized PS at low phospholipid concentration. Immunoblots were performed for detection of SP-A, SP-B, SP-C and His-tag (MSP).

To continue the study of surfactant complexes, the three different PS nanodiscs suspensions were subjected to size-exclusion chromatography in a Superdex 200 column. Nanodiscs assembled with CHAPS-solubilized PS were separated in different peaks according to its size (**Figure 4.9 A**). Peak 1 was composed by a minor proportion of MSP, SP-A and SP-B. Early elution of this fraction would be related to the presence of high molecular weight protein complexes, such as SP-A octadecamer (~ 630 KDa) and, likely, SP-B oligomers. Most of SP-B and SP-C were confined to nanodiscs eluted into two overlapped peaks, were peak 3 contained nanodiscs with SP-B and SP-C and peak 4 was constituted by nanodiscs that seem to contain only a low amount of SP-C. Moreover, free MSP and SP-B were eluted at the end of the SEC, pointing to the presence of free protein not incorporated into discs. On the other hand, nanodiscs formed from cholate-solubilized

PS seemed to consist of a more homogeneous suspension in size, where only SP-B could be detected in the peak containing nanodiscs (peaks 3 and 4) (**Figure 4.9 C**). However, the presence of SP-A and SP-C could not be discarded due to the low PS concentration used for nanodiscs formation. Besides this, it's noteworthy to point out the huge proportion of MSP which is not assembled into nanodiscs, as shown by the last peak of the SEC profile. Comparing nanodiscs formed by CHAPS-solubized PS and by cholate-solubilized PS, both at low concentration of phospholipid (**Figure 4.9 B-C**), it is clear that the use of CHAPS favors the insertion of protein complexes into nanodiscs.

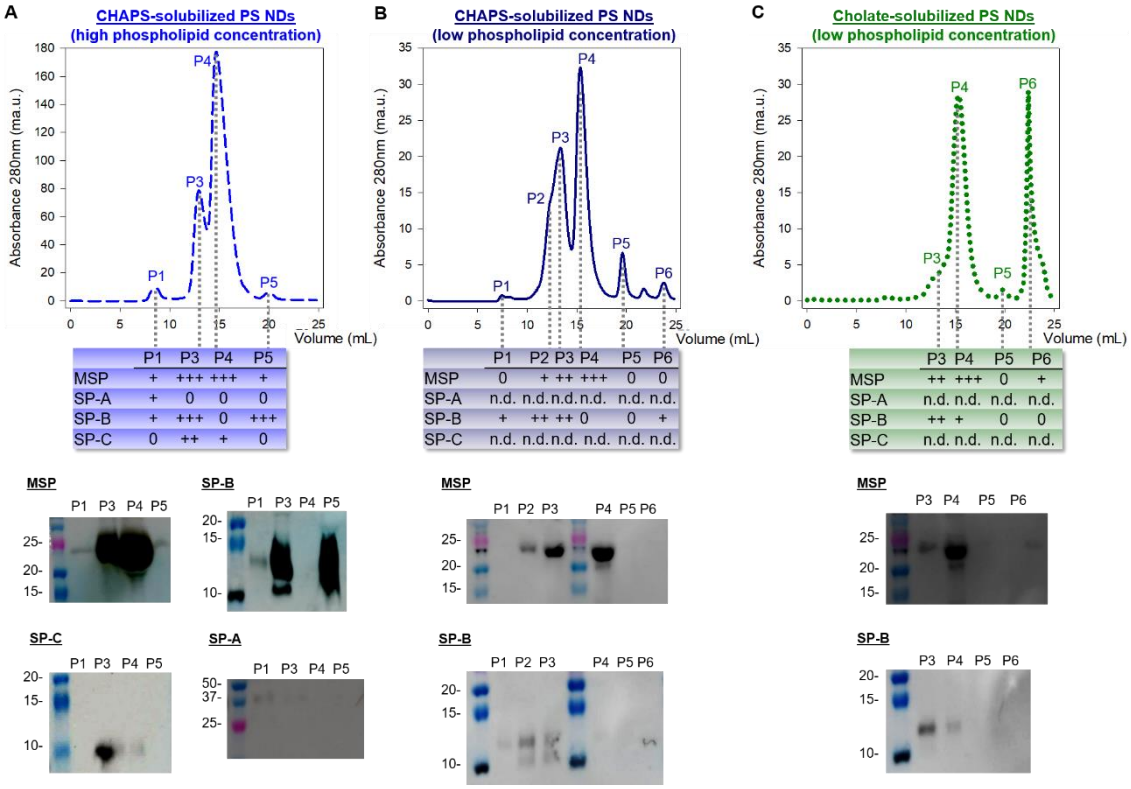

Figure 4.9. Analysis of nanodiscs formed from pulmonary surfactant. Size-exclusion chromatography (SEC) profiles in a Superdex 200 10/300GL column and subsequent SDS-PAGE analysis under reducing conditions of three different preparations of nanodiscs assembled from: **(A)** CHAPS-solubilized PS (224 mM of phospholipid) at molar ratio 6:1 (detergent: phospholipid), **(B)** CHAPS-solubilized PS (56 mM) solubilized by CHAPS at molar ratio 6:1 and **(C)** cholate-solubilized PS (56 mM) at molar ratio 3.5:1. Immunoblots were performed for detection of SP-A, SP-B, SP-C and His-tag (MSP). Tables show the relative amount of protein detected for each chromatography profile; it is also indicated when the protein was not detected (n.d.) throughout the chromatogram.

Following with the characterization of the pulmonary surfactant nanodiscs, the suspension containing nanodiscs from CHAPS-solubilized PS and its fractions obtained by SEC were subjected to a lipid compositional analysis by TLC (Thin Layer Chromatography) (**Figure 4.10**). The idea was to determine whether the different proteins or complexes could be associated to particular lipid species. Results showed that the original PS nanodiscs suspension seemed to be formed mainly by phosphatidylcholine (PC), as well as phosphatidylinositol/phosphatidylserine (PI/PS). Regarding the lipid composition of fractions 1-4 of pulmonary surfactant nanodiscs subjected to SEC,

nanodiscs of peak 3, enriched in SP-B and SP-C, contained mainly PC and PI/PS, as well as phosphatidylethanolamine (PE) and PG, in minor proportion. In the case of peak 4, in which SP-C was previously detected, nanodiscs contained PC and PI/PS, in lower amount. No lipid content was detected for peak 1 and 5, probably due to low sample concentration.

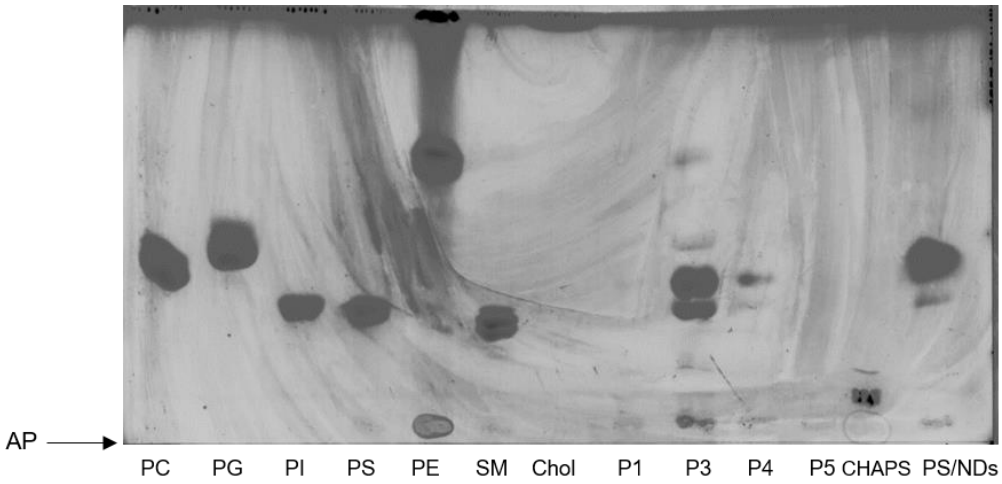

Figure 4.10. Compositional analysis of lipids contained in nanodiscs formed from CHAPS-solubilized PS (224 mM of phospholipid). The original PS nanodiscs suspension (PS/NDs) and fractions obtained from SEC were subjected to a thin layer chromatography (TLC). AP indicates the application point of the samples. Synthetic lipids were also loaded to compare migration of the main surfactant lipids. PC: phosphatidylcholine, PG: phosphatidylglycerol, PI: phosphatidylinositol, PS: phosphatidylserine, PE: phosphatidylethanolamine, SM: sphingomyelin, Chol: cholesterol.

This work analyzed for the first time the composition of lipoprotein complexes in pulmonary surfactant applying the MSP nanodiscs technology, although results obtained suggested that there was scope for improvement. For instance, SEC profiles showed that some SP-B remained out of nanodiscs (**Figure 4.9 A-B**), which could be overcome by increasing the MSP1D1 concentration. Therefore, new pulmonary surfactant nanodiscs were assembled with an increased molar ratio of phospholipid to MSP1D1 of 50:1, in comparison to the ratio 100:1 used in previous experiments. After purification by IMAC of these PS nanodiscs, which contained SP-A, SP-B and SP-C (**Figure 4.11 A**), the sample was subjected to size-exclusion chromatography (**Figure 4.11 B**). SEC profile showed poorly resolved peaks. Despite this, protein composition of different collected fractions was analyzed, showing the presence of a huge amount of assembled empty nanodiscs, which did not contain any surfactant protein (fractions 5/6). Moreover, a considerable amount of non-assembled MSP1D1 was found (fraction 8). All together, the results pointed to a wide excess of MSP1D1 over total pulmonary surfactant content. On the other hand, nanodiscs containing SP-B and SP-C (fractions 3/4) were detected, and a peak containing only SP-B (fractions 1-2) was also found. Although no other protein was detected in this fraction, it is likely that besides SP-B, it also contained a little amount of SP-A, as in peak 1 of **Figure 4.9 A**. In order to attempt the separation of loaded nanodiscs

from empty discs formed as a consequence of the excess of MSP, an ion exchange chromatography was subsequently performed with discrete increasing of ionic strength, taking advantage of the difference in charge between the anionic protein MSP1D1 and the cationic surfactant proteins SP-B and SP-C at pH 7. However, this chromatography did not allow a proper separation of both types of nanodiscs (data not shown).

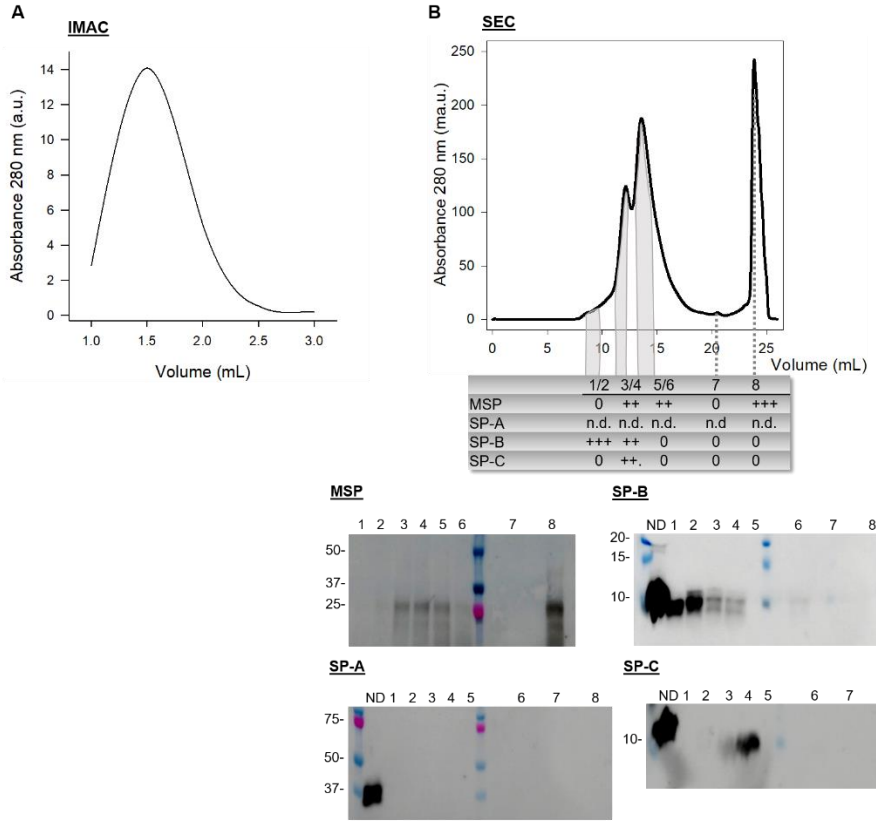

Figure 4.11. Assembly of CHAPS-solubilized surfactant into MSP1D1 nanodiscs, at a molar ratio phospholipid:MSP of 50:1. A) IMAC profile of eluted PS nanodiscs with 500 mM imidazole. **B)** SEC profiles of pulmonary surfactant nanodiscs in Superdex 200 10/300GL column and SDS-PAGE analysis. Immunoblots were performed for detection of SP-A, SP-B, SP-C and His-tag (MSP). Tables show the relative amount of protein detected for each chromatographic fraction; it is also indicated when the protein was not detected (n.d.) throughout the chromatogram. ND: eluted fraction of PS nanodiscs obtained from IMAC.

4.3. DISCUSSION

Solubilization of pulmonary surfactant membranes by CHAPS was implemented in a previous work (Olmeda, 2011). In that work, an extensive study of solubilization of pulmonary surfactant membranes was performed by using different detergents, including CHAPS, dodecyl maltoside and digitonin. CHAPS resulted to be the most efficient detergent to solubilize PS membranes, extracting native complexes of diverse high molecular weights. Further analysis by gradient density centrifugation and size-exclusion chromatography showed that surfactant native complexes purified by this detergent were clustered around two populations, different in density, size and amount of associated lipid, but both containing SP-A, SP-B and SP-C.

In the present work, these native surfactant protein complexes purified in CHAPS were biochemically analyzed by 2D BN/SDS-PAGE. This method allows to identify individual proteins from complexes in combination with immunoblotting or mass spectrometry analysis. Three serum proteins have been detected forming somehow part of pulmonary surfactant complexes: albumin, transferrin and immunoglobulin. It is known that serum proteins can also participate in the progression of lung injury, as their physiological levels increase during lung edema and inflammation (Hallman, Sarnesto and Bry, 1994; Wattiez *et al.*, 1999; Shirahama *et al.*, 2010; Okamoto *et al.*, 2012). However, previous proteomic analysis of healthy human BAL already revealed the presence of these three proteins with relevant physiological, antioxidant and immunological function (Chen *et al.*, 2008; Nguyen *et al.*, 2014). In the case of immunoglobulins, it has been described that collectins SP-A and SP-D interact with these immune molecules in order to modulate the host defense response (Nadesalingam, Reid and Palaniyar, 2005; Lin and Wright, 2006; Vieira, Kung and Bhatti, 2017). In this way, structural studies revealed the presence of immunoglobulins and albumin in the alveolar lining fluid of normal rat lungs, as granular deposits, and closely associated to tubular myelin (Bignon *et al.*, 1975, 1976). Furthermore, albumin and transferrin were also detected in isolated LBs from healthy rat lungs (Wang *et al.*, 2008). The presence of albumin, immunoglobulin and transferrin in the native surfactant complexes purified by CHAPS indicates that these proteins are associated with pulmonary surfactant membranes under physiological conditions and strengthen the hypothesis of a potential role in the alveolar fluid.

Regarding surfactant proteins, 2D BN/SDS-PAGE revealed the existence of high order molecular weight structures containing SP-A, SP-B and SP-C under native conditions. However, protein complexes solubilized by CHAPS were partly disassembled during the first denaturing dimension of the electrophoresis. In this way, SP-A aggregates observed under native conditions underwent a dissociation process during denaturing electrophoresis, towards the generation of dimers, trimers and higher oligomeric structures, such as hexamers or octadecamers, as previously described (Sánchez-Barbero *et al.*, 2005). Concerning SP-C, native complexes of this protein were also observed under native conditions, but were completely disassembled in the presence of SDS into entities below 37 KDa, which would correspond to monomers and dimers. The presence of SP-C oligomers under native conditions is not completely unexpected, as dimerization and further oligomerization have been previously suggested (Kairys, Gilson and Luy, 2004; Luy *et al.*, 2004; Roldan, Pérez-Gil, *et al.*, 2017). In the case of SP-B, unlike SP-C, a significant part of the protein remained associated in complexes with high molecular weight (150-50 KDa) after the denaturing process, pointing to a higher stability of the interactions involved in SP-B supramolecular assemblies.

In this regard, a previous study revealed the existence of an oligomeric structure of SP-B under native conditions (Olmeda *et al.*, 2015). Upon surfactant solubilization by CHAPS, SP-B is assembled into ring-shaped complexes with 10 nm of diameter, visualized by electron microscopy or atomic force microscopy. These obtained particles fitted reasonably well with a three-dimensional structure model of SP-B based on the Saposin B structure, which predicted the potential formation of SP-B oligomers constituted by 5 or 6 SP-B covalent dimers (Olmeda *et al.*, 2015). Considering these data, the expected molecular weights for decamers and dodecamers of SP-B would be 87 and 104.4 KDa, respectively. The electrophoretic analysis of SP-B purified in detergents showed a diffuse pattern of bands of high molecular weight reflecting the existence of multiple associations of SP-B with diverse high order oligomerization states [as shown in Figure 4.3 C and (Olmeda *et al.*, 2015)]. In the present work, the compositional analysis of native complexes in CHAPS-solubilized surfactant by 2D SDS/SDS-PAGE revealed that a significant part of SP-B is assembled into high order oligomers, varying from 50 to 150 KDa. Moreover, under native conditions, SP-B oligomers seemed to be associated to SP-A or SP-C, yielding higher order hetero-oligomers.

In the case of SP-B and SP-C, both proteins were found together in native complexes of molecular weights ranged between 214 and 644 KDa. These native surfactant assemblies have been not only observed in solubilized pulmonary surfactant membranes, but also we have found that SP-B and SP-C are able to assemble into complexes larger than 140 KDa after membrane reconstitution of the organic extract from surfactant. In the same way, SP-B isolated in organic solvent is able to re-establish a high order oligomerization state once reconstituted in POPC/POPG model membranes. Moreover, upon detergent-solubilization of these types of vesicles (containing the whole hydrophobic fraction of PS or isolated SP-B), ring-shaped particles with 10 nm of average diameter were visualized by TEM, in agreement with SP-B oligomers purified by detergent (Olmeda *et al.*, 2015). Besides, these ring-shapes particles similar in size were also observed in detergent-solubilized POPC vesicles containing SP-B. Therefore, anionic phospholipids seemed not to be required for the oligomerization of SP-B, in contrast to what previously suggested (Olmeda *et al.*, 2015).

To sum up, these results would suggest the existence of SP-B/SP-C complexes, although the fact that the two proteins are detected at the same spots in a native electrophoresis or in 2D BN/SDS-PAGE is not necessarily a definitive proof for a real assembly of these proteins, as different complexes might co-localize with similar electrophoretic mobility. Nevertheless, in a very recent FRET (Förster Resonance Energy Transfer) study we have described the existence of SP-B oligomers and SP-B/SP-C heterocomplexes in surfactant membranes (Cabre *et al.*, 2018). That work also proposed that SP-B/SP-C interactions could dissociate arrays of two SP-B oligomers, favoring the

formation of SP-B/SP-C complex. However, the nature of these SP-B/SP-C interactions is not yet completely understood. Crosslinking studies performed during this chapter did not allow to elucidate the stoichiometry of the SP-B oligomer nor of the SP-B/SP-C heterocomplexes, even if these negative results do not imply that such interactions do not exist. There are some factors that may affect the yield of membrane protein crosslinking, among others, solubility of the reagent, the length of its structure and experimental conditions such as pH or temperature. Crosslinking experiments performed throughout the present chapter have looked after several possibilities for these variables. Besides, NHS-ester reagents are the most common used for protein labeling and crosslinking, as they react with primary amines of the side chains of lysines and the N-terminal group of the proteins at physiological pH. Apart from its respective amine terminal groups, SP-B has two lysines whereas SP-C is a 35-amino acid transmembrane polypeptide with only one lysine (K9) located in the junction between the transmembrane poli-valyl helix and the N-terminal amphipathic segment. It is worthy to consider that the scarce number of amine groups and their likely non-favorable location inside both proteins could have hindered the crosslinking reaction between them. Despite this, the existence of SP-B/SP-C complexes have been suggested in both native PS and reconstituted membranes from the organic extract of PS by 2D BN/SDS PAGE and native electrophoresis, respectively. This outcome would support the hypothesis that SP-B/SP-C interactions are involved in the synergistic action of both proteins that facilitate a proper biophysical function of pulmonary surfactant, by enhancing the interfacial adsorption of phospholipids, maintaining the stability of surface active films and modulating the architecture of phospholipid bilayers (Taneva and Keough, 1994d; Schurch *et al.*, 2010; Hobi *et al.*, 2016; Roldan *et al.*, 2016). Moreover, SP-B and SP-C are involved in regulating membrane permeability towards ions, polar and nonpolar molecules in a concerted way (Parra *et al.*, 2011, 2013). The role of SP-B and SP-C on the membrane permeability of pulmonary surfactant system will be extensively addressed in the Chapter 2.

Regarding SP-A/SP-B interactions, two dimensional electrophoresis have revealed the presence of complexes containing both proteins, with a high order of oligomerization. These heterocomplexes could be behind the formation of tubular myelin, which requires SP-B, SP-A, phospholipids and Ca^{2+} (Suzuki, Fujita and Kogishi, 1989). Although the functional role of this lattice structure of surfactant membranes is not known, it might perform a host defense function related to SP-A role in lung immunology (Perez-Gil, 2008). However, these SP-A/SP-B heterocomplexes could also accomplish a biophysical role at the respiratory alveolar surface. SP-B enhances the adsorption of phospholipids into the air-liquid interface. This activity is enhanced in the presence of SP-A (Schurch *et al.*, 1992; Rodriguez-Capote *et al.*, 2001). Besides this, SP-A is able to prevent the inhibition induced by albumin of the surface active film in the presence of SP-B and Ca^{2+},

maintaining minimal surface tensions under compression below 1 mN/m (Venkitaraman *et al.*, 1990). These facts suggest that supramolecular protein complexes of SP-B and SP-A could associate to the interfacial monolayer improving its stability during compression-expansion mechanics. Whether both proteins could be indirectly interacting through lipids (Sarker et al, 2011), or whether native SP-A/SP-B complexes are stabilized by direct protein-protein interactions remains an open question, although this hypothesis might be supported by the fact that SP-A prompts the formation of protein-rich phases in DPPC:PG monolayers containing SP-B (Taneva and Keough, 2000), and also by data obtained by FRET studies among both proteins (Nag *et al.*, 1996).

Lastly, MSP nanodiscs technology was applied to attempt the generation of a solubilized membrane protein library (SMPL) from pulmonary surfactant, and to test the possibility that some of the native surfactant protein or protein/lipid heterocomplexes could be found assembled together into nanodiscs. Some studies can be found at the literature taking advantage of this system for obtaining such membrane proteomes (Civjan *et al.*, 2003; Marty *et al.*, 2013). Nevertheless, nanodiscs are generally used to confine isolated proteins or small complexes, constituting a useful platform for interactomics studies. The implementation of nanodiscs formed from surfactant membranes required a previous optimization of the solubilization method of PS. Eventually, the solubilization of PS membranes with the zwitterionic detergent CHAPS enhanced the incorporation of proteins inside nanodiscs, in comparison to solubilization with cholate. Three different populations of particles were established according to its size, from largest to smallest: 1) aggregates containing MSP, SP-A and SP-B, 2) those with SP-B and SP-C, and 3) the smallest nanodiscs containing SP-C. However, the relative amount of each population is inversely proportional to its size. MSP1D1 generates nanodiscs with ~ 9.7 nm of diameter. Because of that, it is reasonable that confinement of a surfactant membrane patch containing a small protein of 3.7 KDa, SP-C, could be favorable against confining larger proteins such as SP-B oligomers. Moreover, the lipid composition analysis showed that nanodiscs containing SP-B and SP-C were formed essentially by PC, and also contain PI (or PS) and PG. Comparing the lipid composition of the original nanodisc suspension with the fraction of nanodiscs containing SP-B and SP-C, the latest one seemed to be enriched in anionic phospholipid. It is well-known that cationic proteins SP-B and SP-C establish preferential interactions with anionic phospholipids, such as PG and PI (Perez-Gil, Casals and Marsh, 1995). Results obtained in this line suggest that nanodisc technology can be an attractive tool to further investigate the properties of the protein complexes found.

The direct generation of nanodiscs from native surfactant membranes sheds also some light on the establishment of protein-protein interactions in this system. Separation of different types of discs with different size and protein composition confirms the existence

of native protein complexes in surfactant. So, we can conclude that both the electrophoretic analysis of solubilized surfactant membranes or of membranes reconstituted from its individual components, as well as the analysis of the solubilized membrane protein libraries generated from surfactant, strongly suggest the existence of SP-A/SP-B and SP-B/SP-C interactions in surfactant membranes, resulting in the assembly of protein complexes whose physiological role could have essential implications for a proper function of pulmonary surfactant.

Chapter 2

ROLE OF SURFACTANT PROTEIN COMPLEXES ON THE PERMEABILITY AND INTERFACIAL DYNAMICS OF PULMONARY SURFACTANT MEMBRANES

5. ROLE OF SURFACTANT PROTEIN COMPLEXES ON THE PERMEABILITY AND INTERFACIAL DYNAMICS OF PULMONARY SURFACTANT MEMBRANES

5.1. INTRODUCTION

The hydrophobic proteins SP-B and SP-C are determinant for the dynamics of the pulmonary surfactant system. The ability of these proteins to perturb membranes has been extensively studied. Interestingly, SP-B and SP-C are responsible for membrane permeability to ions and to hydrophilic and hydrophobic molecules (Parra *et al.*, 2011, 2013), supposedly through formation of pores into phospholipid membranes. On one hand, SP-B belongs to saposins, a family of membrane-associated proteins that include several cytolysins, which are able to induce membrane pore-forming structures (Olmeda, García-Álvarez and Pérez-Gil, 2013). The oligomeric structure of SP-B orientates parallel to the membrane surface, where would transfer lipids between membranes and interface (Olmeda *et al.*, 2015). On the other hand, the existence of SP-B/SP-C interactions has been described in membranes, which could modulate the proper arrangement of lipid-protein complexes in pulmonary surfactant (Cabre *et al.*, 2018). Furthermore, in the previous chapter we have also found the presence of both proteins at high molecular weight native complexes in surfactant, which also support the hypothesis of the existence of SP-B/SP-C interactions.

In the present chapter, the effects of proteins SP-B and SP-C on the permeability of pulmonary surfactant, as well as model membranes, have been analyzed by visualizing giant vesicles (GVs) made of different lipid/protein composition under fluorescence microscopy. The permeabilization effect of these proteins has been characterized by using polar fluorescent probes, such as calcein or fluorescently-labeled dextrans of different sizes, from 4 to 250 KDa. The latter have been used to determine the size range of molecules that are able to permeate through membranes containing SP-B and/or SP-C. Besides, this study is completed by characterizing the blockage of surfactant membrane permeability towards fluorescein isothiocyanate (FITC)-dextrans by incubation of the lipoprotein complexes with α-SP-B or α-SP-C antibodies.

Finally, to connect the ability of SP-B to permeate membranes with the role of the protein in facilitating the formation and dynamics of pulmonary surfactant films during respiratory cycles, the behavior of SP-B-containing surfactant complexes has been studied by captive bubble surfactometry, in the absence or presence of α-SP-B antibodies.

5.2. RESULTS

5.2.1. SURFACTANT MEMBRANE PERMEABILITY TOWARDS FLUORESCENT POLAR MOLECULES

5.2.1.1. Membrane permeability to fluorescent polar probes and estimation of pore size

Pulmonary surfactant membranes labelled with Rhodamine-DOPE (1,2-dioleoyl-sn-glycero-3-phosphoethanolamine) were reconstituted to form giant vesicles (GVs). Fluorescent microscopy experiments were performed in order to monitor the permeation of fluorescent polar molecules present in the solution through pulmonary surfactant GVs. The size of giant vesicles allowed us to visualize them directly by optical microscopy and evaluate the membrane morphology and the partition of a fluorescent probe in the sample simultaneously.

Figure 5.1 illustrates how calcein, a 623 Da fluorescent polar probe, is able to penetrate through bilayers in GVs made of whole pulmonary surfactant, confirming that pulmonary surfactant membranes are permeable to polar molecules. In order to further characterize the permeability of these membranes, we evaluated the ability of fluorescently labeled dextrans of different sizes, FITC-dextrans from 4 KDa to 250 KDa, to permeate through surfactant GVs. The results revealed that only small dextrans (up to 40 kDa) were able to permeate through surfactant vesicles, showing even higher fluorescence intensities inside the vesicles than at the external medium, whereas surfactant membranes turned out to be non-permeable to dextrans larger than 70 KDa (**Figure 5.1**). Membrane permeability for each dextran size was quantitatively determined as the percentage of permeated (filled) vesicles with respect to the total number of vesicles analyzed. Permeability ratios of surfactant GVs for each dextran size are included in the **table 5.1**.

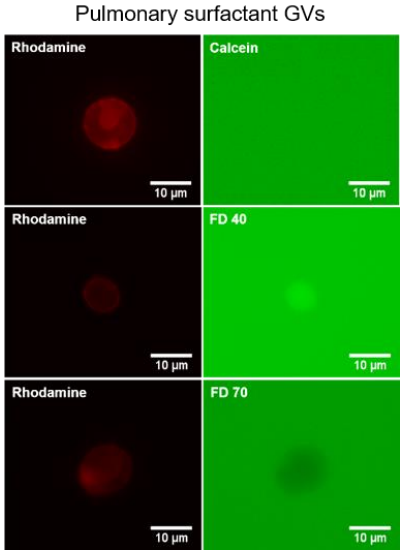

Figure 5.1. Permeability of pulmonary surfactant membranes. GVs made of pulmonary surfactant, labeled with Rhodamine-DOPE and incubated in the presence of calcein or FITC-dextrans with two different chain sizes (40 and 70 KDa). Red fluorescence signal of Rhodamine-DOPE labeled membranes is shown in the first column, and green fluorescence shown in the second column belongs to the corresponding fluorescent polar probe, calcein or FITC-dextrans.

To get a deeper insight of the determinants of this feature of pulmonary surfactant membranes, permeability of vesicles containing different surfactant components was analyzed. Firstly, the whole hydrophobic fraction of surfactant obtained by organic extraction (OE) was used to form GVs, which contained the lipids and hydrophobic proteins SP-B and SP-C. These OE GVs were permeable to FITC-dextrans up to 40 KDa (**Figure 5.2** and **table 5.1**), showing a similar permeability behavior to that of native surfactant membranes.

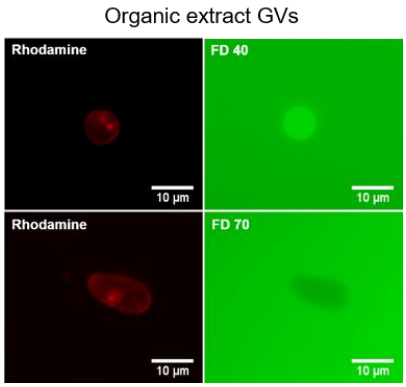

Figure 5.2. Permeability of reconstituted membranes from the organic extract of surfactant. GVs made of the organic extract of surfactant, labeled with Rhodamine-DOPE (red fluorescence signal) were incubated in the presence of FITC-dextrans with two different chain sizes, 40 and 70 KDa (green signal).

In contrast, when the protein-free lipid fraction of surfactant (LF), obtained by LH-20 chromatography of organic extract, was used to form GVs, not even calcein (623 Da) was able to permeate through the membranes, as shown in **Figure 5.3 A**. However, GVs made of the lipid fraction supplemented with the hydrophobic protein fraction of surfactant (PF) at 1% (w/w) returned to be permeable to FITC-dextrans up to 40 KDa, mimicking the permeability size threshold of pulmonary surfactant vesicles (**Figure 5.3 B** and **table 5.1**). In alternative experiments, isolated proteins SP-B and SP-C (separated from each other by LH-60 chromatography) were mixed, maintaining their physiological proportion with the lipid fraction of surfactant, to form GVs that turned out to be permeable to dextrans of higher sizes than the maximal size able to cross native surfactant membranes, becoming non-permeable only to probes larger than 250 KDa (**Figure 5.3 C** and **table 5.1**).

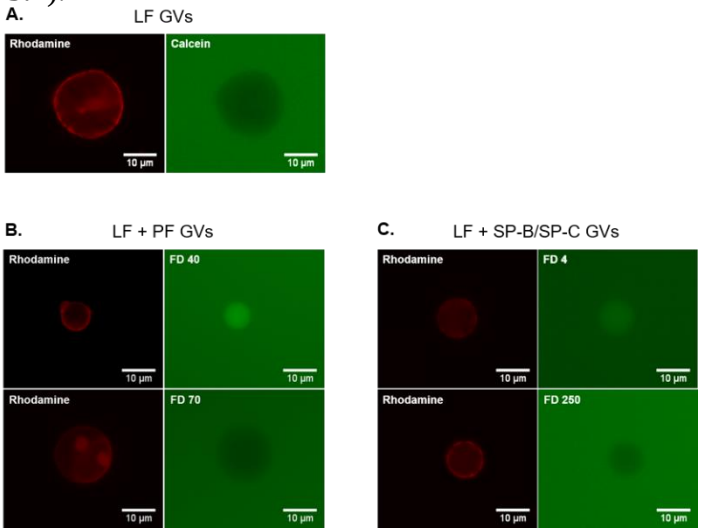

Figure 5.3. Permeability of membranes containing surfactant hydrophobic proteins. GVs were formed by protein-free surfactant lipid fraction (**A**), the lipid fraction supplemented with 1% (w/w) of the hydrophobic surfactant protein fraction (**B**) or with a mixture of purified SP-B and SP-C (0.5% (w/w) of each protein) (**C**). Membranes are labeled with Rhodamine-DOPE (red fluorescent signal) and incubated in a solution containing calcein or FITC-dextrans of two different chain sizes (40 and 70 KDa) (green signal).

Lastly, permeability of GVs made by the surfactant lipid fraction combined with isolated SP-B or SP-C was analyzed. Membranes containing 1% SP-B were found to be permeable to dextrans up to 70 KDa (**Figure 5.4 A**), whereas vesicles containing 1% SP-C showed permeability, in a higher or lower proportion, to every dextran from 4 KDa to 250 KDa (**Figure 5.4 B**). Regarding the morphology of these GVs, vesicles were substantially different depending on its composition. SP-B-supplemented LF GVs were mostly large oligolamellar vesicles, which tended to form vesicle aggregates. In contrast, SP-C GV suspension reflected a population of vesicles heterogeneous in size, with a relevant presence of vesicles smaller than 1 µm, which might be the result of vesicle fragmentation processes.

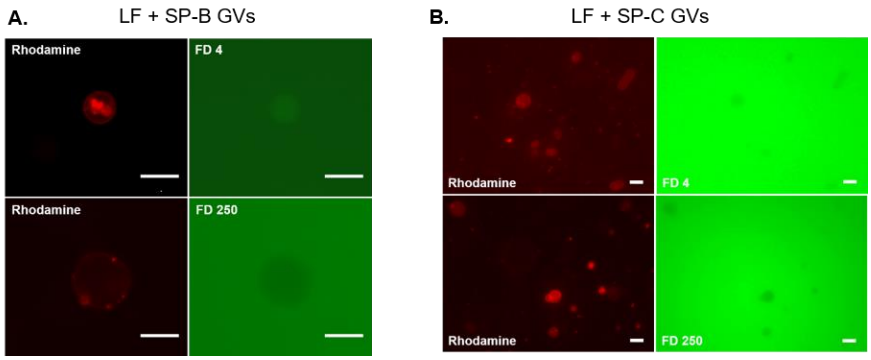

Figure 5.4. Permeability of membranes supplemented with SP-B or SP-C. GVs made of surfactant lipid fraction containing 0.5% (w/w) SP-B (**A**) or 0.5% (w/w) SP-C (**B**) were labeled with Rhodamine-DOPE (red) and incubated in the presence of FITC-dextrans (green) of two different chain sizes (4 and 250 KDa). Scale bars correspond to 10 µm.

For comparison of the several samples studied, **table 5.1** summarizes the permeability ratios to the different FITC-dextrans of the different tested vesicles. Vesicles made of whole native pulmonary surfactant, its organic extract or the mixture of lipid and the hydrophobic protein fractions (LF + PF) showed a comparable permeability, up to 40 KDa dextrans, yielding a cut off in hydrodynamic radius of the permeable dextrans of approximately 4.5 nm. On the other hand, GVs containing the lipid fraction with a mixture of purified SP-B and SP-C, or SP-B alone, yielded a higher threshold (about 6 nm), being permeable to dextrans up to 70 KDa. It is worthy to notice that GVs supplemented with SP-C did not show a marked boundary of permeability, but a progressive decrease of permeability to dextrans from FD40 to FD250. All these results suggest the existence of SP-B/SP-C complexes, with consequences in the pores of surfactant membranes, accounting for the permeability of surfactant to polar molecules.

FITC-dextran	R_h (nm)	PS	OE	LF + PF	LF + SP-B/SP-C	LF + SP-B	LF + SP-C
4 KDa	1.4	100 (0)	100 (0)	100 (0)	100 (0)	100 (0)	49.6 (3.9)
10 KDa	2.3	99 (1)	100 (0)	100 (0)	100 (0)	100 (0)	51 (1.4)
20 KDa	3.3	100 (0)	94 (2.8)	95.2 (1.2)	93 (4.2)	86 (8.5)	40.1 (4.8)
40 KDa	4.5	82 (5.7)	88 (2.8)	86 (2.83)	87.1 (1.6)	81 (4.2)	34.5 (1.7)
70 KDa	6	0 (0)	0 (0)	0 (0)	77 (4.2)	57.8 (3.1)	26.3 (3.2)
250 KDa	8.5	0 (0)	0 (0)	0 (0)	0 (0)	0 (0)	15.8 (2.9)

Table 5.1. Permeability of GVs made by different pulmonary surfactant components to fluorescent dextrans of different size. Tested GVs were made of PS, the native surfactant membranes, OE, the whole hydrophobic fraction of surfactant obtained by organic extraction, LF + PF, a mixture of surfactant lipid fraction and hydrophobic protein fraction 1% (w/w), LF + SP-B/SP-C, lipid fraction with a mixture of purified SP-B and SP-C (0.5% (w/w) of each protein), LF + SP-B, lipid fraction with SP-B 0.5% (w/w) and LF + SP-C, lipid fraction with SP-C 0.5% (w/w). Hydrodynamic radius (R_h) for each FITC-dextran is also indicated. Data are shown as mean percentage of permeable vesicles (standard deviation).

Regarding the lipid component of surfactant membranes, its influence on the generation of these SP-B/SP-C complexes and their effect on permeability was studied in two different model membrane systems. Pure POPC GVs or POPC:POPG (7:3) GVs containing different protein content were incubated with calcein or the set of FITC-dextrans from 4 KDa to 250 KDa. **Table 5.2** shows that the permeability to large polar molecules for pure POPC GVs varied depending on their protein composition, in this order: mixture of purified SP-B/SP-C < PF < SP-B. Meanwhile, POPC:POPG (7:3) GVs containing PF, SP-B/SP-C or SP-B shared the same cut off, being permeable to polar molecules up to 40 KDa. On the other hand, a clear threshold of permeability could not be determined for both SP-C-supplemented GVs, as described before for GVs made of the lipid fraction containing SP-C. Thus, in general, the presence of PG in the composition of GVs was necessary to allow permeability of membranes to dextrans of similar sizes to those permeabilizing through native surfactant.

Fluorescent probe	POPC				POPC: POPG (7: 3)			
	PF	SP-B/SP-C	SP-B	SP-C	PF	SP-B/SP-C	SP-B	SP-C
Calcein (0.6 KDa)	100 (0)	99 (1.4)	100 (0)	62.2 (39.3)	100 (0)	100 (0)	100 (0)	73 (26.9)
FITC-dextran 4 KDa	98.3 (2.4)	0 (0)	98 (2.8)	56.4 (45.9)	100 (0)	98.8 (1.7)	97 (1.2)	62 (29.7)
FITC-dextran 10 KDa	0 (0)	0 (0)	39.1 (10)	39.1(22.4)	93 (1.4)	86 (5.7)	77 (4.2)	45 (17)
FITC-dextran 20 KDa	0 (0)	0 (0)	18 (2.8)	40 (17)	91 (1.4)	70 (2.8)	64.3 (2.2)	37.5 (19.1)
FITC-dextran 40 KDa	0 (0)	0 (0)	0 (0)	31.4 (16.2)	87.1 (1.6)	47.2 (3.9)	46.8 (2.6)	32 (18.4)
FITC-dextran 70 KDa	0 (0)	0 (0)	0 (0)	27.7 (15)	0 (0)	0 (0)	0 (0)	29 (8.5)
FITC-dextran 250 KDa	0 (0)	0 (0)	0 (0)	22.4 (14.3)	0 (0)	0 (0)	0 (0)	22 (9.9)

Table 5.2. Permeability of GVs of two different lipid compositions, POPC and POPC:POPG (7:3), in the presence of different surfactant proteins. Either GVs were supplemented with the hydrophobic protein fraction (PF) 1% (w/w), a mixture of purified SP-B and SP-C (0.5% (w/w) of each protein), SP-B 0.5% or SP-C 0.5% (w/w). Data are shown as mean percentage of permeable vesicles (standard deviation).

5.2.1.2. Blockage of membrane permeability by antibodies

In order to further characterize the effect of these proteins on surfactant membranes, permeability of GVs containing different components of pulmonary surfactant towards FITC-dextrans was evaluated in the presence of antibodies against the hydrophobic surfactant proteins, SP-B and SP-C. The results are summarized in **table 5.3**.

A

FITC-dextran	LF + SP-B	+ α-SP-B	+ α-SP-C
4 KDa	100 (0)	44 (2.8)	97.1 (1.3)
10 KDa	100 (0)	33 (4.2)	96.1 (0.1)
20 KDa	86 (8.5)	22 (2.8)	86 (5.7)
40 KDa	81 (4.2)	11 (4.2)	81 (7.1)
70 KDa	57.8 (3.1)	2 (2.8)	58 (5.7)
250 KDa	0 (0)	0 (0)	0 (0)

B

FITC-dextran	LF + SP-B/SP-C	+ α-SP-B	+ α-SP-C
4 KDa	100 (0)	50.5 (3.6)	46 (2.8)
10 KDa	100 (0)	46 (5.7)	43 (4.2)
20 KDa	93 (4.2)	36 (2.8)	27 (15.6)
40 KDa	87.1 (1.6)	11 (1.4)	10(2.8)
70 KDa	77 (4.2)	0 (0)	0 (0)
250 KDa	0 (0)	0 (0)	0 (0)

C

FITC-dextran	LF + PF	+ α-SP-B	+ α-SP-C
4 KDa	100 (0)	43.3 (4.6)	42.8 (1.7)
10 KDa	100 (0)	42.8 (2.3)	12.4 (0.6)
20 KDa	95.2 (1.2)	30 (14.1)	26.4 (5.9)
40 KDa	86 (2.8)	14 (2.8)	18.5 (6.4)
70 KDa	0 (0)	0 (0)	0 (0)
250 KDa	0 (0)	0 (0)	0 (0)

D

FITC-dextran	OE	+ α-SP-B	+ α-SP-C
4 KDa	100 (0)	45 (1.4)	50 (5.7)
10 KDa	100 (0)	43.4 (0.8)	42.3 (0.4)
20 KDa	94 (2.8)	31.3 (1.8)	27.8 (0.4)
40 KDa	88 (2.8)	8.2 (3.1)	7 (4.2)
70 KDa	0 (0)	0 (0)	0 (0)
250 KDa	0 (0)	0 (0)	0 (0)

Table 5.3. Blockage of permeability of surfactant-based GVs to fluorescent dextrans by α-SP-B or α-SP-C antibodies. Different proteoliposomes were assessed: GVs made of the lipid fraction containing SP-B 0.5% (w/w) (**A**), of the lipid fraction combined with a mixture of purified SP-B and SP-C (0.5% (w/w) of each protein) (**B**) or of the lipid fraction plus the hydrophobic protein fraction 1% (w/w) (**C**), and GVs made by the whole organic extract from pulmonary surfactant (OE) (**D**). GVs pretreated or not with α-SP-B or α-SP-C antisera (1 μM IgG), were incubated with FITC-dextrans from 4 to 250 KDa. Data are shown as mean percentage of permeable vesicles (standard deviation).

GVs made of surfactant lipid fraction supplemented with SP-B were pre-incubated together with α-SP-B polyclonal antiserum (at a final IgG concentration of 1 μM) for 2 hours, before testing their permeability to fluorescent dextrans. Under these conditions, SP-B-containing LF GVs showed a significant reduction in their permeability to polar molecules (**Table 5.3**). To discard non-specific effects of the antibody, the same GVs were also pretreated with α-SP-C polyclonal antiserum (final IgG concentration 1 μM), which showed no blockage of permeability. On the other hand, GVs made of LF

combined with the hydrophobic protein fraction or a mixture of isolated SP-B and SP-C, as well as GVs made by the organic extract of surfactant, underwent a reduction of permeability towards polar molecules when pretreated with either α-SP-B or α-SP-C antisera (**Table 5.3**). As expected, in the case of GVs made of native pulmonary surfactant, pretreatment with different concentrations of α-SP-B or α-SP-C antisera led, in both cases, to a progressive blockage of permeability to polar molecules in a concentration-dependent manner, reaching the highest permeability impairment when pretreated with 5 µM antisera (**Figure 5.5**).

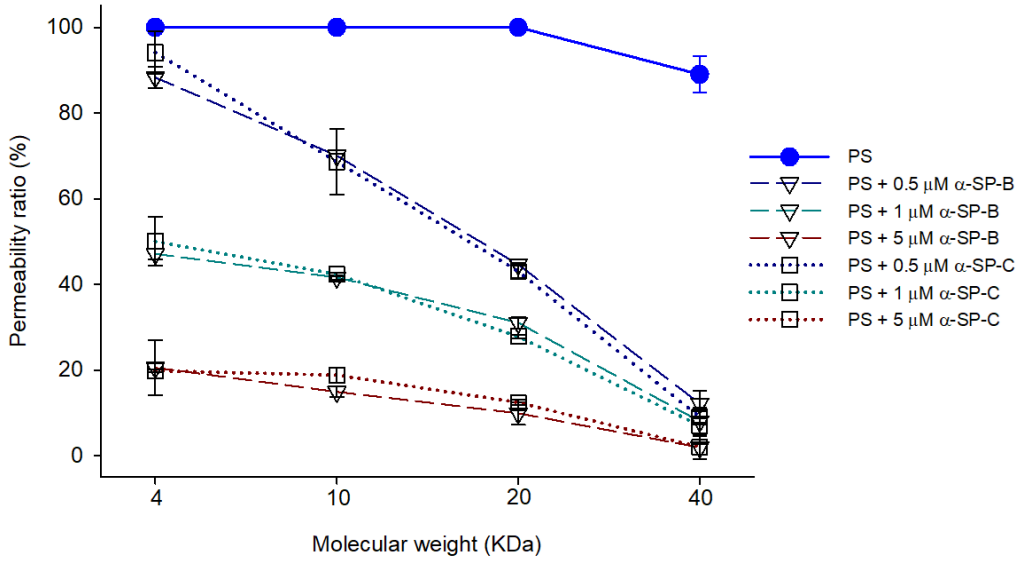

Figure. 5.5. Blockage of permeability towards FITC-dextrans in pulmonary surfactant GVs (PS) by using increasing concentrations of α-SP-B or α-SP-C antisera. Surfactant GVs were pre-treated with α-SP-B or α-SP-C antisera at concentrations of 0.5, 1 and 5 µM IgG. After that, GVs were incubated in FITC-dextrans from 4 to 40 KDa. Permeability ratio (%) was plotted for FITC-dextrans of different sizes.

To verify that the permeability of pulmonary surfactant vesicles was affected specifically by α-SP-B and α-SP-C immunoglobulins present in antisera, and not by any other antisera component, PS GVs were pretreated with 5 µM α-tubulin antiserum, showing no effect on permeability (**table 5.4**). These data confirmed that impairment of permeability in surfactant membranes was carried out by the specific interaction of the antibodies with SP-B and SP-C.

The hydrophilic protein SP-A can be associated with surfactant membranes, accomplishing a role in the biophysics of pulmonary surfactant (Cockshutt, Weitz and Possmayer, 1990; Schurch *et al.*, 1992; Sáenz *et al.*, 2007; Lopez-Rodriguez *et al.*, 2016). To examine whether SP-A would participate in the permeability of pulmonary surfactant membranes, native surfactant GVs were incubated with α-SP-A antiserum, and permeability of vesicles towards FITC-dextrans was analyzed. **Table 5.4** shows that this antibody did not affect the permeability of surfactant GVs to dextrans, suggesting that

SP-A is not involved in the modulation of permeability of surfactant membranes towards polar molecules.

FITC-dextran	PS	+ 5 µM α-SP-B	+ 5 µM α-tubulin	+ 5 µM α-SP-A
4 KDa	100 (0)	20.5 (6.4)	100 (0)	100 (0)
10 KDa	100 (0)	14.9 (1.3)	100 (0)	100 (0)
20 KDa	100(0)	9.9 (2.7)	100(0)	100(0)
40 KDa	89 (4.2)	1.9 (2.7)	94.2 (3)	93.5 (2.1)
70 KDa	0 (0)	0 (0)	0 (0)	0 (0)
250 KDa	0 (0)	0 (0)	0 (0)	0 (0)

Table 5.4. Permeability blockage of surfactant membranes by α-SP-A or a non-related surfactant antiserum. Permeability ratios (%) to FITC-dextrans of native pulmonary surfactant GVs (PS) pre-incubated with α-tubulin or α-SP-A antisera at a final Ig concentration of 5 µM. Data are shown as mean percentage of permeable vesicles (standard deviation).

5.2.2. FUNCTIONAL INHIBITION OF PULMONARY SURFACTANT BY α-SP-B ANTIBODY

In order to study the biophysical activity of pulmonary surfactant (PS) in the presence of a polyclonal α-SP-B antibody at conditions comparable to those producing permeability blockage, we evaluated its tensioactive function by captive bubble surfactometry (CBS). Upon injection of control PS (without pretreatment with the antibody) at a concentration of 4.7 mg/mL of phospholipid, surface tension dropped to 21.9 ± 0.8 mN/m after 5 minutes of initial adsorption and to 23.2 ± 0.6 mN/m after expanding the bubble for 5 minutes. **Figure 5.6** shows how pulmonary surfactant was able to dramatically decrease the surface tension in a few seconds, revealing that, at this low concentration, surfactant was able to efficiently and quickly adsorb and spread along the interface, as previously described (Schurch, Green and Bachofen, 1998). Cycling isotherms of pulmonary surfactant films showed almost no compression/expansion hysteresis along quasi-static and dynamic cycles. Marked hysteresis was only present in the first quasi-static cycle, during which the energy provided by the compression is employed to promote a structural transition of the film at the interface resulting in a depuration of the less active material out of the interface, the so-called “squeeze-out” (Schurch *et al.*, 1994). The subsequent cycles presented a progressive decrease in hysteresis as a result of the irreversible refinement of material at the interface. Pulmonary surfactant reached then minimal surface tensions ≤ 0.8 mN/m with ≤ 20% of area reduction during compression and a maximal surface tension lower than 32 mN/m during expansion.

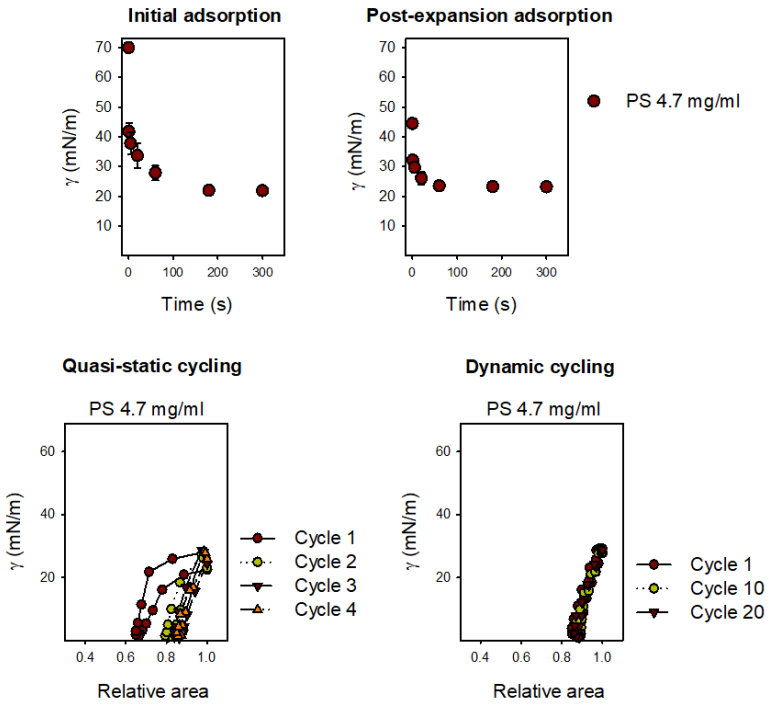

Figure 5.6. Surface active function of pulmonary surfactant. Captive bubble surfactometry of pulmonary surfactant at a phospholipid concentration of 4.7 mg/ml. Top: Initial and post-expansion adsorption kinetics. Data are mean ± standard deviation obtained from 3 independent experiments. Bottom: representative examples of quasi-static and dynamic compression-expansion cycling isotherms (n=3).

Blockage experiments of surfactant membrane permeability towards polar molecules were performed upon pre-incubation of PS GVs with a polyclonal α-SP-B antiserum. It has been previously described that some surface-active components of the serum, such as albumin, compete with pulmonary surfactant to reach the air-liquid interface, impeding the proper adsorption of surfactant and the formation of surfactant film (Lopez-Rodriguez *et al.*, 2012). Thus, evaluation of the functional inhibition of pulmonary surfactant films by α-SP-B antiserum required to set up experimental conditions that avoided the interference of serum in CBS experimental conditions. Pulmonary surfactant (4.7 mg/ml phospholipid) was incubated for 3 hours at 37ºC, together with serum at two different total protein concentrations, 5.1 and 3.8 mg/ml, as determined by Lowry assay. Then, the surface activity of these surfactant preparations was evaluated (**Figure 5.7**).

Pretreatment of PS with both serum concentrations showed efficient initial and post-expansion interfacial adsorption, reaching surface tensions at equilibrium near 20 mN/m. Cycling isotherms of surfactant films formed by PS pretreated with 5.1 mg/ml of serum showed an increased minimal surface tension, about 18 mN/m, with a marked hysteresis in every compression-expansion cycle. During the first dynamic cycle, minimal surface tension dropped to 1 mN/m, but surfactant film was no longer stable along the remaining cycles (**Figure 5.7**). On the other hand, cycling isotherms for PS pretreated with 3.8 mg/ml of serum reached minimal surface tension < 1 mN/m with only about 20% area

reduction during compression, with the exception of the presence of hysteresis in the first quasi-static cycle. Therefore, films formed by PS treated with serum 3.8 mg/ml maintained its interfacial activity.

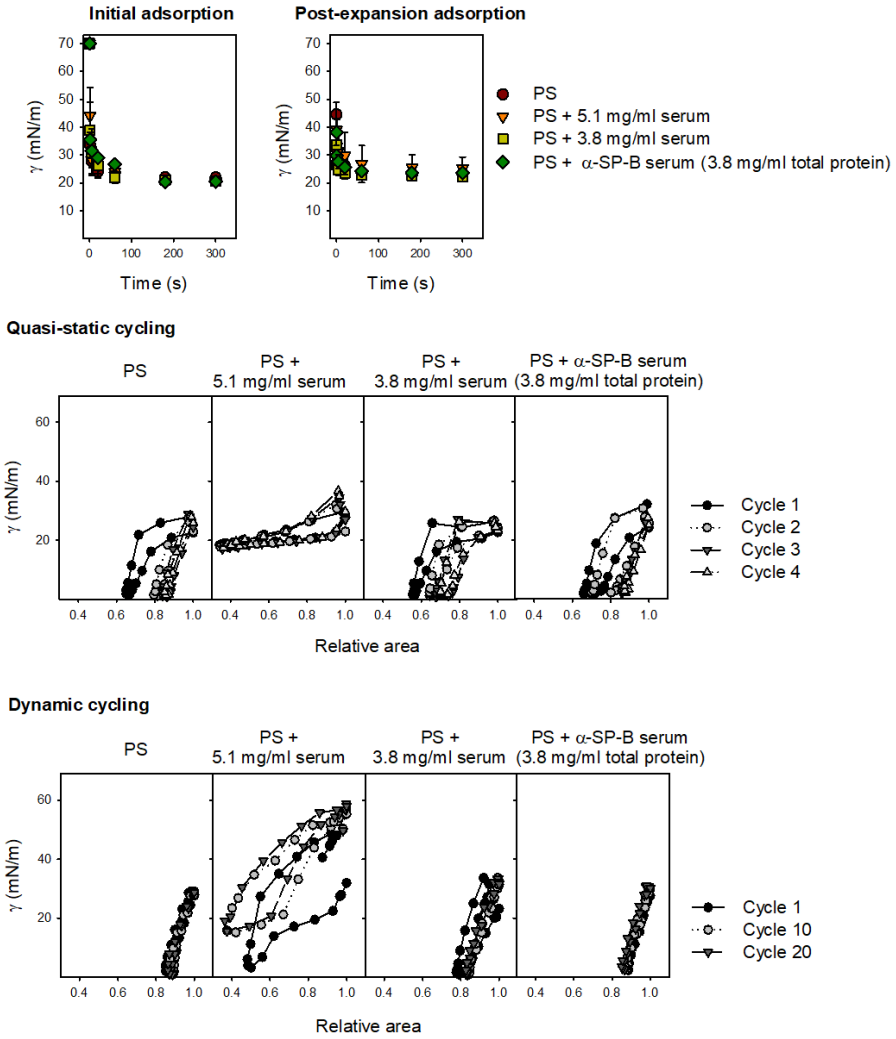

Figure 5.7. Interfacial behavior of surfactant in the presence of serum or α-SP-B antiserum. Captive bubble surfactometry of 4.7 mg/ml surfactant pre-incubated or not with serum or α-SP-B antiserum at different total protein concentrations. Top: Initial and post-expansion adsorption kinetics. Data are mean ± standard deviation obtained from 3 independent experiments. Bottom: representative examples of quasi-static and dynamic compression-expansion cycling isotherms for each sample, n=3.

In the light of the previous results, PS was incubated for 3 hours with polyclonal α-SP-B antiserum at 3.8 mg/ml of protein concentration (4.63 µM IgG) for the evaluation of its surface activity (**Figure 5.7**). α-SP-B-treated PS was able to reduce surface tension near 20 mN/m, showing interfacial adsorption kinetics similar to non-treated PS. Regarding the activity of surfactant film upon cycling, minimal surface tensions < 1 mN/m were reached and, though first and second quasi-static cycle exhibited hysteresis, it disappeared during the remaining cycles. To sum up, the chosen concentration of α-SP-B antiserum, whose serum components do not interfere in the surface activity assay, seems to be not sufficient to inhibit the biophysical function of pulmonary surfactant

through specific SP-B/antibody interaction. Comparing these results with those that lead to blockage of surfactant permeability by α-SP-B antiserum, permeability of GVs resulted entirely blocked with even 0.5 µM of antibody, which correspond to 9.6 Ig/SP-B molar ratio, whereas 4.63 µM of α-SP-B did not inhibit the surface active function of surfactant, corresponding to a Ig/SP-B molar ratio of 0.86. It was obvious that higher concentrations of anti-SP-B antibody were required to achieve the inhibition of the interfacial function of the surfactant.

Facing the possibility that blocking of surfactant function by α-SP-B antiserum could be masked by inhibition mediated by serum itself at high concentration, a purified rabbit polyclonal α-SP-B Ig was chosen to evaluate its effect on the interfacial activity of pulmonary surfactant. In order to correlate α-SP-B blockage results obtained from the biophysical activity analysis of PS with those from the permeability study of surfactant membranes to polar molecules, it was imperative to test the pulmonary surfactant GVs permeability towards FITC-dextrans in the presence of different concentrations of the purified polyclonal α-SP-B Ig. **Table 5.5** compares the effect of α-SP-B antiserum and α-SP-B Ig on the permeability of pulmonary surfactant GVs towards a set of FITC-labeled dextrans. PS treated with any of the antibodies underwent a substantial decrease in permeability upon increasing antibody concentration. Both antiserum and purified Ig, applied in the concentration range 1-5 µM Ig, showed a similar blockage effect on permeability of surfactant GVs to 4 and 40 KDa FITC-dextrans.

		α-SP-B (serum)			α-SP-B Ig		
FITC-dextran	PS	+ 0.5 µM	+ 1 µM	+ 5 µM	+ 0.5 µM	+ 1 µM	+ 5 µM
4	100 (0)	88.3 (2.4)	47.1 (1.3)	20.5 (6.4)	61.3 (1.8)	43.3 (0.6)	31 (3.4)
40	89 (4.2)	12.1 (3)	8 (2.8)	1.9 (2.7)	38.4 (3.9)	11.3 (4.2)	0 (0)

Table 5.5. Permeability blockage of surfactant membranes by α-SP-B antibodies from different sources. Comparative chart of blockage effect on pulmonary surfactant GVs (PS) permeability (in %) towards 4 and 40 KDa FITC-dextrans by α-SP-B antiserum and purified α-SP-B Ig. Data are shown as mean percentage of permeable vesicles (standard deviation).

To study the interfacial activity of pulmonary surfactant (PS) in the presence of the purified polyclonal α-SP-B Ig, surfactant (at 4.7 mg/ml phospholipid) was incubated for 3 hours at 37ºC with different concentrations of the purified α-SP-B Ig (0.5, 5 and 10 µM Ig). Besides, some experimental controls were assessed in parallel: non-treated PS and PS incubated together with 10 µM of a rabbit IgG. Then, surface activity of the samples was evaluated by captive bubble surfactometry. PS pretreated with 0.5 µM of α-SP-B Ig reduced surface tension to 20.9 ± 1.2 mN/m after 5 minutes of injection, and to 20.8 ± 0.2 mN/m after expanding the bubble for 5 minutes (**Figure 5.8** and **table 5.6**). However, for this sample a clearly slower interfacial adsorption kinetics was observed in comparison to PS, in both initial and post-expansion adsorption. Specifically, it required 180 seconds

to reach surface tensions close to the equilibrium, while native surfactant typically reaches the same tension values in less than 20 seconds. Upon cycling, PS treated with 0.5 µM α-SP-B Ig reached very low minimal surface tensions close to 0 mN/m, except for the first quasi-static cycle, 4.4 mN/m. It is noticeable that, unlike untreated PS, that only exhibited hysteresis in the first quasi-static cycle, all quasi-static cycles of PS treated with 0.5 µM α-SP-B Ig showed hysteresis, although it was progressively reduced (**Figure 5.8** and **table 5.7**).

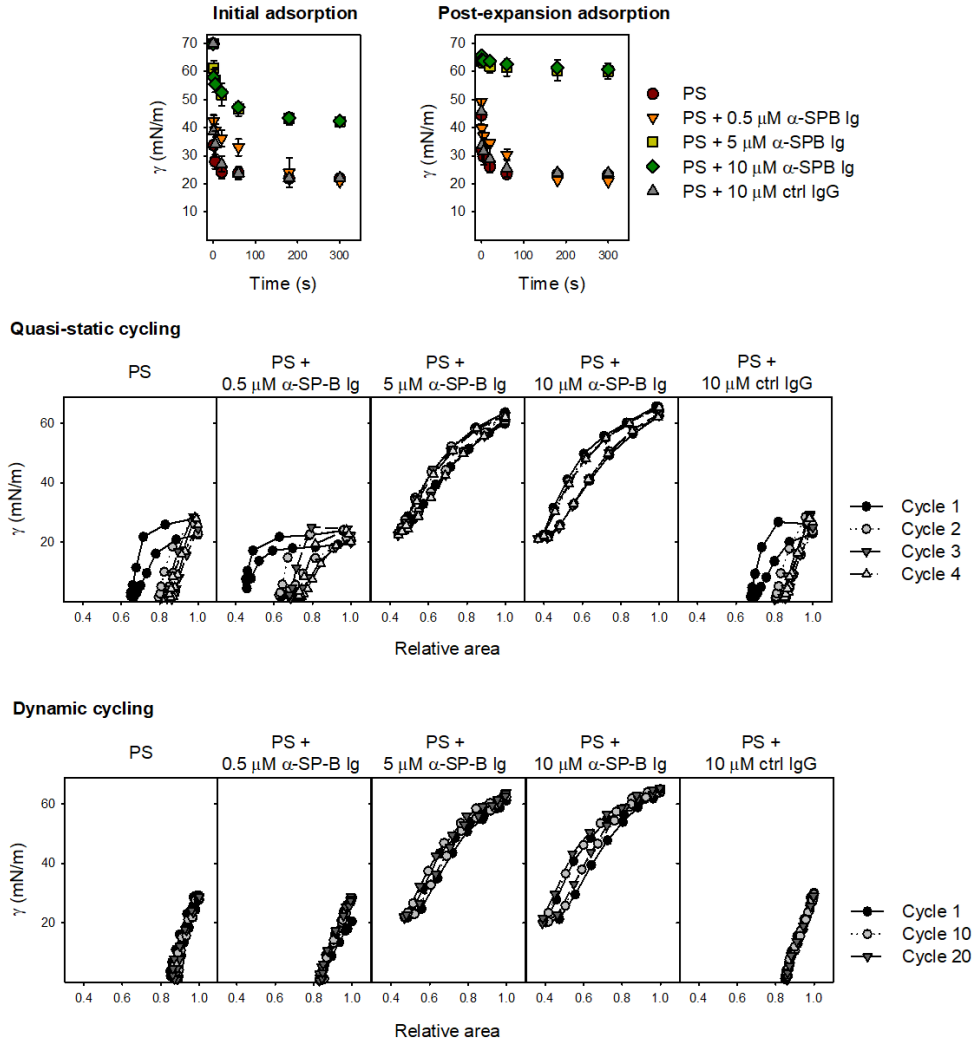

Figure 5.8. Interfacial behavior of surfactant in the presence of α-SP-B Ig. Interfacial adsorption of pulmonary surfactant (4.7mg/ml) pre-incubated with 0.5, 5 or 10 µM of α-SP-B Ig, or 10 µM of a control IgG. Top: Initial and post-expansion adsorption kinetics of the different tested surfactant samples. Data are mean ± standard deviation obtained from 3 independent experiments. Bottom: representative examples of quasi-static and dynamic compression-expansion cycling isotherms for each sample, n=3.

	γ_{eq} (mN/m)	
	IA	PEA
PS	21.9 ± 0.8	23.2 ± 0.6
PS + 10 μM ctrl IgG	22.1 ± 0.6	23.8 ± 0.4
PS + 0.5 μM α-SP-B Ig	20.9 ± 1.2	20.8 ± 0.2
PS + 5 μM α-SP-B Ig	42.2 ± 1.6	60.8 ± 0.4
PS + 10 μM α-SP-B Ig	42.5 ± 1.2	60.1 ± 2.8

Table 5.6. Effect of α-SP-B Ig on initial (IA) and post-expansion (PEA) interfacial adsorption of surfactant. Pulmonary surfactant at 4.7mg/ml (PS) was pre-incubated with 0.5, 5 or 10 μM of α-SP-B Ig, or 10 μM of a control IgG. Data are shown as mean ± standard deviation, n=3.

	Q-stat 4			Dyn 20		
	γ_{min} (mN/m)	γ_{max} (mN/m)	R.A. $_{min}$	γ_{min} (mN/m)	γ_{max} (mN/m)	R.A. $_{min}$
PS	0.8 ± 0.2	28.1 ± 0.4	0.8 ± 0.1	0.8 ± 0.2	31.4 ± 2.3	0.9 ± 0.0
PS + 10 μM ctrl IgG	1.2 ± 0.3	29.5 ± 0.9	0.8 ± 0.1	1.1 ± 0.2	31.5 ± 2.8	0.9 ± 0.0
PS + 0.5 μM α-SP-B Ig	1.2 ± 0.4	25.6 ± 2.2	0.7 ± 0.0	0.8 ± 0.3	28.8 ± 0.0	0.9 ± 0.0
PS + 5 μM α-SP-B Ig	21.7 ± 0.9	54.3 ± 11	0.4 ± 0.0	21.1 ± 0.8	62.2 ± 2.6	0.4 ± 0.0
PS + 10 μM α-SP-B Ig	20.9 ± 0.1	62.8 ± 3.8	0.4 ± 0.0	19.9 ± 0.2	64.4 ± 1.6	0.4 ± 0.0

Table 5.7. Effect of α-SP-B Ig on the behavior of PS films subjected to quasi-static and dynamic compression-expansion cycling. For each sample, the following parameters of the last quasi-static (Q-stat 4) and dynamic (Dyn 20) cycles are shown: minimal surface tension (γ_{min}), maximal surface tension (γ_{max}) and relative area reduction needed for the film to reach minimal tension (R.A. $_{min}$). Pulmonary surfactant at 4.7 mg/ml (PS) was preincubated with 0.5, 5 or 10 μM of α-SP-B Ig, and 10 μM of a control IgG. Data are shown as mean ± standard deviation, n=3.

In contrast, pretreatment of PS with higher α-SP-B Ig concentrations, 5 or 10 μM, showed a clear impairment of surfactant activity (**Figure 5.8**). 5 μM α-SP-B Ig pre-treated PS reached equilibrium surface tensions of 42.2 ± 1.6 mN/m and 60.8 ± 0.4 mN/m after initial and post-expansion adsorption, respectively (**Table 5.6**). In this same way, for 10 μM α-SP-B pre-treated PS, values of surface tension at equilibrium were 42.5 ± 1.2 mN/m for initial and 60.1 ± 2.8 mN/m for post-expansion adsorption. Thus, in the presence of α-SP-B concentration of 5 μM or higher, PS was not able to efficiently form a surface active film at the air-liquid interface, which would decrease surface tension to values near 20 mN/m. Moreover, upon bubble expansion, surface tension only decreased to about 60 mN/m which depicts that some material of the pre-existing monolayer film could spread along the enlarged interface, but the remaining material in the aqueous subphase was not able to adsorb and replenish the interface. In the same line, cycling of PS treated with 5 or 10 μM α-SP-B Ig were highly defective (**Figure 5.8**). Minimal surface tensions only decreased to about 20 mN/m after 60% area reduction (**table 5.7**), revealing that surfactant was fully inhibited in the presence of concentrations of α-SP-B Ig above 5 μM.

On the other hand, to discard non-specific effects of the purified polyclonal antibody on the biophysical function of pulmonary surfactant, the surface activity of PS treated with 10 μM of a rabbit IgG (named as control IgG), was assessed. Control IgG-treated

PS reduced surface tension to 22.1 ± 0.6 mN/m after 5 min of initial adsorption and to 23.8 ± 0.4 after 5 min of bubble expansion (**Figure 5.8** and **table 5.6**). Upon cycling, PS treated with 10 µM control IgG reached minimal surface tensions close to 0 mN/m, with only about 20% area reduction during compression, with the exception of the presence of hysteresis in the first quasi-static cycle (**Figure 5.8** and **table 5.7**). Therefore, 10 µM control IgG did not affect surface activity of PS film.

5.3. DISCUSSION

Previous studies showed that SP-B and SP-C provide pulmonary surfactant with permeability to both membrane and polar probes, as well as ions (Parra *et al.*, 2011, 2013). This chapter addresses a deeper study of the features of surfactant membrane permeability to polar molecules. Additionally, this work present evidences of the dual role of SP-B on membrane permeability and biophysical function of surfactant, which seems to be intrinsically related to the oligomeric protein structure, suggesting that both surfactant functions could be connected, with SP-B acting as the main link.

Studies with FITC-dextrans confirm that the synergic action of SP-B and SP-C modulates the permeability of surfactant membranes towards polar molecules. When both proteins are separated, SP-B promotes aggregation of giant vesicles and their transformation into larger vesicles, in agreement with its ability to promote association and fusion between membranes, (Chang, Nir and Poulain, 1998; Cruz *et al.*, 2000; Ryan *et al.*, 2005). Our results have shown that SP-B is able to make GVs permeable to polar molecules with a defined size threshold. This could suggest that SP-B induces pore formation in membranes. On the other hand, FITC-dextrans of all sizes were able to permeate SP-C-containing vesicles. Moreover, the presence of SP-C was found to destabilize bilayers, promoting fragmentation of vesicles. A previous study proposed that membrane fragmentation induced by SP-C was triggered by SP-C clustering in defined regions of the vesicle (Roldan *et al.*, 2016) However, in the presence of the physiological mixture of both proteins SP-B and SP-C (PF), the morphology of the vesicles is maintained apparently intact. Therefore, SP-B and SP-C seem to modulate each other, providing surfactant membranes with specific properties which are clearly distinct from the activities of each individual protein by itself. The study by (Roldan *et al.*, 2016) has already described this dual behavior of SP-B and SP-C in PS derived membranes. SP-C showed the ability to transform larger vesicles into smaller ones, independently of lipid composition, whereas SP-B promoted the fusion of small vesicles, generating larger vesicles. These fission/fusion activities in membranes were canceled out when both proteins were present, conferring stability to the membrane.

The present work describes the existence of pores in pulmonary surfactant membranes with a hydrodynamic pore radius (r_p) of approximately 4.5 nm. The generation of these pores is induced by SP-B, presumably by assembly of dimers in a supraoligomeric ring-shaped structure of this protein (Olmeda *et al.*, 2015), which has been observed in monolayers and bilayers, as shown in Chapter 3 of the present Thesis. Blockage of membrane permeability by α-SP-B and α-SP-C antibodies revealed that permeability of pore complexes in PS membranes is not only dependent of SP-B, but also SP-C is involved. Blockage generated by α-SP-C antibody could imply that SP-C is directly taking part of pore complexes, or, at least, is modulating the pore size. In this regard, it is interesting to highlight that SP-B alone in surfactant lipid membranes forms pores with a r_p about 6 nm, which are larger than pores described in PS membranes and lipid surfactant membranes supplemented with the hydrophobic surfactant fraction (4.5 nm). SP-C seems therefore to participate in the architecture of the SP-B pore in surfactant membranes by imposing a restraint in pore size. Hence, the present results strongly suggest that protein complexes formed by SP-B and SP-C would modulate the permeability of pulmonary surfactant. We had also previously observed the presence of high molecular weight complexes in native surfactant containing both proteins (chapter 1). A recent study has demonstrated the existence of SP-B/SP-C interactions by time-resolved Förster resonance energy transfer techniques (Cabre *et al.*, 2018), although the detailed structure of the resulting heterocomplex remains unclear. The progressive blockage of permeability to larger FITC-dextrans, as α-SP-B or α-SP-C concentrations increase, suggest that SP-B/SP-C complexes are composed of a defined number of molecules of each protein. However, the stoichiometry of this complex cannot be deduced from the present work due to the polyclonal nature of the antibodies used in this study.

Another interesting conclusion of our results is the fact that a mixture of previously isolated SP-B and SP-C (re-mixed at the physiological SP-B/SP-C proportion, 1:1, by weight) induces a membrane permeability behavior which differs from that in the presence of the hydrophobic protein fraction (PF) (both in simple lipid models or in whole native surfactant lipids). This result is in agreement with those previously found by Parra and coworkers. In that work, the authors described how calcein freely diffuse through POPC GVs supplemented by the mixture of isolated SP-B and SP-C, showing a homogeneous distribution inside and outside of the vesicles, while this probe was gathered mostly inside PF-containing vesicles (Parra *et al.*, 2011). This apparent functional impairment of samples containing the mixture of the purified proteins has been also shown during the comparative analysis of interfacial function of systems prepared by reconstituting defined fractions of native surfactant (Schurch *et al.*, 2010). These evidences would suggest that original SP-B/SP-C complexes are poorly re-established once the proteins are mixed after isolation, maybe because the proper conformation of the

proteins is altered or due to the loss of some unknown component during the purification process. So, these data warn about the risk of inferring conclusions from structural and functional studies of hydrophobic surfactant proteins performed with model systems containing separated SP-B and SP-C.

It is clear that pulmonary surfactant membranes are intrinsically permeable to water-soluble molecules, and that SP-B/SP-C complexes are essential for this feature. Additionally, the anionic phospholipid POPG would be involved in the modulation of the membrane pore structure induced by SP-B/SP-C complexes. Permeability studies in POPC GVs supplemented with different surfactant protein components showed that these vesicles lose the ability to permeate to FITC-dextrans larger than 4 KDa for POPC+ PF, or 20 KDa for POPC+ SP-B, which means a significant reduction of pore size in these bilayers. In POPC:POPG (7:3) GVs, all surfactant protein mixtures led to membranes that were permeable up to FD40. These results suggest that PG participates in the pore structure induced by SP-B/SP-C complexes, probably due to electrostatic interactions between the anionic phospholipid and the hydrophobic cationic surfactant proteins (Perez-Gil, Casals and Marsh, 1995; Takamoto, Lipp, *et al.*, 2001; Cabré *et al.*, 2012). Particularly, it is noteworthy that POPC:POPG (7:3) GVs supplemented with SP-B alone or a mixture of isolated SP-B and SP-C showed pores with estimated r_p of 4.5 nm, whereas LF GVs with similar protein content showed larger pores ($r_p \approx$ 6 nm). Anionic phospholipids, PG and PI, represents only 8-15% by mass of the pulmonary surfactant lipids (Parra and Perez-Gil 2015), in contrast to 30% of PG in the POPC:POPG GVs used for this study. This excess of POPG seems to confer to the membranes the ability to bypass the absence of native SP-B/SP-C complexes, diminishing the SP-B pore diameter, and restoring that of native surfactant. Therefore, anionic phospholipids would accomplish an essential role to finely tune the structural organization of SP-B and SP-C in pulmonary surfactant membranes.

To understand the molecular mechanisms by which SP-B modulates the dynamical behavior of surfactant films, we evaluated the effect of specific SP-B inhibition in these membranes. The application of α-SP-B antibody seemed to affect primarily to the interfacial adsorption ability of surfactant. The highest antibody concentrations (5 μM and 10 μM α-SP-B Ig) prevented the formation of an efficient surfactant film along the air-liquid interface. This deleterious effect became more apparent when evaluating interfacial adsorption upon surface expansion, where surfactant films pre-treated with high α-SP-B Ig concentrations were not able to substantially decrease surface tension, which means that almost no new surfactant material was adsorbed and spread along the newly exposed interface. Moreover, the impairment of formation of a stable surface active film persisted during compression-expansion cycles. Lower α-SP-B Ig concentrations allowed us to analyze subtle changes in the dynamics of the surfactant films in the

presence of this inhibitory agent. Pre-treatment of pulmonary surfactant with 0.5 μM α-SP-B Ig showed slower interfacial adsorption kinetics, although surfactant was finally able to reduce surface tension at similar levels than native surfactant films did in both initial and post-expansion adsorption experiments. However, in the presence of 0.5 μM α-SP-B Ig, surfactant films still became unstable upon cycling, showing difficulties to efficiently reach low surface tensions. Taken together, these results confirm that SP-B is essential to promote interfacial adsorption of lipids and film stability, sustaining very low surface tensions in compressed films, and that pre-treatment with a specific antibody is able to block such tensioactive function

Previous *in vivo* studies demonstrated that intratracheal administration of monoclonal α-SP-B antibodies triggered respiratory distress syndrome, characterized by collapsed alveoli alternating with hyperaerated areas and intraalveolar edema with a moderate inflammatory response (Eijking *et al.*, 1991; Robertson *et al.*, 1991). Besides, Eijking and coworkers contributed with *in vitro* measurements of surface activity by pulsating bubble surfactometry (Eijking *et al.*, 1991), in which 3.1 nM of a monoclonal rat α-SP-B antibody inhibited the function of 5 mg/ml bovine surfactant, showing high minimal surface tension upon compression. Although similar inhibitory levels of pulmonary surfactant have been reported in the present results, the surfactant inactivation was yielded with molar ratio antibody to antigen of 0.093, whereas the previous work used a much lower molar ratio, 0.00046, to achieve the same goal. This discrepancy might be primarily a consequence of different affinities of antibody-antigen interaction, but also due to the presence of serum 10% (v/v) in the monoclonal rat antibody stock used in the study of Eijking, which could partly interfere in surfactant function, as demonstrated in the present chapter.

A three-dimensional structural model of SP-B based on Saposin B structure considered the co-existence of two conformations of SP-B rings, open and closed (Olmeda *et al.*, 2015), which could be important for allowing a proper ability of the protein to promote lipid transfer among surfactant membranes. According to the model, 5 or 6 dimers are associated to form a ring-shaped structure of 10 nm of diameter, which is anchored to the membrane surface. The modeled hexamer of dimers in its closed conformation locates parallel to the membrane surface in a conical shape where the inner pore diameter ranges from 4.75 nm, close to the membrane, to 1.75 nm, projected towards the aqueous environment. Although permeability of whole surfactant membranes to fluorescent dextrans appears to differ from these pore sizes of SP-B, describing an inner pore diameter > 4.5 nm and < 6 nm, we should also consider the possible effects of the ellipsoidal shape of dextran molecules. The opening of dimers would induce pivoting of the whole structure, promoting the exposure of the hydrophobic cavity of the SP-B ring to the acyl chains of the membrane. This structural transition of SP-B ring towards an open

conformation might be promoted through exposure of SP-B to the interface or the establishment of SP-B/SP-B interactions between membranes, which ultimately would catalyze the rapid flow of lipid to the interface or between surfactant membranes (Olmeda *et al.*, 2015; Hobi *et al.*, 2016). The present work has demonstrated that selective blockage of SP-B by antibodies prevents achieving low surface tension and stability of compressed films. Therefore, α-SP-B antibody interaction with SP-B ring would hinder the proper conformational change of the protein, blocking not only the interfacial adsorption of surface active lipid species to the interface but also disturbing film stability during breathing cycles, impeding the formation of a network of interconnected surfactant membranes through SP-B/SP-B interactions upon compression of the interface.

SP-B is the main responsible of promoting surface activity and stability. However, it has been suggested that a cooperative action of SP-B and SP-C could enhance lipid insertion into the interface (Oosterlaken-Dijksterhuis *et al.*, 1991b, 1991a; Wang, Hall and Notter, 1996; Schurch *et al.*, 2010). In the present chapter, it has been described that permeability of pulmonary surfactant membranes to polar molecules is blocked at similar levels by either α-SP-B or α-SP-C antibodies, presumably by interaction with protein complexes formed by SP-B and SP-C. These results are consistent with a recent research that reported that not only α-SP-B antibodies but also α-SP-C antibodies are able to abolish the adsorption of secreted lamellar bodies into the air-liquid interface (Hobi *et al.*, 2016).

Although interfacial activities of SP-B and SP-C partly overlap and both proteins seem to promote the rapid adsorption of phospholipids to the air-liquid interface and ensure the film stability during compression/expansion cycles, different mechanisms have been proposed for each protein. SP-B would be crucial for film stability during compression and re-extension (Schurch *et al.*, 2010), promoting the formation of multilayered membrane reservoirs through connecting neighboring membranes by the apposition of SP-B rings (as it is addressed in Chapter 4 and by (Bernardino de la Serna *et al.*, 2013)). On the other hand, SP-C is not essential to achieve low minimum tension during compression (Schurch *et al.*, 2010), although it allows the attachment of membrane patches to compressed films (von Nahmen *et al.*, 1997; Kramer *et al.*, 2000), which would facilitate the reinsertion of the prepackaged lipid units associated with SP-B. The existence of different mechanisms of action suggests that SP-B and SP-C could play complementary roles that could be modulated by the formation of heterocomplexes in the surface active film and its associated membranes. We have found that SP-B and SP-C even show opposite membrane-activities, fusion and fission respectively, but our results also point to the existence of SP-B/SP-C interactions, and show that establishment of such interactions stabilizes surfactant membranes by counteracting its activities. Here, we propose that SP-B/SP-C complexes could be initially present in surfactant membranes

(**Figure 5.9**). Then, probably as a result of its exposition to air, a conformational change would be triggered and SP-B/SP-C interactions might be dissociated. Disassembly of this heterocomplex, which has been previously also proposed (Cabre *et al.*, 2018), would allow each protein to perform its specific activities in the surroundings of the interfacial film. Future studies could clarify the mechanisms underlying the conformational change triggered into SP-B/SP-C structures.

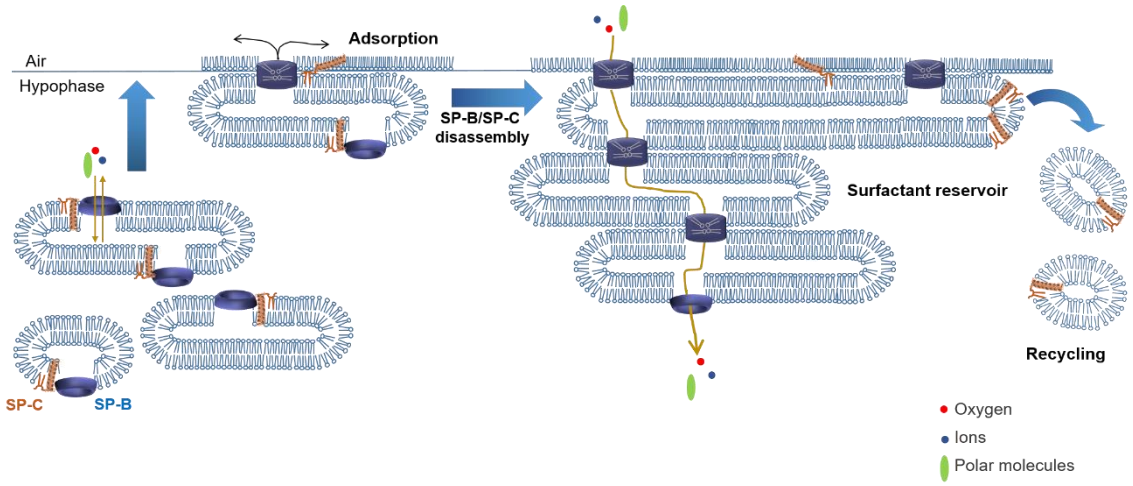

Figure 5.9. Hypothetical model of combined SP-B and SP-C activities on the biophysical function of pulmonary surfactant and membrane permeability. SP-B and SP-C could be forming protein complexes in newly secreted surfactant membranes. The synergetic actions of SP-B and SP-C confer simultaneous permeability to ions, oxygen and polar molecules on surfactant. Upon touching the air-liquid interface, phospholipids are instantaneously adsorbed into the interface due to the cooperative action of SP-B and SP-C. Then, conformational changes would lead to disassembly of SP-B and SP-C, allowing that each protein display its specific activities. SP-B/SP-B interactions could promote membrane connections, generating a dynamic network of membranes interconnected among them and to the interfacial monolayer. The close apposition of SP-B oligomers would constitute the machinery for lipid transfer between connected membranes and between membranes and the monolayer. On the other hand, SP-C could diffuse to regions particularly enriched in less surface-active lipids, such as cholesterol or unsaturated phospholipids, where it could promote membrane fragmentation and conversion into small vesicles targeted for recycling (Roldan *et al.*, 2016).

Finally, results from the present chapter point out that the oligomeric ring-shaped SP-B structure could be simultaneously responsible for both lipid transfer and membrane permeability through the protein pore. Self-interactions of SP-B oligomers would promote the formation of an interconnected membrane network ensuring a rapid and efficient transfer of lipids between membranes, all the way up to the interface. In this line, angle X-ray diffraction experiments have suggested that SP-B accelerates lipid adsorption by inducing the formation of a rate-limiting negatively curved structure (Chavarha *et al.*, 2012, 2015), in a process favored by the presence of PG (Chavarha *et al.*, 2013). On the other hand, SP-B has been suggested to induce permeability through the formation of toroidal pores (Parra *et al.*, 2013). All these findings are consistent with the creation of a SP-B-induced toroidal pore with two types of curvature: negative (concave) curvature in the plane of the bilayer and positive curvature perpendicular to the membrane surface, in line with the structure of the pore induced by the peptide amylin, characterized by NMR

(Smith, Brender and Ramamoorthy, 2009) (**Figure 5.10 B**). Due to the superficial location of the SP-B ring in the bilayer, the protein would induce the formation of toroidal pores that would favor the orientation of lipids to be transferred through the hydrophobic pore constituted by two connected SP-B rings (**Figure 5.10 A**). Through the SP-B pore, the acyl chain of a phospholipid would be shielded in the hydrophobic cavity formed by each SP-B dimer, allowing its polar head group to be oriented towards the center of the pore, in contact with the aqueous environment (Olmeda *et al.*, 2015). In this way, SP-B would drive the lipid transfer between interconnected membranes and bilayers-interface. On the other hand, the presence of these SP-B-induced toroidal pores in bilayers would also serve as a passage for polar molecules to cross between surfactant membranes, through the hydrophilic tunnel generated by lipid polar heads.

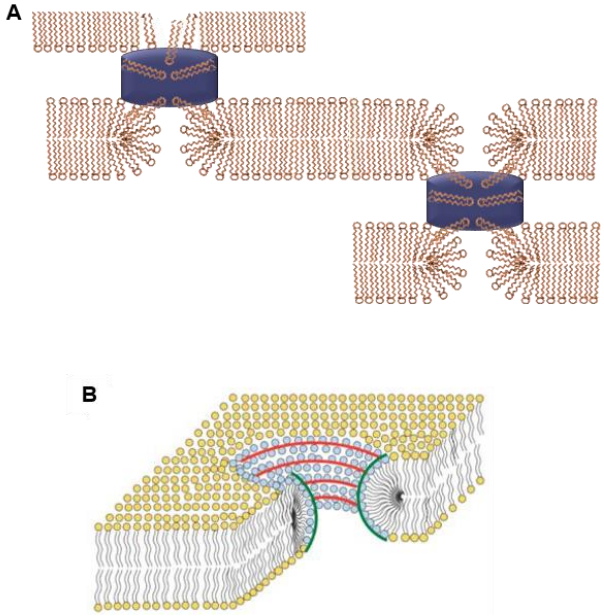

Figure 5.10. Model for lipid transfer induced by SP-B between bilayers and from bilayer to monolayer. A) SP-B induces the formation of toroidal pores, in which the headgroups of phospholipids line their surface. These structures together with the apposition of two SP-B rings would ensure a lipid flow between interconnected bilayers and bilayer-interface. **B)** Schematic representation of the structure of a toroidal pore in a bilayer, constituted by areas with positive curvature, perpendicular to the plane of the bilayer (green lines) and negatively-curved regions, in the plane of the bilayer (red lines). Adapted from (Smith, Brender and Ramamoorthy, 2009).

Regarding the physiological meaning of the polar permeability of surfactant membranes, the presence of SP-B pores in the continuous membrane network would make it accessible to small hydrophilic molecules (those able to pass through a pore with a r_p < 70 KDa), as small peptides involved in innate lung defense, such as defensins or cathelicidins. Furthermore, this permeable membrane system would be relevant for sustaining a proper equilibrium of ions in the alveolar subphase (Parra *et al.*, 2013) and ensuring a rapid diffusion of oxygen from air space through the membrane network (Olmeda *et al.*, 2010). Lastly, the highly permeable character of surfactant membranes could be considered as an advantageous feature which could have an impact in the

administration of hydrophilic drugs directly through the airways. Small hydrophilic active molecules could take advantage of the protein pores to pass through surfactant membranes in the respiratory surface and reach their targets, such as the respiratory epithelium or the bloodstream.

Chapter 3

STRUCTURAL CHARACTERIZATION OF SP-B OLIGOMERS

Results from the structural study of SP-B oligomers by atomic force microscopy were partially included in the article:

Olmeda, B., García-Álvarez B., Gómez MJ., Martínez-Calle M, Cruz A, Pérez-Gil J. (2015). "A model for the structure and mechanism of action of pulmonary surfactant protein B". *FASEB Journal*, 29(10):4236-47.

6. STRUCTURAL CHARACTERIZATION OF SP-B OLIGOMERS

6.1. INTRODUCTION

SP-B is an essential protein for the function of pulmonary surfactant, so that its genetic deficiency leads to lethal respiratory failure at birth (Nogee *et al.*, 1993; Melton *et al.*, 2003). SP-B belongs to the family of saposin-like proteins (SAPLIPs). These proteins are a diverse family of lipid-interacting proteins, defined by a mainly helical secondary structure and the presence of 3 intramolecular disulfide bonds that provide stability to the protein structure (Munford, Sheppard and O'Hara, 1995). Despite these common features shared by SP-B, this protein differs from the rest of them in two main features: the existence of an additional cysteine responsible for the formation of a covalent dimer and the permanent association to lipids, due to its high hydrophobicity. Recently, a 3D model of the SP-B structure was built based on the structure of a member of SAPLIPs, Saposin B, considering the sequence homology between these two proteins and the dimeric state of Saposin B (Olmeda *et al.*, 2015). The model generated for the 3D structure of SP-B predicts an oligomeric organization formed by the association of five or six covalent SP-B dimers. Consistently, native SP-B complexes were purified from CHAPS-solubilized pulmonary surfactant membranes and visualized by negative-staining transmission electron microscopy, revealing the presence of ring-shaped particles of 10 nm of diameter. The 3D volume obtained from the averaged particles was successfully fitted to the structural model of SP-B, confirming the existence of native SP-B oligomers composed by 5 or 6 covalent dimers. Until now, transmission electron microscopy analysis was performed at low resolution, which prevents establishing a fully characterized structure of the SP-B oligomer.

In this chapter, we attempted to get deeper insight into the structural characterization of SP-B oligomers. To get this aim, two specific objectives were covered. Firstly, we studied the oligomeric organization of SP-B in interfacial monolayers and membranes with different lipid composition by atomic force microscopy (AFM) and negative-staining transmission electron microscopy (TEM). Moreover, two different SP-B protein sources were characterized: SP-B complexes purified from CHAPS-solubilized pulmonary surfactant and SP-B isolated from minced lungs using organic solvents.

Secondly, several strategies were applied to obtain native SP-B oligomers with a high sample quality, which would allow the determination of high-resolution SP-B structure by, for instance, electron microscopy or X-ray crystallography. The original protocol established for the purification of native SP-B complexes from detergent-solubilized surfactant gave rise to a heterogeneous suspension with SP-B/detergent complexes of diverse molecular sizes. Here, we attempted to enhance the quality of the sample by the incorporation of additional steps of purification to SP-B oligomers, such as size exclusion

chromatography and GraFix (Gradient Fixation) method. GraFix is a purification process consisting of a density gradient ultracentrifugation in the presence of a gradient of a crosslinking agent, which stabilizes the structure of macromolecules. This method was specifically developed to improve the sample quality for structural determination by negative-staining EM and cryo-EM (Kastner *et al.*, 2008).

Finally, and as an alternative to the use of detergents, we attempted different strategies to isolate and stabilize the SP-B oligomers using amphipols (amphipatic polymers) and POPC or POPC:POPG nanodiscs assembled by MSP1D1, as scaffold protein, or SMA copolymers.

6.2. RESULTS

6.2.1. STRUCTURAL STUDY OF SP-B OLIGOMERS BY ATOMIC FORCE AND TRANSMISSION ELECTRON MICROSCOPY

The structure and distribution of SP-B complexes were studied as assembled in POPC:POPG bilayers and POPC:DPPG monolayers. Besides, a structural analysis of SP-B complexes purified in detergent and organized at an air-liquid interface was performed in the absence of lipids.

6.2.1.1 Structure of SP-B in POPC:POPG bilayers

Suspensions of small unilamellar vesicles (SUVs) containing lipid-protein complexes were directly applied onto mica supports to visualize them by atomic force microscopy (AFM). The samples consisted of 50 μg/ml POPC:POPG (7:3, w:w) supplemented with SP-B isolated in organic solvent or SP-B complexes purified from CHAPS-solubilized pulmonary surfactant, at a protein to lipid ratio of 10% by weight.

Images taken from POPC:POPG bilayers containing SP-B isolated in organic solvent show the presence of circular particles with a central pore (**Figure 6.1 A**). Diameters of over 60 particles were measured, resulting on an average diameter of 15.4 (± 2.7) nm. Similar particles in shape and size were visualized in bilayers containing SP-B purified in detergent, with an average diameter of 14.8 (± 2.6) nm (**Figure 6.1 B**). These ring-shaped particles resemble in size and shape the native SP-B rings purified in detergent and visualized previously in the absence of lipid by TEM (Olmeda *et al.*, 2015). As controls, two different protein-free suspensions of POPC:POPG SUVs were prepared by (1) resuspension of a dried lipid film in Tris buffer, as a control for proteoliposomes with SP-B isolated in organic solvent, or (2) resuspension of the lipid film in buffer supplemented with similar amount of CHAPS to that present in proteoliposomes containing SP-B purified in detergent. Note that the detergent in both samples, the control

and the one containing SP-B purified in CHAPS, was previously removed from vesicle suspensions by adsorption to nonpolar polystyrene adsorbent beads, so that only detergent traces are expected in the preparations. AFM images from POPC:POPG bilayers reconstituted in buffer alone show that lipids were adsorbed forming a flat bilayer surface over the mica (**Figure 6.1 C**). In contrast, bilayers of POPC:POPG reconstituted in buffer with detergent show a humped distribution, suggesting that the reconstitution method in the presence of detergent could have interfered in the adsorption dynamics of the resulting vesicles to the mica support, maybe due to detergent traces (**Figure 6.1 D**). In contrast, bilayers containing SP-B purified in detergent seem to have a lower average height profile than control vesicles reconstituted in the presence of detergent, suggesting that SP-B could favor the adsorption of proteoliposomes onto the mica (**Figure 6.1 B**).

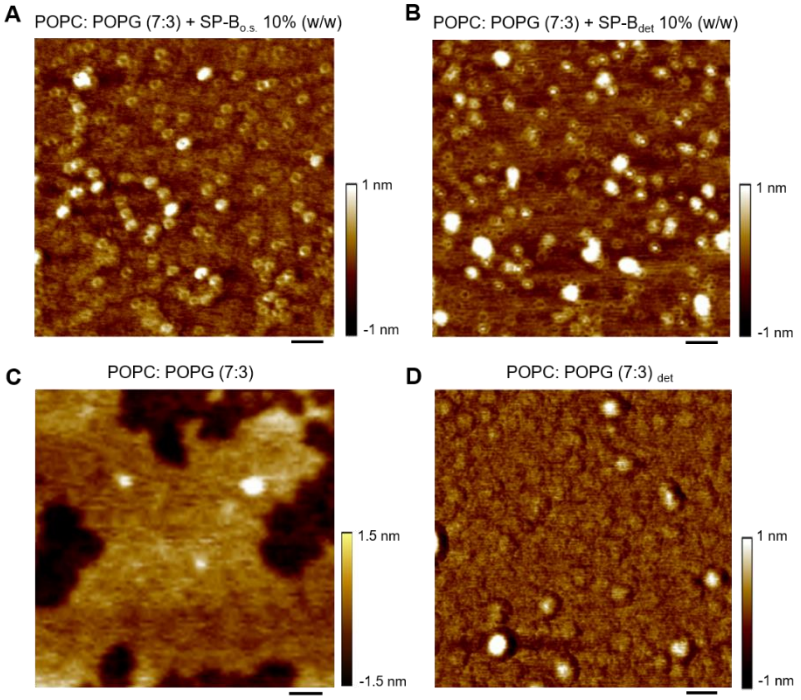

Figure 6.1. Topographical comparison of lipid bilayers containing SP-B isolated in organic solvent (SP-$B_{o.s.}$) or SP-B complexes purified in detergent (SP-B_{det}). AFM images of POPC:POPG (7:3, by weight) SUVs supplemented with 10% (protein/lipid, w/w) of SP-$B_{o.s}$ (**A**) or SP-B_{det} (**B**). Lower panels depict illustrative AFM images of control lipid samples in the absence of protein, which were reconstituted in aqueous buffer alone (**C**) or supplemented with CHAPS at similar concentration than vesicles with SP-B_{det} (**D**). Scale bars, 50 nm.

POPC:POPG vesicles supplemented with SP-B purified in detergent were also visualized under TEM. Images show large membrane layers with an apparent roughness (**Figure 6.2**). The surface of these bilayers seemed to be formed by heterogeneous particles in size and shape that appeared to be closely associated between them, and even form larger fiber-like structures (some examples are labeled with black lines in magnified views of images in **Figure 6.2**). Regarding the size of the particles, it was mainly distributed between 7 and 10 nm of diameter, although smaller particles were also observed at the surface of the vesicles. It is also worth to notice the presence of areas of

interaction between bilayers (see for instance in **Figure 6.2 A** two independent bilayers partly connected through contact sites). A detailed look shows defined structures at these membrane contact sites (labeled with a black arrow in the magnified view), which could correspond to SP-B as a result of its membrane fusion activity, a widely reported function (Poulain, Nir and Hawgood, 1996; Chang, Nir and Poulain, 1998; Ryan *et al.*, 2005). **Figure 6.2 B** could illustrate a final stage of the fusion of two vesicles, when a rift between the fused vesicles was still apparent (pointed with white arrowheads).

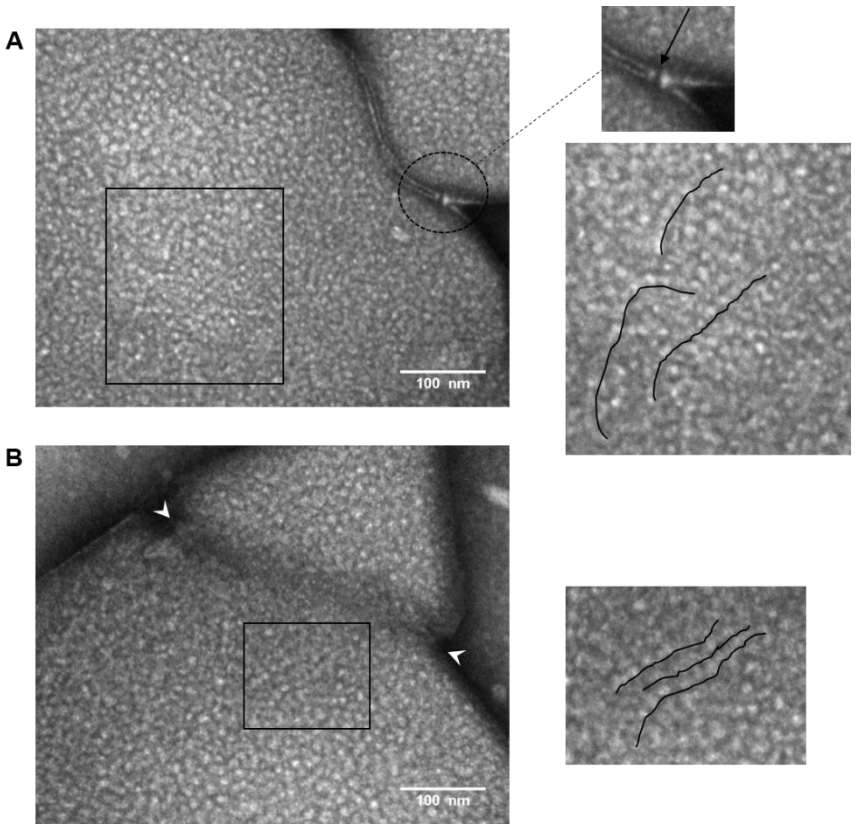

Figure 6.2. TEM images of SP-B complexes purified in detergent (SP-B_{det}) reconstituted into POPC:POPG (7:3, w:w) SUVs, at 10% protein/lipid, by weight. Black lines indicate some examples of particle association in fiber-like structures over the surface of proteoliposomes (magnified views of images A and B). In the upper magnified view of image A, the black arrow points to the contact site between two proteoliposomes, whereas white arrowheads in image B indicate the diffuse boundary between two vesicles that likely underwent a recent fusion process.

6.2.1.2 Structure of SP-B in POPC:DPPG monolayers

The morphology of POPC:DPPG monolayers containing SP-B isolated in organic solvent or SP-B complexes purified from detergent-solubilized pulmonary surfactant was structurally compared by AFM. Two different strategies were used to generate the films: 1) direct application at the interface of organic solvent mixtures containing lipids and SP-B isolated in solvent and 2) deposition at the interface of vesicle suspensions containing SP-B purified in detergent. Since the generation of a interfacial monolayer from vesicles requires destabilization of the continuous bilayer and the lipid insertion into the air-liquid interface, the binary lipid system POPC:DPPG (7:3, w:w), composed by unsaturated and

saturated phospholipids, was selected to enhance lipid adsorption. Unsaturated phospholipids provide the bilayer with the fluidity and dynamic properties required for the structural transformation that allows lipid insertion into the interface, whereas saturated phospholipids are essential to reduce dramatically the surface tension, imposing an extremely ordered monolayer (Lopez-Rodriguez and Perez-Gil, 2014). Organic solvent mixtures of POPC:DPPG, with or without SP-B, were spread onto an air liquid interface to form a single molecule thick film. π-A isotherms for POPC:DPPG (7:3) films compressed at 65 cm^2/min revealed that this binary system underwent a quick LE-LC transition between 13 and 19 mN/m, where the compression work required to achieve lipid packing was scarce (**Figure 6.3 A**). In order to analyze by AFM the topography of lipid films containing or not SP-B isolated in organic solvent, monolayers were compressed to a surface pressure of 15 mN/m and then transferred onto mica supports. AFM images of these POPC:DPPG (7:3) films depict the coexistence of liquid-condensed/liquid-expanded phases or domains, where DPPG condensed domains show a variety of shapes and sizes at the micrometer range (left image, **Figure 6.3 B**). In the case of POPC:DPPG:SP-$B_{o.s.}$ (20% protein/lipid, by weight) films, coexistence of LC/LE phases was also found, but the condensed domains were substantially smaller than in the absence of the protein (right image, **Figure 6.3 B**).

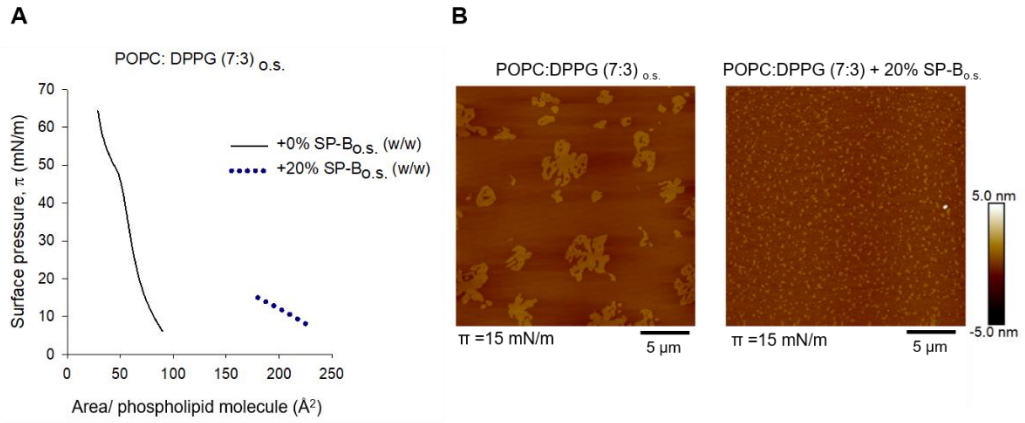

Figure 6.3. Surface pressure measurements and AFM images of solvent-spread interfacial films. Organic solvent mixtures of POPC:DPPG (7:3, by weight) containing or not SP-B isolated in organic solvent (20% SP-$B_{o.s.}$, protein/lipid, by weight) were spread onto the surface of an aqueous buffer trough and the interfacial films were transferred onto mica supports at a constant surface pressure of 15 mN/m. **A)** π-area isotherm. **B)** Height micrographs of an area covering 25 µm of length.

Then, monolayers of POPC:DPPG containing native SP-B complexes purified in detergent were formed from POPC:DPPG SUVs in the absence or presence of 10% or 20% (protein/lipid, w/w) of SP-B purified in detergent. Protein-free liposomes were prepared with the equivalent amount of detergent in the buffer to that of the sample containing the protein, and then, detergent was removed from all samples by adsorption to non-polar beads. Vesicle suspensions were deposited onto the surface of the buffered subphase in the Langmuir trough. As it can be observed in the right part of the π- % area isotherms of **figure 6.4 A**, the presence of SP-B_{det} at high concentration (20%) enhanced

the spreading of the proteolipid material along the air-liquid interface, reaching a surface pressure of 2.5 mN/m after 10 minutes of sample application, in comparison to 0.05 and 0.2 mN/m achieved by vesicles with 0% and 10% of SP-B_{det}, respectively, Once formed, films were subjected to compression up to a maximal surface pressure of 15 mN/m in order to be transferred to mica supports for AFM analysis. Upon compression, films containing 20% SP-B_{det} achieved 15 mN/m of surface pressure with only 30% of surface area reduction. Films in the absence or presence of 10% of the protein needed higher compression rates to achieve an increase in lateral pressure, reaching maximal pressures of only 6.2 and 10 mN/m, respectively. In the particular case of the protein-free lipid film, a sudden loss of material from the interface occurred after compressing up to 6.2 mN/m. This indicates that vesicle-spread monolayers of POPC:DPPG were not able to form effective monolayers, while SP-B_{det} at concentrations ≥ 20% improved the spreading of the vesicles to the interface and promoted the stability of phospholipid monolayers subjected to compression forces. Observed under AFM, POPC:DPPG films at surface pressures between 5 and 6 mN/m showed condensed domains highly variable in size (**Figure 6.4 B**). In the case of films with 10% and 20% of SP-B_{det}, transferred at higher surface pressures, the micrographs showed a distribution of domains similar to that of the monolayer constituted only by lipids at the lower pressures observed.

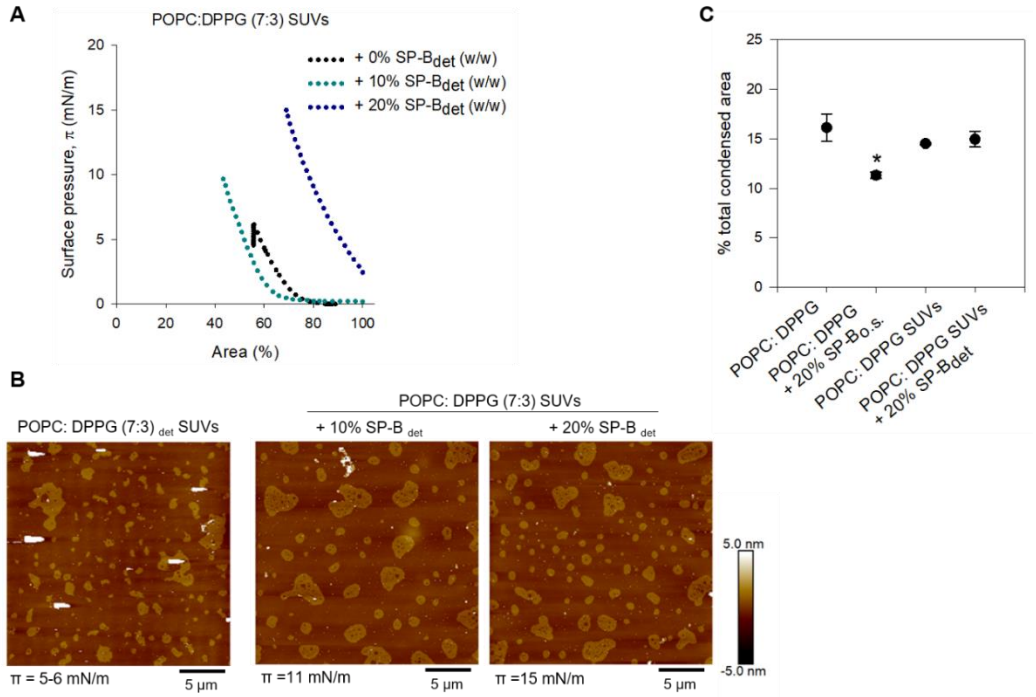

Figure 6.4. Surface pressure measurements and AFM images of vesicle-spread interfacial films. POPC:DPPG (7:3) SUVs containing 0, 10 or 20% (protein/lipid, by weight) of SP-B complexes purified in detergent (SP-B_{det}) were applied onto the buffer surface and transferred onto mica supports. Sample transferring onto mica supports was performed at surface pressures of 5-6, 11 and 15 mN/m for samples containing 0, 10 and 20% of SP-B_{det}, respectively. **A)** π-% area isotherms. **B)** Height micrographs of an area covering 25 µm of length. **C)** Percentage of condensed area of different monolayers was analyzed in height images for both types of films: solvent-spread film, in figure 6.3 and vesicle-spread film, in this figure. Statistical analysis by paired student's t test was performed (* $P<0.05$).

The effect of the protein on the condensation of POPC:DPPG monolayers was quantitatively analyzed. The percentage of condensed domains in solvent-spread monolayers compressed at 15 mN/m decreased significantly in the presence of SP-$B_{o.s.}$ (**Figure 6.4 C**), as previously described in DPPC films (Nag *et al.*, 1997; Cruz *et al.*, 2000). In the case of vesicle-spread monolayers containing SP-B_{det} at surface pressure of 15 mN/m, the percentage of condensed domains showed similar values than pure lipid films at surface pressure of 5-6 mN/m, although they are not comparable due to the difference in lateral pressures between both interfacial films. It has been previously reported that SP-B affects the LC and LE distribution in DPPC and DPPC:DPPG monolayers at microscopic and nanoscopic levels (Cruz *et al.*, 2004). Thus, we quantified not only the area of microdomains but also that of nanodomains (domains with < 100 nm in their larger axis) (**Figure 6.5 B**). SP-$B_{o.s.}$ in solvent-spread POPC:DPPG films caused a marked decrease in the area taken by microdomains over the total condensed area, resulting in an increase in the area occupied by nanodomains. In the case of SP-B_{det} in vesicle-spread lipid films, the protein could also promote the generation of nanodomains, although the potency of this effect cannot be inferred due to the control lipid monolayers were subjected to lower lateral pressures. **Figure 6.5 A** shows that the size of domains in pure lipid solvent-spread films was larger than in films containing SP-B. SP-B_{det} containing lipid films exhibited large condensed areas in combination with numerous smaller microdomains around 200 nm of length. In contrast, SP-$B_{o.s}$ lipid films showed few microdomains and numerous nanodomains. Despite these different sizes of condensed domains in pure lipid films or SP-B containing films, in all monolayers the height of condensed domains was around 1 nm over the liquid-expanded phase background (**Figure 6.5 C**), regardless of the size of domains, in either micro- or nanometer range.

Interestingly, phase images of POPC:DPPG films containing 20% SP-B_{det} show some dark areas within the condensed domains, suggesting that these areas have a different chemical composition (**Figure 6.6 A**). In their corresponding topographic images, it can be observed that these areas show a lower height than the lipid condensed domains (examples of these low, dark areas are tagged with red arrowheads in phase images). As the frequency of appearance is linked to the protein concentration in the film, we propose that these dark areas could be enriched in SP-B. Thus, the number of dark areas in films with 10% SP-B_{det} is reduced compared with those in films containing 20% SP-B_{det}, (compare **Figure 6.6 B** to **A**) whereas they do not appear in pure POPC:DPPG films (data not shown). It is noteworthy to point that these possible protein clusters were not seen in POPC:DPPG films containing 20% SP-$B_{o.s}$. Following with the structural characterization of the condensed domains in films of POPC:DPPG + 20% SP-B_{det}, a magnified view of a large domain of this sample shows an extremely rough surface

(height image in lower panel, **Figure 6.6 A**). Besides the aforementioned low height areas inside the condensed domains, the surface showed a high density of pores (blue arrows point some of these pores in **Figure 6.6 A**). The average inner diameter of these pores was 8.96 (± 1.33) nm, which resembles the pore size of SP-B rings in POPC:POPG bilayers, 8.93 (± 1.15) nm of average inner diameter (see **Figure 6.1 B**). Therefore, AFM image analysis of POPC:DPPG films containing 20% SP-B_{det} suggested the presence of SP-B rings distributed inside the condensed lipid domains, as well as protein clusters, which would be formed as a consequence of the high SP-B concentration.

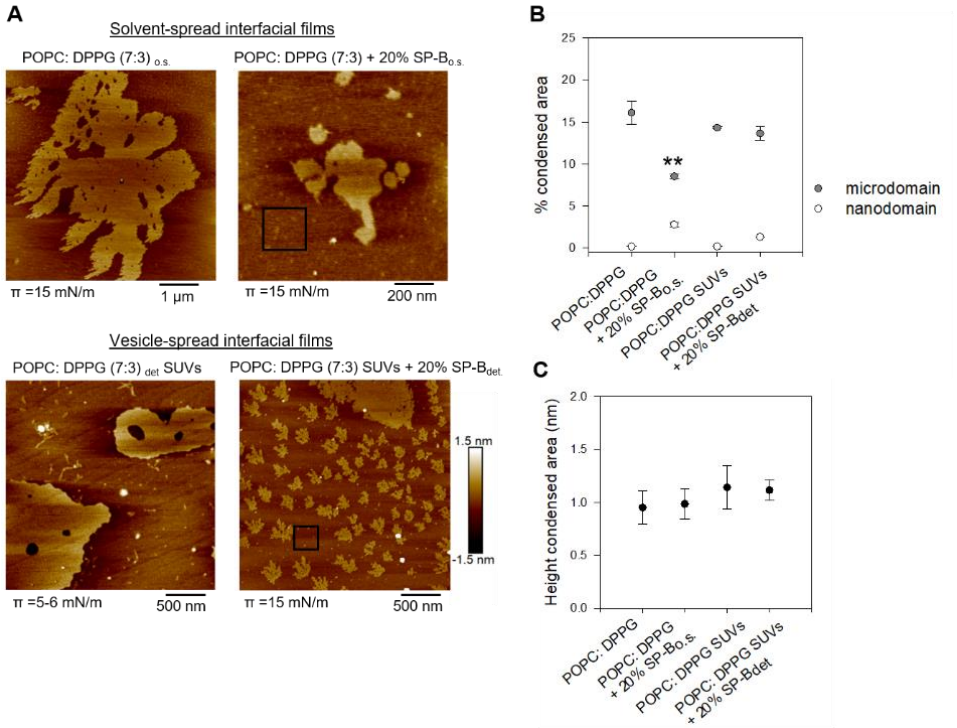

Figure 6.5. Langmuir-Blodgett films of pure POPC:DPPG or POPC:DPPG containing 20% (protein/lipid, by weight) of SP-B isolated in organic solvent (SP-$B_{o.s.}$) or SP-B complexes purified in detergent (SP-B_{det}). A) Height images of different monolayers. Squares tag regions with nanodomains (< 100 nm in their larger axis). **B-C)** Several parameters were quantitatively analyzed in AFM topographic images: % area occupied by micro or nanodomains and height of the condensed domains. Data from pure POPC:DPPG and POPC:DPPG containing 20% SP-B were compared by paired student's t test (** P<0.01 and *** P<0.001).

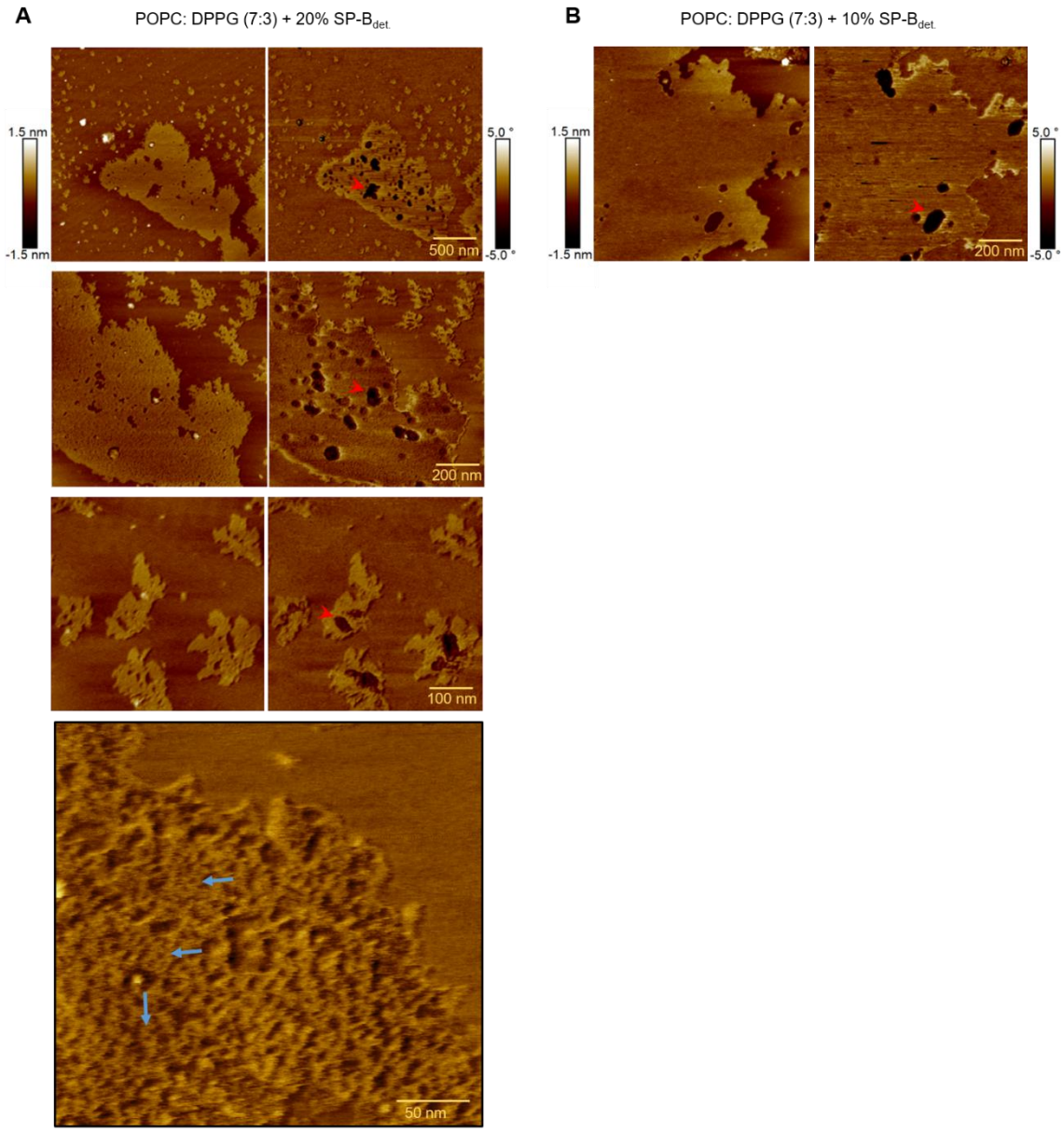

Figure 6.6. AFM image analysis of vesicle-spread interfacial films formed by POPC:DPPG (7:3, w:w) supplemented with SP-B complexes purified in detergent (SP-B_{det}). Monolayers containing 20% **(A)** or 10% **(B)** (protein/lipid; w/w) of SP-B_{det} were transferred at constant surface pressures of 15 or 11 mN/m, respectively. From each pair of micrographs, height (left) and phase (right) images are shown. Besides, lower and larger panel in A) is a magnified height image of a large condensed domain in a monolayer containing 20% SP-B purified in detergent. Red arrowheads in phase images indicate possible protein clusters, whereas blue arrows in the height magnified image point to SP-B rings.

6.2.1.3 Structure of SP-B in interfacial films

SP-B complexes purified from CHAPS-solubilized PS at different concentrations of protein (1 and 2 mg/ml of SP-B_{det}) in the absence of lipids were applied and spread onto the buffered surface of the balance trough. To achieve samples of SP-B_{det} at 1 or 2 mg/ml of protein, purified suspensions of SP-B_{det} were concentrated 10 or 20 times, respectively, in centrifuge tubes supplied with a porous membrane of 10,000 Da of cut off. Interfacial

films of SP-B_{det} were transferred to a mica support at a surface pressure of 11 mN/m (the maximal surface pressure achieved for the film) and analyzed by AFM. SP-B_{det} at a concentration of 2 mg/ml generated films with a variety of protein-detergent structures (**Figure 6.7**): diffused extended structures (**A**), ring-shaped particles (**B**) and also condensed platforms with a height of 0.5 nm over the background, which showed a surface replenished of pores of irregular sizes (**C**). In the case of SP-B_{det} films at lower protein concentration, AFM images showed that the protein was arranged mostly in diffused extended structures and ring-shaped particles (**Figure 6.7 D**). These ring-shaped particles found in films at both SP-B concentrations showed an average diameter of 16.7 (± 4.2), which is consistent with the SP-B rings purified in detergent and visualized by TEM (Olmeda *et al.*, 2015). In order to discard that the structures seen in the SP-B_{det} interfacial films could be artifacts due to the presence of detergent present in the sample, Langmuir-Blodgett films of CHAPS alone were formed. After application of CHAPS at a concentration of 195 mM equivalent to that present in the SP-B 2 mg/ml sample, the material was spread onto the surface of the subphase in the trough and the film was transferred at the maximal surface pressure achieved, 8 mN/m. AFM analysis revealed that CHAPS formed micelles with diameters around 15-30 nm and heights over 1.5 nm, but no other structures could be identified. This fact confirms that the structures observed in films of SP-B purified in detergent are constituted by the protein or protein/detergent assemblies. Upon film compression, the protein could be disposed as thread-like or ring-shaped structures in areas with low SP-B concentration (**Figure 6.7 A, B, D**), whereas more complex structures could be formed as protein concentration increased, as the described large platforms of condensed domains with irregular pores (**Figure 6.7 C**).

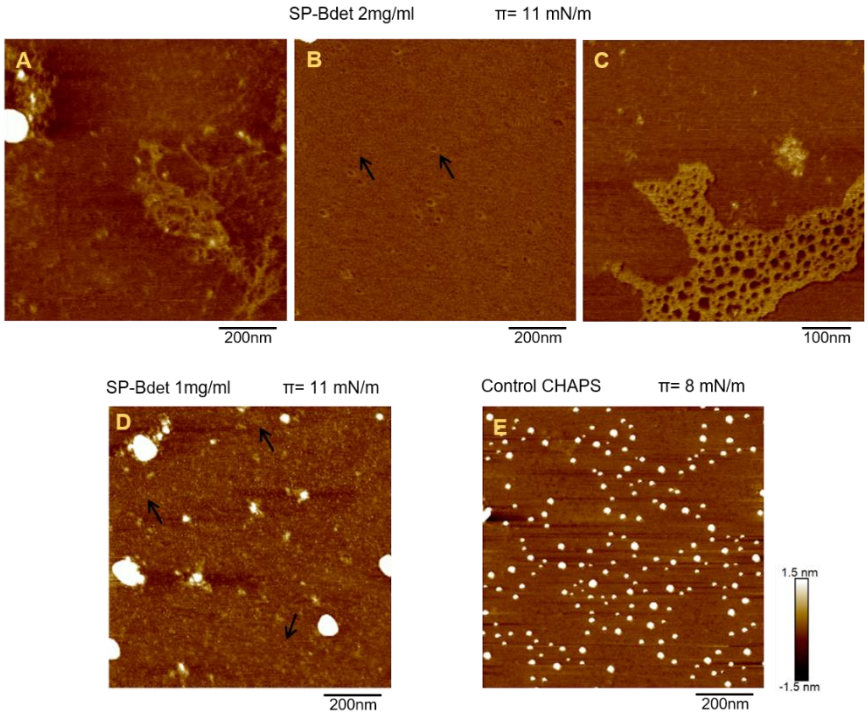

Figure 6.7. Langmuir-Blodgett films of SP-B purified in detergent. Films were formed by deposition onto the interface of SP-B purified in detergent at **(A-C)** 1 mg/ml and **(D)** 2 mg/ml of protein, and transferred at 11 mN/m. **E)** Films of CHAPS at a final concentration of 195 mM. Arrows point to ring-shaped structures.

6.2.2. PURIFICATION OF NATIVE SP-B COMPLEXES FOR HIGH RESOLUTION STRUCTURAL CHARACTERIZATION

Traditionally, hydrophobic surfactant proteins SP-B and SP-C have been purified from organic solvent extraction of pulmonary surfactant or minced lungs. Then, both proteins can be further obtained from the organic extract by two sequential size exclusion chromatographies using organic solvents as eluent. These surfactant proteins can be reconstituted into membranes, preserving most of their original functional properties in the pulmonary surfactant system.

Recently, a new method for native SP-B purification allowed to determine the supramolecular organization of this protein in pulmonary surfactant membranes (Olmeda *et al.*, 2015). Solubilization of pulmonary surfactant by zwitterionic detergent CHAPS (molar ratio detergent:phospholipid 6:1) and a subsequent ion exchange chromatography (IEC) yield native SP-B complexes with a high oligomerization state (**Figure 6.8**). These purified SP-B structures were analyzed by transmission electron microscopy, showing the presence of ring-shaped complexes of 10 nm of diameter, whose structure is consistent with a 3D structural model of SP-B based on the structure of Saposin B. According to this model, each SP-B ring might be formed by the association of 5 or 6 SP-B covalent dimers, although the low resolution of the images together with the heterogeneous nature of the sample did not allow the determination of the structure of the oligomer, including the accurate stoichiometry of the complexes.

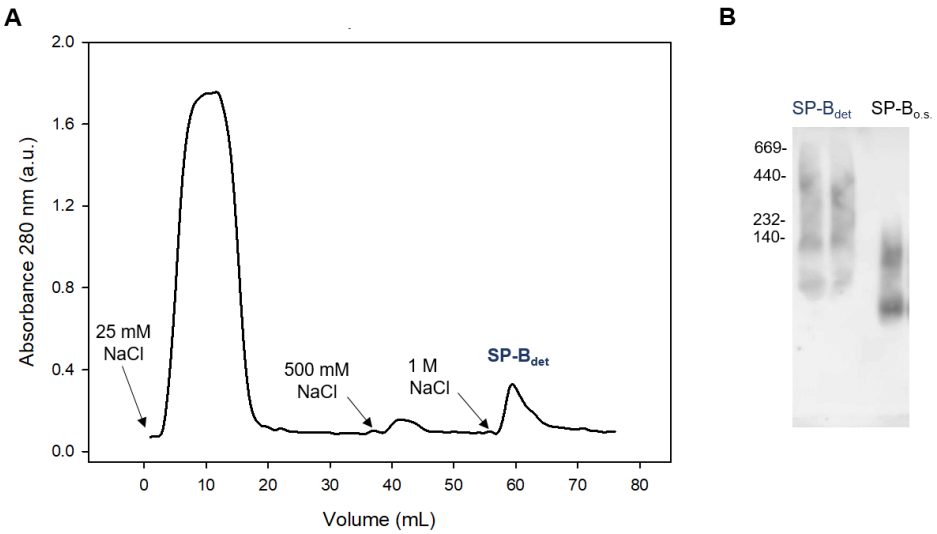

Figure 6.8. Purification of SP-B complexes from CHAPS-solubilized pulmonary surfactant. PS solubilized with CHAPS (detergent:phospholipid molar ratio of 6:1) was loaded onto a Hitrap SP column for ion exchange chromatography (IEC). Phosphate buffers with increasing NaCl concentrations were used. Negatively-charged proteins, such as SP-A, were eluted with 25 mM NaCl. Elution of positively charged proteins required a dramatic increase of ionic strength of buffers, 500 mM NaCl, or even 1M NaCl to ensure the elution of proteins highly attached to the resin. SP-B complexes purified in detergent ($SP\text{-}B_{det}$) were mostly eluted with 1M NaCl-supplemented buffer. **A)** Elution profile of the IEC. **B)** Comparative Blue Native (BN)-PAGE analysis of SP-B complexes purified in detergent ($SP\text{-}B_{det}$) and SP-B isolated in organic solvent ($SP\text{-}B_{o.s.}$). SP-B purified in detergent shows a high oligomerization state, with no clear bands, although the major proportion of the protein seems to be assembled into structures with electrophoretic mobilities corresponding to sizes between 140 and 440 KDa.

Therefore, during this Thesis a number of biochemical methodologies were used with the aim to improve the quality of the samples containing SP-B complexes to a point that could allow obtaining a high-resolution structure of the protein.

6.2.2.1. Size exclusion chromatography of SP-B complexes purified from detergent-solubilized pulmonary surfactant

The first experimental approach consisted on subjecting SP-B complexes purified in detergent to a size exclusion chromatography (SEC) in a fast performance liquid chromatography (FPLC) system. Three different fractions of the previous ion exchange chromatography of CHAPS-solubilized PS were loaded onto the SEC column Superdex 200 10/300GL: a) IEC fraction directly eluted with 1 M NaCl, b) fraction eluted with 0.5 M NaCl (second peak in IEC profile, **Figure 6.8 A**), c) fraction eluted in a second step with 1 M NaCl (third peak in IEC profile, **Figure 6.8 A**), which contained the SP-B rings of 10 nm of diameter observed by TEM. SEC profiles for all the samples contained 2 peaks in common, one eluted at around 9 ml of volume (P1) and a second one that eluted at the end of the chromatography (P3) (**Figure 6.9 A**). The latest peak might be composed by non-assembled protein units, such as SP-B dimers. Besides, IEC fractions eluted with 0.5 M NaCl or directly with 1 M NaCl showed an additional peak between 200 KDa and 12.4 KDa markers (P2). The electrophoretic analysis in the presence of SDS determined that all peaks from each SEC profile contained SP-B, mainly covalent SP-B dimers with a typical electrophoretic mobility of around 20-25 KDa (**Figure 6.9 B**). In contrast, neither SP-A nor SP-C were detected in any of these samples obtained from detergent-solubilized PS.

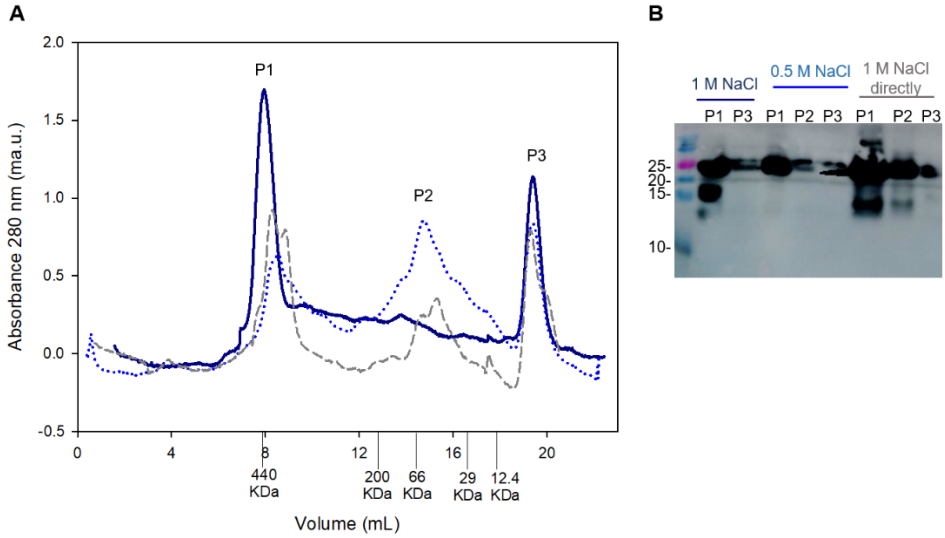

Figure 6.9. Size exclusion chromatography of SP-B complexes purified from detergent-solubilized pulmonary surfactant. A) SEC profiles of Superdex 200 10/300GL column for fractions obtained from IEC of CHAPS-solubilized PS (1) eluted directly with 1 M NaCl (gray dashed line), (2) eluted with 0.5 M NaCl (light blue dotted line), (3) eluted in a second step with 1 M NaCl (dark blue line). Elution volumes of a set of proteins of known molecular weight for SEC column calibration are indicated over x-axis. **B)** Peaks obtained from SEC were analyzed by SDS PAGE in a 16% polyacrylamide gel, followed by α-SP-B western blot.

Fractions obtained from SEC of SP-B complexes purified in the presence of CHAPS and 1M NaCl were also analyzed by non-denaturing electrophoresis (BN-PAGE) and transmission electron microscopy in order to get a deeper structural characterization of SP-B complexes purified in detergent (**Figure 6.10**). BN-PAGE analysis of the original suspension containing SP-B complexes purified in detergent indicates that the sample is composed by supramolecular SP-B assemblies, highly diverse in size (**Figure 6.10 B**). In the case of the fractions obtained from SEC, the non-denaturing electrophoresis showed that SP-B complexes of the different fractions underwent a gradual decrease in size as SEC progressed (**Figure 6.10 B**). BN-PAGE analysis of fraction 1 barely detected SP-B complexes higher than 669 KDa, despite the high absorbance at 280 nm seen for this fraction in the SEC profile. Thus, it is likely that a major part of SP-B was forming part of aggregates which scarcely penetrated into the acrylamide gel. On the other hand, fraction 2 was enriched in SP-B complexes with approximate molecular weights varying from 500 to 200 KDa, whereas fraction 3 contained SP-B complexes with lower molecular weights from around 440 to over 100 KDa. In contrast, bands lower than 66 KDa were detected in fraction 4, similar to those obtained from covalent SP-B dimers isolated in organic solvent (**Figure 6.10 B**). Thus, fraction 4 seemed to contain SP-B dimers, which is in agreement with its late elution in SEC. It is noticeable the discrepancy between the molecular weights of SP-B complexes estimated by BN-PAGE analysis and the estimated molecular weights according to the elution volumes of a set of calibration proteins in the SEC column. This fact could be the consequence of the intrinsic properties of the SEC column (Superdex 200 10/300 GL has a fractionation range for globular proteins of 10,000-600,000 Da) and/ or the presence of self-aggregation process between SP-B complexes after sample collection from SEC.

Finally, the selected fractions from SEC were further analyzed by negative-staining TEM (**Figure 6.10 C**). On the contrary to the expected size separation provided by the chromatography, all fractions showed significant sample heterogeneity. In the case of micrographs from fractions 1-3, ring-shaped particles of 10 nm of diameter were observed, which resembled, in size and shape, those previously described in preparations of SP-B complexes purified from CHAPS-solubilized PS (Olmeda *et al.*, 2015). Fraction 1 also contained large aggregates of protein/detergent micelles, as suggested before in BN-PAGE analysis of this fraction. In contrast, images from fraction 4 seemed to contain small particles, diverse in morphology, which are partly masked by background noise. To sum up, size exclusion chromatography of SP-B complexes purified from CHAPS-solubilized PS allowed to obtain samples enriched in ring-shaped structures but without accomplishing the requirements of sample purity and quality for unraveling the structure of native SP-B complexes at high resolution.

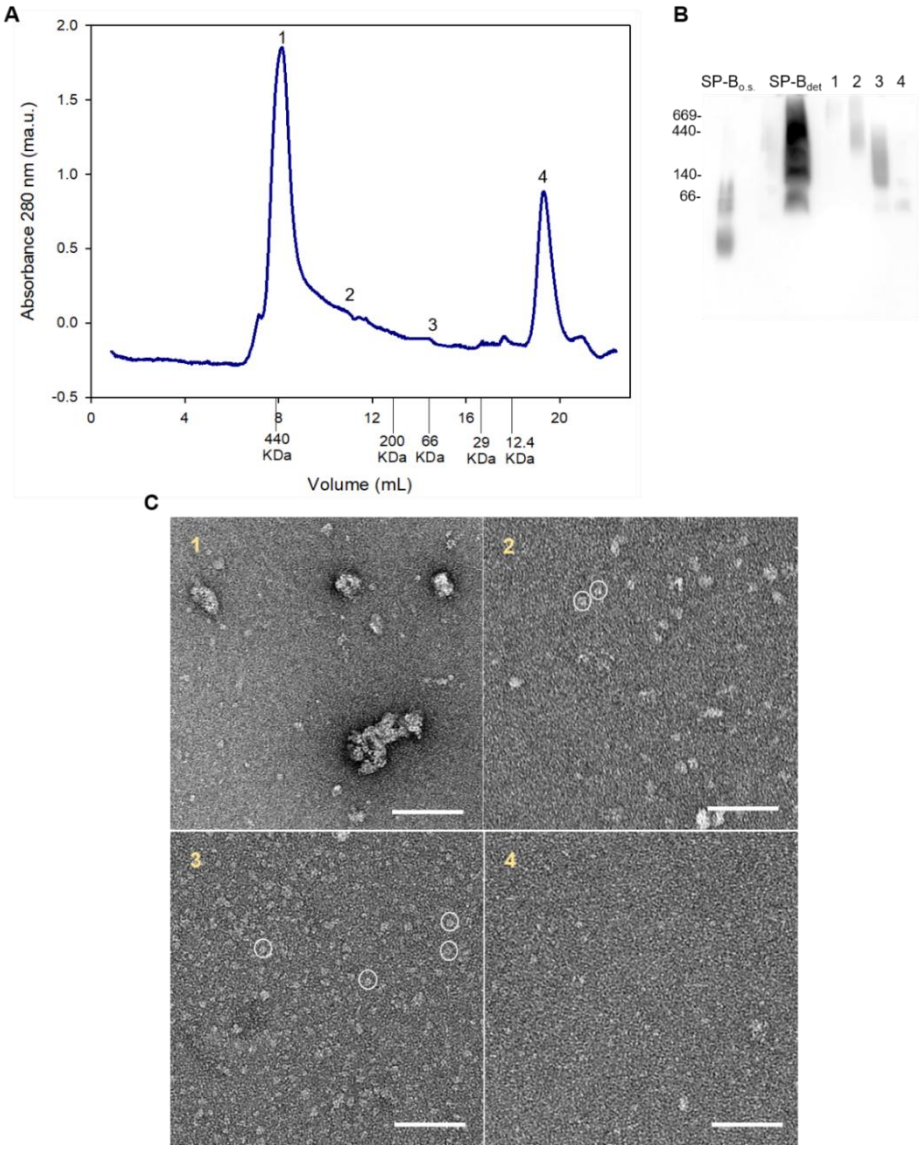

Figure 6.10. Structural characterization of different samples obtained from SEC of SP-B complexes purified in detergent in the presence of 1 M NaCl. A) SEC profile of Superdex 200 10/300GL column. Elution volumes of a set of proteins of known molecular weight for SEC column calibration are indicated over x-axis. **B)** Blue native-PAGE of the original sample containing SP-B complexes ($SP\text{-}B_{det}$) and the obtained fractions from SEC. In addition, a sample containing SP-B isolated in organic solvent ($SP\text{-}B_{o.s.}$) was included in the electrophoretic analysis. BN-PAGE was performed on a 5-20% polyacrylamide gel followed by α-SP-B western blot. **C)** Representative micrographs of selected fractions from SEC taken by negative-staining transmission electron microscopy. White circles indicate ring-shaped structures of 10 nm of diameter. Scale bars, 100nm.

Prior to further structural characterization of SP-B complexes purified in detergent, it was necessary to establish the optimal storage and handling conditions to prevent the alteration of the structure of protein assemblies. So, SP-B complexes were challenged to freezing-thawing cycles or sample concentration processes, and the resulting protein stability was analyzed by SEC profiles. After 1 freezing-thawing cycle, new eluted peaks appeared at around 18 and 23 ml. In addition to those, upon a second freezing-thawing cycle, intermediate peaks emerged in detriment of the main peak containing SP-B

aggregates. Thus, consecutive freezing-thawing cycles of SP-B purified in detergent leads to a progressive disassembly of high molecular weight SP-B particles into SP-B entities of lower molecular weight (**Figure 6.11 A**). On the other hand, upon 20 times sample concentration in centrifuge tubes supplied with a porous membrane of 10,000 Da of cut off, SEC profile of SP-B purified in detergent did not result substantially altered (**Figure 6.11 B**). However, lower molecular weight SP-B entities were lost, as their size was below the cut off of the membrane in tubes.

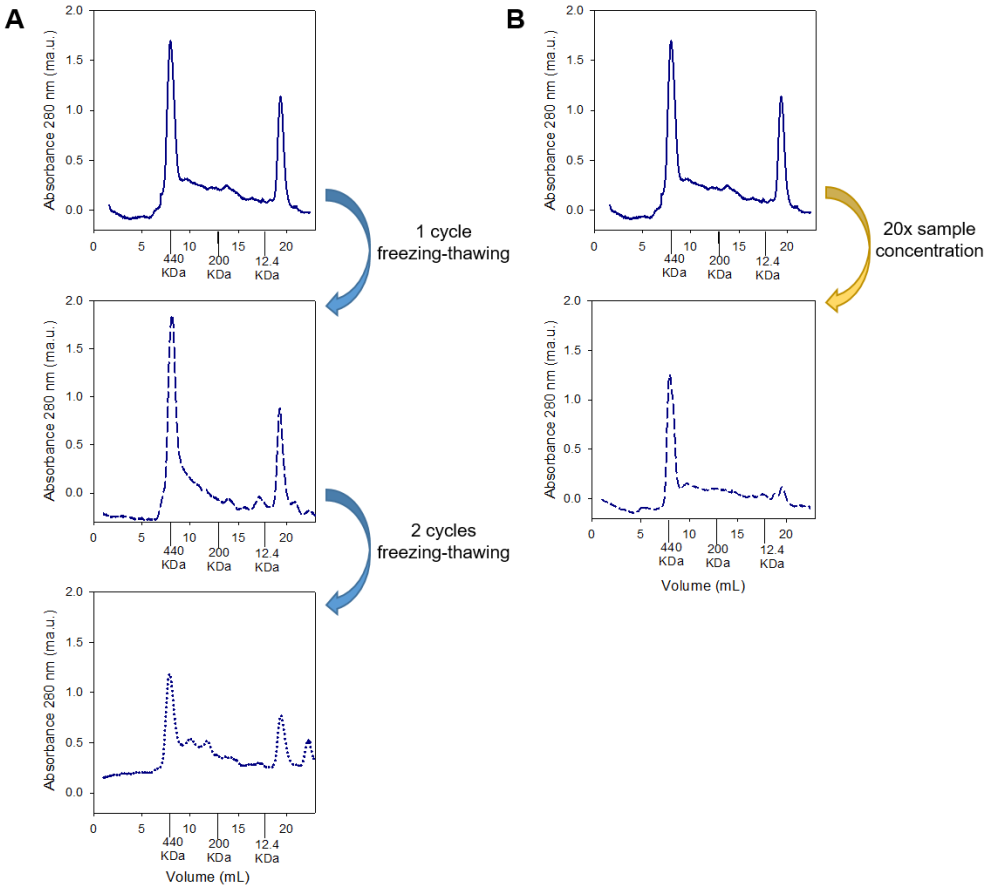

Figure 6.11. Stability of SP-B purified from CHAPS-solubilized PS upon successive freezing-thawing cycles (A) or 20x sample concentration (B). SEC profiles in Superdex 200 10/300GL column are shown where the elution volumes of a set of proteins of known molecular weight are indicated over x-axis.

6.2.2.2. Stabilization of SP-B complexes by GraFix method

This method consists on a purification process by density gradient ultracentrifugation in the presence of a crosslinker gradient, which stabilizes the structure of individual macromolecules and prevents them from aggregation. In order to purify homogeneous samples of SP-B complexes in detergent that could allow its structural characterization at high resolution, SP-B purified from CHAPS-solubilized PS was subjected to a glycerol density gradient ultracentrifugation with an additional gradient of glutaraldehyde, as crosslinker agent. The effect of the crosslinker over the stabilization of SP-B complexes was evaluated by comparison with a glycerol density gradient ultracentrifugation in the absence of glutaraldehyde. In order to set up this method for purification of SP-B

complexes, a number of experiments with different gradients of glycerol and glutaraldehyde were performed, although only the results of the best experimental conditions achieved are shown here. The profile of a 15-45% glycerol gradient ultracentrifugation in the absence of glutaraldehyde (black symbols, **Figure 6.12 A**) together with the SDS-PAGE analysis under non-reducing conditions (**Figure 6.12 B**) showed that a fraction of SP-B purified in detergent was pelleted during centrifugation, while the remaining SP-B was distributed along the tube with a major presence at the top of the tube, in 15-26% glycerol solution. SP-B was detected in major bands of 20 KDa, corresponding to SP-B dimers. In the case of samples with a high SP-B concentration also SP-B monomers can be slightly detected in the western blot.

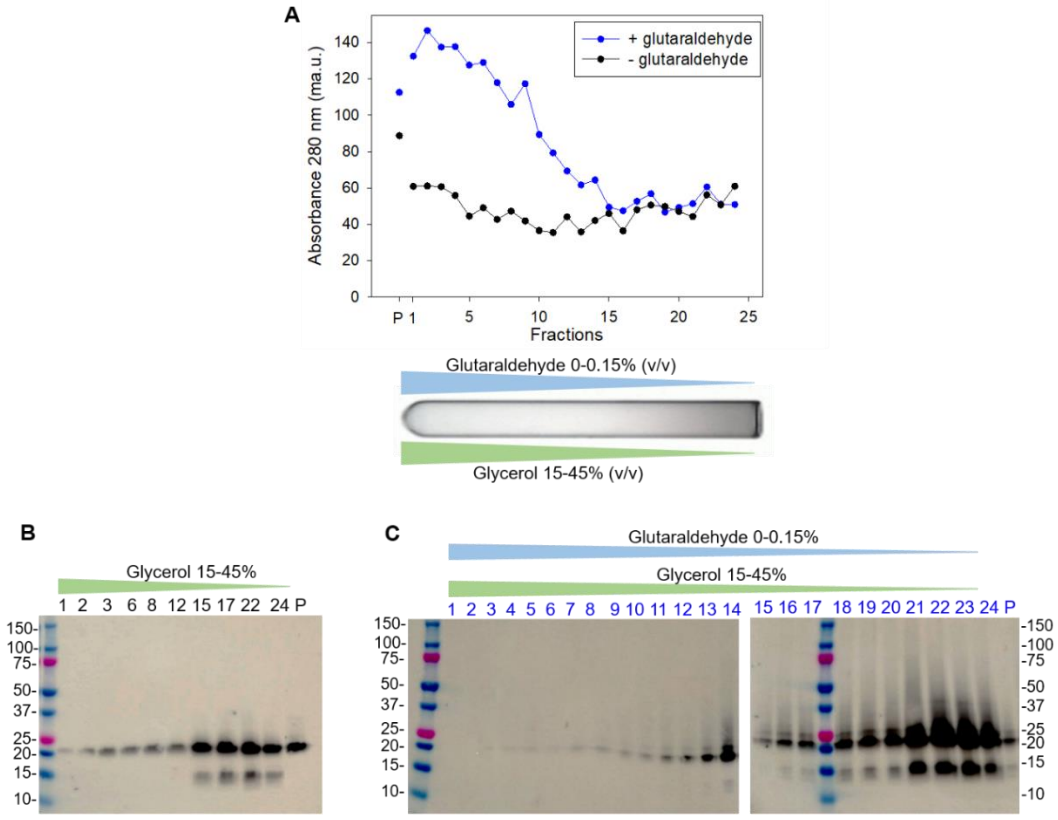

Figure 6.12. Stabilization of SP-B complexes purified from CHAPS-solubilized PS by GraFix method. SP-B purified in detergent was subjected to glycerol-density gradient ultracentrifugation in the presence or absence of an additional glutaraldehyde gradient. After ultracentrifugation, samples were collected from bottom to top of the centrifuge tube and absorbance at 280 nm was measured. **A)** Profile of density gradient ultracentrifugation with (blue) or without (black) glutaraldehyde. In the lower panels, α-SP-B western blots are shown, corresponding to SDS-PAGE analysis under non-reducing conditions of fractions obtained from gradient ultracentrifugation in the absence **(B)** or presence **(C)** of the glutaraldehyde gradient. P corresponds to samples obtained from solubilization of the pellet in buffer.

On the other hand, the glutaraldehyde/glycerol gradient ultracentrifugation revealed that the presence of the crosslinker agent partly prevented the protein from pelleting during ultracentrifugation (blue symbols, **Figure 6.12 A**). SP-B was distributed along ¾ of the tube, with a major presence in 15-19% glycerol solution (**Figure 6.12 C**), where the protein was detected in bands around 20 KDa (SP-B dimer) and higher bands at 25

KDa and 37 KDa, which would correspond to trimers or tetramers of SP-B. These SP-B supradimeric assemblies were detected in solutions with 0-0.06% crosslinker agent, although SP-B tetramers are restricted to 0.006-0.02% glutaraldehyde solutions. As previously seen in gradient ultracentrifugation in the absence of crosslinker, SP-B monomer bands were also observed in samples with high SP-B concentrations. Therefore, the glutaraldehyde gradient did not achieve an efficient stabilization of SP-B complexes, formed by decamers or dodecamers of SP-B.

6.2.2.3. Purification of SP-B complexes by amphipols

As an alternative to detergents, SP-B complexes purified from CHAPS-solubilized PS were stabilized by amphipatic polymers, shortly named as amphipols. Sample suspensions were prepared by addition of amphipols to SP-B complexes purified in CHAPS and subsequent detergent removal. In order to achieve the purification of decamers or dodecamers of SP-B, different suspensions with a wide range of amphipol A8-35/SP-B ratios (from 0.25:1 to 8:1, w/w) were prepared and then analyzed by non-denaturing electrophoresis (**Figure 6.13 A**). For amphipol to protein ratios below 1:1, SP-B was detected as a smear with molecular weights from about 100 KDa up to higher than 669 KDa, so it is very likely that a huge proportion of SP-B would be forming aggregates. In contrast, for amphipol to protein ratios above 1:1, the smear above 140 KDa disappeared, and diffused bands below 66 KDa became more apparent as ratio increases. In the case of amphipol/SP-B ratio 1:1, most of SP-B was detected over 66 KDa and up to ~200 KDa. Previously, ring-shaped SP-B structures had been visualized by TEM in SP-B complexes purified in detergent with similar molecular weights range estimated by BN-PAGE (**Figure 6.10**). Therefore, further characterization of SP-B solubilized in amphipols was performed using the amphipol/SP-B ratio, 1:1. SP-B complexes solubilized in amphipols were analyzed by negative-staining TEM. Micrographs showed the presence of particles with high heterogeneity in size and shape (**Figure 6.13 B**). Four types of structures seemed to be predominant: 1) spherical particles of around 4-5 nm (arrowheads), which might fit with self-assembled polymers of A8-35 (Gohon *et al.*, 2011), 2) fibril structures (arrow) which seemed to be constituted by small round particles, 3 and 4) two types of ring-shaped structures with approximate diameters of 10 nm or 14 nm (white and yellow circles, respectively), which might be constituted by SP-B and amphipols. Since membrane protein/amphipol complexes might slightly increase in size compared with the protein solubilized in detergent (Popot, 2010), it is possible that particles of 14 nm would be composed of SP-B rings stabilized by amphipols, whereas SP-B complexes solubilized in a remainder fraction of CHAPS would constitute the 10 nm-particles.

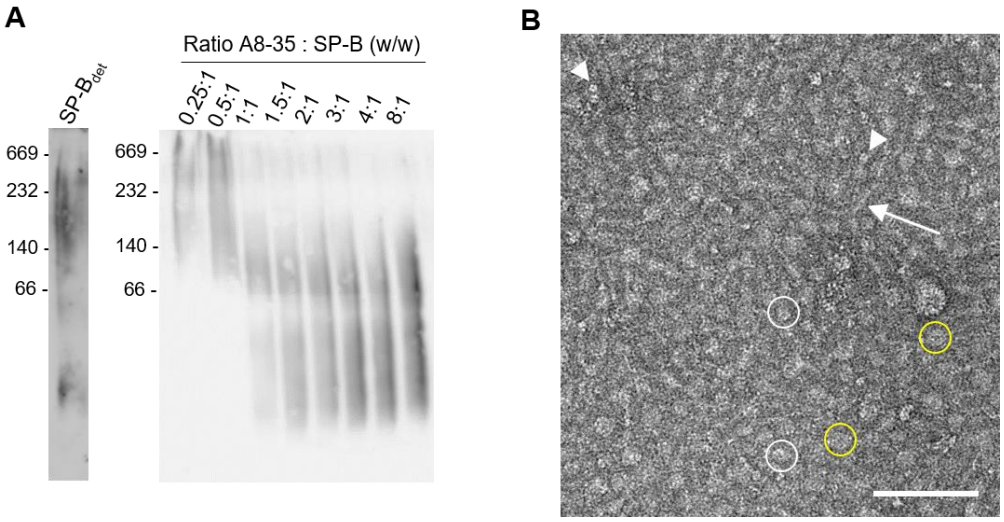

Figure 6.13. Purification of SP-B complexes in amphipol A8-35. A) α-SP-B western blot after BN-PAGE analysis of SP-B complexes solubilized with amphipols at different mass ratios A8-35/ SP-B (right membrane) and the original suspension of SP-B complexes purified in detergent (left membrane). Samples were analyzed by α-SP-B western blot of BN-PAGE in 4-20% polyacrylamide gel. **B)** Representative TEM image of a negatively stained sample of SP-B purified in amphipols (mass ratio A8-35/SP-B, 1:1). Ring-shaped particles with diameters of around 10 nm or 14 nm are labeled within white and yellow circles, respectively. Arrowheads point to particles of around 4-5 nm of diameter, whereas arrow marks a fiber-like structure. Scale bar, 100 nm.

In order to achieve more homogeneous samples, SP-B complexes solubilized in amphipols at a mass ratio A8-35/SP-B of 1:1 were subjected to a size exclusion chromatography (SEC) in a Superdex 200 10/300 column (**Figure 6.14 A**). The chromatogram showed a main peak with a left-shoulder, which might be composed of aggregates. At the end of the SEC profile, some peaks could be observed, that might correspond to SP-B structures of low molecular weight associated or not with amphipols. The main peak of the SEC profile seems to be formed by two peaks overlapped with a high absorbance at 280 nm (P1 and P2). BN-PAGE of P1 and P2 confirmed that these fractions contained SP-B complexes solubilized in amphipols at different oligomerization states (**Figure 6.14 B**). P1 contained mainly SP-B complexes with approximate molecular weights between 200 KDa and 669 KDa, whereas P2 is composed of a wide range of SP-B assemblies, from lower than 66 KDa to about 500 KDa, although SP-B seemed to be enriched in regions between 140 to 440 KDa and below 66 KDa.

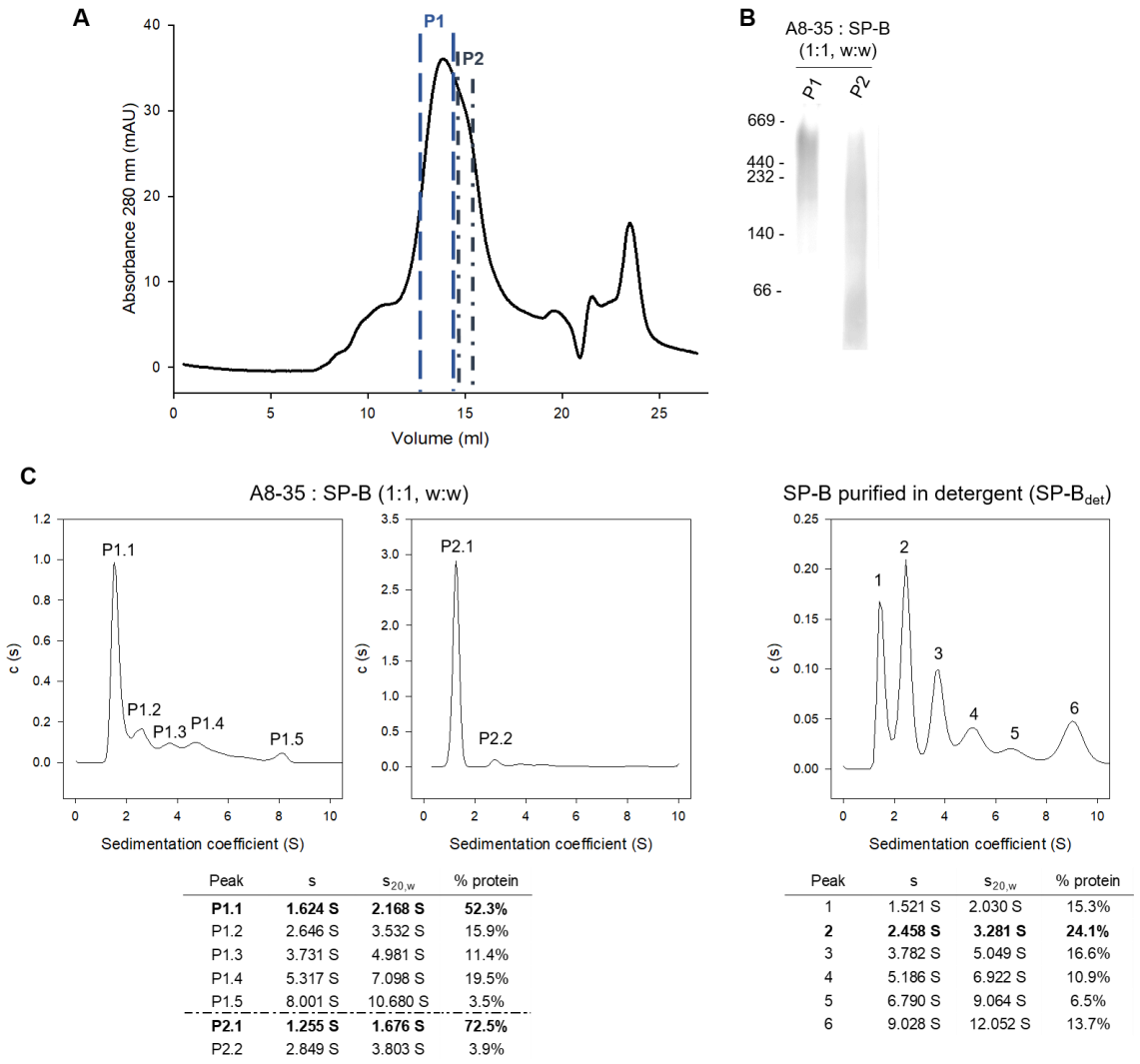

Peak	s	$s_{20,w}$	% protein
P1.1	**1.624 S**	**2.168 S**	**52.3%**
P1.2	2.646 S	3.532 S	15.9%
P1.3	3.731 S	4.981 S	11.4%
P1.4	5.317 S	7.098 S	19.5%
P1.5	8.001 S	10.680 S	3.5%
P2.1	**1.255 S**	**1.676 S**	**72.5%**
P2.2	2.849 S	3.803 S	3.9%

Peak	s	$s_{20,w}$	% protein
1	1.521 S	2.030 S	15.3%
2	**2.458 S**	**3.281 S**	**24.1%**
3	3.782 S	5.049 S	16.6%
4	5.186 S	6.922 S	10.9%
5	6.790 S	9.064 S	6.5%
6	9.028 S	12.052 S	13.7%

Figure 6.14. Characterization of SP-B complexes purified in amphipols (mass ratio A8-35/ SP-B, 1:1). A) SEC profile in Superdex 200 10/300GL column, indicating fractions P1 and P2 collected for subsequent analysis. **B)** α-SP-B western blot after BN-PAGE of P1 and P2 fractions from SEC. **C)** Velocity sedimentation-analytical ultracentrifugation experiments for P1 and P2 fractions from SEC of SP-B solubilized in amphipols (left panels) and for SP-B complexes purified in detergent (right panel). Tables show the calculated sedimentation coefficient (s), the corrected sedimentation coefficient for water as solvent and temperature of 20 °C and the percentage of protein present on each peak, over the total protein in the sample.

Finally, to further characterize the complexes present in the SP-B/amphipol sample, velocity sedimentation experiments in an analytical ultracentrifuge were performed from SEC fractions P1 and P2 containing SP-B solubilized in amphipols, as well as from the original suspension of SP-B complexes purified in detergent (**Figure 6.14 C**). Velocity sedimentation profile of the latter showed that it is a highly heterogeneous suspension, in which SP-B is distributed between 6 main different populations with different sedimentation coefficient, where the most abundant population (24.1%) had a sedimentation coefficient, $s_{20,w}$, of 3.281 S (**right panel, figure 6.14 C**). For samples obtained from SEC of SP-B solubilized in amphipols, velocity sedimentation-AUC showed a moderate heterogeneity of samples (**left panels, figure 6.14 C**). P1 sample was

composed by a main peak with a $s_{20,w}$ value of 2.168 S, which represents 52.3% of total sample, and four additional minority populations, with a maximal $s_{20,w}$ value of 10.68 S. On the other hand, the number of populations in the P2 sample was reduced to two populations, where the most abundant, with a 72.5%, showed a $s_{20,w}$ value of 1.676 S. As it can be observed, results from velocity sedimentation experiments showed a high heterogeneity of the samples, so that they are not suitable for equilibrium sedimentation-analytical ultracentrifugation experiments, which could provide accurate information about the exact mass of each protein species. To sum up, it has been demonstrated that amphipols are able to solubilize SP-B previously purified in detergent, although they fail in stabilizing an oligomeric SP-B structure of a defined molecular size.

6.2.2.4. Purification of SP-B into MSP1D1 nanodiscs

In this case, the SP-B source was not purified from CHAPS-solubilized PS, but SP-B isolated in organic solvent and later reconstituted into POPC vesicles. SP-B isolation into His_6tag-MSP1D1 nanodiscs was attempted following a similar strategy to that previously developed for SP-C solubilization in nanodiscs (Roldán *et al.*, 2014). Suspensions of nanodiscs with different molar ratios of phospholipid to MSP1D1 (40:1; 50:1 and 60;1), but at a fixed MSP1D1:SP-B molar ratio of 4:1, were prepared by addition of cholate-solubilized MSP1D1 to POPC vesicles containing SP-B and solubilized by CHAPS. After detergent removal, different particle suspensions were subjected to a size exclusion chromatography in Superdex 200 10/300GL column for further compositional analysis. SEC profiles for all ratios assayed showed two different populations, which eluted at 12.4 ml and around 15.5 ml, both containing MSP1D1, as shown by the presence of 25 KDa bands in silver-staining SDS-PAGE (**Figure 6.15 A-B**). Faint bands above 25 KDa would correspond to MSP1D1 assemblies that were not entirely denatured and reduced before the electrophoretic analysis, or to traces of contaminant proteins from the recombinant expression of the MSP1D1. Considering the elution volumes for both peaks, the first peak would correspond to MSP1D1 self-assembled to form nanodiscs, whereas the second peak would contain free units of MSP1D1. Regarding SP-B, 15-20 KDa bands corresponding to the surfactant protein were only detected in the nanodisc suspension with the lowest molar ratio phospholipid: MSP1D1, 40:1, although SP-B could not be confined into MSP1D1 nanodiscs, as shown by its presence in the second peak. On the contrary, SP-B might have remained associated to lipids (or even to detergent traces, coming from the process of SP-B solubilization into nanodiscs), which eluted simultaneously with free MSP1D1 (**Figure 6.15 B**). This interpretation of the results is in agreement with those from SP-C solubilization into POPC nanodiscs (Roldán *et al.*, 2014), where SP-C-free POPC nanodiscs formed by the self-assembly of His_6tag-

MSP1D1 eluted at 12.5 ml in Superdex 200 10/300GL column at similar experimental conditions (Roldán López *et al.*, 2017). Thus, in the present work, MSP1D1, at least under the assayed ratios and lipid conditions, does not seem able to incorporate SP-B into assembled nanodiscs.

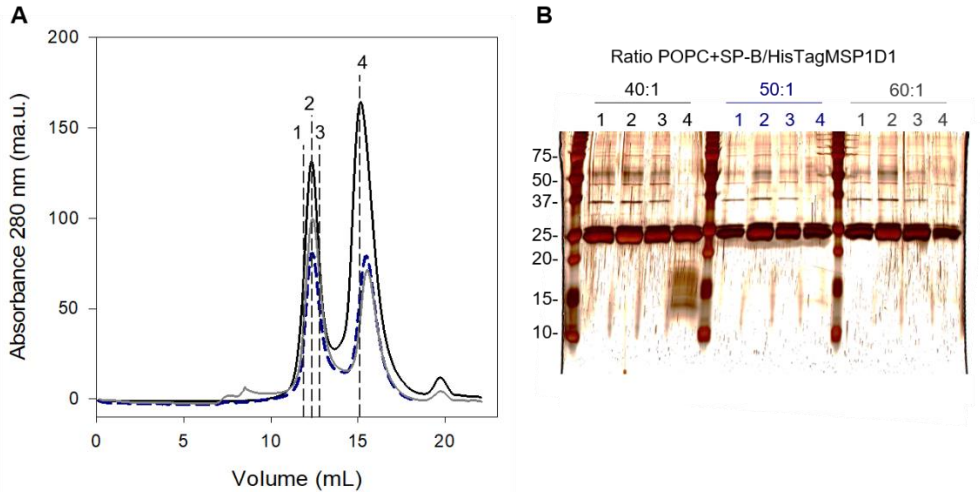

Figure 6.15. Purification of SP-B complexes into MSP1D1 nanodiscs. A) SEC profiles of SP-B nanodiscs obtained at different molar ratios of phospholipid to MSP1D1, 40:1, 50:1 and 60:1. **B)** Selected fractions 1-4 collected from each chromatography were analyzed by silver-staining of SDS-PAGE under-reducing conditions in a 12% polyacrylamide gel. 25 KDa bands correspond to His_6tag-MSP1D1 monomers, whereas 15-20 KDa bands to SP-B.

6.2.2.5. Purification of SP-B into SMA lipid particles

In this work, POPC:POPG vesicles containing SP-B 10% (by weight) were solubilized with styrene maleic anhydride (SMA) copolymers. The size of the resulting lipid nanoparticles can be determined by both the ratio of the mixture of styrene and maleic anhydride polymers and the number of assembled copolymers, which one can easily modulate by the lipid to copolymer ratio (Craig *et al.*, 2016). So, a high lipid/SMA ratio favors the formation of large particles, although the homogeneity of the suspension could be compromised by a scarce membrane solubilization. In our case, the SMA copolymer used was styrene/maleic anhydride at molar ratio 3:1 and lipid nanoparticles were performed at a lipid/copolymer weight ratio of 1:1.5, based on previous literature referring to the solubilization of KCNE1 protein channel isolated into POPC:POPG SMALPs of 14 nm of diameter (Zhang *et al.*, 2017), and the successful confinement of SP-C into POPC lipid nanoparticles using this same ratio (Roldan, Cruz, *et al.*, 2017). Once SP-B/SMALPs were generated, the particle suspension was subjected to a size exclusion chromatography in a Superdex 200 10/300GL column to purify particles from free-copolymer. The chromatogram showed that the suspension contains particles of a wide range of sizes, resulting in the presence of a broad peak of absorbance (**Figure 6.16 A**). It is convenient to mention that SMA copolymer adsorbs at UV wavelengths (Oluwole *et al.*, 2017), so that the secondary peak eluted at the end of the chromatogram could be formed by free SMA and/ or SP-B. In parallel, SMALPs were generated from

POPC:POPG liposomes in the absence of protein. This control sample showed a SEC profile with the main peak narrower than in the case of SP-B/SMALPs (**Figure 6.16 A**). Selected fractions obtained from SEC of SP-B/SMALPs suspension were analyzed by non-denaturing electrophoresis, showing that SP-B was present in a band of about 100 KDa (blue arrowhead) and as smeared bands with molecular weights between 200 and 669 KDa (**Figure 6.16 B**). P1 sample seemed to be particularly aggregated, as a wide amount of protein was not able to penetrate through the gel.

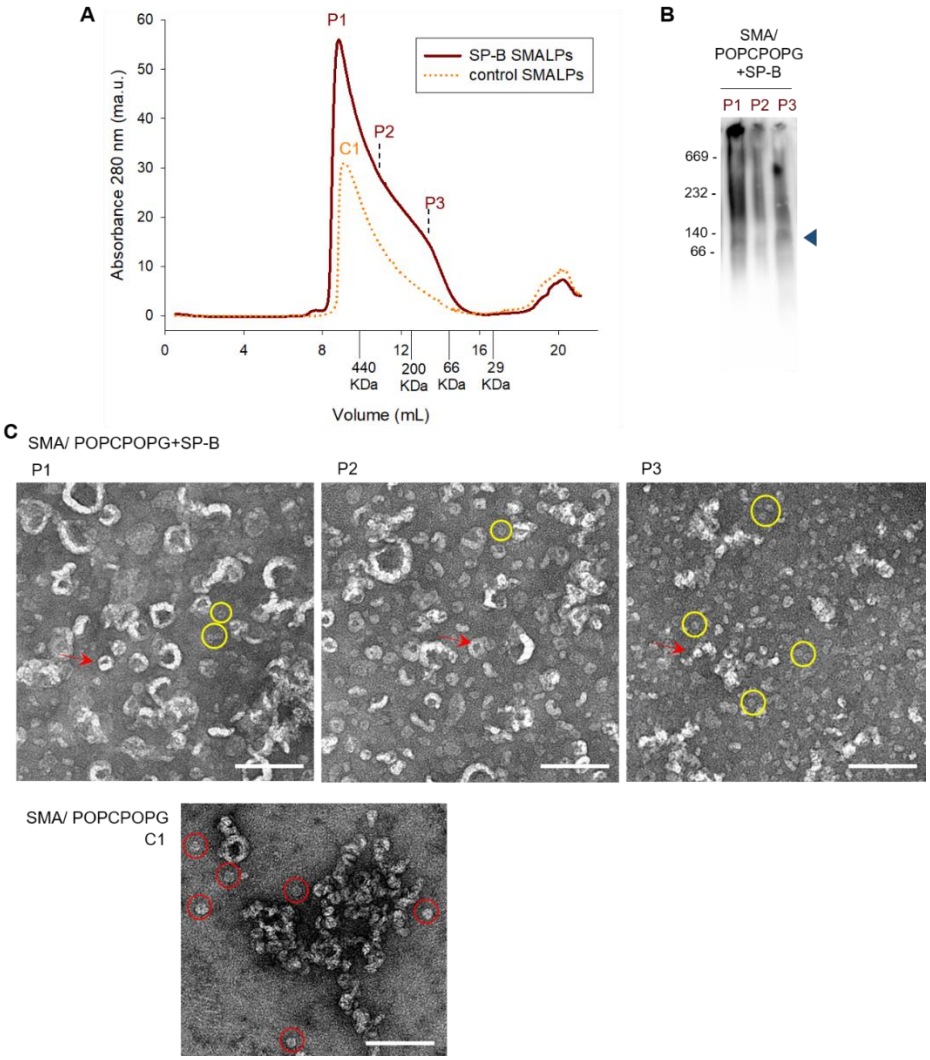

Figure 6.16. Solubilization and purification of SP-B into SMA lipid particles (SMALPs). A) SEC of suspensions composed by SMA lipid particles without protein (orange dashed line) or containing SP-B (dark red line) in Superdex 200 10/300GL column. **B)** SEC fractions of SP-B/SMALPs were analyzed by α-SP-B western blot of BN PAGE in a 4-20% polyacrylamide gel. Blue tag points a 100 Kda band of SP-B present in all analyzed fractions of SP-B/SMALPs. **C)** Negative-staining TEM images of SEC fractions from SP-B/SMALPs (upper panels) and from control SMALPs without protein (lower panel). Yellow circles in SP-B/SMALPs images identify low contrast ring-shaped particles with an average diameter of 10.1 (± 0.6) nm, whereas red circles in control SMALPs point to high contrast particles with average diameter of 14 (± 1.2) nm. Arrowheads indicate round particles with high diffraction contrast. Scale bars, 100 nm.

To keep on characterizing SP-B/SMALPs, the selected SEC samples were analyzed by negative-staining TEM. In general, all samples showed high structural heterogeneity (**Figure 6.16 C**), as SEC profiles and BN-PAGE analysis suggested before (**Figure 6.16 A-B**). Representative images from P1 and P2 samples showed large aggregates and round particles of high diffraction contrast (arrowheads), which became smaller in P3. Particles and aggregates with high diffraction contrast by negative-staining TEM were also seen in POPC:POPG SMALPS in the absence of protein, suggesting that these entities are constituted by the copolymer, which is in accordance with previous published works (Craig *et al.*, 2016; Zhang *et al.*, 2017). On the other hand, images taken from SP-B/SMALPs samples (P1-P3) did not clearly show nanodiscs of defined size containing protein complexes inside. Nevertheless, all SP-B/SMALPs samples showed some ring-shaped particles with lower contrast with an average diameter of 10.1 (± 0.6) nm (white circles) that are not present in POPC:POPG SMALPs. These ring-shaped particles are consistent with native SP-B complexes purified in detergent (Olmeda *et al.*, 2015). Therefore, it is likely that at least part of SP-B would not have been participating in the structure of SMA lipid nanoparticles, but presumably would remain associated only with phospholipids. Further optimization of experimental conditions for SP-B purification into SMALPs could lead to enhance sample quality in order to characterize a high-resolution SP-B structure.

6.3. DISCUSSION

The first evidence of the oligomeric structure of SP-B in pulmonary surfactant was the purification of native SP-B complexes from PS membranes by detergent solubilization (Olmeda *et al.*, 2015). In such preparations, the presence of ring-shaped particles of 10 nm of diameter were revealed by TEM (Olmeda *et al.*, 2015). These SP-B complexes could be formed by the association of 5 or 6 covalent dimers, as a theoretical 3D structural model of SP-B predicts. The existence of native SP-B oligomers has been supported by our results, which show that SP-B dimers isolated in organic solvent are reassembled in membranes forming a ring-shaped structure, consistent in size and shape with native SP-B complexes purified in detergent. Besides, AFM and TEM analysis of bilayers and monolayers containing SP-B complexes showed a preferential orientation of the protein, where the ring-shaped particle was located parallel over the polar lipid surface. This orientation is in agreement with that predicted by the model of SP-B oligomer, in which protein-membrane interaction is hold by the interaction between polar sides of helices 1 and 5 with the phospholipid headgroup, as well as with FRET experiments which assign a superficial topology to the protein, at the headgroup region of lipids (Cabré *et al.*, 2012; Olmeda *et al.*, 2015). Moreover, in the case of interfacial films formed by SP-B

complexes purified in detergent in the absence of lipids, SP-B rings were also located parallel to the air-liquid interface. The preferential orientation of the structure in membranes and interfacial films could be linked to the function of the protein in the pulmonary system, interconnecting membranes (Bernardino de la Serna *et al.*, 2013) and ensuring both fast adsorption of surfactant and a high stability during respiratory dynamics (Schurch *et al.*, 2010). In fact, fusion of lipid membranes promoted by SP-B was observed by TEM in the form of scars between bilayers. Besides the orientation of the structure with respect to the membrane, the information obtained by TEM images also suggests the existence of tight lateral contacts between SP-B particles, as the appearance of fiber-like protein structures could reflect. However, experimental artifacts cannot be discarded as the cause of the generation of the observed fibers due to the high protein concentration of the preparation (10% protein to lipid, by weight), which could induce a non-physiological protein aggregation.

SP-B promotes film stability under mechanical stress and enhances monolayer compressibility to achieve optimal lipid packing (Krol *et al.*, 2000; Diemel *et al.*, 2002; Cruz *et al.*, 2004). In this work, we have analyzed the effect of SP-B on POPC:DPPG films generated by two application methods: 1) placing the surfactant mixture in organic solvent on the air-liquid surface of the through and 2) by deposition of vesicles onto the surface. In contrast to solvent-spread monolayers, the generation of a monolayer film from a vesicle suspension was less efficient, as it was also previously described by (Cruz *et al.*, 2000). The formation of a vesicle-spread monolayer might be probably limited by the opening of bilayers and the transfer of lipid packages to the interface. Our results showed that the presence of SP-B complexes purified in detergent in those vesicles enhanced the transfer of lipids from vesicles to the air-liquid interface and their spreading, allowing the efficient formation of a monolayer film, which, in contrast to vesicles lacking SP-B, was stable at least at the low compression pressures achieved (π = 15 mN/m).

SP-B oligomers were only visualized in monolayers generated from vesicle suspensions containing SP-B purified in detergent, not in solvent-spread films with SP-B. Although a functional characterization of these monolayers would be necessary to determine how the different organization of the protein influences its function in the interfacial film, we hypothesize that the presence of SP-B complexes would imply an enhancement of the film stability upon compression-expansion cycles. Results in Chapter 2 strongly suggested that native SP-B complexes in surfactant membranes were essential for the optimal surface function of surfactant films. Moreover, a comparative study between solvent- and vesicle-spread films reported higher stabilization effects of SP-B on compressed monolayers generated from vesicle spreading (Cruz *et al.*, 2000). We propose that this enhancement in stability upon film compression would be a consequence

of the assembly of SP-B into the oligomeric structure upon reconstitution into lipid vesicles.

SP-B altered the structural organization of condensed domains of POPC/DPPG films at the micro- and the nanoscale. SP-B in solvent-spread films caused a marked decrease of both size and total amount of microdomains, whereas the number of nanodomains increased. Similar effects were previously reported for SP-B in solvent-spread films of DPPC and DPPC:DPPG (Cruz *et al.*, 2004). In the case of vesicle-spread films, SP-B complexes purified in detergent could have a similar effect on the structure of condensed domains of POPC:DPPG films. However, a detailed AFM image analysis of condensed domains in vesicle-spread monolayers suggested the presence of SP-B inside the condensed domains, mostly in ring-shaped structures, but also the existence of some areas enriched in protein, which would be formed by SP-B clusters. Therefore, SP-B complexes present in vesicles maintain its native structure once surfactant material spreads forming a monolayer. The presence of SP-B clusters above 10% of protein (by weight) could suggest that the concentration of SP-B in monolayers exceeds the solubility limit of the protein in lipid films. A number of previous publications reported that the distribution of fluorescently-labeled SP-B is confined to the liquid-expanded phase in solvent-spread DPPC films (Nag *et al.*, 1997; Cruz *et al.*, 2000). Analysis at higher resolution of monolayers using AFM showed that SP-B in solvent-spread films forms protein clusters at the boundaries of liquid-expanded/liquid-condensed phases in DPPC and DPPC:DPPG films (Cruz *et al.*, 2004). Moreover, AFM images of compressed films of DPPG containing SP-B in organic solvent showed the presence of ring-shaped protein structures in the liquid-expanded phase, not associated to condensed domains (Olmeda *et al.*, 2015). Regarding the lipid system used in our study, POPC:DPPG (7:3, w:w), it is predictable that SP-B establishes preferential interactions with the anionic phospholipid DPPG in the monolayer, as it was previously described in membranes (Baatz, Elledge and Whitsett, 1990; Perez-Gil, Casals and Marsh, 1995; Cabré *et al.*, 2012). However, at a low surface pressure of π=15 mN/m, a fraction of DPPG would be forming condensed domains and the remaining would be located at the liquid-expanded phase together with POPC. Thus, the preferential partitioning of SP-B in DPPG condensed domains could be at least partly explained by mere attractive electrostatic interactions between the cationic protein and the negatively charged phospholipid.

In the second part of the present chapter, we addressed the improvement of the purification of SP-B complexes as a prior step to determine the high-resolution structure of the SP-B oligomer by electron microscopy or X-ray crystallography. High-resolution structural techniques require a high homogeneity of the sample and a proper stability of the protein (Carpenter *et al.*, 2008; Thompson *et al.*, 2016). Size exclusion chromatography of SP-B purified in detergent allowed the obtaining of samples

containing ring-shaped SP-B complexes of 10 nm of diameter, free of aggregates and low molecular weight SP-B species, such as dimers. However, non-denaturing electrophoretic analysis and negative-staining TEM images showed that these suspensions enriched in SP-B complexes still had a heterogeneous composition, making them unsuitable for high-resolution structural characterization. Alternatively, we attempted to increase the quality of the sample of SP-B complexes purified in detergent by a method called GraFix (Kastner *et al.*, 2008), which consists on a glycerol gradient ultracentrifugation in the presence of a glutaraldehyde gradient, as crosslinking agent. Glutaraldehyde partly stabilizes SP-B complexes preventing the unspecific aggregation produced during the ultracentrifugation in the absence of the crosslinker. However, the GraFix methodology was not able to stabilize SP-B complexes of the expected molecular weights (87 or 104.4 KDa, depending on whether the complex is formed by the association of 5 or 6 covalent SP-B dimers) (Olmeda *et al.*, 2015). Glutaraldehyde is a bifunctional crosslinking reagent that reacts with amine groups to form Schiff's bases. The efficiency of the crosslinking reaction strongly depends on the proximity of the amine-reactive groups of the protein. For glutaraldehyde crosslinking, amine groups should be at a distance of about 4.8 Å (Wine *et al.*, 2007). As previously argued in the crosslinking experiments between surfactant hydrophobic proteins in Chapter 1, the 3D model of SP-B based on Saposin B structure predicts that the minimal interdimer distances between amino groups of lysines or lysine with amino terminal segment of SP-B are 10.8 and 9.7 Å, respectively, which exceeds significantly the distance between reactive amine groups subjected to glutaraldehyde crosslinking. Thus, crosslinking reaction by glutaraldehyde is not suitable to stabilize the association of 5 or 6 SP-B dimers of the native SP-B complex described in PS membranes.

On the other hand, as an alternative to the use of the zwitterionic detergent CHAPS, an extensive study of SP-B complexes stabilized by amphipols was performed (Kleinschmidt and Popot, 2014). The non-denaturing electrophoretic analysis showed the presence of SP-B complexes of high molecular weight. Besides, the negative-staining TEM images confirmed the existence of ring-shaped particles of 10 nm of diameter, consistent in size and shape with SP-B structures purified in detergent (Olmeda *et al.*, 2015). Nevertheless, the analytical ultracentrifugation of SP-B/amphipols samples determined that the major proportion of the suspension was formed by entities of low molecular weight in a highly heterogeneous sample, suggesting that amphipols were not able to stabilize efficiently SP-B complexes of high molecular weight. Some works pointed that stability and homogeneity of a membrane protein can be further improved by forming ternary complexes consisting of membrane protein, detergent and amphipols (Champeil *et al.*, 2000; Zoonens *et al.*, 2007). Thus, this possibility could be investigated for stabilization of SP-B complexes in the future.

Finally, SP-B complexes were attempted to be confined within membrane nanodiscs prepared by using two different strategies: the membrane scaffold protein MSP1D1 or the copolymer styrene-maleic acid (SMA). In the case of MSP1D1, nanodiscs of POPC were formed, but SP-B could not be incorporated into them. The assembly of two molecules of MSP1D1 in the presence of detergent-solubilized membranes generates nanodiscs of ~ 9.7 nm of diameter (Denisov *et al.*, 2004). Despite the nanodisc size is on the edge to confine ring-shaped SP-B particles of 10 nm of diameter, we previously demonstrated the presence of native SP-B and SP-C complexes into MSP1D1 nanodiscs obtained from detergent solubilized-pulmonary surfactant (Chapter 1). That means that the confinement of SP-B into nanodiscs could be favored by the presence of native surfactant membranes. It is very likely that the anionic phospholipids present in PS, such as PG or PS, accomplish a relevant role by establishing interactions with the cationic charges of the SP-B, favoring the incorporation of SP-B into MSP nanodiscs. On the other hand, SMA lipid nanoparticles were generated from POPC:POPG vesicles containing SP-B. The main advantage of SMALPs over MSP nanodiscs is the possibility to build particles of a desired size by setting the ratio of lipid to SMA copolymer. After subjecting them to a size exclusion chromatography, the electrophoretic analysis showed that SP-B complexes eluted together with SMA lipid nanoparticles. However, TEM micrographs showed that SP-B/SMALPs suspensions were formed by a wide variety of particles and aggregates, which makes difficult to identify SP-B-containing lipid nanoparticles. This heterogeneity could be due to an inappropriate balance between SMA and proteoliposomes, which could be overcome in the future by optimizing the lipid-to-SMA ratio, combined with the use of SMA containing different ratios of styrene/maleic anhydride, which also have influence in the size of the obtained nanoparticles.

Throughout this chapter, the existence of native SP-B oligomers has been determined in lipid membranes containing SP-B from two different sources, SP-B dimers isolated in organic solvent and native SP-B complexes purified from CHAPS-solubilized pulmonary surfactant. Monolayers generated from vesicles supplemented with SP-B complexes purified in detergent showed SP-B rings and protein clusters in condensed domains. Moreover, SP-B rings showed a preferential orientation parallel to the plane of the lipid monolayer or bilayer, and in the absence of lipids, SP-B rings purified in detergent locates parallel to the interface. As mentioned before, this preferential orientation might be intrinsically related to the action of SP-B in the surface behavior of pulmonary surfactant, where SP-B catalyzes the adsorption of lipids and stabilizes the active film by the generation of a surfactant reservoir, mediating tight contacts between membranes. In addition, several membrane protein purification strategies were carried out in order to obtain a high quality sample of SP-B oligomers which could allow the determination of SP-B structure at high resolution. In the light of the obtained results, we can conclude that

solubilization of SP-B complexes in the zwitterionic detergent CHAPS or in amphipols did not yield a sufficient pure and stable sample. Conversely, nanodisc and lipid nanoparticle technologies could be potentially useful to purify an adequate sample of SP-B complexes attached to the surface of negatively charged membranes. However, further studies are required to optimize the yield of SP-B oligomer isolation into lipid discs. For instance, the use of other variants of membrane scaffolding protein MSP and mixtures of copolymers, as well as an appropriate lipid composition, could have a strong impact in the generation of these nanodiscs.

Chapter 4

FLUORESCENCE SPECTROSCOPY APPLIED TO THE STUDY OF THE SUPRAMOLECULAR ORGANIZATION OF SP-B

The experiments included in this chapter was performed during a short-term stay in the Centre for Molecular Chemistry and Physics (Lisbon University, Portugal) assisted and supervised by Dr. Luís Miguel Santos Loura, Pr. Mário Nuno Berberán Santos and Pr. Manuel Prieto. This stay was funded by an EMBO short-term fellowship (7343).

7. FLUORESCENCE SPECTROSCOPY APPLIED TO THE STUDY OF THE SUPRAMOLECULAR ORGANIZATION OF SP-B

7.1. INTRODUCTION

Förster resonance energy transfer (FRET) has been widely used to study protein-protein and protein-lipid interactions, providing relevant information at molecular level given its spatial resolution in the nanometer range.

FRET between identical fluorophores, called homo-FRET, has been revealed as a powerful tool to determine the oligomerization of free and membrane-bound proteins (Lillo *et al.*, 2002; Otto *et al.*, 2003; Bader *et al.*, 2011; Chan, Kaminski and Kaminski Schierle, 2011; Melo *et al.*, 2014). When energy homotransfer is efficient between the fluorophores of a labeled oligomeric protein, the oligomer stoichiometry of the protein can be determined by analyzing the effect of energy transfer on the fluorescence anisotropy of the system. Upon excitation with a polarized light, if a population of fluorophores undergoes homo-FRET, the fluorescence anisotropy will decrease because the fluorophores directly excited by the polarized light can then transfer energy to other fluorophores whose dipole orientations are little (or not at all) correlated with the orientation of the electric field vector of the excitation light. The probability that the fluorophore directly excited by the polarized light will emit a photon decreases with the number of the fluorophores involved in energy homotransfer processes in the cluster. As previously shown by (Runnels and Scarlata, 1995), when the distances between fluorophores within an oligomer are below $0.8R_0$, the anisotropy is inversely proportional to the number of fluorophores if depolarizing rotation is absent.

The first aim of this chapter was to attempt the determination of the SP-B oligomer stoichiometry in synthetic negatively charged membranes and in pulmonary surfactant-derived membranes using homo-FRET methodologies. With this purpose, the extent of homo-FRET among BODIPY-labeled SP-B molecules involved in the protein complex was measured by steady-state and time-resolved fluorescence anisotropy.

Besides the analysis of oligomerization of the native SP-B complex, we investigated the structure of SP-B/membrane aggregates. SP-B interacts peripherally with phospholipid membranes, with its amphipathic helical regions oriented parallel to the membrane surface and establishing electrostatic interactions between its positively charged residues and anionic phospholipids (G Vandenbussche *et al.*, 1992; Morrow *et al.*, 1993; Perez-Gil, Casals and Marsh, 1995; Cruz *et al.*, 1998; Cabré *et al.*, 2012). SP-B has been reported to promote perturbations in membranes leading to aggregation and fusion between vesicles, lipid mixing, and rapid leakage of their content (Oosterlaken-Dijksterhuis *et al.*, 1992; Poulain *et al.*, 1992; Ryan *et al.*, 2005). Furthermore, it has

been proposed that SP-B initiates transfer of lipids between membranes or to the interface through lipid packing disturbance, where the amino-terminal segment of the protein plays a crucial role (Serrano *et al.*, 2006).

Hetero-FRET is particularly useful to study the structural effects of proteins on the organization of the bilayers, due to its large sensitivity to distances in the 1-10 nm scale (Loura, de Almeida and Prieto, 2001; Loura *et al.*, 2006; Coutinho *et al.*, 2008). In the present work, time-resolved FRET experiments combined with a careful analysis based on a meaningful model provided quantitative topological information regarding the interaction of SP-B with POPC:POPG model membranes.

7.2. RESULTS

7.2.1. STUDY OF THE STOICHIOMETRY OF THE SP-B OLIGOMER BY HOMO-FRET

The main goal of the present work is to use homo-FRET measurements to determine the stoichiometry of fluorescently-labeled SP-B in membranes. The presence of homoaggregates of BODIPY/SP-B dimers in surfactant and model lipid membranes has been suggested by steady-state and time-resolved quenching experiments (Cabre *et al.*, 2018). Besides this, the photophysical properties of BODIPY probes make them a useful tool for homotransfer processes (Karolin *et al.*, 1994), so that BODIPY/SP-B was chosen to evaluate the oligomerization state of the protein by homo-FRET fluorescence anisotropy.

The purification process of SP-B involves the use of organic solvents due to its highly hydrophobic character. Under these conditions, its structural conformation is a covalent dimer of 18 KDa stabilized by an intermolecular disulfide bond between Cys 48 residues (Johansson, Curstedt and Jornvall, 1991). In the present work, SP-B purified in organic solvent was covalently derivatized with BODIPY-FL preferentially at its N-terminal segment. In order to determine the stoichiometry of the SP-B complex in membranes, different mixtures of labeled and unlabeled protein were used to generate SP-B oligomers with different fractional labeling (f) in large unilamellar vesicles (LUVs) made of POPC:POPG (7:3, molar ratio). The extent of homo-FRET in the different oligomer species was evaluated by steady-state and time-resolved anisotropy measurements.

Figure 7.1 illustrates the overlap of excitation and emission spectra of BODIPY-FL/SP-B. The homo-FRET Föster radius of BODIPY-FL, R_0, is 5.7 nm (Johnson, Kang and Haugland, 1991). Furthermore, the excitation spectrum of BODIPY-FL/SP-B shows a strong $S_0 \rightarrow S_1$ transition located at 508 nm and a weak $S_0 \rightarrow S_2$ transition, with a maximum intensity at 358 nm. Due to intrinsic characteristics of the equipment, time-

resolved experiments were performed by exciting the sample at a wavelength within the second singlet (S_2), whereas steady-state anisotropy was measured at two different excitation wavelengths that correspond to both excitation singlets, S_1 and S_2.

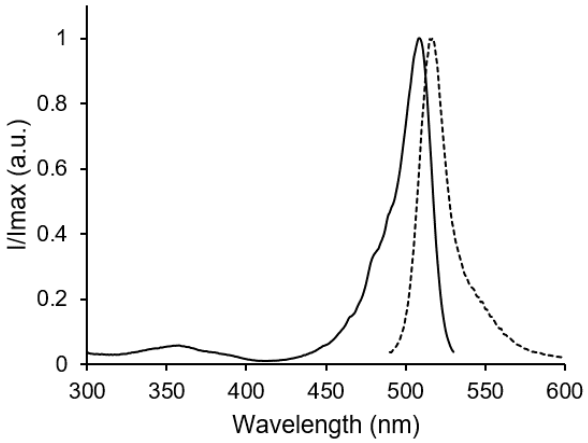

Figure 7.1. Relative excitation and emission spectra of BODIPY-FL/SP-B. Spectra were obtained from POPC:POPG (7:3, mol:mol) LUVs (0.3 mM phospholipid concentration) containing BODIPY-FL/SP-B (0.6% protein/lipid molar ratio). Excitation and emission intensity spectra were obtained at $\lambda_{excitation}$ of 335 nm (solid line) and $\lambda_{emission}$ of 530 nm (dashed line).

Firstly, steady-state fluorescence anisotropy of vesicle suspensions containing BODIPY/SP-B was measured at different fractional labeling (**Figure 7.2** and **table 7.1**). In the case of extreme dilution of BODIPY/SP-B ($f = 0.10$), in which the amount of labeled protein was ten times lower than that of full-labeled protein, the anisotropy values were 0.176 ± 0.003 at λ_{exc} of 470 nm and 0.085 ± 0.010 at 335 nm. These anisotropy values are compatible with the expected anisotropy for a dimer of BODIPY/SP-B, $r_{dimer} = r_0/2$, because the fundamental anisotropy (r_0) of BODIPY-FL shows values of 0.37 and 0.175 at λ_{exc} of 470 nm and 335 nm, respectively (Karolin *et al.*, 1994). According to the 3D model of the SP-B oligomer based on Saposin B structure, 6 dimers could be forming the SP-B complex (Olmeda *et al.*, 2015). Thus, considering the existence of homo-FRET among dimers of the hexameric complex, the anisotropy limit values for the full-labeled SP-B oligomer ($f = 1$) would be 0.031 and 0.015 at $\lambda_{excitation}$ of 470 nm and 335 nm, where $r_{hexamer\ of\ dimers} = r_0/12$. Conversely, the full-labeled SP-B oligomer ($f = 1$) showed a slightly decrease in anisotropy compared to the highly diluted BODIPY/SP-B sample, but this reduction was not large enough to support a supradimeric organization of BODIPY/SP-B. In the same line, the steady-state measurements of samples with intermediate fractional labeling showed anisotropy values only compatible with dimers of BODIPY/SP-B.

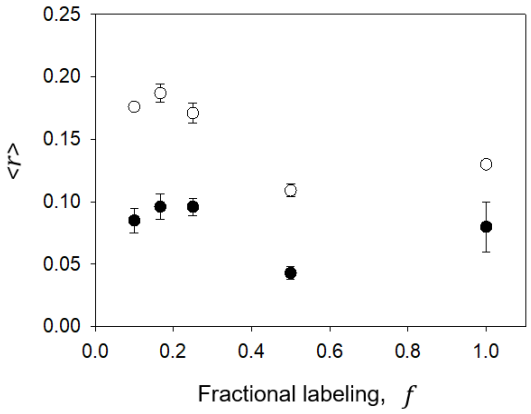

Figure 7.2. Extent of homo-FRET in BODIPY/SP-B oligomers. Steady-state anisotropy measurements at $\lambda_{excitation}$ of 335 nm (black circles) and 470 nm (white circles) of BODIPY/SP-B at different fractional labelling reconstituted into POPC:POPG (7:3, mol/mol) LUVs.

To gain a detailed description of the depolarizing motions of BODIPY/SP-B that occurred in the fluorescence timescale, time-resolved fluorescence anisotropy decays of vesicle suspensions containing BODIPY/SP-B at different fractional labeling were measured, providing information about the amplitude of motion and its rotational correlation time. Anisotropy decays of BODIPY/SP-B were described by two correlation times, independently of the fractional labeling of the sample. In all cases, the anisotropy decays were interpreted as the product of two independent depolarizing processes, since the second rotational times ϕ_2 were about 20-fold longer than the shorter ones ϕ_1 (**Table 7.1**). The fast correlation time reflects the restricted movements resulting from local motions of the covalently bound probe and/or mobility of the protein segment to which the probe is linked. In homo-FRET experiments with fluorescently-labeled proteins, this fast depolarization component is typically due to FRET. On the contrary, the slow correlation time would be related to the overall rotation of the protein in the lipid environment or the whole vesicle in solution (Lipari and Szabo, 1980).

f	β_1	Φ_1 (ns)	β_2	Φ_2 (ns)	$r(0)$	r_∞	$\langle r \rangle_{calc}$	$\langle r \rangle_{\lambda=335\ nm}$	$\langle r \rangle_{\lambda=470\ nm}$
0.10	0.04	1.31	0.07	21.62	0.11	0.07	0.062	0.085 (± 0.010)	0.176 (±0.003)
0.17	0.03	0.85	0.07	18.34	0.11	0.07	0.061	0.096 (±0.010)	0.187 (±0.007)
0.25	0.04	2.00	0.06	34.60	0.10	0.06	0.061	0.096 (±0.007)	0.171 (±0.008)
0.50	0.04	1.10	0.07	22.60	0.11	0.07	0.066	0.043 (±0.005)	0.109 (± 0.005)
1.00	0.05	0.71	0.06	13.53	0.11	0.06	0.057	0.080 (± 0.020)	0.130 (±0.002)

Table 7.1. Time-resolved fluorescence parameters (amplitudes, β_i; rotational correlation times, ϕ_i; residual anisotropy, r_∞) of 0.3 mM POPC:POPG (7:3, mol/mol) LUVs containing BODIPY/SP-B (at different fractional labeling, f, with fixed 0.67% protein/lipid molar ratio). Parameters were obtained from fitting equation 3.4.5 (in 3.4 section of Materials and methods) to the anisotropy decays measured at $\lambda_{excitation}$ of 335 nm. The table also shows the experimental steady-state anisotropy, $\langle r \rangle_{\lambda=335\ nm}$ and $\langle r \rangle_{\lambda=470\ nm}$, and the one calculated using the parameters obtained from the time-resolved analysis, $\langle r \rangle_{calc}$ (equation 3.4.6, in 3.4 section of Materials and methods).

The anisotropy decay of a dimer that undergoes energy transfer process with additional rotational diffusion can be defined by:

$$r = \frac{r_0}{2} \cdot (1 + e^{-2kt}) \cdot e^{-t/\tau_r} \qquad \text{(Eq. 7.1)}$$

being k, the rate of energy transfer and τ_r, the slow rotational correlation time of the system. This equation can be rewritten as a sum of two exponential decays, where the first term defines the depolarizing component due to FRET and the second term describes depolarization caused by rotational diffusion of the fluorophore:

$$r = \frac{r_o}{2} \cdot \left(e^{-\left(2k+\frac{1}{\tau_r}\right)t} + e^{-\frac{t}{\tau_r}} \right)$$

(Eq. 7.2)

Comparing this theoretical formalism of the anisotropy decay with the empirical equation, $\langle r \rangle_t = \beta_1 e^{-t/\phi_1} + \beta_2 e^{-t/\phi_2}$, the first correlation time, ϕ_1, is attributed to $1/2k$, as $1/\tau_r$ can be neglected, and the slow rotational correlation time is described by the second correlation time, ϕ_2.

The recovered values for ϕ_2 defined the local slow motions of the dimer in the bilayer, as the contribution of rotation of the whole vesicle can be neglected. The theoretical prediction from the Perrin equation (Perrin, 1926) for the overall rotation of a vesicle of 100 nm of diameter was 130 µs, in aqueous solution at 23 ºC, suggesting that ϕ_2 in the range of ns described the slow motion of BODIPY/SP-B in the context of the whole rotation of the protein bound to the vesicle.

At infinite times, when $\phi_1 \ll \phi_2$, the residual anisotropy (r_∞) could approximate to $r = \beta_2$ in the empirical formalism fitting to anisotropy decays. The r_∞ values for all BODIPY/SP-B samples were 0.06-0.07 (**Table 7.1**), which is close to the anisotropy at long times predicted for a dimer by the equation, $r = r_0/2 = 0.088$. Following with the analysis, time-zero anisotropy values, $r(0) = 0.10 - 0.11$, (**Table 7.1**) were below the fundamental anisotropy for BODIPY-FL at $\lambda_{excitation}$of 335 nm ($r_0 = 0.175$), indicating the existence of ultrafast motions of the fluorophore which could not be registered within the time resolution of the instrumental setup. Moreover, the steady-state anisotropy calculated from the obtained time-resolved parameters by analysis of anisotropy decays ($\langle r \rangle_{calc}$) showed a deviation compared to experimental steady-state at $\lambda_{excitation}$of 335 nm ($\langle r \rangle_{\lambda=335\,nm}$) for each sample (**Table 7.1**). This could be also attributed to the substantial loss of initial information in the anisotropy decays due to very fast depolarization processes.

The distances between molecules of BODIPY-labeled protein involved in depolarization caused by homo-FRET can be calculated from obtained first correlation times, ϕ_1, and using the equation that relates the rate of energy transfer, k_T, with the donor-acceptor distances, assuming lifetime (τ_D) of BODIPY/SP-B= 4.085 ns (Cabre *et al.*, 2018).

$$k_T = \frac{1}{\tau_D}\left(\frac{R_0}{r}\right)^6$$

(Eq. 7.3)

In the case of the infinitely diluted BODIPY/SP-B sample ($f = 0.10$), the estimated distance between probes of the covalent SP-B dimer was 48.4 Å (**table 7.2**). Donor-acceptor distances were maintained about this value for all samples, suggesting once more that the energy transfer only occurs between covalent BODIPY/SP-B dimer, regardless of the fractional labeling of the sample.

f	Radius (Å)
0.10	48.4
0.17	52
0.25	45.1
0.50	49.8
1.00	53.6

Table 7.2. Distances between BODIPY-linked and N-terminal regions of SP-B dimer calculated from the parameters obtained from time-resolved anisotropy analysis. 0.3 mM POPC:POPG (7:3, mol/mol) LUVs containing BODIPY/SP-B (at different fractional labeling, f, with fixed 0.67% molar ratio of protein to lipid).

A previous fluorescence spectroscopy study showed the interaction between SP-C and homoaggregates of SP-B (Cabre *et al.*, 2018). In that work, quenching studies of wild-type SP-B by SP-C in surfactant lipid membranes showed that SP-C up to a SP-C/SP-B molar ratio of 0.125% led to an increase in tryptophan fluorescence intensity over the intensity observed for SP-B in the absence of SP-C, suggesting that low SP-C densities would cause the dissociation of interconnected SP-B hexamers. In the present work, as we could not detect efficient FRET extent corresponding to the SP-B hexamer by anisotropy measurements, we hypothesized that SP-B oligomers could be participating in a higher molecular structure through apposition of SP-B complexes, leading to fluorescence quenching events that hampered the extent of FRET along all probes contained in a full-labeled BODIPY/SP-B hexamer. Thus, fluorescence anisotropy was evaluated in vesicle suspensions made by surfactant lipids, containing BODIPY/SP-B with different fractional labeling and SP-C (at protein-to-lipid molar ratios of 0.7% and 0.088%, respectively) (**table 7.3**). Steady-state anisotropy measurements at both excitation wavelengths (335 and 470 nm) showed similar values for the extremely diluted BODIPY/SP-B ($f = 0.10$) in the absence and in the presence of SP-C (compare **tables 7.1** and **7.3**). In the case of full-labeled BODIPY/SP-B ($f = 1$), the observed steady-state anisotropy values were scarcely lower than those observed for the diluted labeled protein in the presence of SP-C (**table 7.3**), suggesting the sole presence of BODIPY/SP-B dimers. These observations were corroborated by the analysis of anisotropy decays of each sample, where the residual anisotropy (r_∞) values obtained were 0.08 and 0.06 for diluted and full-labeled BODIPY/SP-B samples, respectively, which resemble well the

long times anisotropy expected for a dimer, as mentioned above. Therefore, SP-C did not contribute to enhance the extent of homo-FRET among BODIPY/SP-B molecules.

f	β_1	Φ_1 (ns)	β_2	Φ_2 (ns)	$r(0)$	r_∞	$\langle r \rangle_{calc}$	$\langle r \rangle_{\lambda=335\ nm}$	$\langle r \rangle_{\lambda=470\ nm}$
0.10	0.04	1.35	0.08	27.00	0.11	0.08	0.069	0.077 (± 0.013)	0.189 (±0.011)
1.00	0.04	1.03	0.06	17.50	0.10	0.06	0.051	0.043 (±0.003)	0.133 (±0.002)

Table 7.3. Time-resolved fluorescence parameters (amplitudes, β_i; rotational correlation times, ϕ_i; residual anisotropy, r_∞) of 0.357 mM of surfactant lipid fraction (LF) LUVs containing SP-C (0.088% protein/lipid molar ratio) and BODIPY/SP-B (at different fractional labeling, f, with fixed protein/lipid molar ratio of 0.67%). Parameters were obtained from fitting equation 3.4.5 (in 3.4 section of Materials and methods) to the anisotropy decays measured at $\lambda_{excitation}$ of 335 nm. The table also shows the experimental steady-state anisotropy, $\langle r \rangle_{\lambda=335\ nm}$ and $\langle r \rangle_{\lambda=470\ nm}$, and the one calculated using the parameters obtained from the time-resolved analysis, $\langle r \rangle_{calc}$ (equation 3.4.6, in 3.4 section of Materials and methods).

Finally, to evaluate a potential effect of the probe on the structure of SP-B oligomer, POPC:POPG (7:3) vesicles containing BODIPY/SP-B or SP-B (0.67% molar protein/lipid) were visualized by atomic force microscopy. Micrographs of both samples showed the presence of ring-shaped particles with similar averaged diameters (14.5 ± 2.7 nm, for BODIPY/SP-B, and 15.3 ± 3.9 nm for SP-B) (**Figure 7.3**). These particles are consistent in size and shape with the SP-B oligomers previously described by transmission electron and atomic force microscopies (Olmeda *et al.*, 2015).

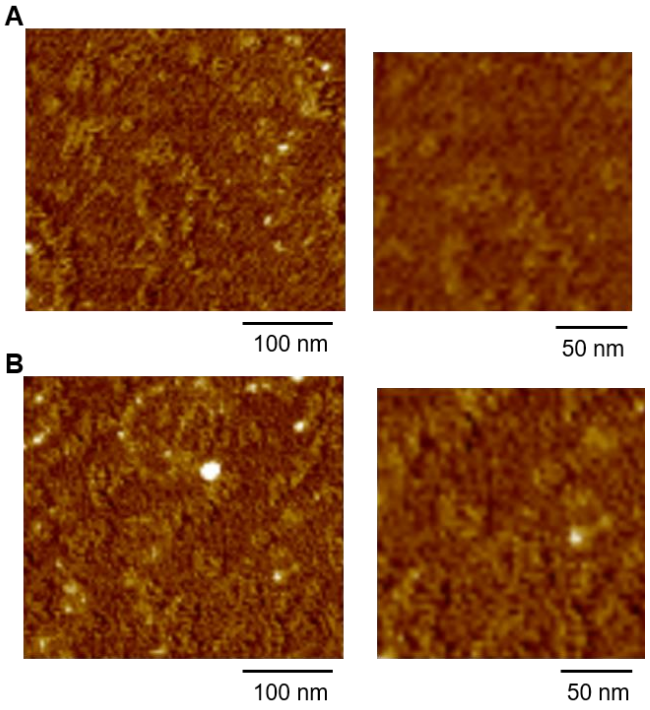

Figure 7.3. AFM micrographs of oligomers of BODIPY/SP-B and SP-B in bilayers. BODIPY/SP-B **(A)** or SP-B **(B)** (0.67% protein/lipid molar ratio) were reconstituted into small unilamellar vesicles of POPC:POPG (7:3, molar) at 65 µM final lipid concentration. Both samples showed ring-shaped particles. The averaged diameter of these rings were 14.5 (± 2.7) nm, for BODIPY/SP-B and 15.3 (± 3.9) nm for SP-B. Depth of images is 3 nm. Magnified images are shown on the right.

7.2.2. MULTILAMELLAR STRUCTURES INDUCED BY SP-B: A FRET STUDY

The structure of aggregates formed by SP-B in negatively-charged membranes made of POPC:POPG, 7:3 molar ratio, were analyzed using FRET methodologies. FRET experiments were performed between donor and acceptor membrane probes,

BODIPY(500/510)-PC and ORB, respectively, or between SP-B labeled with BODIPY-FL as donor, and ORB as acceptor.

7.2.2.1. R_0 calculations

All energy transfer experiments performed involved the use of BODIPY derivative probes and octadecyl rhodamine B (ORB). Emission spectra of BODIPY-FL/SP-B and BODIPY(500/510)-PC (donors) overlap with the absorption spectrum of ORB (acceptor), which makes these probes suitable as a FRET pair (**Figure 7.4**).

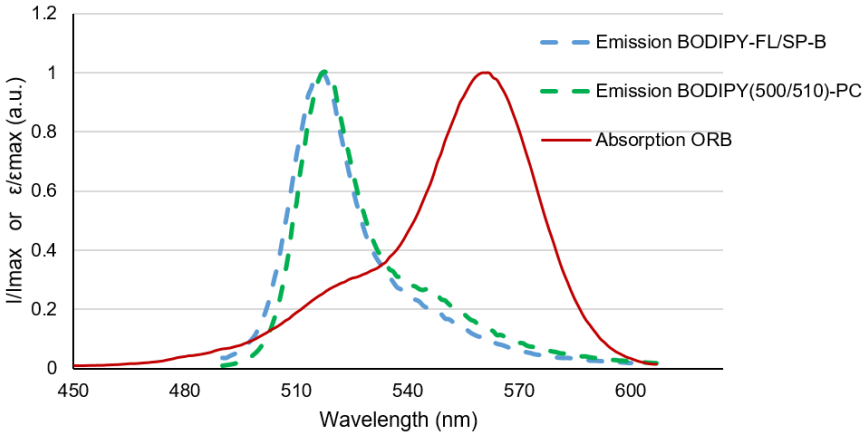

Figure 7.4. Corrected normalized fluorescence emission spectra of BODIPY-FL/SP-B and BODIPY(500-510)-PC (both with excitation at 335 nm) and ORB absorption spectrum. Spectra were obtained from samples of POPC:POPG (7:3, mol:mol) LUVs (0.5 mM phospholipid concentration) supplemented with BODIPY-FL/SP-B, BODIPY(500-510)-PC or ORB. Probe/lipid molar ratios were 1:1000 for BODIPY derivatives and 1:400 for ORB.

Förster radius (R_0), or the critical distance at which the transfer efficiency is 50% for an isolated donor-acceptor pair, was calculated for both FRET pairs, BODIPY-PC/ORB and BODIPY-SP-B/ORB, using the relationship (Lakowicz, 2006):

$$R_0 = 0.2108 \cdot [\kappa^2 \cdot \Phi_D \cdot n^{-4} \cdot \int_0^{\infty} I_D(\lambda) \cdot \varepsilon_A(\lambda) \cdot \lambda^4 \cdot d\lambda]^{1/6} \qquad \text{(Eq. 7.4)}$$

where κ^2 is the orientation factor (assumed in this study as 2/3, the dynamical isotropic value, whose validity for fluid bilayers is extensively discussed in (Van Der Meer, Coker III and Chen, 1994; Loura, Fedorov and Prieto, 1996)), Φ_D is the donor quantum yield in the absence of acceptor, n is the refractive index, λ is the wavelength, $I_D(\lambda)$ is the normalized donor emission spectrum and $\varepsilon_A(\lambda)$ is the molar absorption spectrum of the acceptor.

The quantum yield of the donor, Φ_D, was estimated for BODIPY-FL/SP-B reconstituted into LUVs to be 0.78, assuming proportionality between the quantum yield and the area under the intensity decay. For BODIPY(500-510)-PC, the published value of quantum yield of the probe in ethanol was used (Φ_D= 0.90) (Haugland, 2002). From these values and the measured spectra, R_0 of 5.5 and 5.7 nm were calculated for BODIPY-PC/ORB and BODIPY-SP-B/ORB FRET pairs, respectively.

From the analysis of time resolved donor decays in the absence ($i_D(t)$) and in the presence of acceptors ($i_{DA}(t)$), FRET efficiency, E_t, can be calculated by

$$E_t = 1 - \int_0^\infty i_{DA}(t)dt \Big/ \int_0^\infty i_D(t)dt$$

(Eq. 7.5)

7.2.2.2. FRET modelling

Time-resolved FRET experiments can also offer quantitative topological information regarding the interaction of the protein SP-B with POPC:POPG model membranes. To get this aim, two different experimental configurations were considered: 1) FRET between membrane probes (**Figure 7.5 A-B**) and 2) FRET between BODIPY/SP-B and an acceptor membrane probe (**Figure 7.5 C-E**). For each FRET pair, different formalisms were developed based on (Coutinho *et al.*, 2008), describing different donor/acceptor distributions.

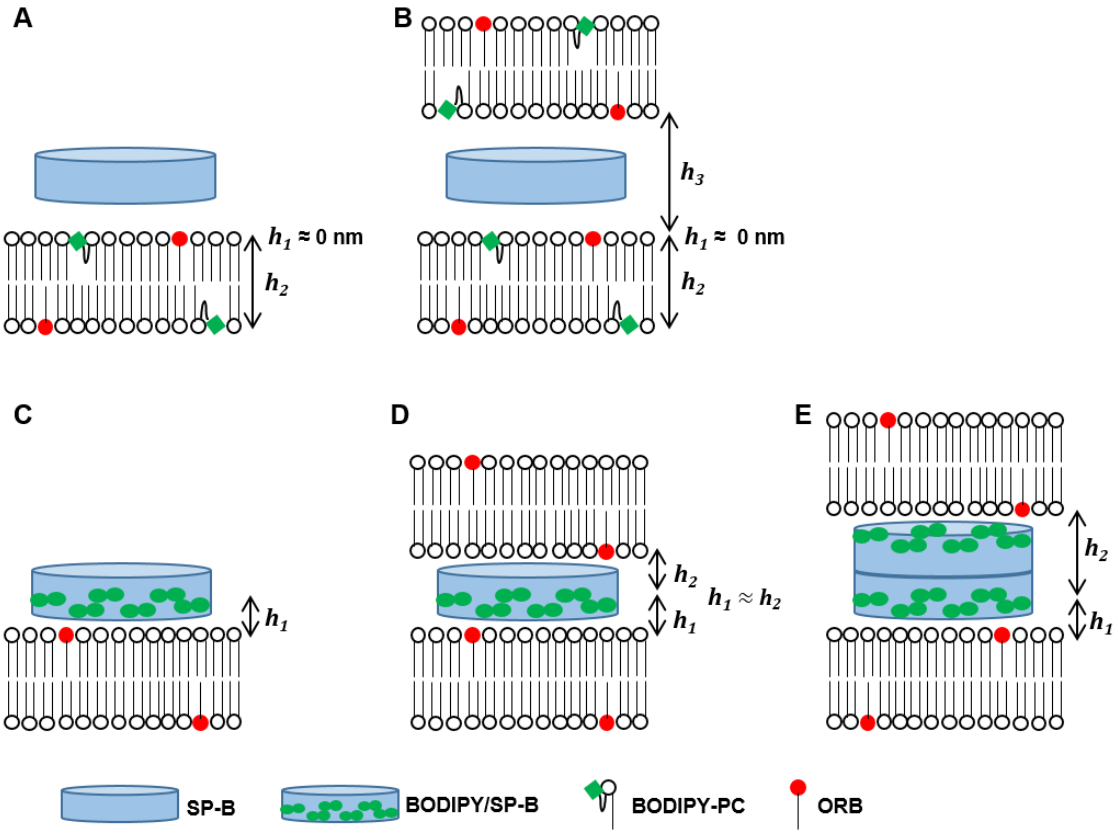

Figure 7.5. Schematic diagrams of the FRET models used for the study of bilayer stacking induced by SP-B. FRET between two membrane probes (**A** and **B**) or between SP-B labeled with BODIPY and acceptor membrane probe (**C–E**). **A** and **C** depict topological models for SP-B interaction with only one bilayer, whereas **B, D** and **E** illustrates arrangements for SP-B-mediated aggregation of bilayers. These models only considered the interaction between two bilayers, since the contribution of a third bilayer to the FRET would result negligible given the Förster radii of the FRET pairs. h_1, h_2 and h_3 indicate the donor-acceptor distances for each FRET situation.

Figure 7.5 A illustrates a FRET scenario between membrane probes in the absence of vesicle aggregation. Each donor fluorophore transfers energy to acceptor molecules located in the same leaflet at transverse distance h_1, or located in the opposite leaflet of the bilayer at distance h_2. So, the donor decay in the presence of uniformly distributed acceptor is defined by:

$$i_{DA}(t) = i_D(t)\rho(t, h_1)\rho(t, h_2) \quad \text{(Eq. 7.6)}$$

where

$$i_D = \sum_i A_i \exp(-t/\tau_i) \quad \text{(Eq. 7.7)}$$

is the donor decay in the absence of acceptor, given by a sum of exponentials. The FRET contributions were calculated from (Davenport *et al.*, 1985):

$$\rho(t, h) = \exp(-tkChF(t, h)) \quad \text{(Eq. 7.8)}$$

where

$$C = \Gamma(2/3)n\pi R_0^2 \quad \text{(Eq. 7.9)}$$

and

$$F(t, h) = \int_0^\infty \frac{1 - exp[(-t/\tau)(R_0/h)^6\alpha^6]}{\alpha^3} d\alpha \quad \text{(Eq. 7.10)}$$

$k = 2/R_0^2$, n is the surface density of acceptors, τ is the average donor lifetime in the absence of acceptor (Loura *et al.*, 2006), and Γ is the complete gamma function.

If $h_1 \ll R_0$, where donor and acceptor probes show identical transverse location, the corresponding FRET contribution is simplified

$$\rho(t, h_1) \cong \rho(t) = \exp\left[-C(t/\tau)^{1/3}\right] \quad \text{(Eq. 7.11)}$$

Figure 7.5 B illustrates the situation of SP-B-induced bilayer aggregation. Here, a new acceptor plane becomes available for each donor at distance h_3. Thus, an additional term is inserted in the donor decay law,

$$i_{DA}(t) = i_D(t)\rho(t, h_1)\rho(t, h_2)\rho(t, h_3) \quad \text{(Eq. 7.12)}$$

Figure 7.5 C depicts the FRET situation between donors bound to SP-B protein and acceptor membrane probe without vesicle aggregation. Each donor fluorophore can only sense acceptors that share the same transverse location

$$i_{DA}(t) = i_D(t)\rho(t, h_1) \quad \text{(Eq. 7.13)}$$

Figure 7.5 D-E refers to FRET from BODIPY/SP-B to two planes of acceptor of different bilayers. Both cartoons depict the situation of vesicle aggregation induced by the protein, although they differ on the mechanism by which the protein mediates contacts between bilayers, through a single SP-B oligomer (D) or through the vertical apposition of two SP-B oligomers (E). In the case depicted in **Figure 7.5 E**, the donor decay is given by

$$i_{DA}(t) = i_D(t)\rho(t, h_1)\rho(t, h_2) \qquad \text{(Eq. 7.14)}$$

If the membrane aggregation is induced by only one single SP-B oligomer (**Figure 7.5 D**), then $h_1 \approx h_2$ (similar distance from donors to both acceptor planes).

7.2.2.3. Partitioning of ORB into POPC:POPG membranes

Time-resolved experiments presented in this chapter were performed between BODIPY derivatives as FRET donor molecules, and ORB as the FRET acceptor membrane probe. ORB is a cationic amphiphilic fluorescent probe which is able to bind and insert into a lipid bilayer, with the acyl chain of 18 carbons protruding into the bilayer and the fluorophore located at the level of the polar heads of phospholipids. In the aqueous phase, ORB can be found as fluorescent monomers or forming non-fluorescent aggregates, with a critical aggregation concentration of 14 nM (Kenichi and Yoshinori, 1994; Buranda *et al.*, 2010). The aim of the present study is to analyze the organization of SP-B into membrane aggregates by FRET detection between the membrane probes BODIPY-PC (donor) and ORB (acceptor) or between the SP-B labeled with BODIPY and ORB inserted into the membrane, so that an uncharacterized partial incorporation of ORB in the membranes could hinder the interpretation of the FRET analysis. Thus, it was necessary to determine the optimal liposome concentration that ensures the complete incorporation of ORB into membranes. Suspensions of POPC:POPG (7:3, mol/mol) LUVs at different phospholipid concentration with a fixed concentration of ORB (0.75 µM) were prepared and their fluorescence intensity was measured (at excitation wavelength of 505 nm). In order to favor the partitioning of ORB into liposomes, the probe was dried together with the lipid mixture and then reconstituted into vesicles. The plot of fluorescence intensity depicts how ORB soluble in water scarcely showed fluorescence, whereas its fluorescence intensity raises as phospholipid concentration increases, until reaching a plateau up to 0.2 mM of POPC:POPG liposomes (**Figure 7.6**).

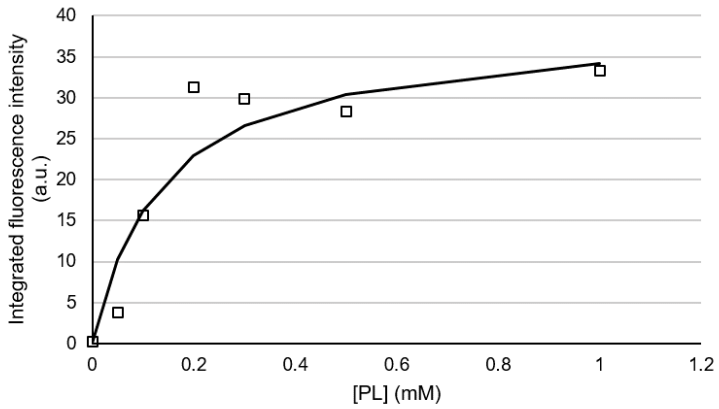

Figure 7.6. Partitioning of the acceptor probe, ORB, into membranes. Integrated fluorescence intensity over the emission spectrum, at an excitation wavelength of 505 nm, in the absence or presence of POPC:POPG LUVs at different phospholipid concentrations, from 0.05 to 1 mM.

The partition coefficient, K_p, of ORB into POPC:POPG vesicles was calculated from the intensity measurements by using the following equation (Santos, Prieto and Castanho, 1998):

$$I - I_w = \frac{(I_L - I_W)K_p\,\gamma_L\,[L]}{1 + K_p\,\gamma_L\,[L]} \qquad \text{(Eq. 7.15)}$$

where I_L and I_W are the limit fluorescence intensity with all the probe in lipid phase or in water, respectively, γ_L is the molar volume of lipid phase, and $[L]$ is the lipid concentration. By plotting the values $I - I_w$ measured at 505 nm versus $[L]$ of the different suspensions of ORB-labeled vesicles and fitting to a hyperbolic regression, a value of K_p = 9.9 (±5.2)·10^3 was obtained, considering γ_{POPC}= 0.754 M^{-1} (Koenig and Gawrisch, 2005) and γ_{POPG}= 0.723 M^{-1} (Marsh, 2013).

The membrane-bound solute mole fraction of ORB, x_L, for a defined lipid concentration is described by:

$$x_L = \frac{K_{p,x}[L]}{[W] + K_{p,x}[L]} \qquad \text{(Eq. 7.16)}$$

where $[W]$ is the molar concentration of water, approximately 55.5 M at 25ºC (Santos, Prieto and Castanho, 2003), and $K_{p,x}$ is the mole-fraction partition constant, which is related with K_p by the following equation:

$$K_p = K_{p,x}(\gamma_W/\gamma_L) \qquad \text{(Eq. 7.17)}$$

Using equations 7.16 and 7.17, the molar fraction of ORB inserted into 0.5 mM POPC:POPG (7:3, molar) LUVs was estimated to be x_L= 0.79 (with a range of uncertainty of 0.64-0.85). Since a high proportion of the probe partitionates into POPC:POPG membranes at a phospholipid concentration of 0.5 mM, the following experiments were performed with POPC:POPG LUVs at this phospholipid concentration.

The aim of the present work was to characterize the structure of aggregates formed by SP-B and negatively-charged membranes using FRET methodologies. To do this, two different FRET experiments were designed: 1) between BODIPY/SP-B as donor and membrane probe as acceptor; and 2) between membrane probes, BODIPY-PC and ORB. Moreover, two different methodologies of sample preparation were compared: A) SP-B or BODIPY/SP-B reconstituted together with labeled lipids to form vesicles; and B) SP-B or BODIPY/SP-B was added to preformed labeled vesicles. Combination of the sample

preparation methods for sample preparation with the designed FRET experiments gave rise to four different experiments, whose results are explained below.

7.2.2.4. SP-B reconstituted into liposomes: FRET between BODIPY/SP-B and the lipid probe

To study the effect of SP-B on the organization of membrane aggregates, time-resolved FRET experiments were performed using BODIPY/SP-B, as donor, and the membrane probe ORB, as acceptor, which showed a R_0 value of 5.5 nm. For this FRET experiment, increasing concentrations of BODIPY/SP-B were reconstituted into POPC:POPG (7:3, molar ratio) LUVs labeled with or without ORB. Time-resolved donor intensity decays were measured in the presence or in the absence of the acceptor for each BODIPY/SP-B concentration. **Figure 7.7 A** depicts how, as BODIPY/SP-B concentration increases, FRET efficiency between probes diminishes, which shows that the distance between BODIPY/SP-B and the membrane probe ORB become longer. To discard that this decrease in FRET could be related to a progressive loss of the donor in the vesicle suspensions, ratios of donor absorption (ε_D) to acceptor absorption (ε_A) were analyzed for each sample (**Figure 7.7 B**). $\varepsilon_D/\varepsilon_A$ ratios were increased proportionally to the BODIPY/SP-B concentration in vesicle suspension, except for the vesicles supplemented with the highest protein concentration (4.17 µM BODIPY/SP-B). For this sample, it is likely that a minor fraction of BODIPY/SP-B was not successfully reconstituted into the lipid vesicles due to the high protein/lipid molar ratio, 0.8 % (10% protein to lipid by mass). Thus, in general, the progressive FRET decrease observed with increasing concentrations of BODIPY/SP-B was not caused primarily by a loss of donor, except for 4.17 µM BODIPY/SP-B. We also considered the possibility that BODIPY/SP-B contained in MLVs could have promoted the formation of large membrane aggregates that would hinder the generation of LUVs of 100 nm by extrusion, yielding a substantial loss, not only of donor molecules, but of total material during the process, which would be larger, the higher protein concentrations. To test this hypothesis, donor and acceptor were quantified from absorption spectra of the original MLVs and the generated LUVs samples. **Figure 7.7 C** depicts the percentage of recovery for donor and acceptor probes upon extrusion of the vesicle suspensions, showing that the loss of material caused by the extrusion process affects similarly to both probes, BODIPY/SP-B and ORB. Absorptions of donor and acceptor molecules decreased between 10 and 20% in LUVs, independently of the [BODIPY/SP-B] contained in the original suspensions. Thus, the marked reduction in FRET efficiency between BODIPY/SP-B and ORB as increasing concentrations of labeled protein could not be explained by a loss of constituents during the vesicle preparation. An alternative explanation for the progressive longer distances between ORB

membrane probe and BODIPY bound to SP-B at increasing protein concentrations, represented by a decrease in FRET efficiency, could be the potential appearance of repulsive interactions forces between the cationic membrane probe ORB and the cationic charges of the SP-B, whose net charge is + 7 (Hawgood, Derrick and Poulain, 1998), that would imply the physical separation of donor and acceptor molecules.

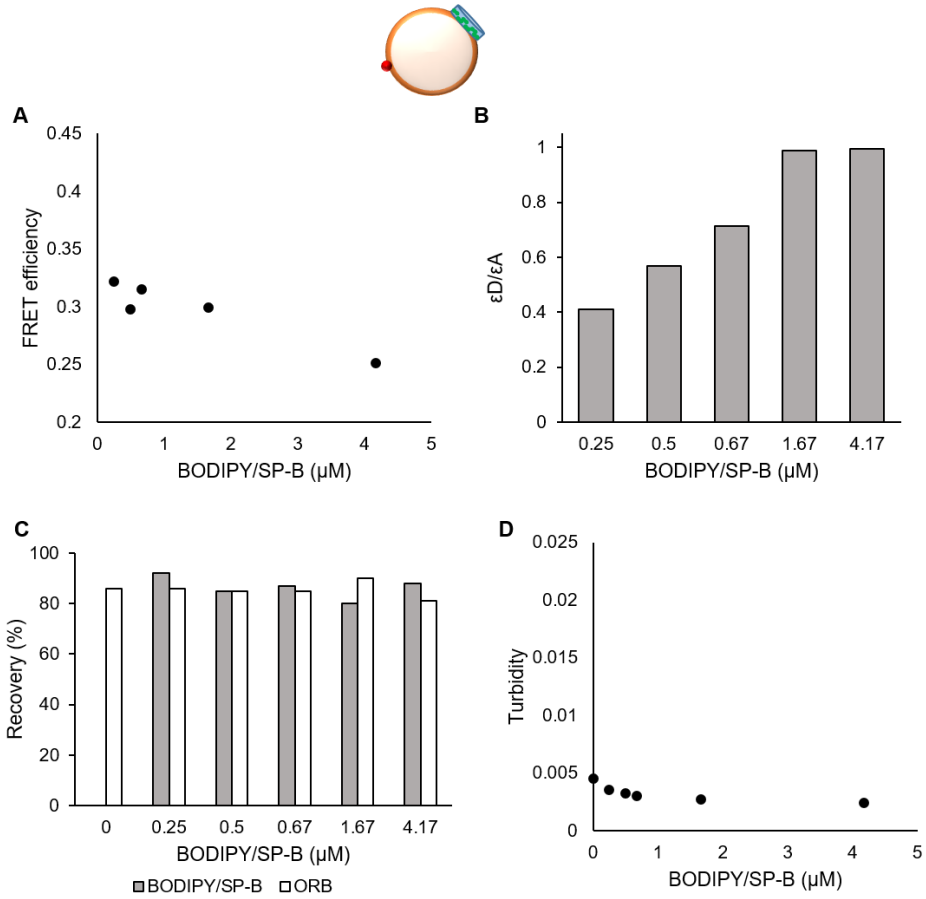

Figure 7.7. Membrane aggregation induced by BODIPY/SP-B, reconstituted into liposomes. Increasing amounts of BODIPY/SP-B (0; 0.25; 0.5; 0.67; 1.67; 4.17 μM BODIPY/SP-B, final concentration) were reconstituted in 0.5 mM POPC:POPG (7:3, molar ratio) LUVs labeled with ORB (probe/phospholipid molar ratio, 1:400). **A)** FRET efficiency between BODIPY/SP-B and ORB. **B)** Absorption donor to acceptor ratios for the different samples. **C)** Recovery (in percentage, %) of BODIPY/SP-B and ORB, calculated from absorption spectra of the samples before and after the extrusion of the vesicles. **D)** Turbidity of LUVs induced by BODIPY/SP-B. The extent of light scattering was determined by absorbance at 630 nm.

In addition to time-resolved FRET experiments, the ability of SP-B to induce membrane aggregation was also evaluated by absorption measurements of the different vesicle suspensions at a wavelength of 360 nm, showing no increase in turbidity as protein concentration increases (**Figure 7.7 D**). All together, the lack of increase in FRET efficiency and in turbidity as BODIPY/SP-B concentration increased, suggested the inability of the labeled protein to promote membrane aggregation, in contrast to the extensive published evidences describing membrane association and fusion induced by native SP-B (Cruz *et al.*, 1997; Chang, Nir and Poulain, 1998; Ryan *et al.*, 2005; Cabre *et al.*, 2009).

7.2.2.5. SP-B reconstituted into liposomes: FRET between lipid probes

To continue with the FRET-based study of membrane aggregation induced by SP-B, different amounts of wild-type SP-B were reconstituted in POPC:POPG (7:3) LUVs, labeled with BODIPY-PC (donor) and ORB (acceptor), at 0.5 mM phospholipid concentration. This FRET pair showed a R_0=5.7 nm. Analysis of time-resolved FRET experiments showed that all samples displayed similar FRET efficiencies independently of the SP-B concentration (**Figure 7.8 A**). In the same line, there was no increase in turbidity associated to the increase of protein concentration in vesicle suspensions (**Figure 7.8 B**). Therefore, these results suggested that wild-type SP-B was not able to promote vesicle aggregation, as it has also previously been shown for BODIPY/SP-B.

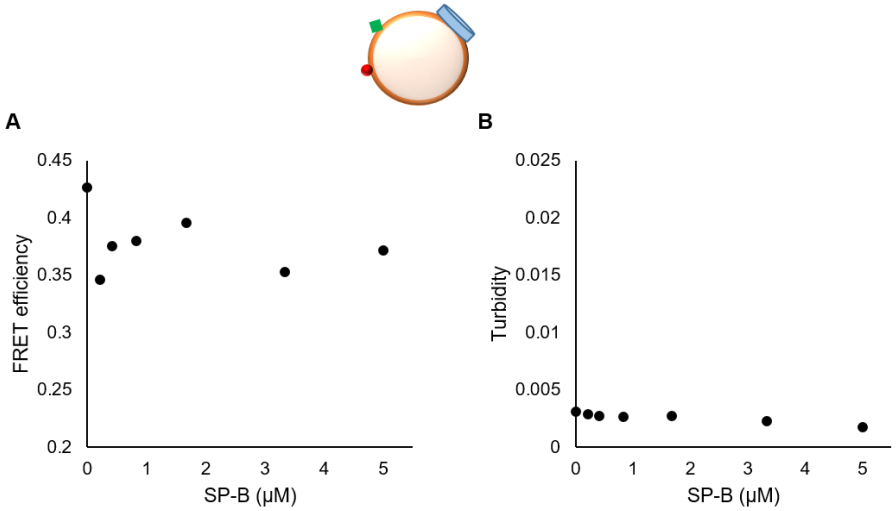

Figure 7.8. Membrane aggregation induced by non-labeled SP-B, reconstituted into liposomes. Increasing amounts of SP-B (0; 0.22; 0.42; 0.83; 1.67; 3.3 and 5 μM SP-B, final concentration) were reconstituted in 0.5 mM POPC:POPG (7:3, molar ratio) LUVs, labeled with BODIPY-PC and ORB (probe/phospholipid molar ratios, 1:1000 and 1:400, respectively). **A)** FRET efficiency between BODIPY-PC and ORB. **B)** Turbidity of LUVs induced by SP-B. The extent of light scattering was determined by absorbance at 630 nm.

7.2.2.6. SP-B added to preformed vesicles: FRET between lipid probes

In the light of these results, we attempted another experimental approach consisting on the addition of 5 μl of SP-B solubilized in methanol (at different protein concentrations) to preformed POPC:POPG LUVs labeled with BODIPY-PC and ORB. Absorption measurements of the samples at a wavelength of 630 nm showed higher turbidity of the vesicle suspensions as the protein concentration increases (**Figure 7.9 A**). Therefore, addition of SP-B in methanolic solution induced vesicle aggregation.

Time-resolved FRET experiments were performed using the FRET pair BODIPY-PC/ORB, with a large R_0 (5.7 nm). Once SP-B in methanolic solution was added to the labeled POPC:POPG LUVs, fluorescence donor decays in the absence or in the presence

of acceptor were measured. Time-resolved experiments showed that FRET efficiency increased upon SP-B addition (**Figure 7.9 B**), confirming that SP-B was able to induce membrane aggregation. Absorption spectra of the different samples showed similar maximal absorption values for ORB, except for samples with 0.44 and 2.5 µM of SP-B, where ORB absorption at 562 nm were slightly higher (data not shown). The analysis of absorption ratios of donor to acceptor molecules ($\varepsilon_D/\varepsilon_A$) in the vesicle suspensions showed the existence of slight differences of the probes concentrations between samples (**Figure 7.9 C**). Particularly, D/A absorption ratios were diminished for samples containing 0.44 and 2.5 µM of SP-B. Thus, the acceptor concentration in these samples was above the expected value, which likely caused an overestimation of FRET efficiency values for 0.44 and 2.5 µM of SP-B, as one can appreciate in **Figure 7.9 B**. Moreover, it is also possible that the highest protein concentration (5 µM of SP-B) could have been produced a repulsion effect on ORB, leading to a non-uniform distribution of membrane probes and a subsequent decrease in FRET efficiency at this protein concentration, as it was proposed before for BODIPY/SP-B reconstituted into liposomes labeled with ORB (**Figure 7.7 A**).

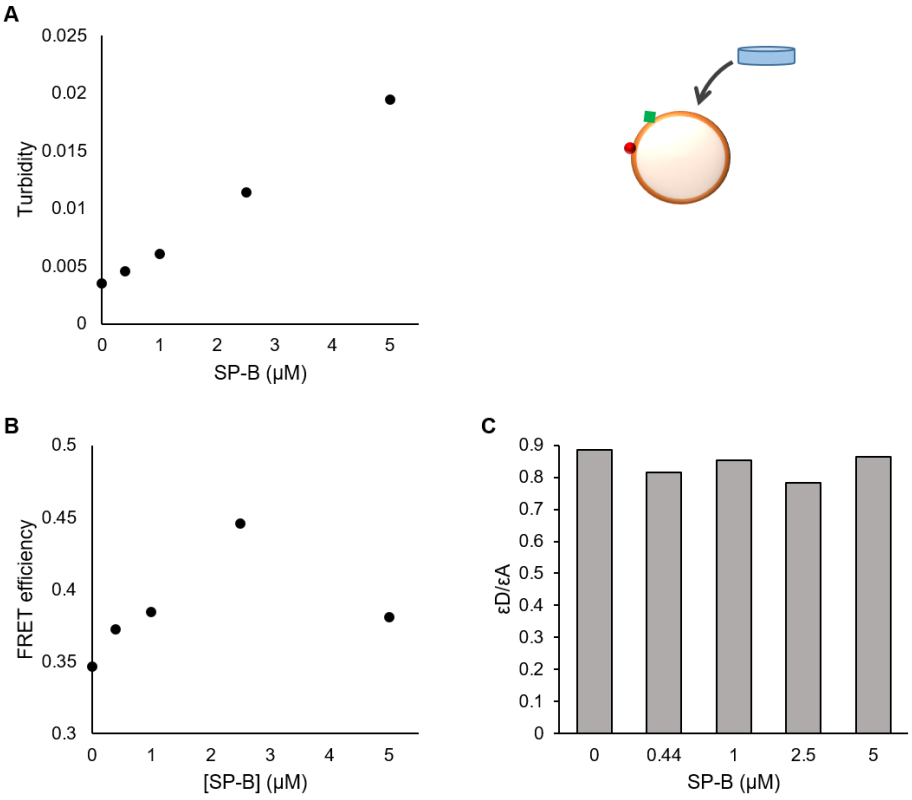

Figure 7.9. Membrane aggregation induced by addition of SP-B in methanolic solution to preformed liposomes. A fixed volume of 5 µl of a methanolic solution containing different SP-B amounts were added to 0.5 mM POPC:POPG (7:3, molar ratio) LUVs, labeled with BODIPY-PC and ORB (phospholipid/probe molar ratios, 1:1000 and 1:400, respectively). Increasing final SP-B concentrations in the vesicle suspensions were: 0; 0.4; 1; 2.5; 5 µM SP-B. **A)** Turbidity of LUVs induced by SP-B. The extent of light scattering was determined by absorbance at 630 nm. **B)** FRET efficiency between BODIPY-PC (donor) and ORB (acceptor). **C)** Donor to acceptor absorption ratios for the different samples.

Additionally, time-resolved donor fluorescence decay curves were analyzed using the formalisms described in section 7.2.2.2 FRET theoretical background, (eq. 7.6 and 7.12, and **figures 7.5 A-B**) (**Table 7.4**). For FRET between membrane probes, the model predicts that donors and acceptors in the same leaflet of the bilayer locate at the same plane, at a fixed distance $h_1 \approx 0$ nm. The fluorophore of ORB locates at the lipid interface, whereas BODIPY-PC has a main population where the fluorophore loops to the interface and another one, with the fluorophore embedded within the bilayer (Kaiser and London, 1998). Considering the coexistence of these two populations, the repeat distance recovered from this model geometry would probably correspond to the major one. Following, the distance between donor and acceptor fluorophores in opposite leaflets of the bilayer, h_2 , was determined by fitting fluorescence decays in the absence of SP-B with diverse h_2 values to the equation 7.6. The best fit was achieved with h_2 = 3.9 nm for POPC:POPG (7:4, mol:mol) bilayers. In this same line, a previous work determined by time-resolved FRET methodology that the thickness of POPC:POPS (4:1, molar ratio) was 3.7 nm (Coutinho *et al.*, 2008). Fixing $h_1 \approx 0$ nm and $h_2 \approx 3.9$ nm, a third plane of acceptors was attempted at variable distance h_3 . The implementation of a third plane of acceptors for samples with [SP-B] ≤ 1 µm did not led to an improvement in the fitness compared to the two acceptor planes model. However, for higher SP-B concentrations (≥ 2.5 µM), the incorporation of a third plane of acceptors resulted in a refinement of the goodness of the fit (X^2) and a decrease of h_3 up to 8.1 nm for the highest protein concentration (5 µM SP-B). In addition, the acceptor surface density for the different protein concentrations settled around a constant value, except for suspension with 2.5 µM SP-B. The imbalance for this sample might be due to an excessive acceptor concentration in the lipid mixture, as previously observed (**Figure 7.9 C**).

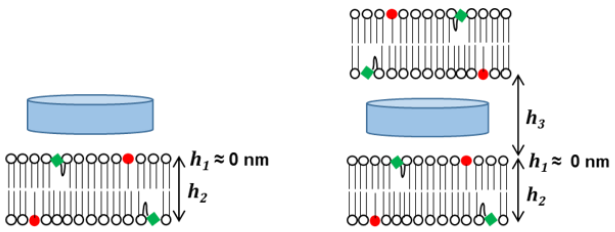

	Single bilayer		Aggregated bilayers		
	$h_1 \approx 0$ nm; $h_2 = 3.9$ nm		$h_1 \approx 0$ nm; $h_2 = 3.9$ nm; h_3, optimized		
[SP-B] (µM)	n	X_G^2	h_3	n	X_G^2
0	0.00295	1.10	>10	0.00286	1.11
0.4	0.00316	1.08	>10	0.00308	1.12
1	0.00329	1.03	>10	0.00319	1.04
2.5	0.00407	1.08	9.3	0.00385	1.05
5	0.00331	1.11	8.1	0.00301	1.06

Table 7.4. Comparison of the fitting parameters recovered for single bilayer and aggregated bilayers models applied to FRET experiments between membrane probes BODIPY-PC and ORB, in the presence of increasing concentrations of SP-B. Parameters obtained from pairwise global analysis of the time-resolved decays of BODIPY-PC (donor) in the absence and in the presence of ORB (acceptor). *n* is the number of acceptors/nm^2. The time-resolved FRET data were analyzed

assuming BODIPY-PC looping, so $h_1 \approx 0$; and $h_2 = 3.9$ nm was recovered from fitting the data obtained from the protein free sample to the single bilayer model.

7.2.2.7. SP-B added to preformed vesicles: FRET between BODIPY/SP-B and lipid probe

The ability of BODIPY/SP-B to induce vesicle aggregation was confirmed by absorption measurements at 630 nm (**Figure 7.10 A**). Upon addition of increasing concentrations of BODIPY/SP-B in methanolic solution (at final protein concentrations from 0 to 4.40 µM), the turbidity of the vesicle suspension increased, describing a sigmoidal curve. At the highest protein concentration assessed, both SP-B and BODIPY-SP-B induced vesicle aggregation to a similar extent (**Figures 7.9 A** and **7.10 A**).

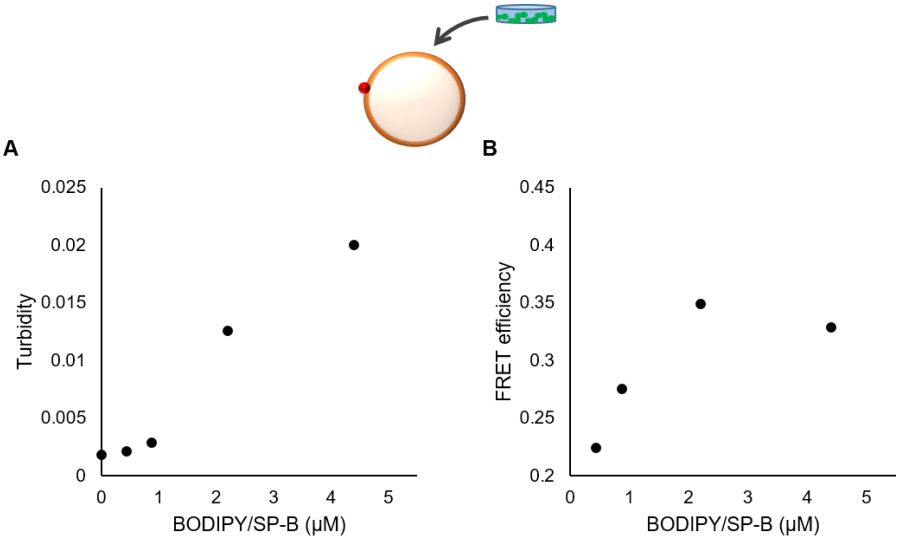

Figure 7.10. Membrane aggregation induced by addition of BODIPY/SP-B in methanolic solution. A fixed volume of 5 µl of a methanolic solution containing different BODIPY/SP-B amounts were added to 0.5 mM POPC:POPG (7:3, molar ratio) LUVs labeled with ORB (probe/phospholipid molar ratio, 1:400). Increasing final SP-B concentrations in the vesicle suspensions were: 0; 0.44; 0.88; 2.20 and 4.40 µM BODIPY/SP-B. **A)** Turbidity of LUVs induced by SP-B. The extent of light scattering was determined by absorbance at 630 nm. **B)** FRET efficiency between BODIPY/SP-B (donor) and ORB (acceptor).

Time-resolved FRET experiments were performed using BODIPY/SP-B and ORB as the FRET pair, with a value of R_0= 5.5 nm. Addition of increasing BODIPY/SP-B concentrations led to a progressive increase in FRET efficiency (**Figure 7.10 B**). For protein concentrations between 0.44 and 2.5 µM of BODIPY/SP-B the efficiency underwent an apparently linear increase and then remained constant for higher protein concentrations. Therefore, FRET efficiencies suggested the existence of multibilayer structures induced by [BODIPY/SP-B] ≥ 2.5 µM. From previous FRET experiments in BODIPY/SP-B reconstituted into liposomes labeled with ORB, we proposed that there was a segregation process between the protein and the lipid probe due to the existence of repulsive electrostatic forces (**Figure 7.7 A**). The apparent stabilization of FRET efficiency values for BODIPY/SP-B concentrations higher than 2.5 µM could have been

as a consequence of the combined effect of an increased vesicle aggregation and the repulsion process between the protein and ORB.

For an extensive study of the organization of the membranes in the presence of BODIPY/SP-B, the experimental fluorescence donor decays in the presence and absence of acceptor were analyzed using the formalisms described in the section 7.*2.2.2* (eq. 7.13-14 and **figure 7.5 C-E**). The distance (h_1 = 2.5 nm) between the protein donor to one acceptor plane was fixed from the best fit to the donor decay of vesicle suspension with the lowest protein concentration (0.44 µM BODIPY/SP-B). This single acceptor plane showed a well-fitting model for [BODIPY/SP-B] ≤ 0.88 µM (**Table 7.5**). On the contrary, in the case of higher protein concentration, it did not fit to such a single bilayer model. Comparing the two FRET models under consideration, X^2 values underwent a significant improvement (> 24%) in samples with [BODIPY/SP-B] ≥ 2.2 µM when an additional second plane was inserted, at a distance (h_2) of around 5-5.5 nm. **Figure 7.11** shows decays of donor emission in the absence and in the presence of acceptor for samples with [BODIPY/SP-B] = 4.4 µM, and depicts how the experimental data fit better to the aggregated bilayer model, as is evident from residual weights and autocorrelation plots.

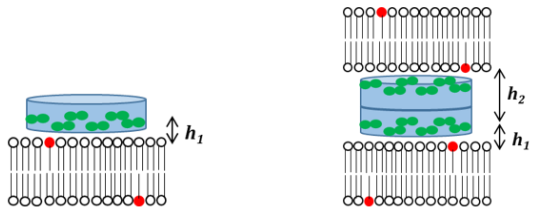

	Single bilayer		Aggregated bilayers		
	h_1 = 2.5 nm		h_1 = 2.5 nm; h_2, optimized		
[BODIPY/SP-B] (µM)	n	X_G^2	h_2	n	X_G^2
0.44	0.00297	1.20	>10	0.00292	1.21
0.88	0.0042	1.22	>10	0.00413	1.22
2.2	0.00649	1.83	5.5	0.00416	1.12
4.4	0.00575	1.49	5	0.0037	1.13

Table 7.5. Comparison of the fitting parameters recovered for single bilayer and aggregated bilayers models applied to FRET experiments between BODIPY/SP-B and ORB. Parameters obtained from pairwise global analysis of the time-resolved decays of BODIPY/SP-B (donor) in the absence and in the presence of ORB (acceptor). n is the number of acceptors/ nm^2. The distance h_1 = 2.5 nm was recovered from fitting the data obtained from the sample with the lowest [BODIPY/SP-B] (0.44 µM) to the single bilayer model.

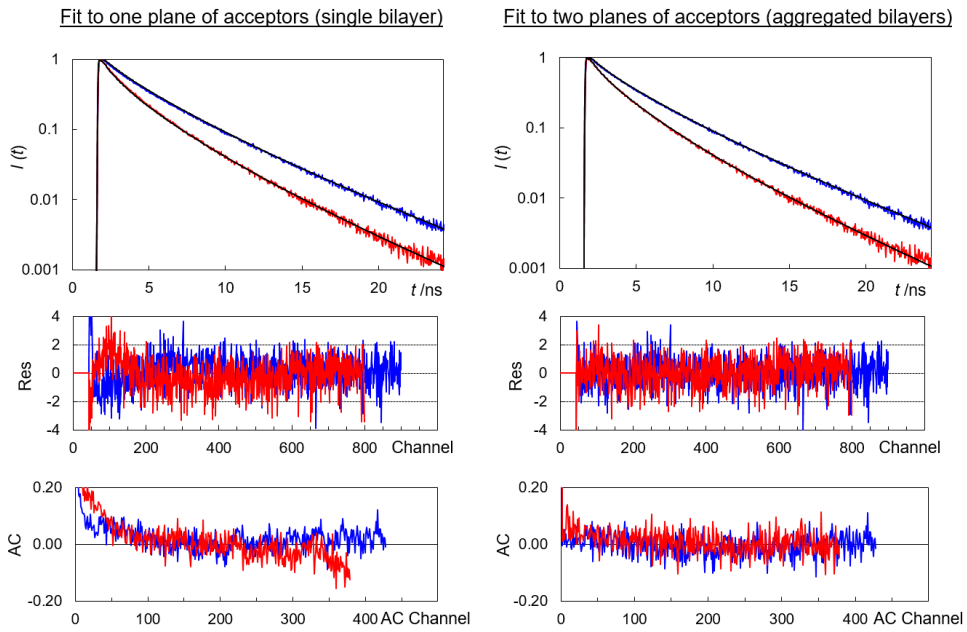

Figure 7.11. Time-resolved fluorescence intensity decays of BODIPY/SP-B. Upper panels: BODIPY/SP-B fluorescence decay in the absence (donor only, blue) and presence of ORB (donor + acceptor, red) in 0.5 mM POPC:POPG (7:3, mol/mol) LUVs, upon addition of 4.4 μM BODIPY/SP-B. The fittings of donor fluorescence decays to single bilayer (left) and to aggregated bilayers model (right) are compared. Weighted residual plots (middle panels) and autocorrelation plots (lower panels) for the fits of donor and donor + acceptor decays to the single bilayer (left) and aggregated bilayers models (right).

Additionally, these time-resolved donor decays were analyzed using a linear combination of the formalisms for one-acceptor plane and two-acceptor planes, with fixed distances h_1 = 2.5 nm and h_2 = 5 nm (**Table 7.6**). The fraction of donor molecules that transfer energy to one acceptor plane or to two acceptor planes was calculated for each protein concentration. So, for the lowest BODIPY/SP-B concentration, all donors transferred energy to only one acceptor plane at a distance h_1 = 2.5 nm. Conversely, for [BODIPY/SP-B] ≥ 2.5 μM, the whole fraction of donors sensed the two acceptor planes. Thus, all BODIPY/SP-B molecules are involved in vesicle aggregation at these high protein concentrations. An intermediate situation was reported for samples with [BODIPY/SP-B] = 0.88 μM, where the best fit to this linear combination model indicated that 70% of donors transferred energy only to a single acceptor plane, against 30% of donors that did it to two acceptor planes.

	Combination of single and aggregated bilayers		
	h_1 = 2.5 nm; h_2 = 5 nm		
[BODIPY/SP-B] (μM)	$f_{2planes}$	n	X_G^2
0.44	0.001	0.00296	1.20
0.88	0.299	0.00356	1.20
2.2	1	0.00388	1.13
4.4	1	0.00344	1.12

Table 7.6. Linear combination of the single bilayer and the aggregated bilayers models applied to FRET experiments between BODIPY/SP-B and ORB. Parameters obtained from pairwise global analysis of the time-resolved decays of BODIPY/SP-B (donor) in the absence and in the presence of ORB (acceptor). For each protein concentration, the fraction of donors transferring energy to two planes of acceptors, $f_{2planes}$, was calculated for the fixed distances h_1 = 2.5 nm and h_2 = 5 nm. n is the number of acceptors/nm^2.

7.3. DISCUSSION

7.3.1. STOICHIOMETRY OF THE SP-B OLIGOMER BY HOMO-FRET

In the first section of the results presented in this chapter, a homo-FRET study was approached to determine the degree of oligomerization of the SP-B complex in synthetic lipid membranes, as well as in pulmonary surfactant-derived membranes. Previously, it had been described that SP-B adopts a supradimeric structure in membranes. A 3D model of SP-B based on the structure of Saposin B predicted that five or six covalent SP-B dimers could self-assemble by specific interactions involving N-terminal and C-terminal helical segments into a ring-shaped structure (described in chapter 3 and in (Olmeda *et al.*, 2015)). To confirm experimentally the stoichiometry of SP-B oligomers, SP-B derivatized with a BODIPY probe on its amino terminal segment was used to evaluate the extent of energy transfer within the SP-B oligomer.

The relatively large homo-FRET Förster radius of BODIPY-FL probe, R_0 = 5.7 nm, makes in principle this fluorophore suitable for efficient donor-donor energy migration in macromolecular complexes. As a theoretical 3D model for SP-B oligomer already exists (Olmeda *et al.*, 2015), distances between amino groups of amino-terminal regions of each SP-B molecule in the protein complex were measured, which allowed a first assumption of the convenience of a fluorophore for homo-FRET along the SP-B complex. **Figure 7.12** illustrates the SP-B oligomer formed by the association of six covalent dimers, where the distance between NH_2-terminal groups of both monomers forming the covalent SP-B dimer is 5.31 nm, whereas the amino-amino interdimer distances lower to 1.87 and 2.51 nm. Therefore, the Förster radius of BODIPY is large enough to allow energy transfer between the subunits as an efficient process.

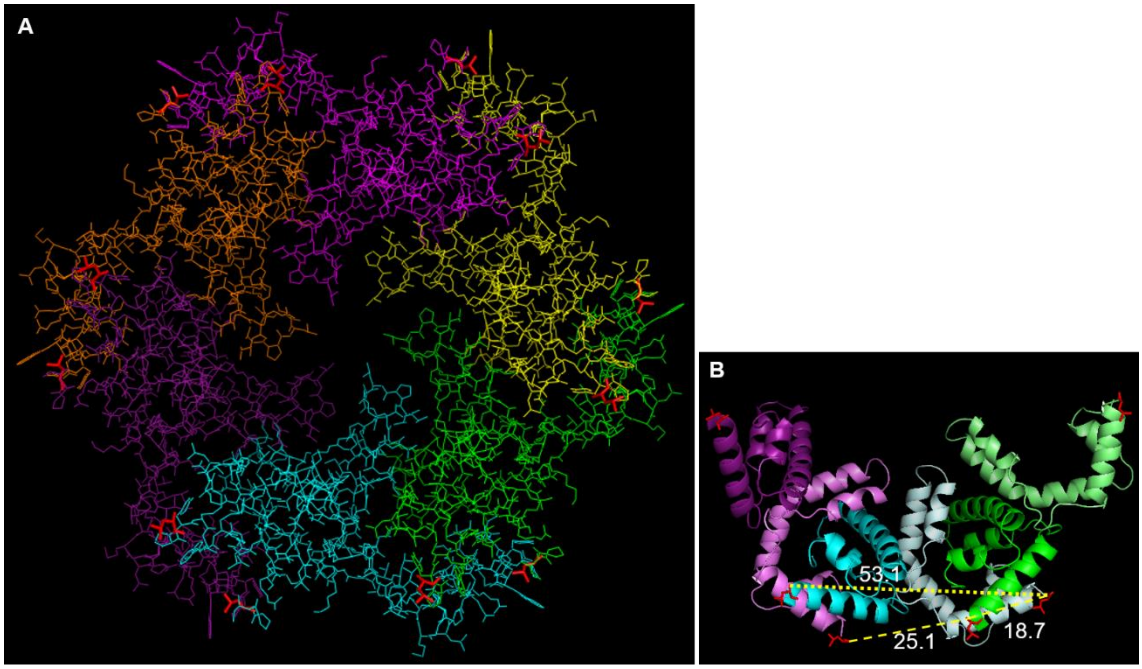

Figure 7.12. Three-dimensional model of SP-B oligomer based on the structure of Saposin B (Olmeda *et al.*, 2015). A) The SP-B complex shown is formed by the association of six covalent dimers, each of them represented in a different color. The amino group of amino-terminal region of each monomer is tagged in red. **B)** Detail of three adjacent covalent dimers inside the tridimensional model of SP-B oligomer. Covalent dimers are represented in different range of colors: purple, blue and green, with their respective monomers colored in dark and light tones. Distance between amino-groups of amino-terminal segments of the same covalent dimer is tagged with a dotted line, whereas distances between adjacent covalent dimers are represented with long dashed lines. Distance values are reported in angstroms.

The extent of homo-FRET among BODIPY/SP-B molecules in POPC:POPG model membranes was analyzed by fluorescence anisotropy. Both steady-state and time-resolved anisotropy measurements suggested the presence of BODIPY/SP-B dimers, but no higher degrees of oligomerization. Similar results were also obtained for BODIPY/SP-B in surfactant lipid membranes with little amounts of SP-C. Despite potential SP-B/SP-C interactions described in a previous work (Cabre *et al.*, 2018), and also suggested by results obtained in chapters 1 and 2 of this Thesis, the presence of SP-C did not induce an increase in the energy transfer neither between BODIPY/SP-B molecules involved in a large complex, nor among the fluorophores within the dimer. Nevertheless, AFM micrographs of BODIPY/SP-B in POPC:POPG membranes showed that labeled protein is assembled into ring-shaped particles with a diameter of 14.5 (± 2.7) nm, similar to the particles size observed in in POPC:POPG bilayers containing wild-type SP-B, and consistent with SP-B oligomers previously described (Olmeda *et al.*, 2015). It is important to remark that the labeling efficiency of the protein with BODIPY was high (91%), although we could not determine whether the ring-shaped complexes seen by AFM correspond to fully-labeled SP-B complexes, only wild type SP-B or a mixture of both proteins.

The dimer detected by homo-FRET anisotropy measurements (for infinite dilution of BODIPY/SP-B ($f = 0.10$)) showed a distance between fluorophores of 4.84 nm. This distance was maintained around this value for samples with higher fractional labeling, where slight deviations observed in the length would be due to residual interdimer homo-FRET. Since the amino terminal groups of the monomers forming the covalent SP-B dimer are located at 5.31 nm (**Figure 7.12**), it is reasonable to suggest that the dimer structure of BODIPY/SP-B detected by homo-FRET is, indeed, the covalent SP-B dimer. At this point, it is convenient to indicate that the oligomer model was built up using the human SP-B sequence lacking the first four amino acid residues (FPIP). It is known that prolines in the N-terminal segment of SP-B (residues 1-9) are involved in the spatial orientation of this segment with respect to α-helix 1 (Serrano *et al.*, 2006). Thus, the lack of FPIP in the SP-B model could vary noticeably the location of the N-terminal region compared to the full-sequence of SP-B, which could explain the slight difference (+ 0.47 nm) in the intradimer N-terminal distance measured in the SP-B oligomer model, compared to the distance recovered by homo-FRET.

The stoichiometry of a number of protein complexes associated to lipid membranes has been previously analyzed successfully by homo-FRET time-resolved spectroscopic studies (Yeow and Clayton, 2007; Hofman *et al.*, 2010; Melo *et al.*, 2014). However, this is not the case for BODIPY/SP-B oligomers, as our results indicated that energy transfer only occurred between fluorophores of the same covalent dimer, not between those of adjacent dimers. The extent of energy migration between a population of fluorophores located at distances $< R_0$ can be affected by self-quenching processes; fluorophores in close contact can form a non-fluorescent complex, or upon contact, the excited fluorophore returns to the ground state without emission of a photon (collisional quenching), leading to a strong decrease in the fluorescence lifetime of the donor. A previous work reported solely a slight decrease of lifetime for 2 μM of full-labeled BODIPY/SP-B in POPC vesicles (comparable protein and lipid concentrations to the conditions used in this work) (Cabre *et al.*, 2018), thus there was no evidence of the presence of collisional quenching that would hinder the extent of homo-FRET among BODIPY/SP-B subunits in the oligomer structure. Moreover, in the case that quenching events between fluorophores of adjacent dimers would be taking place in full-labeled BODIPY/SP-B oligomer, the energy migration between intradimer fluorophores would be also hampered because BODIPYs from adjacent dimers alternate along the structure (see **Figure 7.12**). Therefore, the inability to detect the high degree of oligomerization of BODIPY/SP-B complex by homo-FRET, which was presumably observed by atomic force microscopy, was not due neither to quenching processes, nor to unfavorable orientation of BODIPYs from adjacent dimers, as samples underwent ultrafast initial depolarization, which contributes to randomize orientations. It therefore remains an open

question the interpretation of the anomalous FRET behavior in SP-B oligomers that seem to assemble similarly to non-fluorescent SP-B forms. The final answer to the actual stoichiometry of SP-B complexes, as well as the particular disposition of N-terminal groups, will come from alternate experimental approaches different from fluorescence spectroscopy, such as X-ray crystallographic analysis.

7.3.2. MULTILAMELLAR STRUCTURES INDUCED BY SP-B: A FRET STUDY

FRET reports an interbilayer distance of 7.5 nm

FRET measurements are a sensitive tool to obtain quantitative information of the topological changes in membrane arrangements induced by proteins, as previously reported (Loura *et al.*, 2006; Coutinho *et al.*, 2008). In this work, we studied the interaction of native or fluorescently labeled SP-B with POPC:POPG model bilayers using time-resolved FRET methodology.

SP-B is a hydrophobic protein widely known for promoting membrane perturbations leading to vesicle aggregation, lipid exchange and membrane fusion (Oosterlaken-Dijksterhuis *et al.*, 1992; Poulain *et al.*, 1992; Cruz *et al.*, 1997; Ryan *et al.*, 2005). In the present work, and as it was reported in these previous studies, the addition of SP-B and BODIPY/SP-B in methanolic solution to vesicle suspensions confirmed, by turbidity measurements, the ability of both proteins to induce vesicle aggregation.

As a first approach in FRET data analysis, fluorescence intensity decays of the donor were described as a sum of exponential functions, and the recovered fitting parameters were used to calculate the experimental FRET efficiencies between BODIPY/SP-B or BODIPY-PC, as donor molecules, and ORB, as acceptor membrane probe. Upon addition of SP-B or SP-B labeled with BODIPY-FL in methanolic solution, FRET efficiencies reached maximal values for protein concentrations ≥ 2.2 μM of BODIPY/SP-B and ≥ 2.5 μM SP-B, suggesting that a high protein concentration induces vesicle aggregation. Although both proteins led to a rise in FRET efficiency, the relative increase in efficiency was higher for BODIPY/SP-B (compare **Figure 7.9 B** and **7.10 B**). This was an expected result as donor-acceptor distances between protein-bound donor and the membrane probe, ORB, are shorter than distances between the FRET pair constituted by membrane probes, BODIPY-PC/ORB, resulting in a higher efficiency of energy transfer.

However, despite FRET efficiency is a useful parameter to inform about the relative proximity between probes, it cannot resolve changes in membrane lipid organization. For this, more sophisticated models to fit FRET experimental data are required (Loura *et al.*, 2006; Coutinho *et al.*, 2008). In this work, the analysis of the fluorescence decays was performed using FRET formalisms corresponding to single bilayer or aggregated bilayers

models. In the case of experiments with BODIPY-SP-B/ORB FRET pair, it was determined that [BODIPY/SP-B] ≥ 2.2 µM induced the formation of membrane aggregated structures, where the bilayers connected by SP-B were located at a distance of approximately 7.5 nm (h_1+h_2) (see **table 7.5, figure 7.13 A**). Using a linear combination of the formalisms describing the models for single bilayer and aggregated bilayers, we determined that none of BODIPY/SP-B molecules were connecting vesicles at 0.44 µM of labeled protein. When the protein concentration was increased up to 0.88 µM, a minor fraction of BODIPY/SP-B (about 30% of total protein) was involved in the connection between two bilayers. This proportion increased up to 100% of BODIPY/SP-B connecting bilayers, for protein concentration ≥ 2.2 µM (**table 7.6**). On the other hand, the analysis of time-resolved FRET experiments between membrane probes suggested that membrane aggregation induced by SP-B took place from [SP-B] ≥ 2.5 µM. Recovered distances h_3 underwent a reduction inversely proportional to [SP-B]. For instance, the sample with 2.5 µM of SP-B showed a good fitting to the aggregated bilayers model with an interbilayer distance (h_3) of 9.1 nm, whereas for 5 µM of SP-B the recovered distance was 8.1 nm (see **table 7.4, figure 7.13 B**). Although this distance is consistent with the ~7.5 nm interbilayer distance from the protein-bound donor/membrane acceptor FRET system, it is reasonable to suggest that the range of protein concentrations assayed do not allow to confirm whether this distance h_3 would be stabilized to around 8.1 nm for higher SP-B concentrations. Besides, in the case of experiments using BODIPY/SP-B and ORB as FRET pair, the interbilayer distance (h_1+h_2) is expected to be determined more accurately because the recovered distances refer to the attachment point between the two bilayers. Beyond these considerations, it is clear that both FRET experimental configurations resolved successfully the study of membrane aggregation induced by SP-B.

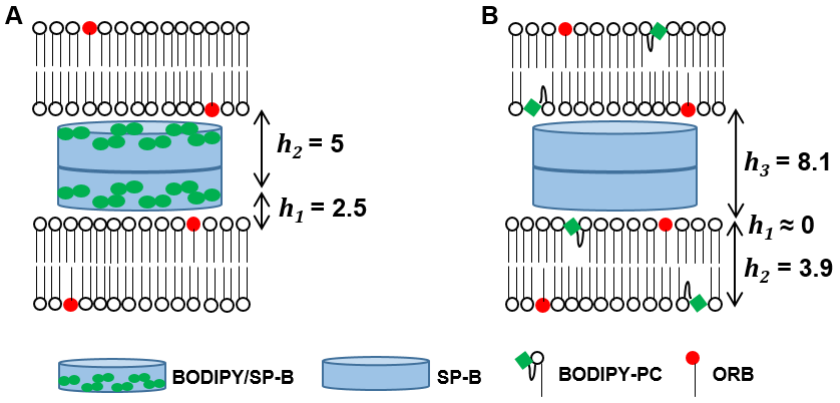

Figure 7.13. Schematic representation of the distances determined by FRET pairs BODIPYSP-B/ORB (A) and BODIPY-PC/ORB (B) in membrane-membrane interaction induced by SP-B.

SP-B shows an oligomeric organization in surfactant membranes, as well as in lipid model monolayers and bilayers (Olmeda *et al.*, 2015 and see chapters 1 and 3). Transmission electron and atomic force micrographs revealed that SP-B is assembled as

ring-shaped structures of 10 nm of diameter, which stand parallel to the surface of lipid layers. According to the 3D model structure based on Saposin B structure, the SP-B oligomer, formed by the association of six dimers, is projected around 3.7 nm over the lipid layer. Considering this height value, the apposition of two SP-B rings, one on top of each other, would connect two membranes with an interbilayer distance of 7.4 nm, which is in close agreement with the distance predicted by our time-resolved FRET experiments. Therefore, this work confirms that SP-B/SP-B interaction mediates contacts between membranes, as suggested by quartz crystal microbalance with dissipation (QCM-D) experiments (Cabre *et al.*, 2009). SP-B participates in vesicle aggregation processes (Cruz *et al.*, 1997) by allowing membrane interactions that deform vesicles which evolve to the formation of multilamellar structures (Cabre *et al.*, 2009), with two SP-B oligomers connecting adjacent membranes. This membrane perturbation process would be governed by the combined action of SP-B/SP-B interactions and lipid-protein interactions. Due to the large interplanar distances induced by the protein (7.5 nm), the present time-resolved FRET study could not detect possible stacking of membranes beyond two connected bilayers.

The previous oligomerization study of BODIPY/SP-B by homo-FRET did not prove higher oligomerization degree of the protein than the covalent dimer. If we assume that labeling of SP-B with BODIPY at its N-terminal region would have hindered the assembly of SP-B dimers into the ring-shaped oligomer, one could speculate that two covalent dimers of BODIPY/SP-B might mediate the connection between two bilayers, reporting interbilayer distance similar to those obtained by SP-B, which are consistent with the height of two juxtaposed modelled SP-B oligomers. However, it is unlikely that a sole covalent SP-B dimer could adopt a similar configuration in a phospholipid bilayer than covalent dimers inside the SP-B oligomer do, in which the interaction of the protein with the membrane surface is mediated by N-terminal and C-terminal amphipathic helical segments of two non-covalent SP-B dimers.

Influence of sample preparation methods: addition of SP-B onto preformed vesicles versus SP-B reconstituted in vesicles

Effective vesicle aggregation induced by SP-B was detected after addition of SP-B in methanolic solution onto preformed vesicles (**Figures 7.9** and **7.10**). Previous work reported lipid mixing activity of SP-B applied to preformed PC or DPPC vesicles by the same method (Poulain *et al.*, 1992; Poulain, Nir and Hawgood, 1996). Upon injection of the protein in small volumes of methanol, SP-B would be able to interact with the bilayers, adopting a tertiary structure similar to that formed by SP-B reconstituted from a dried proteolipid film, showing analogous promoting effects of adsorption of phospholipid

vesicles into the air-liquid interface (Cruz *et al.*, 1997). Nevertheless, neither turbidity nor FRET efficiency measurements of samples containing SP-B reconstituted into liposomes evidenced the presence of vesicle aggregation (**Figures 7.7** and **7.8**). This is in line with a previous work that showed that addition of SP-B onto preformed vesicles causes an instantaneous and extensive aggregation of vesicles in contrast to SP-B reconstituted together with liposomes (Cruz *et al.*, 1997). The method of proteoliposome preparation might influence the SP-B orientation in the vesicle. Thus, SP-B reconstituted together with lipids would be located in both leaflets of the bilayer, while the injection of SP-B to preformed liposomes would favor the preferential location of the protein in external leaflets of the vesicle, increasing the number of protein molecules available to mediate contact between vesicles. We propose that, due to this different disposition of the protein reconstituted into the vesicles, the effective protein concentration of these samples could be lower than in the case of the protein added in methanol, and not enough to generate detectable levels of membrane aggregation, as is illustrated in **Figure 7.14**. Our results are in line with previous evidences that suggests SP-B injected onto preformed vesicles causes an instantaneous and extensive aggregation of vesicles, in contrast to SP-B reconstituted together with liposomes (Cruz *et al.*, 1997). However, electron microscopy analysis showed that SP-B reconstituted in vesicles is also able to promote aggregation of lipid vesicles and the formation of multilayered surfactant assemblies (Parra *et al.*, 2011; Bernardino de la Serna *et al.*, 2013). Considering these evidences, it is likely that longer incubation time of sample containing SP-B reconstituted in vesicles would lead to a greater extent of vesicle aggregation that could be detected by turbidity and FRET measurements.

The distinct preparation methods of SP-B vesicles appear to lead to different SP-B/membrane structures, whose activities differs very slightly. In the context of the pulmonary surfactant, it has been proposed that the process that follows SP-B added in methanol to interact with phospholipid membranes could be more representative to the interaction of SP-B with lipids in the surfactant cycle in vivo (Cruz *et al.*, 1997). During the proteolytic processing of pro-SP-B, the mature segment of the protein would be covered by N-terminal and C-terminal propeptides until the cleavage of mature protein, instant in which SP-B interacts with lipids and participates in lamellar body biogenesis by promoting membrane remodeling. The processing of proSP-B to generate the mature form of the protein could be somehow analogous to the exposure of hydrophobic regions of SP-B in organic solvents to lipid vesicles.

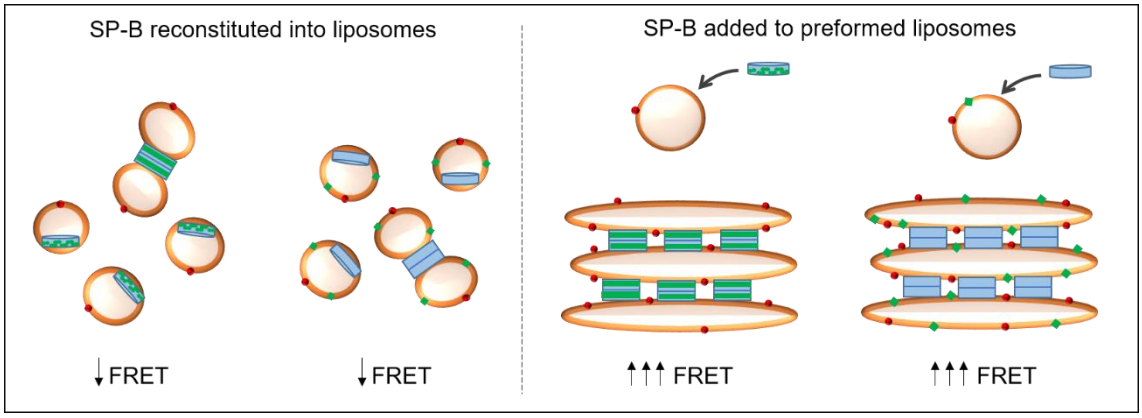

Figure 7.14. Schematic representation of the effect of the two methods of sample preparation assessed on vesicle aggregation induced by SP-B.

7.3.3. CONCLUDING REMARKS

In this chapter, FRET methodologies were applied to determine structural and functional features of SP-B oligomers. Despite homo-FRET experiments did not allow to determine the stoichiometry of the SP-B oligomer in lipid membranes, time-resolved FRET measurements revealed that SP-B in methanolic solution is able to self-assemble into native oligomers attached to the membrane surface and induce membrane stacking through protein-protein interactions.

SP-B has been suggested as essential for ensuring an efficient flow of lipid molecules between different surfactant structures and with the associated-interfacial film. The close apposition of membrane layers to interfacial monolayers induced by SP-B was reported by AFM and QCM-D analysis (Krol *et al.*, 2000; Diemel *et al.*, 2002; Cabre *et al.*, 2009). Our time-resolved FRET approach resolved, at nanoscale, the structure of multibilayer organization induced by SP-B, and supports for the first time with experimental data, the apposition of two SP-B ring-shaped oligomers that had been previously suggested as an important feature for the optimal function of surfactant (Olmeda *et al.*, 2015).

The present study provides quantitative topological information about the structure of protein-membrane aggregates induced by SP-B. These structures would not only be essential for lipid adsorption to the interface, but also would be required for allowing the proper biogenesis of lamellar bodies, their unraveling to form diverse extracellular forms and the generation of the multibilayer reservoir of surfactant membranes necessary to stabilize the respiratory surface during breathing dynamics (reviewed in (Perez-Gil, 2008)).

Chapter 5

ROLE OF SP-B ON THE EXOCYTOSIS OF LAMELLAR BODIES IN ALVEOLAR TYPE II CELLS

The experiments included in this chapter was performed during a short-term stay in the Institute of General Physiology (Ulm University, Germany) assisted and supervised by Pr. Manfred Frick and Pr. Paul Dietl. This stay was partially funded by a fellowship from Spanish Ministry of Economy and Competitiveness (EEBB-I-2015-10363). The results of this study were published in the article:

Martínez-Calle, M., Olmeda, B., Dietl, P., Frick, M., Pérez-Gil, J. (2018). "Pulmonary surfactant protein SP-B promotes exocytosis of lamellar bodies in alveolar type II cells". *FASEB Journal*, 32 (8): 4600-4611.

8. ROLE OF SP-B ON THE EXOCYTOSIS OF LAMELLAR BODIES IN ALVEOLAR TYPE II CELLS

8.1. INTRODUCTION

Pulmonary surfactant is synthesized and secreted by alveolar type II (ATII) cells. Prior to secretion, surfactant lipids and hydrophobic proteins are assembled into highly packed membranous structures, called lamellar bodies (LBs). LBs are acidic secretory organelles which range in size from 1.0 to 2.0 μM (Weaver, Na and Stahlman, 2002). The continuous availability of surfactant at the air-liquid interface is controlled by highly-regulated exocytosis of LBs. Alveolar mechanical stretching during inspiration is the main physiological stimulus for LB exocytosis. Large inflation of the lungs lead to an increase of the cytoplasmic calcium concentration, which triggers surfactant secretion (Nicholas, Power and Barr, 1982; Wirtz and Dobbs, 1990; Frick *et al.*, 2004).

Several agonists and molecular mechanisms are involved in the regulation of surfactant release (reviewed in (Rooney, 2001)). Among others, the purinergic-induced signaling pathway in ATII cells has been widely characterized. Purinergic agonists, such as ATP or UTP, activate $P2Y_2$ receptors, expressed in these cells. Their activation results in formation of inositol 1,4,5-triphosphate (IP_3) and diacylglycerol (DAG), and subsequent Ca^{2+} release from intracellular stores and PKC activation, respectively, which ultimately trigger LB fusion with the plasma membrane and surfactant secretion. ATP is a very potent stimulus for surfactant secretion *in vitro*, but it also seems to be relevant in alveolar mechanotransduction (Patel *et al.*, 2005).

Ca^{2+} plays a central role as a second messenger in the regulation of surfactant exocytosis, both in lungs and in isolated alveolar type II cells (Nicholas, Power and Barr, 1982; Wirtz and Dobbs, 1990; Haller *et al.*, 1998; Ashino *et al.*, 2000; Frick *et al.*, 2001, 2004). The transient elevation of cytoplasmic calcium concentration, $[Ca^{2+}]_c$, with an amplitude over 320 nM Ca^{2+} activates the fusion machinery, composed of several cytoskeletal elements, which prompts the fusion of LBs with plasma membrane and the final surfactant release ((Haller *et al.*, 1999); fusion machinery reviewed in (Olmeda, Martinez-Calle and Perez-Gil, 2017)).

In this chapter, a wide study of the effect of SP-B on the secretion of lamellar bodies by rat primary ATII cell cultures was performed. This study was primarily carried out using a fluorescent-based method developed by Haller and co-workers (Haller *et al.*, 1998), which enables real-time monitoring of surfactant release in stimulated primary ATII cell cultures by the fluorescence signal of styril dye FM1-43 in combination with Fura-2 measurements. This method has the unique advantage of detecting single exocytotic events, as phospholipid staining by FM1-43 results in bright fluorescence

when the dye in the extracellular medium gains access to surfactant through the fusion pore. In parallel, Fura-2 measurements report changes in $[Ca^{2+}]_c$ occurring in single stimulated cells.

8.2. RESULTS

8.2.1. EFFECT OF EXTRACELLULAR SP-B ON LAMELLAR BODY EXOCYTOSIS BY ATII CELLS

The possible role of surfactant protein SP-B on regulation of pulmonary surfactant exocytosis in alveolar type II cells has been tested by treating primary ATII cell cultures with phospholipid vesicles containing SP-B. **Figure 8.1 A** shows that POPC:POPG (7:3, w:w) vesicles containing SP-B (final protein concentration 13 μM) promoted lamellar bodies exocytosis in 65% of ATII cells, a 7.8-fold increase compared to cells maintained in control buffer. In comparison, ATP, a well-known surfactant secretagogue, induced LB fusion in 25% of ATII cells. Thus, SP-B induced a 3.4-fold higher LB exocytosis response than ATP. The combined treatment of cells with ATP and SP-B-containing vesicles did not result in an enhancement of LB exocytosis as a result of a cooperative action. Several control experimental conditions were also assayed to discard that surfactant secretion by ATII cells could have been affected by the mere exposure to liposomes. The results showed that cells treated with vesicles without protein did not exhibit a higher percentage of fusion than cells in control buffer, whereas cells treated simultaneously with ATP and vesicles without protein showed levels of surfactant secretion similar to those obtained by ATP alone. In the light of these results, we can conclude that SP-B could be a potent inducer of surfactant exocytosis by alveolar type II cells.

It has been well-established that surfactant secretion is highly regulated by cytoplasmic calcium concentration, $[Ca^{2+}]_c$, in ATII cells. Changes in cytoplasmic calcium concentration over time were registered by the ratiometric fluorescence intensity of Fura-2. Stimulation with ATP induced a Ca^{2+} signal consisting of a peak followed by a plateau (**Figure 8.1 B, upper panel**). Previous work determined that such ATP-induced peak phase is generated from the release of Ca^{2+} from intracellular stores and it is related to an early exocytotic activity, whereas a late Ca^{2+} entry from the extracellular medium elicits a Ca^{2+} plateau phase and late fusion events (Frick *et al.*, 2001; Dietl, Haller and Frick, 2012). Fura-2 ratio measurements revealed that, as in the case of ATP, SP-B stimulated Ca^{2+} signaling in ATII cells (**Figure 8.1 B, lower panel**). Similar to ATP, SP-B also triggered an intracellular Ca^{2+} peak, and a subsequent sustained increase in $[Ca^{2+}]$c over time. **Figure 1C** illustrates, after 1 minute of cell treatment with SP-B vesicles, how ratiometric Fura-2 fluorescence increases and, almost simultaneously, the fusion of LBs

with the plasma membrane occurs. This event is shown by the subsequent burst of bright FM1-43 fluorescence as this probe enters into the surfactant lipid-filled LB compartment through the open fusion pore.

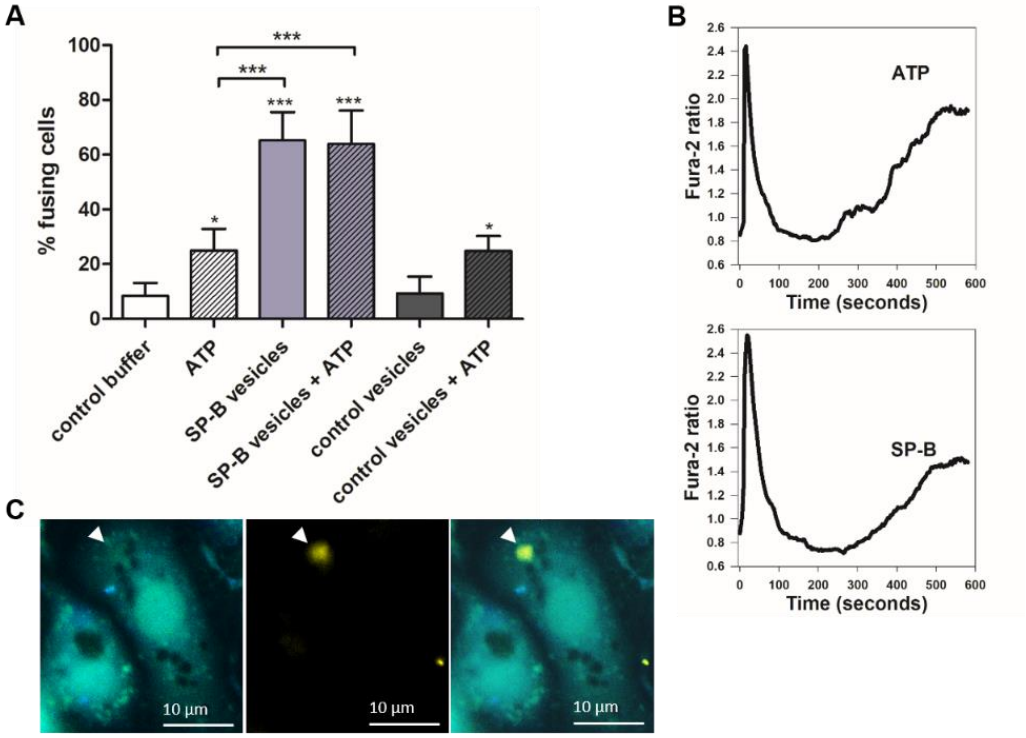

Figure 8.1. SP-B promotes lamellar body exocytosis in ATII cells. A) Stimulation of lamellar body fusion with plasma membrane in ATII cells by treatment with 100 µM ATP and/or vesicles containing SP-B at a final protein concentration of 13 µM. Control conditions tested included vesicles without protein and cell bath solution, named as control buffer. ANOVA was performed, where each experimental condition was compared to control buffer using Dunn's multiple comparison test. Additionally, SP-B vesicles, ATP + SP-B vesicles and ATP were analyzed by paired student's t test (* $P < 0.05$ and *** $P < 0.001$). **B)** Representative plot of time course of Fura-2 ratio in response to 100 µM ATP or vesicles containing SP-B at a final protein concentration of 13 µM. **C)** Typical images from an ATII cell culture, 1 minute after stimulation with SP-B vesicles (13 µM final protein concentration). Left image shows ratiometric Fura-2 fluorescence in the cytoplasm; dark spots (no fluorescence) in the cytoplasm represents lamellar bodies. The image in the center shows a lamellar body fusion event seen as a local increase of FM1-43 fluorescence at the site of the fusion pore in the plasma membrane of the ATII cell. An overlay of these images is shown (right). White arrows point to the site of LB fusion. In the left image note that once LB fuses with plasma membrane, it is no longer detected in the cytoplasm (absence of a dark spot).

In order to characterize the efficiency of SP-B to stimulate LB exocytosis, we next analyzed this issue upon treatment with different SP-B concentrations (**Figure 8.2**). LB exocytosis underwent a linear growth in response to increasing concentrations of SP-B, until reaching a plateau when cells were treated with SP-B concentrations above 13 µM.

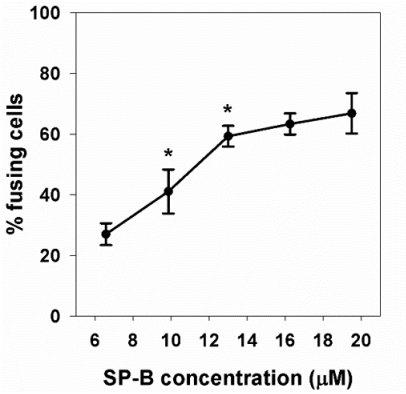

Figure 8.2. Characterization of the activity of SP-B as inducer of lamellar body exocytosis and evaluation of its effect on ATII cell viability. Concentration-response curve, where increasing SP-B concentrations (from 6.6 to 19.5 μM SP-B) *versus* exocytotic response were plotted. Lipid concentration in all vesicle samples was kept constant. ANOVA with all pairwise multiple comparison procedures (Holm-Sidak method) was performed (* P<0.05).

Besides, we tested the viability of the cells challenged with SP-B vesicles. As shown in **Figure 8.3**, vesicles containing SP-B at a final protein concentration of 13 μM did not compromise cell viability through permeabilization of the plasma membrane, revealed by the inability of propidium iodide, a DNA-binding fluorescent probe, to enter the cells, which is a typical consequence of cell damage. This SP-B concentration was therefore effective at stimulation of surfactant secretion but non-toxic for ATII primary cell cultures. Hence, we established this SP-B final concentration as our reference concentration for the following experiments. In most of them, unless otherwise stated, all vesicles used were made by POPC:POPG (7:3, w:w).

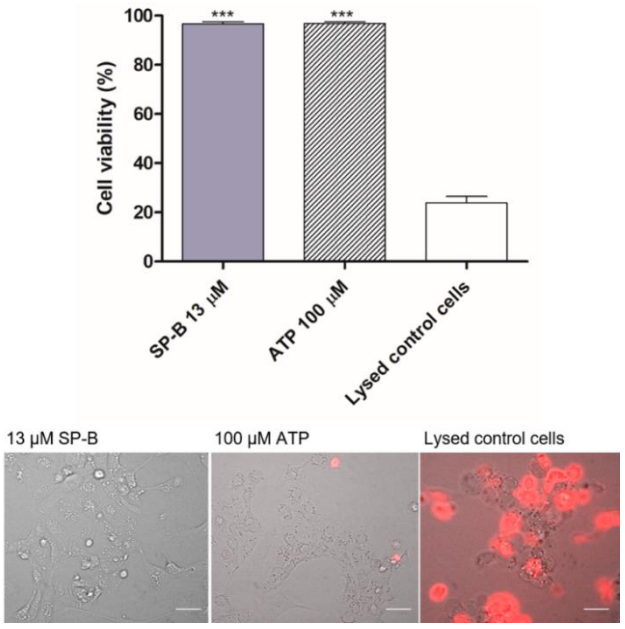

Figure 8.3. Effect of the extracellular SP-B on ATII cell viability. Cytotoxicity analysis by permeability to propidium iodide (PI). Cell uptake of PI was assessed after 15 min incubation with 100 μM ATP or vesicles containing SP-B (13 μM). As a control of cell damage, cell culture buffer was replaced by distilled water prior to propidium iodide incubation. Percentage of cells showing viability (lack of PI permeation) was plotted for each treatment. Data were analyzed by ANOVA, followed by Dunn's multiple comparison test (*** P<0.001). Overlay images of PI (red)-associated nuclear fluorescence and bright field are shown; scale bar, 50 μM.

8.2.2. EFFECT OF DIFFERENT SURFACTANT LIPID-PROTEIN MIXTURES ON LAMELLAR BODY EXOCYTOSIS IN ATII CELLS

The dynamics of surfactant films formed at the air-water interface of the alveoli is supported by the activities of proteins SP-B and SP-C. A likely cooperative action of both proteins at the respiratory surface has been suggested (Schurch *et al.*, 2010), and even the

existence of SP-B/SP-C complexes in surfactant membranes has been recently proposed (Cabre *et al.*, 2018). Both proteins are also involved together in the permeability of surfactant membranes, as previously described in chapter 2 of this Thesis. Therefore, we next investigated whether SP-C, together with SP-B, might also be involved in the regulation of surfactant secretion by alveolar type II cells. To test this, samples containing different mixtures of the surfactant components were analyzed. Vesicles containing SP-C alone were not able to trigger lamellar bodies exocytosis in ATII cells (**Figure 8.4 A**). However, vesicles containing both purified hydrophobic proteins, SP-B and SP-C, stimulated LB exocytosis at similar levels than vesicles containing SP-B alone (**Figure 8.4 B**). This exocytotic activity was also achieved when ATII cells were treated with vesicles formed by the organic fraction of the pulmonary surfactant, which contains the native lipids and the original proportion of hydrophobic proteins (**Figure 8.4 C**). Therefore, SP-B was able to promote lamellar body exocytosis independently of the presence of SP-C, showing the latter no effect on this feature.

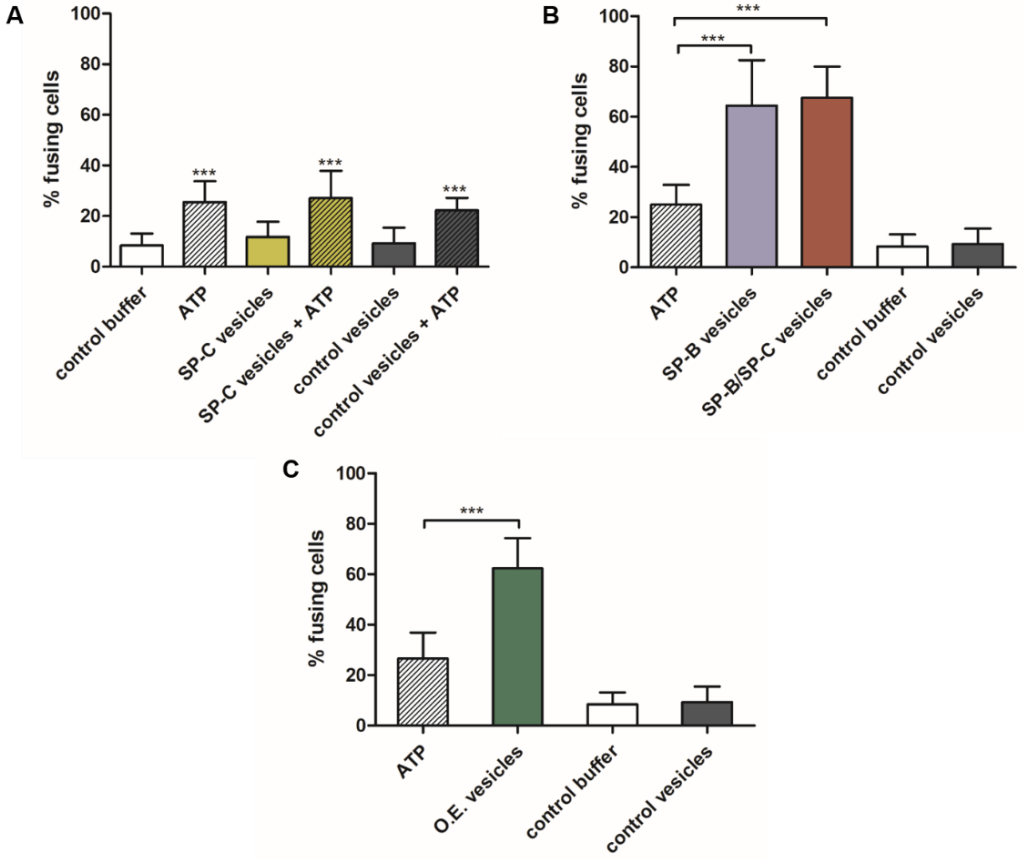

Figure 8.4. Effect of different surfactant protein mixtures on the exocytosis of LBs in primary ATII cell cultures. A) Cell treatment with vesicles containing SP-C. **B)** Cell treatment with vesicles containing a combination of purified SP-B and SP-C compared to treatment with vesicles containing SP-B alone. **C)** Treatment with vesicles formed by the organic extract of pulmonary surfactant (O.E.), containing all surfactant lipids and the physiological proportion of the hydrophobic proteins SP-B and SP-C. Vesicles tested in all these experiments are composed of SP-C and/or SP-B, with each protein at a final concentration of 13 µM. Control treatments included addition of 100 µM ATP, control vesicles without any protein or cell bath solution (control buffer). For panel A, data were analyzed using one-way ANOVA, followed by Dunn's multiple comparison test. Data from panels B and C were analyzed by paired student's t test (*** $P<0.001$).

Apart from the classical method to purify SP-B dimers in organic solvent, native SP-B complexes from pulmonary surfactant can be obtained by its solubilization with detergent (Olmeda *et al.*, 2015). Structural characterization of these SP-B particles revealed a supramolecular organization of five or six SP-B dimers that adopt a ring-shaped protein structure, functionally competent to promote formation and proper dynamics of interfacial phospholipid films. **Figure 8.5** shows that both, vesicles containing native SP-B complexes originally solubilized in detergent or SP-B obtained in organic solvent, were able to promote LB exocytosis at similar efficiency levels.

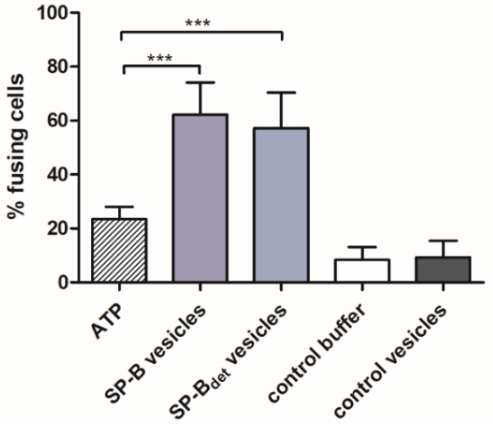

Figure 8.5. SP-B oligomers stimulates LB exocytosis in ATII cells. A) Cells were treated with vesicles containing detergent-solubilized SP-B complexes ($SP\text{-}B_{det}$) in comparison to those treated with vesicles containing SP-B purified in organic solvent. Control treatments included addition of 100 µM ATP, control vesicles without any protein or cell bath solution (control buffer). Data were analyzed by paired student's t test (*** $P<0.001$).

Due to the cationic nature of SP-B, the protein establishes electrostatic interactions with anionic phospholipids in bilayers (Perez-Gil, Casals and Marsh, 1995; Cabré *et al.*, 2012). Therefore, we analyzed a likely influence of the anionic phospholipids on the ability of SP-B to induce LB exocytosis in ATII cells (**Figure 8.6**). With this aim, ATII cell cultures were treated with SP-B reconstituted in POPC or POPC:POPG (7:3, w:w) vesicles. The results showed that SP-B incorporated in negatively-charged vesicles promoted slightly higher levels of LB secretion than SP-B in zwitterionic vesicles, suggesting that the anionic phospholipid POPG would enhance the activity of SP-B as inducer of LB exocytosis.

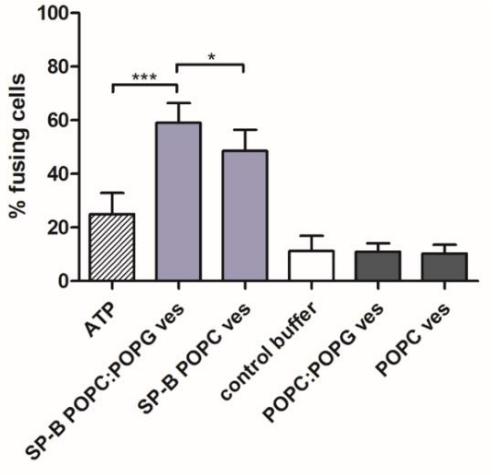

Figure 8.6. Influence of anionic phospholipid on stimulation of LB exocytosis by SP-B. ATII cell cultures were treated with POPC or POPC:POPG (7:3) vesicles, containing SP-B. Control treatments included addition of 100 µM ATP, cell bath solution (control buffer), or control vesicles made of POPC or POPC: POPG (7:3, w:w) in the absence of protein. Data were analyzed by paired student's t test (* $P<0.05$ and *** $P<0.001$).

8.2.3. BLOCKAGE OF SP-B-INDUCED LAMELLAR BODY EXOCYTOSIS BY ANTIBODIES

In this work, we have shown that extracellular pulmonary surfactant, specifically through an effect promoted by SP-B, would play a role in the regulation of its own secretion. To confirm this outcome, we performed a set of experiments to test whether SP-B-mediated LB exocytosis could be blocked when vesicles containing different surfactant components were pre-incubated with antibodies against surfactant proteins SP-B or SP-C (**Figure 8.7**). As expected, blockage of SP-B vesicles with α-SP-B antibody arrested the induction of LB secretion by ATII cells in a dose-dependent manner (**Figure 8.7 A**). To discard a non-specific effect of the antibody, SP-B vesicles were treated with α-SP-C antibody, which showed no alteration in the SP-B ability to stimulate LB exocytosis (**Figure 8.7 B**). Vesicles made up by organic extract from pulmonary surfactant showed a reduced ability to stimulate LB secretion when they were pre-exposed to α-SP-B antibody as well as, surprisingly, upon pre-exposure to α-SP-C antibody (**Figure 8.7 C**). Interestingly, when the cells were treated with vesicles containing a mixture of purified proteins SP-B and SP-C, pre-treatment with α-SP-B antibody led to a blockage of LB exocytosis, but no effect was observed when the vesicles were pre-treated with α-SP-C antibody (**Figure 8.7 D**). Thus, the blocking effect of the α-SP-C antibody towards SP-B-promoted secretion stimulatory function when both proteins are co-purified, but not when they are separated and later combined. These results strongly suggest a disruption of SP-B/SP-C interactions during the purification process, as previously described in chapter 2 regarding the effect of both proteins in surfactant permeability, which could be caused by a possible loss of unknown factors or by alteration of the proteins conformation once SP-B/SP-C complexes are dissociated.

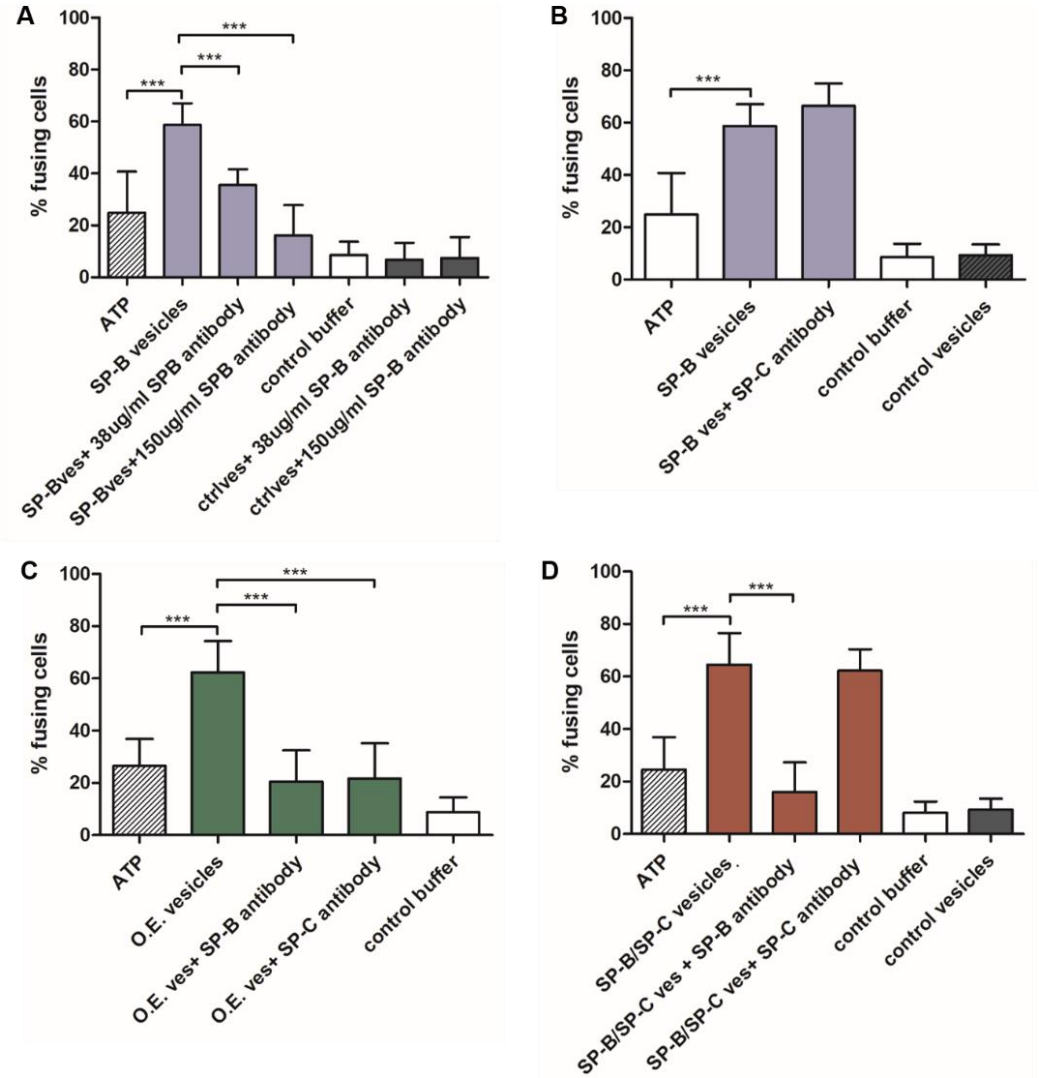

Figure 8.7. Blockage by antibodies of SP-B-stimulation of LB exocytosis in ATII cells. ATII cell cultures were treated with vesicles containing SP-B **(A, B)**, vesicles made up of organic extract from pulmonary surfactant **(C)** or vesicles containing a combination of isolated SP-B and SP-C **(D)**. The vesicles were pre-incubated with either α-SP-B or α-SP-C antibodies (150 µg/ml of antibody concentration, unless otherwise stated). Control treatments included addition of 100 µM ATP, control vesicles without any protein or cell bath solution (control buffer). Data were analyzed by paired student's t test (*** $P<0.001$).

8.2.4. UNRAVELING THE SIGNALING PATHWAY BY WHICH SP-B INDUCES LAMELLAR BODY EXOCYTOSIS IN ATII CELLS

In order to get deeper insight into the effect of SP-B on LB secretion, besides evaluating LB fusion with plasma membrane the exocytotic response was studied focusing on the percentage of cells responding to the stimulus, by analysis of Ca^{2+} signaling through Fura-2 measurements. **Figure 8.8 A** shows that both ATP and SP-B-containing vesicles induced Ca^{2+} signal in the majority of cells (about 90% of cells). However, regarding the fusion activity, SP-B vesicles induced lamellar body fusion in 65% of cells, while ATP, despite promoting a robust Ca^{2+} response, only caused LB

fusion in 25% of cells (**Figure 8.8 B**). Therefore, SP-B seems to stimulate surfactant secretion in a more efficient and potent way than ATP.

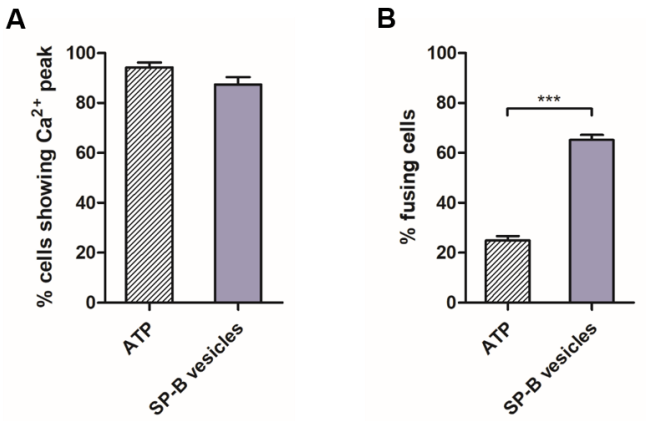

Figure 8.8. Effect of ATP or SP-B on the proportion of ATII cells showing LB fusion with plasma membrane. (A) Effect of ATP or SP-B on the percentage of cells showing LB fusion-associated calcium signal. **(B)** Effect of ATP or SP-B on the proportion of cells with fusion activity. ATII cells were stimulated with 100 µM ATP or vesicles containing SP-B at a final concentration of 13 µM. Values are means ± SEM. Data were analyzed by paired student's t test (*** $P<0.001$).

With the aim of unraveling the signaling pathway by which SP-B promotes lamellar body fusion and subsequent surfactant release from ATII cells, SP-B-stimulated LB exocytosis was assessed in the presence of different antagonists, chemical agents and ionic conditions. A significant decrease in the levels of SP-B-induced LB exocytosis was found when cell cultures were treated with suramin, an agonist of $P2Y_2$ purinergic receptors, or when extracellular ATP was depleted by addition of apyrase (**Figure 8.9 A**). These results suggest that SP-B-induced LB exocytosis is mediated by ATP through activation of the $P2Y_2$ purinergic receptors. Attempts to detect a SP-B-promoted direct increase in ATP concentration at the extracellular medium revealed a trend of SP-B to induce higher extracellular concentration of ATP (**Figure 8.9 B**), which resulted non-significant as a consequence of high inter-experimental variability. The recent finding that ATP is also stored and secreted within LBs (Fois *et al.*, 2018), together with the variability of the number of exocytotic events per cell, may be behind that high variability in total extracellular ATP levels as detected at prolonged times. We still speculate that the source of a primary local rise in ATP concentration could be the release of intracellular ATP towards the extracellular medium, which could be triggered by SP-B. Connexin and pannexin channels have been proposed as ATP release pathways in a broad range of cell types. To test whether this type of channels could be involved in SP-B-induced ATP release by ATII cells, inhibitors of pannexin/connexin channels were used. Treatment of cells with flufenamic acid (FFA) or carbenoxolone (CBX) caused a marked reduction of SP-B-induced LB secretion (**Figure 8.9 A**). In the light of these results, we propose that extracellular SP-B, via a yet unknown mechanism, results in opening of hemichannels and ATP release towards the hypophase in primary ATII cells. This released ATP then

triggers a local autocrine or paracrine activation of $P2Y_2$ receptors, inducing purinergic-signaling mediated LB exocytosis.

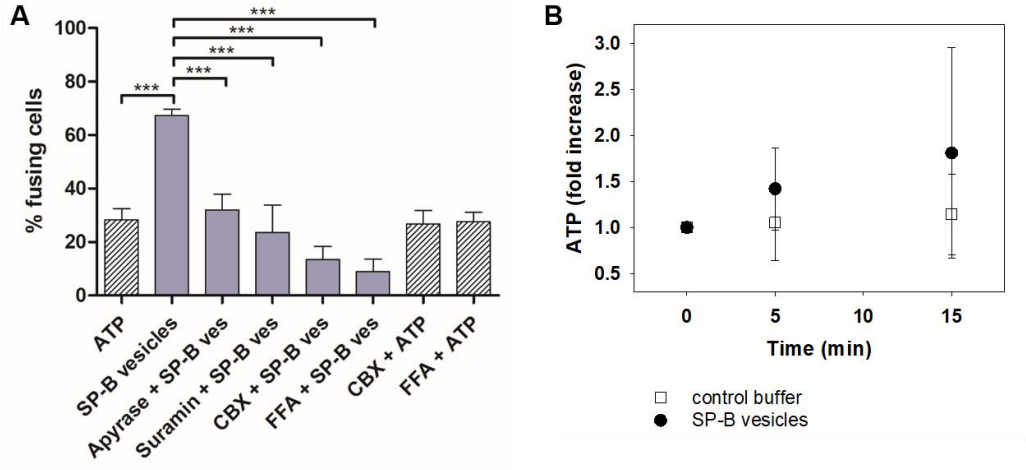

Figure 8.9. SP-B induces LB exocytosis via activation of P2Y2 purinergic pathway through ATP release by ATII cells. (A) Evaluation of SP-B-stimulated LB exocytosis in the presence of several inhibitors of purinergic pathway, suramin and apyrase, and pannexin/connexin hemichannels, flufenamic acid (FFA) and carbenoxolone (CBX) (under conditions detailed in Materials and Methods). Vesicles containing SP-B at a final concentration of 13 µM were used for ATII cell stimulation of exocytosis, whereas ATP 100 µM was used as a control for stimulation. Values are means ± SEM. Data were analyzed by paired student's t test (*** $P<0.001$). **(B)** Time-course of ATP release (fold increase) in ATII cell cultures non-treated (white squares) or treated (black circles) with SP-B vesicles. Results have been averaged from 7 independent experiments. Extracellular ATP was quantified by the luciferase assay. Data show mean +- SD. T-test analysis were performed between non- and SP-B-treated cells at 5 and 10 min, showing non-significant differences.

To further substantiate our hypothesis that SP-B induces LB exocytosis through an ATP release mechanism and the subsequent activation of purinergic $P2Y_2$ receptors, the impact of SP-B on intracellular Ca^{2+} signals was evaluated. Regulated surfactant secretion is linked to a rise in intracellular Ca^{2+} concentration that is essential to recruit the exocytotic machinery. Stimulation with ATP results in a Ca^{2+} signal consisting of an early peak, sustained by intracellular Ca^{2+} release, and a delayed plateau phase, as a result from Ca^{2+} entry (Frick *et al.*, 2001; Dietl, Haller and Frick, 2012). In line with our hypothesis, that SP-B triggers LB fusion via release of ATP through channels, inhibitors flufenamic acid (FFA) or carbenoxolone (CBX) significantly reduced the percentage of cells showing a Ca^{2+} peak upon SP-B treatment (**Figure 8.10 A**). Also, presence of extracellular suramin or apyrase, as well as depletion of intracellular Ca^{2+} stores using the endoplasmic Ca^{2+}-ATPase inhibitor thapsigargin, abolished the SP-B induced Ca^{2+} peak. Inhibition of Ca^{2+} peaks was in accordance with a reduction in SP-B-induced LB exocytosis (**Figure 8.10 A and 8.10 B**). Surprisingly, removal of extracellular Ca^{2+} alone (which does not affect the ATP-induced initial Ca^{2+} peak resulting from release of Ca^{2+} from intracellular stores) also decreased significantly the frequency of SP-B induced-Ca^{2+} peaks and LB exocytosis (**Figure 8.10 A and 8.10 B**). This could indicate that extracellular Ca^{2+} might be required upstream of the SP-B-mediated activation of the purinergic pathway. For instance, Ca^{2+} might somehow mediate SP-B binding to

particular sites of the ATII plasma membrane or modulate ATP release through channels. Nevertheless, further research will be needed to clarify the role of extracellular Ca^{2+} in SP-B-stimulated surfactant secretion by ATII cells.

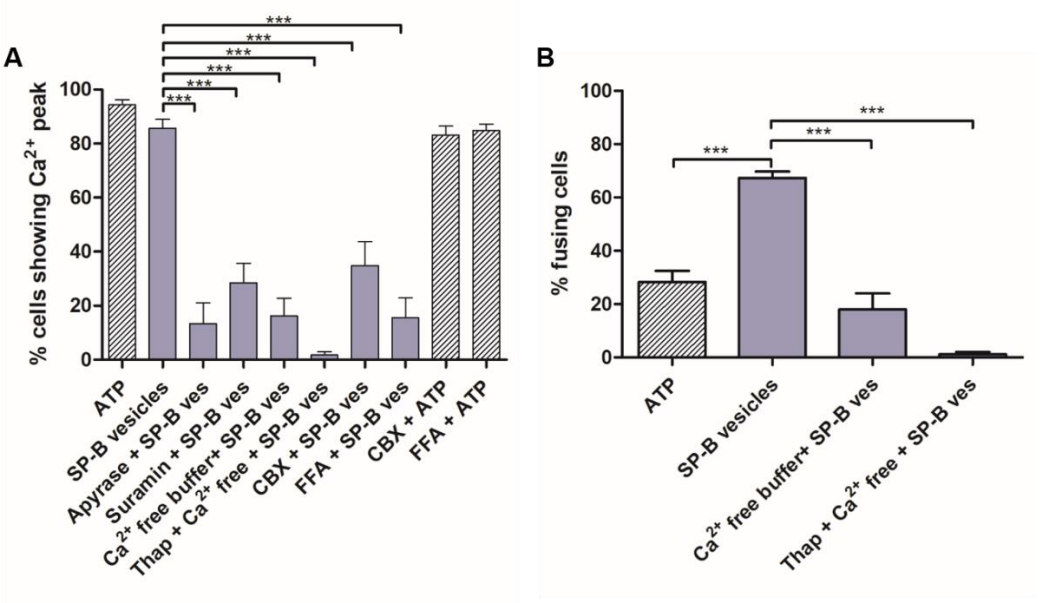

Figure 8.10. Relevance of Ca2+ in SP-B-induced LB exocytosis in ATII cells. Evaluation of SP-B-induced Ca2+ signal **(A)** and SP-B-induced LB exocytosis **(B)** in the presence of several inhibitors of purinergic pathway, suramin and apyrase, pannexin/connexin hemichannels inhibitors, carbenoxolone (CBX) and flufenamic acid (FFA), and thapsigargin (Thap), inhibitor of the sarco/endoplasmic reticulum Ca^{2+} ATPase, as well as some saline conditions, depleted Ca^{2+} from cell bath solution (procedure detailed in Materials and Methods). ATII cells were stimulated with vesicles containing SP-B at a final concentration of 13 µM or 100 µM ATP for control of stimulation. Values are mean ± SEM. Data were analyzed by paired student's t test (*** P<0.001).

To discard a potential cytotoxic effect of these treatments, we assessed the percentage of cells whose plasma membrane was damaged and allowed permeabilization of the probe FM1-43 and the subsequent staining of internal membranes (**Table 8.1** and **Figure 8.11**). In all the conditions tested, the percentage of viable cells was always higher than 96.7 %.

% cell viability						
	SP-B vesicles-stimulated cells					
SP-B vesicles	Apyrase	Suramin	Thapsigargin + Ca^{2+} free	Ca^{2+} free	FFA	CBX
97.9 (1.8)	99.4 (0.9)	98.5 (2.2)	98.8 (1.04)	99.5 (0.9)	99 (1.4)	99.4 (0.9)

% cell viability		
	ATP-stimulated cells	
ATP	FFA	CBX
96.7 (2.9)	98 (1.6)	99 (1.4)

Table 8.1. Cell viability during SP-B- or ATP-stimulated LB fusion experiments. Fraction of viable (non-damaged) ATII cells in the presence of apyrase (50 U/ml), 800 µM suramin, 200 nM thapsigargin, 100 µM flufenamic acid, 10 µM carbenoxolone or Ca^{2+}-free extracellular solution. Cytotoxicity of the different treatments was evaluated from the proportion of ATII cells that uptake FM1-43 into their internal membranes. Data are shown as % cell viability (SD).

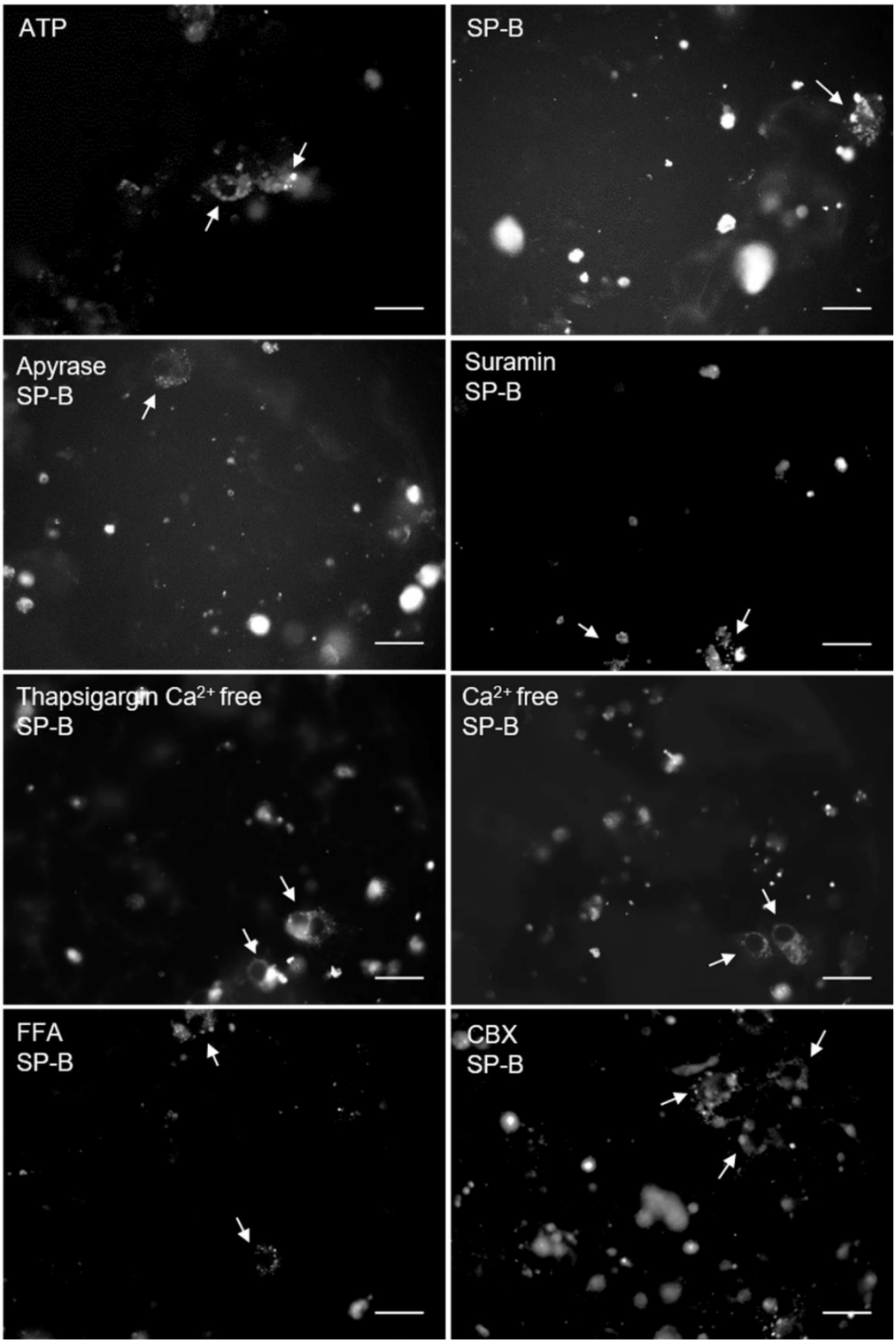

Figure 8.13. Cytotoxicity of different exocytosis stimulators and inhibitors on ATII cell cultures. Representative images from SP-B or ATP-stimulated LB fusion experiments in the presence of 50 U/ml apyrase, 800 µM suramin, 200 nM thapsigargin, 100 µM flufenamic acid (FFA), 10 µM carbenoxolone (CBX) or Ca^{2+} free-extracellular solution. Cells whose plasma membrane integrity is damaged (white arrows) show a strong FM1-43 labeling of the internal membranes, specially the pool of lamellar bodies in the cytoplasm. Additionally, FM1-43 signal stains vesicles and secreted LBs in solution, as well as LBs in late stages of secretion that remain attached to the cell. Scale bars show 25µm.

In order to identify the putative ATP release channel regulated by extracellular SP-B, a co-immunoprecipitation assay with an anti-SP-B antibody was performed on a preparation of plasma membrane from rat primary ATII cell cultures pre-incubated with SP-B vesicles. The assay consisted of several steps, from light to harsh treatments, to elute SP-B and SP-B-bound protein complexes. The electrophoretic analysis of the different eluted samples showed the presence of multiple bands for most of the elution treatments (**Figure 8.11**). Several silver-stained bands were subjected to protein identification by mass spectrometry, revealing that the bands of around 20 KDa from SDS-eluted samples contained porcine SP-B (red arrowhead). However, none of the remaining analyzed bands (black arrowheads) was successfully identified as plasma membrane proteins from ATII cells. Specifically, bands 2 and 3 were identified as bovine serum albumin, protein present in some of the buffers used during co-immunoprecipitation, whereas band 5 contained keratin, a common protein contaminant. Analysis of bands 1 and 4 did not provide conclusive results.

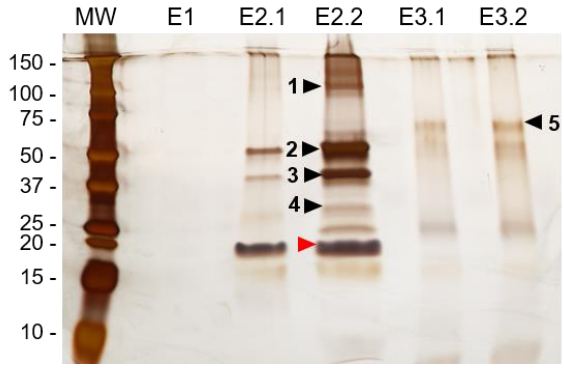

Figure 8.11. Co-immunoprecipitation assay of SP-B vesicles with plasma membrane of ATII cells. SDS/PAGE was performed on gradient gels of 4-20% acrylamide. For immunoprecipitation, α-SP-B antibody was used. Protein elution was performed under several conditions. MW: molecular weight; E1: 0.2 M glycine eluted fraction; E2.1 and E2.2: two consecutive SDS eluted fractions; E3.1 and E3.2: β-mercaptoethanol eluted fractions. After SDS/PAGE, labeled bands were analyzed by mass spectrometry analysis, indicating the presence of porcine SP-B (red arrowhead), bovine serum albumin (bands 2 and 3) and keratin (band 5). No protein was successfully identified from bands 1 and 4.

8.3. DISCUSSION

Surfactant secretion is highly regulated in alveolar type II cells by a concerted action of several physicochemical agents, such as mechanical stimulation or CO_2, and several agonists are known to activate surfactant secretion pathways. Here we demonstrate that surfactant protein SP-B is a potent factor stimulating the secretion of lamellar bodies by alveolar type II cells. SP-B stimulation prompts a rise in cytoplasmic calcium concentration, which is sufficient to trigger fusion of LBs with the plasma membrane and surfactant release. The increase of $[Ca^{2+}]_c$ would be related to intracellular Ca^{2+} release, and is followed by a plateau phase of the Ca^{2+} signal, sustained by Ca^{2+} entry from the

extracellular space. In the light of the present results, we propose the following model of the mechanisms behind SP-B-induced surfactant secretion (**Figure 8.12**). Initially, extracellular SP-B leads to a local ATP release from ATII cells through channels via a yet unknown mechanism that likely involves Ca^{2+}-dependent binding of SP-B to ATII cells. ATP then activates purinergic $P2Y_2$ receptors in an autocrine/paracrine fashion, which results in hydrolysis of phosphatidylinositol (3,4,5)-trisphosphate (PIP_3) into IP_3 by phospholipase C (PLC). IP_3 activates receptors (IP_3R) on intracellular Ca^{2+} stores and leads to release of Ca^{2+} into the cytoplasm, prompting LB exocytosis. In addition to activation of the purinergic pathway, ATP could mediate the entry of Ca^{2+} from the extracellular medium (probably via $P2X_4$ receptors (Miklavc, Thompson and Frick, 2013)), which triggers a late exocytotic activity. Previous work had already shown similar autocrine ATP-stimulated surfactant secretion in response to mechanical stretching (Patel *et al.*, 2005).

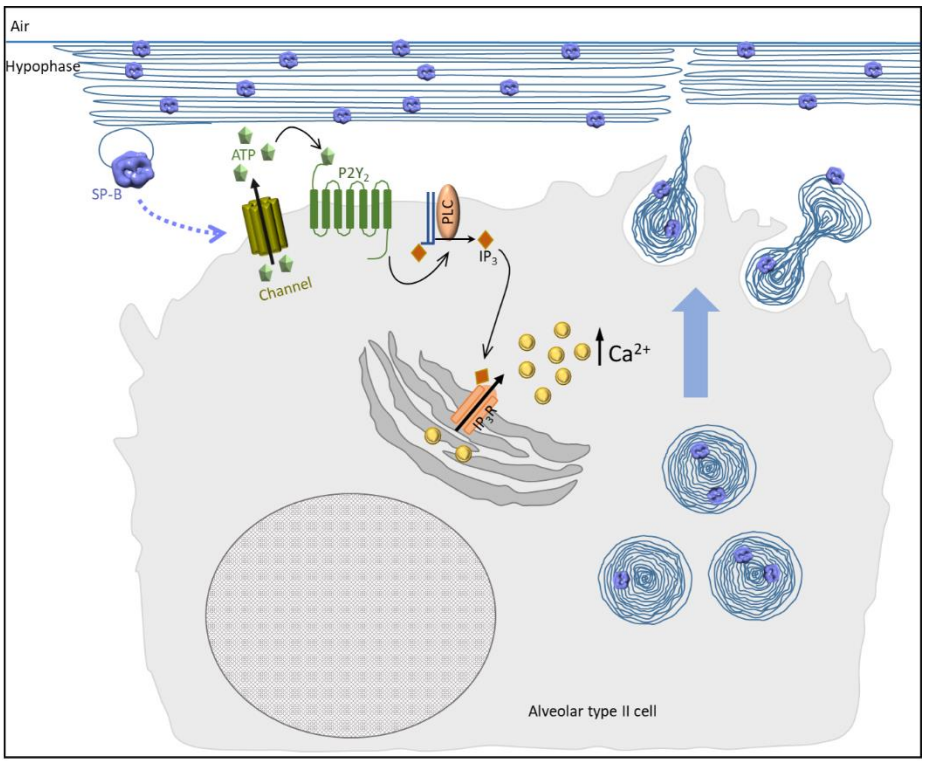

Figure 8.12. Pulmonary surfactant protein SP-B as a key element for pulmonary surfactant to regulate its own secretion by ATII cells. Secreted SP-B stimulates surfactant secretion via hemichannel-mediated ATP release. ATP released into the extracellular fluid triggers the activation of $P2Y_2$ purinergic receptors, which leads to the generation of IP_3 and concomitant Ca^{2+} release from intracellular Ca^{2+} stores via IP_3 receptors. Rise in $[Ca^{2+}]_c$ triggers lamellar body fusion with plasma membrane and surfactant release.

Although we propose that SP-B-induced ATP release is mediated by opening of channels in alveolar type II cells, further experiments will be required to identify the specific channel involved, as well as the extent and the location of the specific sites at which ATP release is primarily triggered by the action of SP-B at the plasma membrane of ATII cell. Several studies have reported a connection between Pannexin-1-dependent

ATP release and activation of purinergic $P2Y_2$ receptors in a variety of cell types (Séror *et al.*, 2011; Lu *et al.*, 2012; Velasquez and Eugenin, 2014). Moreover, pannexin-1 hemichannels are expressed in A549 cells, an ATII cell-derived line, where they may elicit hypotonicity-induced ATP release (Seminario-Vidal *et al.*, 2011). Pannexin-1 might therefore be a good candidate to mediate ATP release in SP-B-stimulated ATII cells, something that should be confirmed by further studies. Another feature that still remains unclear is the mechanism by which SP-B might activate the opening of channels and ATP release. This process could be driven directly by SP-B or through an intermediate molecular machinery, which could involve a plasma membrane protein receptor in ATII cells. At this point, the co-immunoprecipitation assay of SP-B with plasma membrane of ATII cells did not shed light about the identity of a putative receptor of SP-B. A future extension of this work should pursue the identification of molecular events linking the activation of channels with SP-B action at the plasma membrane of ATII cells.

Regarding the blocking assays with antibodies, the results suggest, once again, that SP-B is associated with SP-C in surfactant membranes, although SP-C would not be directly involved in stimulation of surfactant secretion. This is consistent with a previous study that revealed the existence of SP-B/SP-C complexes in secreted LBs, which would form a "gating" machinery allowing the unravelling of surfactant membranes of the LB and their rapid spreading once at the air-liquid interface (Hobi *et al.*, 2016). Regarding the implication of anionic phospholipids in SP-B-induced LB secretion, our results suggest that POPG could modulate the structural disposition of the SP-B oligomer to achieve an optimal activity. This effect of POPG over the structural conformation of the SP-B oligomer was also stated in Chapter 2, where the presence of the anionic phospholipid was found to be important for achieving the native pulmonary surfactant permeability to polar molecules.

Despite surfactant secretion is primarily stimulated by mechanical stretching of the epithelial alveoli during breathing, our results show for the first time that SP-B may act as a positive regulatory key element of pulmonary surfactant exocytosis via purinergic signaling pathway. The participation of other surfactant proteins in the regulation of surfactant exocytosis has been previously described. Hydrophilic surfactant protein SP-A inhibits surfactant secretion through the specific receptor SPAR via activation of phosphatidylinositol 3-Kinase (PI_3K) in ATII cells (Dobbs *et al.*, 1987; Rice *et al.*, 1987; Strayer, Yang and Jerng, 1993; White and Strayer, 2000). Several lines of evidence support the existence of possible interactions between SP-A and SP-B. Both proteins are required for the formation of tubular myelin, another type of highly ordered array of surfactant membranes, which suggests a likely specific interaction between them (Perez-Gil, 2008). Other experimental results have also suggested SP-A/SP-B relationships via direct protein-protein interactions (Taneva and Keough, 2000) or mediated by lipids

(Sarker, Jackman and Booth, 2011). Besides this, the results obtained in Chapter 1 also pointed the possibility of the existence of SP-A/SP-B complexes in native surfactant membranes. In the light of the present results, we propose that pulmonary surfactant might regulate its own secretion through the coordinated action of SP-B-inducing and SP-A-inhibiting activities. Combined effects of SP-B and SP-A on surfactant secretion might be elicited by the interaction of extracellular forms of both proteins.

To conclude, the present work showed evidences of the relevance of SP-B in the alveolar homeostasis. SP-B would not be only essential for the optimal surface active function of surfactant at the interface, but also our current *in vitro* results suggests that SP-B acts as a potent stimulating agent of purinergic-mediated surfactant secretion by ATII cells, ensuring that a proper density of newly secreted surfactant complexes are assembled at the respiratory interface.

GENERAL DISCUSSION

9. GENERAL DISCUSSION

In this work, three main features of pulmonary surfactant have been extensively analyzed: membrane aggregation as a basis to rearrange surfactant structures, membrane permeability through the generation of pores generation which allow the flow of both polar solutes and lipids, and stimulation of surfactant secretion by alveolar type II cells. In all of these three activities, the action of protein SP-B has been found to be essential.

Throughout this Thesis, the existence of a supramolecular organization of SP-B in pulmonary surfactant has been repeatedly proven. Besides native SP-B complexes purified from detergent-solubilized surfactant membranes, SP-B dimers from both the whole organic extract of pulmonary surfactant or the protein isolated in organic solvent are able to self-assemble yielding a ring-shaped structure of the SP-B oligomer that locates over the polar head groups of bilayers and monolayers. Besides these structures, a more complex organization of the oligomers, in the form of fibers or protein clusters, could be also inferred from our results, though their structure and functional implication has to be still further investigated.

It was previously known that the ability of SP-B to induce tight connections between membranes yields the generation of multilayered structures associated to the interface (Taneva and Keough, 1994b; Krol *et al.*, 2000; Diemel *et al.*, 2002; Cruz *et al.*, 2004; Cabre *et al.*, 2009; Bernardino de la Serna *et al.*, 2013) that appear to be crucial for sustaining the surface active film against the mechanical stress induced by continuous compression-expansion cycles (Schurch *et al.*, 2010). Time-resolved FRET experiments performed in this Thesis provide quantitative information of the topology of membrane aggregates induced by SP-B, confirming that the connection between two neighboring bilayers is mediated by the vertical apposition of two SP-B ring-shaped oligomers. These structures would be relevant for the role of SP-B not only on the biophysical function of pulmonary surfactant at the alveolar interface, but also on the biogenesis of lamellar bodies and the structural rearrangements that undergo surfactant once secreted into the alveolar subphase (Perez-Gil, 2008).

Regarding the permeability properties of surfactant, the selective blockage of SP-B with antibodies allowed to determine that SP-B ring-shaped structures are responsible for the formation of pores in surfactant membranes, which allow the flow of polar molecules, as well as the lipid transfer through interconnected membranes of the surfactant reservoir, and between those membranes and the interfacial monolayer. As mentioned above, SP-B mediates the connection between membranes through the interaction of two SP-B oligomers, which would constitute a lipid transfer machinery, shielding the acyl chains of phospholipids in hydrophobic cavities provided by SP-B dimers and exposing the polar head groups towards the aqueous solvent, as previously proposed by (Olmeda *et al.*,

2015). Thus, SP-B rings are essential to ensure optimal interfacial adsorption and stability of the surface active film during respiratory cycles, so that permeability of surfactant membranes appears to be a consequence of the architecture of the SP-B machinery specialized in lipid transfer between interconnected bilayers and between bilayers and monolayer. Furthermore, the existence of such pores would, as a consequence, provide surfactant membranes with the ability to facilitate diffusion of ions, gases, such as oxygen, poorly soluble in water, or small peptides involved in innate defense, ensuring a proper ion balance in the alveolar subphase (Parra *et al.*, 2013) and a rapid oxygen diffusion from air space (Olmeda *et al.*, 2010).

In addition to study the role of SP-B on membrane permeability and on the surface behavior of pulmonary surfactant, the stimulating effect of SP-B on surfactant secretion by alveolar type II cells was also revealed for the first time. Extracellular membrane-associated SP-B promotes lamellar body fusion with plasma membrane and subsequent surfactant secretion via $P2Y_2$ purinergic pathway in primary ATII cell cultures. We propose that stimulation of LB exocytosis could be triggered by SP-B rings that are not participating in connections between surfactant membranes. These free SP-B oligomers might be available to interact with ATII cells triggering the activation of purinergic $P2Y_2$ receptors via channel-mediated ATP release, leading finally to lamellar body fusion with plasma membrane and surfactant secretion. The final stage of surfactant secretion stimulation would be reached once the hypophase is fullly replenished with a sufficiently dense network of surfactant membranes, in which most of the secreted SP-B rings would be participating in connections between membranes or between those and the interfacial monolayer. In this way, extracellular SP-B complexes may act as a feedback mechanism to ensure availability of enough surfactant to convert the alveolar interface into a so-called "membrane interface" (Olmeda *et al.*, 2015), optimized to facilitate rapid transfer of lipids, as well as transit of polar molecules, ions and gases. Future work should confirm whether the proposed SP-B regulatory mechanism also regulates pulmonary surfactant pools and alveolar homeostasis *in vivo*.

A considerable outcome of this work is the importance of the preservation of native interactions in the whole surfactant system. Despite the crucial role of SP-B in the investigated activities of surfactant, interactions of this protein with the many other components of the system have been found to be significant. It has been widely described that SP-B establishes preferential electrostatic interactions with anionic phospholipids through its cationic amino acids (Baatz, Elledge and Whitsett, 1990; Perez-Gil, Casals and Marsh, 1995; Cabré *et al.*, 2012). Our results are in agreement with these published data, as PG, the most abundant anionic phospholipid in PS, becomes relevant to ensure the proper function of SP-B in pulmonary surfactant with respect two key features: membrane permeability and stimulation of surfactant secretion by alveolar type II cells.

However, in contrast to a previous work that considered that anionic phospholipids could be necessary for the oligomerization of SP-B (Olmeda *et al.*, 2015), here we have demonstrated that PG is not essential for SP-B dimers isolated in organic solvent to oligomerize in a phospholipid environment, displaying a structure similar to those complexes formed in the presence of PG or the native SP-B complexes purified in detergent. We speculate that PG is still crucial at surfactant layers to promote a solid anchor of SP-B rings at the surface of membranes and monolayers. Only with that solid attachment, SP-B rings could play their key role to I) facilitate efficient flow of surface active species and II) stabilize multilayered structures along breathing mechanics.

Besides lipids, SP-B oligomers also demonstrated to be associated with other surfactant proteins. Recently, a time-resolved fluorescence spectroscopy study has demonstrated a direct interaction between SP-B oligomers and SP-C (Cabre *et al.*, 2018). Here, our results suggest the integration of both proteins into native complexes of surfactant solubilized by detergents. Furthermore, it has been certainly proven that the original activities of SP-B and SP-C when kept together from the organic extract of surfactant, are not preserved after their physical separation during their purification process, highlighting the importance of potential native protein-protein interactions. Additionally, as in the case of PG, the presence of SP-C has been found to be relevant for maintaining the proper native surfactant permeability through SP-B-generated pores. As previously discussed, interaction of SP-B and SP-C would be crucial for the spatial and temporal modulation of their cooperative and counteracting activities, necessary for the optimal function of the system.

On the other hand, the physical interaction of SP-B with the collectin SP-A has been also deduced from 2D BN/SDS-PAGE of surfactant membranes solubilized by CHAPS. Further investigations would be necessary to determine whether SP-A and SP-B establish direct protein/protein interaction or whether it could be mediated by other molecules, such as lipids. Some important physiological implications can be attributed to such interactions, because the cooperation of both proteins in several aspects of surfactant structure or function has been previously described (Hawgood *et al.*, 1987; Palaniyar *et al.*, 1999). Moreover, as a consequence of our results, a new coordinated role of SP-B and SP-A could be ascribed to both proteins at the tight regulation of surfactant secretion by type II cells.

As a concluding remark, the present Thesis confirms that SP-B is a central cornerstone in the pulmonary surfactant system at a higher level than envisioned before, with SP-B participating at every stage of the surfactant cycle. Firstly, SP-B is required to achieve the optimal surface activity of pulmonary surfactant at the interface, where the connection between membranes established by SP-B rings results essential. Secondly, SP-B is

involved in the proper assembly of surfactant membranes inside the lamellar bodies (Stahlman *et al.*, 2000). And lastly, extracellular SP-B stimulates the surfactant exocytosis via purinergic pathway, ensuring a proper density of secreted surfactant at the alveolar interface.

In the light of these evidences, it is no surprising that lack of SP-B is incompatible with life. The production of human SP-B is therefore a priority if future therapeutic strategies in respiratory medicine have to go through restoration of a proper SP-B-based surfactant network in the lungs of patients.

CONCLUSIONS

10. CONCLUSIONS

1. The native oligomeric structure of SP-B is able to be re-assembled from SP-B dimers dissolved in organic solvent once it is reconstituted with lipids in aqueous environments. The preferential orientation of these SP-B ring-shaped complexes, parallel to the plane of lipid bilayers or monolayers, is related to its function.

2. The presence of anionic phospholipid PG modulates the oligomeric structure of SP-B, being necessary for an optimal function of the protein.

3. SP-B participates in native heterocomplexes together with proteins SP-A or SP-C. Direct interactions SP-A/SP-B and SP-B/SP-C could not be proven in the present work.

4. Permeability of surfactant membranes to polar molecules is the consequence of the synergistic action of both SP-B and SP-C in bilayers. SP-B is able to induce the formation of pores of a defined size in membranes, whereas SP-C participates in the architecture of these pores by constricting the pore size.

5. The native SP-B oligomer is responsible of lipid transfer between surfactant membranes and the interface, ensuring the optimal surface function of pulmonary surfactant.

6. SP-B ring-shaped structures could be simultaneously responsible for both lipid transfer and membrane permeability through SP-B pores.

7. SP-B sustains multilamellar structures in surfactant by connecting membranes through the vertical apposition of two SP-B rings. These SP-B/SP-B interactions would be at the core of the role of SP-B on the biophysical function of pulmonary surfactant at the alveolar interface, but also might be involved in the generation of lipid packing during lamellar body biogenesis.

8. Extracellular membrane-associated SP-B induces lamellar body exocytosis by activation of $P2Y_2$ purinergic signaling pathways in alveolar type II cells. SP-B prompts Ca^{2+}-dependent surfactant secretion via ATP release from ATII cells. Thus, SP-B is not only relevant for the biophysical function of pulmonary surfactant, but also a central element in the surfactant homeostasis at the alveolar spaces by regulating its secretion.

BIBLIOGRAPHY

11. BIBLIOGRAPHY

Agassandian, M. and Mallampalli, R. K. (2013) 'Surfactant phospholipid metabolism', *Biochim Biophys Acta*, 1831(3), pp. 612–625. doi: 10.1016/j.bbalip.2012.09.010.

Akinbi, H. T., Breslin, J. S., Ikegami, M., Iwamoto, H. S., Clark, J. C., Whitsett, J. A., Jobe, A. H. and Weaver, T. E. (1997) 'Rescue of SP-B knockout mice with a truncated SP-B proprotein. Function of the C-terminal propeptide', *J Biol Chem*, 272(15), pp. 9640–9647.

de Almeida, R. F. M., Loura, L. M. S., Fedorov, A. and Prieto, M. (2005) 'Lipid Rafts have Different Sizes Depending on Membrane Composition: A Time-resolved Fluorescence Resonance Energy Transfer Study', *Journal of Molecular Biology*, 346(4), pp. 1109–1120. doi: https://doi.org/10.1016/j.jmb.2004.12.026.

Andersson, M., Curstedt, T., Jornvall, H. and Johansson, J. (1995) 'An amphipathic helical motif common to tumourolytic polypeptide NK-lysin and pulmonary surfactant polypeptide SP-B', *FEBS Lett*. 1995/04/10, 362(3), pp. 328–332. doi: 0014-5793(95)00268-E [pii].

Arroyo, R., Martín-González, A., Echaide, M., Jain, A., Brondyk, W. H., Rosenbaum, J., Moreno-Herrero, F. and Pérez-Gil, J. (2018) 'Supramolecular Assembly of Human Pulmonary Surfactant Protein SP-D', *Journal of Molecular Biology*, 430(10), pp. 1495–1509. doi: 10.1016/j.jmb.2018.03.027.

Ashino, Y., Ying, X., Dobbs, L. G. and Bhattacharya, J. (2000) '[Ca(2+)](i) oscillations regulate type II cell exocytosis in the pulmonary alveolus', *Am J Physiol Lung Cell Mol Physiol*, 279(1), pp. L5-13.

Baatz, J. E., Elledge, B. and Whitsett, J. A. (1990) 'Surfactant protein SP-B induces ordering at the surface of model membrane bilayers', *Biochemistry*. 1990/07/17, 29(28), pp. 6714–6720.

Bader, A. N., Hoetzl, S., Hofman, E. G., Voortman, J., van Bergen en Henegouwen, P. M. P., van Meer, G. and Gerritsen, H. C. (2011) 'Homo-FRET imaging as a tool to quantify protein and lipid clustering.', *Chemphyschem : a European journal of chemical physics and physical chemistry*. Germany, 12(3), pp. 475–483. doi: 10.1002/cphc.201000801.

Ban, N., Matsumura, Y., Sakai, H., Takanezawa, Y., Sasaki, M., Arai, H. and Inagaki, N. (2007) 'ABCA3 as a lipid transporter in pulmonary surfactant biogenesis', *J Biol Chem*, 282(13), pp. 9628–9634. doi: 10.1074/jbc.M611767200.

Banares-Hidalgo, A., Perez-Gil, J. and Estrada, P. (2014) 'Acidic pH triggers conformational changes at the NH2-terminal propeptide of the precursor of pulmonary surfactant protein B to form a coiled coil structure', *Biochim Biophys Acta*, 1838(7), pp. 1738–1751. doi: 10.1016/j.bbamem.2014.03.016.

Batenburg, J. J. (1992) 'Surfactant phospholipids: synthesis and storage', *Am J Physiol*, 262(4 Pt 1), pp. L367-85.

Bates, S. R. (2010) 'P63 (CKAP4) as an SP-A receptor: implications for surfactant turnover', *Cell Physiol Biochem*, 25(1), pp. 41–54. doi: 10.1159/000272062.

Bates, S. R., Dodia, C., Tao, J. Q. and Fisher, A. B. (2008) 'Surfactant protein-A plays an important role in lung surfactant clearance: evidence using the surfactant protein-A gene-targeted mouse', *Am J Physiol Lung Cell Mol Physiol*, 294(2), pp. L325-33. doi: 10.1152/ajplung.00341.2007.

Baumgart, F., Ospina, O. L., Mingarro, I., Rodríguez-Crespo, I. and Pérez-Gil, J. (2010) 'Palmitoylation of Pulmonary Surfactant Protein SP-C Is Critical for Its Functional Cooperation with SP-B to Sustain Compression/Expansion Dynamics in Cholesterol-Containing Surfactant

Films', *Biophysical Journal*. The Biophysical Society, 99(10), pp. 3234–3243. doi: 10.1016/j.bpj.2010.08.070.

Beers, M. F. and Mulugeta, S. (2005) 'Surfactant protein C biosynthesis and its emerging role in conformational lung disease', *Annu Rev Physiol*, 67, pp. 663–696. doi: 10.1146/annurev.physiol.67.040403.101937.

Bernardino de la Serna, J., Vargas, R., Picardi, V., Cruz, A., Arranz, R., Valpuesta, J. M., Mateu, L. and Perez-Gil, J. (2013) 'Segregated ordered lipid phases and protein-promoted membrane cohesivity are required for pulmonary surfactant films to stabilize and protect the respiratory surface', *Faraday Discuss*, 161, pp. 535–589. doi: 10.1039/c2fd20096a.

Bignon, J., Chahinian, P., Feldmann, G. and Sapin, C. (1975) 'Ultrastructural immunoperoxidase demonstration of autologous albumin in the alveolar capillary membrane and in the alveolar lining material in normal rats', *The Journal of Cell Biology*. The Rockefeller University Press, 64(2), pp. 503–509.

Bignon, J., Jaurand, M. C., Pinchon, M. C., Sapin, C. and Warnet, J. M. (1976) 'Immunoelectron microscopic and immunochemical demonstrations of serum proteins in the alveolar lining material of the rat lung.', *The American review of respiratory disease*. United States, 113(2), pp. 109–120. doi: 10.1164/arrd.1976.113.2.109.

Blanco, O. and Perez-Gil, J. (2007) 'Biochemical and pharmacological differences between preparations of exogenous natural surfactant used to treat Respiratory Distress Syndrome: role of the different components in an efficient pulmonary surfactant', *Eur J Pharmacol*. 2007/06/05, 568(1–3), pp. 1–15. doi: S0014-2999(07)00510-9 [pii]10.1016/j.ejphar.2007.04.035.

Bligh, E. G. and Dyer, W. J. (1959) 'A rapid method of total lipid extraction and purification', *Canadian Journal of Biochemistry and Physiology*, 37(8), pp. 911–917. doi: 10.1139/o59-099.

Brasch, F., Johnen, G., Winn-Brasch, A., Guttentag, S. H., Schmiedl, A., Kapp, N., Suzuki, Y., Muller, K. M., Richter, J., Hawgood, S. and Ochs, M. (2004) 'Surfactant protein B in type II pneumocytes and intra-alveolar surfactant forms of human lungs', *Am J Respir Cell Mol Biol*. 2003/09/16, 30(4), pp. 449–458. doi: 10.1165/rcmb.2003-0262OC2003-0262OC [pii].

Brasch, F., Ochs, M., Kahne, T., Guttentag, S., Schauer-Vukasinovic, V., Derrick, M., Johnen, G., Kapp, N., Muller, K. M., Richter, J., Giller, T., Hawgood, S. and Buhling, F. (2003) 'Involvement of napsin A in the C- and N-terminal processing of surfactant protein B in type-II pneumocytes of the human lung', *J Biol Chem*, 278(49), pp. 49006–49014. doi: 10.1074/jbc.M306844200.

Breyton, C., Pucci, B. and Popot, J.-L. (2010) *Amphipols and Fluorinated Surfactants: Two Alternatives to Detergents for Studying Membrane Proteins In vitro, Methods in molecular biology (Clifton, N.J.)*. doi: 10.1007/978-1-60761-344-2_14.

Buranda, T., Wu, Y., Perez, D., Chigaev, A. and Sklar, L. A. (2010) 'Real time partitioning of octadecyl rhodamine B into bead supported lipid bilayer membranes reveals quantitative differences in saturable binding sites in DOPC and 1:1:1 DOPC/SM/Cholesterol membranes', *The journal of physical chemistry. B*, 114(3), pp. 1336–1349. doi: 10.1021/jp906648q.

Butler, P. L. and Mallampalli, R. K. (2010) 'Cross-talk between remodeling and de novo pathways maintains phospholipid balance through ubiquitination', *J Biol Chem*, 285(9), pp. 6246–6258. doi: 10.1074/jbc.M109.017350.

Cabré, E. J., Loura, L. M. S., Fedorov, A., Perez-Gil, J. and Prieto, M. (2012) 'Topology and lipid selectivity of pulmonary surfactant protein SP-B in membranes: Answers from fluorescence', *Biochimica et Biophysica Acta - Biomembranes*, 1818(7), pp. 1717–1725. doi: 10.1016/j.bbamem.2012.03.008.

Cabre, E. J., Malmstrom, J., Sutherland, D., Perez-Gil, J. and Otzen, D. E. (2009) 'Surfactant

protein SP-B strongly modifies surface collapse of phospholipid vesicles: insights from a quartz crystal microbalance with dissipation', *Biophys J*. 2009/08/05, 97(3), pp. 768–776. doi: S0006-3495(09)01016-9 [pii]10.1016/j.bpj.2009.04.057.

Cabre, E. J., Martinez-Calle, M., Prieto, M., Fedorov, A., Olmeda, B., Loura, L. M. S. and Perez-Gil, J. (2018) 'Homo- and hetero-oligomerization of hydrophobic pulmonary surfactant proteins SP-B and SP-C in surfactant phospholipid membranes.', *The Journal of biological chemistry*. United States. doi: 10.1074/jbc.RA117.000222.

Campbell, N. A., Reece, J. B. and Mitchell, L. G. (1999) *Biology*. 5th editio. Boston: Benjamin Cummings.

Carpenter, E. P., Beis, K., Cameron, A. D. and Iwata, S. (2008) 'Overcoming the challenges of membrane protein crystallography', *Current Opinion in Structural Biology*. Elsevier Science, 18(5), pp. 581–586. doi: 10.1016/j.sbi.2008.07.001.

Casals, C., Miguel, E. and Perez-Gil, J. (1993) 'Tryptophan fluorescence study on the interaction of pulmonary surfactant protein A with phospholipid vesicles.', *The Biochemical journal*. England, 296 (Pt 3, pp. 585–593.

Castanho, M. A. R. B., Santos, N. C. and Loura, L. M. S. (1997) 'Separating the turbidity spectra of vesicles from the absorption spectra of membrane probes and other chromophores', *European biophysics journal*. Springer, 26(3), pp. 253–259.

Catoire, L. J., Warnet, X. L. and Warschawski, D. E. (2014) 'Micelles, Bicelles, Amphipols, Nanodiscs, Liposomes, or Intact Cells: The Hitchhiker's Guide to the Study of Membrane Proteins by NMR BT - Membrane Proteins Production for Structural Analysis', in Mus-Veteau, I. (ed.). New York, NY: Springer New York, pp. 315–345. doi: 10.1007/978-1-4939-0662-8_12.

Cerrada, A., Haller, T., Cruz, A. and Perez-Gil, J. (2015) 'Pneumocytes Assemble Lung Surfactant as Highly Packed/Dehydrated States with Optimal Surface Activity', *Biophys J*, 109(11), pp. 2295–2306. doi: 10.1016/j.bpj.2015.10.022.

Champeil, P., Menguy, T., Tribet, C., L Popot, J. and le Maire, M. (2000) *Interaction of Amphipols with Sarcoplasmic Reticulum Ca2+-ATPase, The Journal of biological chemistry*. doi: 10.1074/jbc.M000470200.

Chan, F. T. S., Kaminski, C. F. and Kaminski Schierle, G. S. (2011) 'HomoFRET fluorescence anisotropy imaging as a tool to study molecular self-assembly in live cells.', *Chemphyschem : a European journal of chemical physics and physical chemistry*. Germany, 12(3), pp. 500–509. doi: 10.1002/cphc.201000833.

Chang, R., Nir, S. and Poulain, F. R. (1998) 'Analysis of binding and membrane destabilization of phospholipid membranes by surfactant apoprotein B', *Biochim Biophys Acta*. 1998/06/19, 1371(2), pp. 254–264. doi: S0005-2736(98)00031-5 [pii].

Chattopadhyay, A. and Harikumar, K. G. (1996) 'Dependence of critical micelle concentration of a zwitterionic detergent on ionic strength: Implications in receptor solubilization', *FEBS Letters*, 391(1–2), pp. 199–202. doi: 10.1016/0014-5793(96)00733-8.

Chavarha, M., Loney, R. W., Kumar, K., Rananavare, S. B. and Hall, S. B. (2012) 'Differential effects of the hydrophobic surfactant proteins on the formation of inverse bicontinuous cubic phases.', *Langmuir : the ACS journal of surfaces and colloids*. United States, 28(48), pp. 16596–16604. doi: 10.1021/la3025364.

Chavarha, M., Loney, R. W., Rananavare, S. B. and Hall, S. B. (2013) 'An anionic phospholipid enables the hydrophobic surfactant proteins to alter spontaneous curvature', *Biophys J*, 104(3), pp. 594–603. doi: 10.1016/j.bpj.2012.12.041.

Chavarha, M., Loney, R. W., Rananavare, S. B. and Hall, S. B. (2015) 'Hydrophobic surfactant

proteins strongly induce negative curvature.', *Biophysical journal*. United States, 109(1), pp. 95–105. doi: 10.1016/j.bpj.2015.05.030.

Chen, J., Ryu, S., Gharib, S. A., Goodlett, D. R. and Schnapp, L. M. (2008) 'Exploration of the normal human bronchoalveolar lavage fluid proteome', *Proteomics. Clinical applications*, 2(4), pp. 585–595. doi: 10.1002/prca.200780006.

Cheong, N., Zhang, H., Madesh, M., Zhao, M., Yu, K., Dodia, C., Fisher, A. B., Savani, R. C. and Shuman, H. (2007) 'ABCA3 is critical for lamellar body biogenesis in vivo', *J Biol Chem*, 282(33), pp. 23811–23817. doi: 10.1074/jbc.M703927200.

Civjan, N. R., Bayburt, T. H., Schuler, M. A. and Sligar, S. G. (2003) 'Direct solubilization of heterologously expressed membrane proteins by incorporation into nanoscale lipid bilayers.', *BioTechniques*. England, 35(3), pp. 556-560,562-563.

Clark, J. C., Wert, S. E., Bachurski, C. J., Stahlman, M. T., Stripp, B. R., Weaver, T. E. and Whitsett, J. A. (1995) 'Targeted disruption of the surfactant protein B gene disrupts surfactant homeostasis, causing respiratory failure in newborn mice', *Proc Natl Acad Sci U S A*. 1995/08/15, 92(17), pp. 7794–7798.

Cockshutt, A. M., Weitz, J. and Possmayer, F. (1990) 'Pulmonary surfactant-associated protein A enhances the surface activity of lipid extract surfactant and reverses inhibition by blood proteins in vitro.', *Biochemistry*. United States, 29(36), pp. 8424–8429.

Coutinho, A., Loura, L. M. S., Fedorov, A. and Prieto, M. (2008) 'Pinched Multilamellar Structure of Aggregates of Lysozyme and Phosphatidylserine-Containing Membranes Revealed by FRET', *Biophysical Journal*, pp. 4726–4736. doi: 10.1529/biophysj.108.134379.

Craig, A. F., Clark, E. E., Sahu, I. D., Zhang, R., Frantz, N. D., Al-Abdul-Wahid, M. S., Dabney-Smith, C., Konkolewicz, D. and Lorigan, G. A. (2016) 'Tuning the size of styrene-maleic acid copolymer-lipid nanoparticles (SMALPs) using RAFT polymerization for biophysical studies.', *Biochimica et biophysica acta*. Netherlands, 1858(11), pp. 2931–2939. doi: 10.1016/j.bbamem.2016.08.004.

Crapo, J. D., Young, S. L., Fram, E. K., Pinkerton, K. E., Barry, B. E. and Crapo, R. O. (1983) 'Morphometric characteristics of cells in the alveolar region of mammalian lungs.', *The American review of respiratory disease*. United States, 128(2 Pt 2), pp. S42-6. doi: 10.1164/arrd.1983.128.2P2.S42.

Crouch, E. C. (1998) 'Structure, biologic properties, and expression of surfactant protein D (SP-D)', *Biochim Biophys Acta*, 1408(2–3), pp. 278–289.

Crouch, E. and Wright, J. R. (2001) 'Surfactant proteins a and d and pulmonary host defense.', *Annual review of physiology*. United States, 63, pp. 521–554. doi: 10.1146/annurev.physiol.63.1.521.

Cruz, A., Casals, C., Keough, K. M. and Perez-Gil, J. (1997) 'Different modes of interaction of pulmonary surfactant protein SP-B in phosphatidylcholine bilayers', *Biochem J*. 1997/11/14, 327 (Pt 1, pp. 133–138.

Cruz, A., Casals, C., Plasencia, I., Marsh, D. and Perez-Gil, J. (1998) 'Depth profiles of pulmonary surfactant protein B in phosphatidylcholine bilayers, studied by fluorescence and electron spin resonance spectroscopy', *Biochemistry*. 1998/07/02, 37(26), pp. 9488–9496. doi: 10.1021/bi971558vbi971558v [pii].

Cruz, A., Vazquez, L., Velez, M. and Perez-Gil, J. (2004) 'Effect of pulmonary surfactant protein SP-B on the micro- and nanostructure of phospholipid films', *Biophys J*. 2003/12/26, 86(1 Pt 1), pp. 308–320. doi: S0006-3495(04)74106-5 [pii]10.1016/S0006-3495(04)74106-5.

Cruz, A., Worthman, L. A., Serrano, A. G., Casals, C., Keough, K. M. and Perez-Gil, J. (2000)

‘Microstructure and dynamic surface properties of surfactant protein SP-B/dipalmitoylphosphatidylcholine interfacial films spread from lipid-protein bilayers’, *Eur Biophys J*. 2000/09/01, 29(3), pp. 204–213.

Daniels, C. B. and Orgeig, S. (2003) ‘Pulmonary surfactant: the key to the evolution of air breathing.’, *News in physiological sciences : an international journal of physiology produced jointly by the International Union of Physiological Sciences and the American Physiological Society*. United States, 18, pp. 151–157.

Davenport, L., Dale, R. E., Bisby, R. H. and Cundall, R. B. (1985) ‘Transverse location of the fluorescent probe 1, 6-diphenyl-1, 3, 5-hexatriene in model lipid bilayer membrane systems by resonance excitation energy transfer’, *Biochemistry*. ACS Publications, 24(15), pp. 4097–4108.

Denisov, I. G., Grinkova, Y. V, Lazarides, A. A. and Sligar, S. G. (2004) ‘Directed self-assembly of monodisperse phospholipid bilayer Nanodiscs with controlled size.’, *Journal of the American Chemical Society*. United States, 126(11), pp. 3477–3487. doi: 10.1021/ja0393574.

Denisov, I. G. and Sligar, S. G. (2017) ‘Nanodiscs in Membrane Biochemistry and Biophysics.’, *Chemical reviews*. United States, 117(6), pp. 4669–4713. doi: 10.1021/acs.chemrev.6b00690.

Dico, A. S., Taneva, S., Morrow, M. R. and Keough, K. M. (1997) ‘Effect of calcium on phospholipid interaction with pulmonary surfactant protein C.’, *Biophysical Journal*, 73(5), pp. 2595–2602.

Diemel, R. V, Snel, M. M. E., Waring, A. J., Walther, F. J., van Golde, L. M. G., Putz, G., Haagsman, H. P. and Batenburg, J. J. (2002) ‘Multilayer Formation upon Compression of Surfactant Monolayers Depends on Protein Concentration as Well as Lipid Composition: AN ATOMIC FORCE MICROSCOPY STUDY ’, *Journal of Biological Chemistry* , 277(24), pp. 21179–21188. doi: 10.1074/jbc.M111758200.

Dietl, P., Haller, T. and Frick, M. (2012) ‘Spatio-temporal aspects, pathways and actions of Ca(2+) in surfactant secreting pulmonary alveolar type II pneumocytes’, *Cell Calcium*, 52(3–4), pp. 296–302. doi: 10.1016/j.ceca.2012.04.010.

Divangahi, M., King, I. L. and Pernet, E. (2015) ‘Alveolar macrophages and type I IFN in airway homeostasis and immunity.’, *Trends in immunology*. England, 36(5), pp. 307–314. doi: 10.1016/j.it.2015.03.005.

Dobbs, L. G., Gonzalez, R. and Williams, M. C. (1986) ‘An improved method for isolating type II cells in high yield and purity’, *Am Rev Respir Dis*, 134(1), pp. 141–145. doi: 10.1164/arrd.1986.134.1.141.

Dobbs, L. G., Wright, J. R., Hawgood, S., Gonzalez, R., Venstrom, K. and Nellenbogen, J. (1987) ‘Pulmonary surfactant and its components inhibit secretion of phosphatidylcholine from cultured rat alveolar type II cells’, *Proc Natl Acad Sci U S A*, 84(4), pp. 1010–1014.

Dörr, J. M., Scheidelaar, S., Koorengevel, M. C., Dominguez, J. J., Schäfer, M., van Walree, C. A. and Killian, J. A. (2016) ‘The styrene–maleic acid copolymer: a versatile tool in membrane research’, *European Biophysics Journal*. Berlin/Heidelberg: Springer Berlin Heidelberg, 45, pp. 3–21. doi: 10.1007/s00249-015-1093-y.

Duck-Chong, C. G. (1978) ‘The isolation of lamellar bodies and their membranous content from rat lung, lamb tracheal fluid and human amniotic fluid’, *Life Sciences*, 22(22), pp. 2025–2030. doi: https://doi.org/10.1016/0024-3205(78)90549-0.

Eijking, E. P., Strayer, D. S., van Daal, G. J., Tenbrinck, R., Merritt, T. A., Hannappel, E. and Lachmann, B. (1991) ‘In vivo and in vitro inactivation of bovine surfactant by an anti-surfactant monoclonal antibody.’, *The European respiratory journal*. England, 4(10), pp. 1245–1250.

Fisher, A. B., Dodia, C. and Chander, A. (1994) ‘Inhibition of lung calcium-independent

phospholipase A2 by surfactant protein A', *Am J Physiol*, 267(3 Pt 1), pp. L335-41.

Fois, G., Winkelmann, V. E., Bareis, L., Staudenmaier, L., Hecht, E., Ziller, C., Ehinger, K., Schymeinsky, J., Kranz, C. and Frick, M. (2018) 'ATP is stored in lamellar bodies to activate vesicular P2X₄ in an autocrine fashion upon exocytosis', *The Journal of General Physiology*, 150(2), p. 277 LP-291.

Fois, G., Wittekindt, O., Zheng, X., Felder, E. T., Miklavc, P., Frick, M., Dietl, P. and Felder, E. (2012) 'An ultra fast detection method reveals strain-induced Ca(2+) entry via TRPV2 in alveolar type II cells', *Biomech Model Mechanobiol*, 11(7), pp. 959–971. doi: 10.1007/s10237-011-0365-4.

Frick, M., Bertocchi, C., Jennings, P., Haller, T., Mair, N., Singer, W., Pfaller, W., Ritsch-Marte, M. and Dietl, P. (2004) 'Ca2+ entry is essential for cell strain-induced lamellar body fusion in isolated rat type II pneumocytes', *Am J Physiol Lung Cell Mol Physiol*, 286(1), pp. L210-20. doi: 10.1152/ajplung.00332.2003.

Frick, M., Eschertzhuber, S., Haller, T., Mair, N. and Dietl, P. (2001) 'Secretion in alveolar type II cells at the interface of constitutive and regulated exocytosis', *Am J Respir Cell Mol Biol*, 25(3), pp. 306–315. doi: 10.1165/ajrcmb.25.3.4493.

Fullagar, W. K., Aberdeen, K. A., Bucknall, D. G., Kroon, P. A. and Gentle, I. R. (2003) 'Conformational changes in SP-B as a function of surface pressure', *Biophys J*. 2003/09/26, 85(4), pp. 2624–2632. doi: S0006-3495(03)74685-2 [pii]10.1016/S0006-3495(03)74685-2.

Garavito, R. M. and Ferguson-Miller, S. (2001) 'Detergents as Tools in Membrane Biochemistry', *Journal of Biological Chemistry*, pp. 32403–32406. doi: 10.1074/jbc.R100031200.

Gerson, K. D., Foster, C. D., Zhang, P., Zhang, Z., Rosenblatt, M. M. and Guttentag, S. H. (2008) 'Pepsinogen C proteolytic processing of surfactant protein B', *J Biol Chem*, 283(16), pp. 10330–10338. doi: 10.1074/jbc.M707516200.

Glasser, S. W., Detmer, E. A., Ikegami, M., Na, C. L., Stahlman, M. T. and Whitsett, J. A. (2003) 'Pneumonitis and emphysema in sp-C gene targeted mice', *J Biol Chem*. 2003/01/10, 278(16), pp. 14291–14298. doi: 10.1074/jbc.M210909200M210909200 [pii].

Goerke, J. (1998) 'Pulmonary surfactant: functions and molecular composition', *Biochim Biophys Acta*. 1998/11/14, 1408(2–3), pp. 79–89. doi: S0925-4439(98)00060-X [pii].

Gohon, Y., Vindigni, J.-D., Pallier, A., Wien, F., Celia, H., Giuliani, A., Tribet, C., Chardot, T. and Briozzo, P. (2011) 'High water solubility and fold in amphipols of proteins with large hydrophobic regions: oleosins and caleosin from seed lipid bodies.', *Biochimica et biophysica acta*. Netherlands, 1808(3), pp. 706–716. doi: 10.1016/j.bbamem.2010.12.002.

Goñi, F. M. (2014) 'The basic structure and dynamics of cell membranes: An update of the Singer–Nicolson model', *Biochimica et Biophysica Acta (BBA) - Biomembranes*, 1838(6), pp. 1467–1476. doi: 10.1016/j.bbamem.2014.01.006.

Gunther, A., Schmidt, R., Feustel, A., Meier, U., Pucker, C., Ermert, M. and Seeger, W. (1999) 'Surfactant subtype conversion is related to loss of surfactant apoprotein B and surface activity in large surfactant aggregates. Experimental and clinical studies', *Am J Respir Crit Care Med*, 159(1), pp. 244–251. doi: 10.1164/ajrccm.159.1.9612005.

Gupta, N., Manevich, Y., Kazi, A. S., Tao, J.-Q., Fisher, A. B. and Bates, S. R. (2006) 'Identification and characterization of p63 (CKAP4/ERGIC-63/CLIMP-63), a surfactant protein A binding protein, on type II pneumocytes.', *American journal of physiology. Lung cellular and molecular physiology*. United States, 291(3), pp. L436-46. doi: 10.1152/ajplung.00415.2005.

Guttentag, S., Robinson, L., Zhang, P., Brasch, F., Buhling, F. and Beers, M. (2003) 'Cysteine protease activity is required for surfactant protein B processing and lamellar body genesis', *Am J*

Respir Cell Mol Biol, 28(1), pp. 69–79. doi: 10.1165/rcmb.2002-0111OC.

Haller, T., Auktor, K., Frick, M., Mair, N. and Dietl, P. (1999) 'Threshold calcium levels for lamellar body exocytosis in type II pneumocytes', *Am J Physiol*, 277(5 Pt 1), pp. L893-900.

Haller, T., Dietl, P., Pfaller, K., Frick, M., Mair, N., Paulmichl, M., Hess, M. W., Furst, J. and Maly, K. (2001) 'Fusion pore expansion is a slow, discontinuous, and Ca2+-dependent process regulating secretion from alveolar type II cells', *J Cell Biol*, 155(2), pp. 279–289. doi: 10.1083/jcb.200102106.

Haller, T., Dietl, P., Stockner, H., Frick, M., Mair, N., Tinhofer, I., Ritsch, A., Enhorning, G. and Putz, G. (2004) 'Tracing surfactant transformation from cellular release to insertion into an air-liquid interface', *Am J Physiol Lung Cell Mol Physiol*, 286(5), pp. L1009-15. doi: 10.1152/ajplung.00342.2003.

Haller, T., Ortmayr, J., Friedrich, F., Volkl, H. and Dietl, P. (1998) 'Dynamics of surfactant release in alveolar type II cells', *Proc Natl Acad Sci U S A*, 95(4), pp. 1579–1584.

Hallman, M., Sarnesto, A. and Bry, K. (1994) 'Interaction of transferrin saturated with iron with lung surfactant in respiratory failure.', *Journal of applied physiology (Bethesda, Md. : 1985)*. United States, 77(2), pp. 757–766. doi: 10.1152/jappl.1994.77.2.757.

Haugland, R. P. (2002) *Handbook of fluorescent probes and research products*. Molecular Probes.

Hawgood, S., Benson, B. J., Schilling, J., Damm, D., Clements, J. A. and White, R. T. (1987) 'Nucleotide and amino acid sequences of pulmonary surfactant protein SP 18 and evidence for cooperation between SP 18 and SP 28-36 in surfactant lipid adsorption.', *Proceedings of the National Academy of Sciences of the United States of America*. United States, 84(1), pp. 66–70.

Hawgood, S., Derrick, M. and Poulain, F. (1998) 'Structure and properties of surfactant protein B', *Biochim Biophys Acta*. 1998/11/14, 1408(2–3), pp. 150–160. doi: S0925-4439(98)00064-7 [pii].

Hawgood, S. and Poulain, F. R. (2001) 'The pulmonary collectins and surfactant metabolism.', *Annual review of physiology*. United States, 63, pp. 495–519. doi: 10.1146/annurev.physiol.63.1.495.

Hills, B. A. (1999) 'An alternative view of the role(s) of surfactant and the alveolar model.', *Journal of applied physiology (Bethesda, Md. : 1985)*. United States, 87(5), pp. 1567–1583. doi: 10.1152/jappl.1999.87.5.1567.

Hobi, N., Giolai, M., Olmeda, B., Miklavc, P., Felder, E., Walther, P., Dietl, P., Frick, M., Perez-Gil, J. and Haller, T. (2016) 'A small key unlocks a heavy door: The essential function of the small hydrophobic proteins SP-B and SP-C to trigger adsorption of pulmonary surfactant lamellar bodies', *Biochim Biophys Acta*, 1863(8), pp. 2124–2134. doi: 10.1016/j.bbamcr.2016.04.028.

Hofman, E. G., Bader, A. N., Voortman, J., van den Heuvel, D. J., Sigismund, S., Verkleij, A. J., Gerritsen, H. C. and van Bergen en Henegouwen, P. M. P. (2010) 'Ligand-induced EGF receptor oligomerization is kinase-dependent and enhances internalization.', *The Journal of biological chemistry*. United States, 285(50), pp. 39481–39489. doi: 10.1074/jbc.M110.164731.

Ikegami, M., Grant, S., Korfhagen, T., Scheule, R. K. and Whitsett, J. A. (2009) 'Surfactant protein-D regulates the postnatal maturation of pulmonary surfactant lipid pool sizes', *J Appl Physiol (1985)*, 106(5), pp. 1545–1552. doi: 10.1152/japplphysiol.91567.2008.

Ikegami, M., Korfhagen, T. R., Whitsett, J. A., Bruno, M. D., Wert, S. E., Wada, K. and Jobe, A. H. (1998) 'Characteristics of surfactant from SP-A-deficient mice', *Am J Physiol*, 275(2 Pt 1), pp. L247-54.

Ikegami, M., Takabatake, N. and Weaver, T. E. (2002) 'Intersubunit disulfide bridge is not required for the protective role of SP-B against lung inflammation', *J Appl Physiol*. 2002/07/23, 93(2), pp. 505–511. doi: 10.1152/japplphysiol.01137.2001.

Johansson, J. and Curstedt, T. (1997) 'Molecular structures and interactions of pulmonary surfactant components', *Eur J Biochem*. 1997/03/15, 244(3), pp. 675–693.

Johansson, J., Curstedt, T. and Jornvall, H. (1991) 'Surfactant protein B: disulfide bridges, structural properties, and kringle similarities', *Biochemistry*. 1991/07/16, 30(28), pp. 6917–6921.

Johansson, J., Szyperski, T., Curstedt, T. and Wuthrich, K. (1994) 'The NMR structure of the pulmonary surfactant-associated polypeptide SP-C in an apolar solvent contains a valyl-rich alpha-helix', *Biochemistry*. 1994/05/17, 33(19), pp. 6015–6023.

Johansson, L. B. A. and Niemi, A. (1987) 'Electronic energy transfer in anisotropic systems. 1. Octadecylrhodamine B in vesicles', *The Journal of Physical Chemistry*. American Chemical Society, 91(11), pp. 3020–3023. doi: 10.1021/j100295a075.

Johnson, I. D., Kang, H. C. and Haugland, R. P. (1991) 'Fluorescent membrane probes incorporating dipyrrometheneboron difluoride fluorophores', *Analytical Biochemistry*, 198(2), pp. 228–237. doi: 10.1016/0003-2697(91)90418-S.

Jouhet, J. (2013) *Importance of the hexagonal lipid phase in biological membrane organization, Frontiers in plant science*. doi: 10.3389/fpls.2013.00494.

Kairys, V., Gilson, M. K. and Luy, B. (2004) 'Structural model for an AxxxG-mediated dimer of surfactant-associated protein C.', *European journal of biochemistry*. England, 271(11), pp. 2086–2092. doi: 10.1111/j.1432-1033.2004.04107.x.

Kaiser, R. D. and London, E. (1998) 'Determination of the depth of BODIPY probes in model membranes by parallax analysis of fluorescence quenching.', *Biochimica et biophysica acta*. Netherlands, 1375(1–2), pp. 13–22.

Karolin, J., Johansson, L. B. A., Strandberg, L. and Ny, T. (1994) 'Fluorescence and Absorption Spectroscopic Properties of Dipyrrometheneboron Difluoride (BODIPY) Derivatives in Liquids, Lipid Membranes, and Proteins', *Journal of the American Chemical Society*, 116(17), pp. 7801–7806. doi: 10.1021/ja00096a042.

Kastner, B., Fischer, N., Golas, M. M., Sander, B., Dube, P., Boehringer, D., Hartmuth, K., Deckert, J., Hauer, F., Wolf, E., Uchtenhagen, H., Urlaub, H., Herzog, F., Peters, J. M., Poerschke, D., Luhrmann, R. and Stark, H. (2008) 'GraFix: sample preparation for single-particle electron cryomicroscopy.', *Nature methods*. United States, 5(1), pp. 53–55. doi: 10.1038/nmeth1139.

Keating, E., Zuo, Y. Y., Tadayyon, S. M., Petersen, N. O., Possmayer, F. and Veldhuizen, R. A. W. (2012) 'A modified squeeze-out mechanism for generating high surface pressures with pulmonary surfactant.', *Biochimica et biophysica acta*. Netherlands, 1818(5), pp. 1225–1234. doi: 10.1016/j.bbamem.2011.12.007.

Kelly, K. and Jacobs, R. (2011) *Phospholipid Biosynthesis, AOCS Lipid Library*. doi: 10.21748/lipidlibrary.39191.

Kenichi, N. and Yoshinori, F. (1994) 'PHOTOLUMINESCENT PROPERTIES OF OCTADECYLRHODAMINE B IN WATER, IN ALCOHOLS AND IN MIXED WATER-ALCOHOL SOLUTIONS', *Photochemistry and Photobiology*. Wiley/Blackwell (10.1111), 60(6), pp. 563–566. doi: 10.1111/j.1751-1097.1994.tb05148.x.

Kishore, U., Greenhough, T. J., Waters, P., Shrive, A. K., Ghai, R., Kamran, M. F., Bernal, A. L., Reid, K. B. M., Madan, T. and Chakraborty, T. (2006) 'Surfactant proteins SP-A and SP-D: structure, function and receptors.', *Molecular immunology*. England, 43(9), pp. 1293–1315. doi: 10.1016/j.molimm.2005.08.004.

Kittelberger, N., Breunig, M., Martin, R., Knolker, H. J. and Miklavc, P. (2016) 'The role of myosin 1c and myosin 1b in surfactant exocytosis', *J Cell Sci*, 129(8), pp. 1685–1696. doi: 10.1242/jcs.181313.

Kleinschmidt, J. and Popot, J.-L. (2014) *Folding and stability of integral membrane proteins in amphipols, Archives of Biochemistry and Biophysics*. doi: 10.1016/j.abb.2014.10.01.

Knowles, T. J., Finka, R., Smith, C., Lin, Y.-P., Dafforn, T. and Overduin, M. (2009) 'Membrane proteins solubilized intact in lipid containing nanoparticles bounded by styrene maleic acid copolymer.', *Journal of the American Chemical Society*. United States, 131(22), pp. 7484–7485. doi: 10.1021/ja810046q.

Koenig, B. W. and Gawrisch, K. (2005) 'Specific volumes of unsaturated phosphatidylcholines in the liquid crystalline lamellar phase.', *Biochimica et biophysica acta*. Netherlands, 1715(1), pp. 65–70. doi: 10.1016/j.bbamem.2005.07.006.

Korczynski, J. and Włodarczyk, J. (2009) *[Fluorescence lifetime imaging microscopy (FLIM) in biological and medical research], Postepy biochemii*.

Korfhagen, T. R., Sheftelyevich, V., Burhans, M. S., Bruno, M. D., Ross, G. F., Wert, S. E., Stahlman, M. T., Jobe, A. H., Ikegami, M., Whitsett, J. A. and Fisher, J. H. (1998) 'Surfactant protein-D regulates surfactant phospholipid homeostasis in vivo', *J Biol Chem*, 273(43), pp. 28438–28443.

Kramer, A., Wintergalen, A., Sieber, M., Galla, H. J., Amrein, M. and Guckenberger, R. (2000) 'Distribution of the surfactant-associated protein C within a lung surfactant model film investigated by near-field optical microscopy.', *Biophysical journal*. United States, 78(1), pp. 458–465. doi: 10.1016/S0006-3495(00)76608-2.

Krol, S., Ross, M., Sieber, M., Kunneke, S., Galla, H. J. and Janshoff, A. (2000) 'Formation of three-dimensional protein-lipid aggregates in monolayer films induced by surfactant protein B', *Biophys J*. 2000/08/02, 79(2), pp. 904–918. doi: S0006-3495(00)76346-6 [pii]10.1016/S0006-3495(00)76346-6.

Kuroki, Y. and Akino, T. (1991) 'Pulmonary surfactant protein A (SP-A) specifically binds dipalmitoylphosphatidylcholine.', *The Journal of biological chemistry*. United States, 266(5), pp. 3068–3073.

Kuroki, Y., Gasa, S., Ogasawara, Y., Shiratori, M., Makita, A. and Akino, T. (1992) 'Binding specificity of lung surfactant protein SP-D for glucosylceramide.', *Biochemical and biophysical research communications*. United States, 187(2), pp. 963–969.

De La Serna, J. B., Perez-Gil, J., Simonsen, A. C. and Bagatolli, L. A. (2004) 'Cholesterol rules: Direct observation of the coexistence of two fluid phases in native pulmonary surfactant membranes at physiological temperatures', *Journal of Biological Chemistry*, 279(39), pp. 40715–40722. doi: 10.1074/jbc.M404648200.

Lakowicz, J. R. (2006) *Principles of fluorescence spectroscopy, Principles of Fluorescence Spectroscopy*. doi: 10.1007/978-0-387-46312-4.

Liang, B. and Tamm, L. K. (2018) 'Solution NMR of SNAREs, complexin and α-synuclein in association with membrane-mimetics', *Progress in Nuclear Magnetic Resonance Spectroscopy*, 105, pp. 41–53. doi: https://doi.org/10.1016/j.pnmrs.2018.02.001.

Lillo, M. P., Cañadas, O., Dale, R. E. and Acuña, A. U. (2002) 'Location and Properties of the Taxol Binding Center in Microtubules: A Picosecond Laser Study with Fluorescent Taxoids', *Biochemistry*. American Chemical Society, 41(41), pp. 12436–12449. doi: 10.1021/bi0261793.

Lin, P. M. and Wright, J. R. (2006) 'Surfactant protein A binds to IgG and enhances phagocytosis of IgG-opsonized erythrocytes.', *American journal of physiology. Lung cellular and molecular*

physiology. United States, 291(6), pp. L1199-206. doi: 10.1152/ajplung.00188.2006.

Lin, S., Ikegami, M., Moon, C., Naren, A. P. and Shannon, J. M. (2015) 'Lysophosphatidylcholine Acyltransferase 1 (LPCAT1) Specifically Interacts with Phospholipid Transfer Protein StarD10 to Facilitate Surfactant Phospholipid Trafficking in Alveolar Type II Cells', *J Biol Chem*, 290(30), pp. 18559–18574. doi: 10.1074/jbc.M115.666701.

Lipari, G. and Szabo, A. (1980) 'Effect of librational motion on fluorescence depolarization and nuclear magnetic resonance relaxation in macromolecules and membranes.', *Biophysical Journal*, 30(3), pp. 489–506.

Long, A. R., O'Brien, C. C., Malhotra, K., Schwall, C. T., Albert, A. D., Watts, A. and Alder, N. N. (2013) 'A detergent-free strategy for the reconstitution of active enzyme complexes from native biological membranes into nanoscale discs.', *BMC biotechnology*. England, 13, p. 41. doi: 10.1186/1472-6750-13-41.

Lopez-Rodriguez, E., Ospina, O. L., Echaide, M., Taeusch, H. W. and Perez-Gil, J. (2012) 'Exposure to polymers reverses inhibition of pulmonary surfactant by serum, meconium, or cholesterol in the captive bubble surfactometer.', *Biophysical journal*. United States, 103(7), pp. 1451–1459. doi: 10.1016/j.bpj.2012.08.024.

Lopez-Rodriguez, E., Pascual, A., Arroyo, R., Floros, J. and Perez-Gil, J. (2016) 'Human Pulmonary Surfactant Protein SP-A1 Provides Maximal Efficiency of Lung Interfacial Films', *Biophys J*, 111(3), pp. 524–536. doi: 10.1016/j.bpj.2016.06.025.

Lopez-Rodriguez, E. and Perez-Gil, J. (2014) 'Structure-function relationships in pulmonary surfactant membranes: from biophysics to therapy', *Biochim Biophys Acta*, 1838(6), pp. 1568–1585. doi: 10.1016/j.bbamem.2014.01.028.

Loura, L. M., Fedorov, A. and Prieto, M. (1996) 'Resonance energy transfer in a model system of membranes: application to gel and liquid crystalline phases', *Biophysical journal*. Elsevier, 71(4), pp. 1823–1836.

Loura, L. M. S., de Almeida, R. F. M. and Prieto, M. (2001) 'Detection and Characterization of Membrane Microheterogeneity by Resonance Energy Transfer', *Journal of Fluorescence*, 11(3), pp. 197–209. doi: 10.1023/A:1012249117580.

Loura, L. M. S., Coutinho, A., Silva, A., Fedorov, A. and Prieto, M. (2006) 'Structural effects of a basic peptide on the organization of dipalmitoylphosphatidylcholine/dipalmitoylphosphatidylserine membranes: a fluorescent resonance energy transfer study.', *The journal of physical chemistry. B*. United States, 110(15), pp. 8130–8141. doi: 10.1021/jp055855i.

Lu, D., Soleymani, S., Madakshire, R. and Insel, P. a. (2012) 'ATP released from cardiac fibroblasts via connexin hemichannels activates profibrotic P2Y2 receptors', *The FASEB Journal*, 26(6), pp. 2580–2591. doi: 10.1096/fj.12-204677.

Luy, B., Diener, A., Hummel, R.-P., Sturm, E., Ulrich, W.-R. and Griesinger, C. (2004) 'Structure and potential C-terminal dimerization of a recombinant mutant of surfactant-associated protein C in chloroform/methanol.', *European journal of biochemistry*. England, 271(11), pp. 2076–2085. doi: 10.1111/j.1432-1033.2004.04106.x.

le Maire, M., Champeil, P. and Møller, J. V (2000) 'Interaction of membrane proteins and lipids with solubilizing detergents', *Biochimica et Biophysica Acta (BBA) - Biomembranes*, 1508(1), pp. 86–111. doi: https://doi.org/10.1016/S0304-4157(00)00010-1.

Malacrida, L., Astrada, S., Briva, A., Bollati-Fogolin, M., Gratton, E. and Bagatolli, L. A. (2016) 'Spectral phasor analysis of LAURDAN fluorescence in live A549 lung cells to study the hydration and time evolution of intracellular lamellar body-like structures', *Biochim Biophys Acta*, 1858(11), pp. 2625–2635. doi: 10.1016/j.bbamem.2016.07.017.

Mann, T. L. and Krull, U. J. (2003) ‘Fluorescence polarization spectroscopy in protein analysis’, *Analyst*. Royal Society of Chemistry, 128(4), pp. 313–317.

Marquardt, D. W. (1963) ‘An Algorithm for Least-Squares Estimation of Nonlinear Parameters’, *Journal of the Society for Industrial and Applied Mathematics*, 11(2), pp. 431–441. doi: 10.1137/0111030.

Marsh, D. (2013) *CRC Handbook of lipid bilayers*.

Marty, M. T., Wilcox, K. C., Klein, W. L. and Sligar, S. G. (2013) ‘Nanodisc-solubilized membrane protein library reflects the membrane proteome.’, *Analytical and bioanalytical chemistry*. Germany, 405(12), pp. 4009–4016. doi: 10.1007/s00216-013-6790-8.

Mason, R. (2006) *Biology of alveolar type II cells*, *Respirology (Carlton, Vic.)*. doi: 10.1111/j.1440-1843.2006.00800.x.

Massaro, D., Clerch, L. and Massaro, G. D. (1981) ‘Surfactant aggregation in rat lungs: influence of temperature and ventilation.’, *Journal of applied physiology: respiratory, environmental and exercise physiology*. United States, 51(3), pp. 646–653. doi: 10.1152/jappl.1981.51.3.646.

McCormack, F. X. and Whitsett, J. A. (2002) ‘The pulmonary collectins, SP-A and SP-D, orchestrate innate immunity in the lung’, *J Clin Invest*, 109(6), pp. 707–712. doi: 10.1172/JCI15293.

Van Der Meer, B. W., Coker III, G. and Chen, S. Y. (1994) ‘Resonance Energy Transfer: Theory and Data’, *VCH Publishers, NewYork*.

Melo, A. M., Fedorov, A., Prieto, M. and Coutinho, A. (2014) ‘Exploring homo-FRET to quantify the oligomer stoichiometry of membrane-bound proteins involved in a cooperative partition equilibrium.’, *Physical chemistry chemical physics : PCCP*. England, 16(34), pp. 18105–18117. doi: 10.1039/c4cp00060a.

Melton, K. R., Nesslein, L. L., Ikegami, M., Tichelaar, J. W., Clark, J. C., Whitsett, J. A. and Weaver, T. E. (2003) ‘SP-B deficiency causes respiratory failure in adult mice’, *Am J Physiol Lung Cell Mol Physiol*. 2003/03/18, 285(3), pp. L543-9. doi: 10.1152/ajplung.00011.200300011.2003 [pii].

Miklavc, P., Ehinger, K., Sultan, A., Felder, T., Paul, P., Gottschalk, K. E. and Frick, M. (2015) ‘Actin depolymerisation and crosslinking join forces with myosin II to contract actin coats on fused secretory vesicles’, *J Cell Sci*, 128(6), pp. 1193–1203. doi: 10.1242/jcs.165571.

Miklavc, P., Frick, M., Wittekindt, O. H., Haller, T. and Dietl, P. (2010) ‘Fusion-activated Ca(2+) entry: an “active zone” of elevated Ca(2+) during the postfusion stage of lamellar body exocytosis in rat type II pneumocytes’, *PLoS One*, 5(6), p. e10982. doi: 10.1371/journal.pone.0010982.

Miklavc, P., Hecht, E., Hobi, N., Wittekindt, O. H., Dietl, P., Kranz, C. and Frick, M. (2012) ‘Actin coating and compression of fused secretory vesicles are essential for surfactant secretion--a role for Rho, formins and myosin II’, *J Cell Sci*, 125(Pt 11), pp. 2765–2774. doi: 10.1242/jcs.105262.

Miklavc, P., Mair, N., Wittekindt, O. H., Haller, T., Dietl, P., Felder, E., Timmler, M. and Frick, M. (2011) ‘Fusion-activated Ca2+ entry via vesicular P2X4 receptors promotes fusion pore opening and exocytotic content release in pneumocytes’, *Proc Natl Acad Sci U S A*, 108(35), pp. 14503–14508. doi: 10.1073/pnas.1101039108.

Miklavc, P., Thompson, K. E. and Frick, M. (2013) ‘A new role for P2X4 receptors as modulators of lung surfactant secretion.’, *Frontiers in cellular neuroscience*, 7(1662–5102 (Electronic)), p. 171. doi: 10.3389/fncel.2013.00171.

Miklavc, P., Wittekindt, O. H., Felder, E. and Dietl, P. (2009) ‘Ca2+-dependent actin coating of

lamellar bodies after exocytotic fusion: a prerequisite for content release or kiss-and-run', *Ann N Y Acad Sci*, 1152, pp. 43–52. doi: 10.1111/j.1749-6632.2008.03989.x.

Mingarro, I., Lukovic, D., Vilar, M. and Perez-Gil, J. (2008) 'Synthetic pulmonary surfactant preparations: new developments and future trends', *Curr Med Chem*. 2008/02/22, 15(4), pp. 393–403.

Morrow, M. R., Perez-Gil, J., Simatos, G., Boland, C., Stewart, J., Absolom, D., Sarin, V. and Keough, K. M. (1993) 'Pulmonary surfactant-associated protein SP-B has little effect on acyl chains in dipalmitoylphosphatidylcholine dispersions', *Biochemistry*. 1993/04/27, 32(16), pp. 4397–4402.

Munford, R. S., Sheppard, P. O. and O'Hara, P. J. (1995) 'Saposin-like proteins (SAPLIP) carry out diverse functions on a common backbone structure.', *Journal of Lipid Research* , 36(8), pp. 1653–1663.

Nadesalingam, J., Reid, K. B. M. and Palaniyar, N. (2005) 'Collectin surfactant protein D binds antibodies and interlinks innate and adaptive immune systems.', *FEBS letters*. England, 579(20), pp. 4449–4453. doi: 10.1016/j.febslet.2005.07.012.

Nag, K., Pérez-Gil, J., Ruano, M. L., Casals, C. and Keough, K. M. W. (1996) 'Association of fluorescent labelled pulmonary surfactant protein A (SP-A) and B (SP-B) with dipalmitoylphosphatidylcholine (DPPC) monolayer films', *39th Annual Meeting of Canadian Federation of Biological Societies. London, Ontario*.

Nag, K., Taneva, S. G., Perez-Gil, J., Cruz, A. and Keough, K. M. (1997) 'Combinations of fluorescently labeled pulmonary surfactant proteins SP-B and SP-C in phospholipid films.', *Biophysical journal*. United States, 72(6), pp. 2638–2650. doi: 10.1016/S0006-3495(97)78907-0.

von Nahmen, A., Post, A., Galla, H.-J. and Sieber, M. (1997) 'The phase behavior of lipid monolayers containing pulmonary surfactant protein C studied by fluorescence light microscopy', *European Biophysics Journal*, 26(5), pp. 359–369. doi: 10.1007/s002490050090.

Neuland, K., Sharma, N. and Frick, M. (2014) 'Synaptotagmin-7 links fusion-activated Ca(2)(+) entry and fusion pore dilation', *J Cell Sci*, 127(Pt 24), pp. 5218–5227. doi: 10.1242/jcs.153742.

Nguyen, E. V, Gharib, S. A., Schnapp, L. M. and Goodlett, D. R. (2014) 'Shotgun MS proteomic analysis of bronchoalveolar lavage fluid in normal subjects', *Proteomics. Clinical applications*, 8(0), pp. 737–747. doi: 10.1002/prca.201300018.

Nicholas, T. E., Power, J. H. and Barr, H. A. (1982) 'The pulmonary consequences of a deep breath', *Respir Physiol*, 49(3), pp. 315–324.

Nogee, L. M. (2004) 'Alterations in SP-B and SP-C expression in neonatal lung disease.', *Annual review of physiology*. United States, 66, pp. 601–623. doi: 10.1146/annurev.physiol.66.032102.134711.

Nogee, L. M., de Mello, D. E., Dehner, L. P. and Colten, H. R. (1993) 'Brief report: deficiency of pulmonary surfactant protein B in congenital alveolar proteinosis', *N Engl J Med*. 1993/02/11, 328(6), pp. 406–410. doi: 10.1056/NEJM199302113280606.

Ochs, M., Johnen, G., Muller, K. M., Wahlers, T., Hawgood, S., Richter, J. and Brasch, F. (2002) 'Intracellular and intraalveolar localization of surfactant protein A (SP-A) in the parenchymal region of the human lung', *Am J Respir Cell Mol Biol*, 26(1), pp. 91–98. doi: 10.1165/ajrcmb.26.1.4570.

Ochs, M., Nyengaard, J. R., Jung, A., Knudsen, L., Voigt, M., Wahlers, T., Richter, J. and Gundersen, H. J. G. (2004) 'The Number of Alveoli in the Human Lung', *American Journal of Respiratory and Critical Care Medicine*. American Thoracic Society - AJRCCM, 169(1), pp.

120–124. doi: 10.1164/rccm.200308-1107OC.

Ogasawara, Y., Kuroki, Y. and Akino, T. (1992) 'Pulmonary surfactant protein D specifically binds to phosphatidylinositol.', *The Journal of biological chemistry*. United States, 267(29), pp. 21244–21249.

Okamoto, T., Miyazaki, Y., Shirahama, R., Tamaoka, M. and Inase, N. (2012) 'Proteome analysis of bronchoalveolar lavage fluid in chronic hypersensitivity pneumonitis.', *Allergology international : official journal of the Japanese Society of Allergology*. England, 61(1), pp. 83–92. doi: 10.2332/allergolint.11-OA-0315.

Olmeda, B. (2011) *Relaciones estructura-función del sistema surfactante pulmonar: detección de complejos multiproteicos nativos y participación del surfactante en la difusión interfacial del oxígeno*.

Olmeda, B., Garcia-Alvarez, B., Gomez, M. J., Martinez-Calle, M., Cruz, A. and Perez-Gil, J. (2015) 'A model for the structure and mechanism of action of pulmonary surfactant protein B', *FASEB J*, 29(10), pp. 4236–4247. doi: 10.1096/fj.15-273458.

Olmeda, B., García-Álvarez, B. and Pérez-Gil, J. (2013) 'Structure-function correlations of pulmonary surfactant protein SP-B and the saposin-like family of proteins', in *European Biophysics Journal*, pp. 209–222. doi: 10.1007/s00249-012-0858-9.

Olmeda, B., Martinez-Calle, M. and Perez-Gil, J. (2017) 'Pulmonary surfactant metabolism in the alveolar airspace: Biogenesis, extracellular conversions, recycling.', *Annals of anatomy = Anatomischer Anzeiger : official organ of the Anatomische Gesellschaft*. Germany, 209, pp. 78–92. doi: 10.1016/j.aanat.2016.09.008.

Olmeda, B., Villén, L., Cruz, A., Orellana, G. and Perez-Gil, J. (2010) 'Pulmonary surfactant layers accelerate O2 diffusion through the air-water interface', *Biochimica et Biophysica Acta - Biomembranes*, 1798(6), pp. 1281–1284. doi: 10.1016/j.bbamem.2010.03.008.

Oluwole, A. O., Danielczak, B., Meister, A., Babalola, J. O., Vargas, C. and Keller, S. (2017) 'Solubilization of Membrane Proteins into Functional Lipid-Bilayer Nanodiscs Using a Diisobutylene/Maleic Acid Copolymer.', *Angewandte Chemie (International ed. in English)*. Germany, 56(7), pp. 1919–1924. doi: 10.1002/anie.201610778.

Oosterlaken-Dijksterhuis, M. A., van Eijk, M., van Golde, L. M. and Haagsman, H. P. (1992) 'Lipid mixing is mediated by the hydrophobic surfactant protein SP-B but not by SP-C.', *Biochimica et biophysica acta*. Netherlands, 1110(1), pp. 45–50.

Oosterlaken-Dijksterhuis, M. A., Haagsman, H. P., van Golde, L. M. and Demel, R. A. (1991a) 'Characterization of lipid insertion into monomolecular layers mediated by lung surfactant proteins SP-B and SP-C.', *Biochemistry*. United States, 30(45), pp. 10965–10971.

Oosterlaken-Dijksterhuis, M. A., Haagsman, H. P., van Golde, L. M. and Demel, R. A. (1991b) 'Interaction of lipid vesicles with monomolecular layers containing lung surfactant proteins SP-B or SP-C.', *Biochemistry*. United States, 30(33), pp. 8276–8281.

Orwick, M. C., Judge, P. J., Procek, J., Lindholm, L., Graziadei, A., Engel, A., Grobner, G. and Watts, A. (2012) 'Detergent-free formation and physicochemical characterization of nanosized lipid-polymer complexes: Lipodisq.', *Angewandte Chemie (International ed. in English)*. Germany, 51(19), pp. 4653–4657. doi: 10.1002/anie.201201355.

Osanai, K., Mason, R. J. and Voelker, D. R. (1998) 'Trafficking of newly synthesized surfactant protein A in isolated rat alveolar type II cells', *Am J Respir Cell Mol Biol*, 19(6), pp. 929–935. doi: 10.1165/ajrcmb.19.6.3292.

Otto, H., Lamparter, T., Borucki, B., Hughes, J. and Heyn, M. P. (2003) 'Dimerization and Inter-Chromophore Distance of Cph1 Phytochrome from Synechocystis, as Monitored by Fluorescence

Homo and Hetero Energy Transfer', *Biochemistry*. American Chemical Society, 42(19), pp. 5885–5895. doi: 10.1021/bi026946y.

Palaniyar, N., Ikegami, M., Korfhagen, T., Whitsett, J. and McCormack, F. X. (2001) 'Domains of surfactant protein A that affect protein oligomerization, lipid structure and surface tension', *Comp Biochem Physiol A Mol Integr Physiol*, 129(1), pp. 109–127.

Palaniyar, N., Ridsdale, R. A., Hearn, S. A., Possmayer, F. and Harauz, G. (1999) 'Formation of membrane lattice structures and their specific interactions with surfactant protein A', *Am J Physiol*, 276(4 Pt 1), pp. L642-9.

Palaniyar, N., Ridsdale, R. A., Holterman, C. E., Inchley, K., Possmayer, F. and Harauz, G. (1998) 'Structural changes of surfactant protein A induced by cations reorient the protein on lipid bilayers.', *Journal of structural biology*. United States, 122(3), pp. 297–310. doi: 10.1006/jsbi.1998.4004.

Parra, E., Alcaraz, A., Cruz, A., Aguilella, V. M. and Perez-Gil, J. (2013) 'Hydrophobic pulmonary surfactant proteins SP-B and SP-C induce pore formation in planar lipid membranes: evidence for proteolipid pores', *Biophys J*, 104(1), pp. 146–155. doi: 10.1016/j.bpj.2012.11.014.

Parra, E., Moleiro, L. H., Lopez-Montero, I., Cruz, A., Monroy, F. and Perez-Gil, J. (2011) 'A combined action of pulmonary surfactant proteins SP-B and SP-C modulates permeability and dynamics of phospholipid membranes', *Biochem J*. 2011/06/18, 438(3), pp. 555–564. doi: BJ20110681 [pii]10.1042/BJ20110681.

Parra, E. and Perez-Gil, J. (2015) 'Composition, structure and mechanical properties define performance of pulmonary surfactant membranes and films', *Chem Phys Lipids*, 185, pp. 153–175. doi: 10.1016/j.chemphyslip.2014.09.002.

Patel, A. S., Reigada, D., Mitchell, C. H., Bates, S. R., Margulies, S. S. and Koval, M. (2005) 'Paracrine stimulation of surfactant secretion by extracellular ATP in response to mechanical deformation', *Am J Physiol Lung Cell Mol Physiol*, 289(3), pp. L489-96. doi: 10.1152/ajplung.00074.2005.

Perez-Gil, J. (2008) 'Structure of pulmonary surfactant membranes and films: the role of proteins and lipid-protein interactions', *Biochim Biophys Acta*, 1778(7–8), pp. 1676–1695. doi: 10.1016/j.bbamem.2008.05.003.

Perez-Gil, J., Casals, C. and Marsh, D. (1995) 'Interactions of hydrophobic lung surfactant proteins SP-B and SP-C with dipalmitoylphosphatidylcholine and dipalmitoylphosphatidylglycerol bilayers studied by electron spin resonance spectroscopy', *Biochemistry*, 34(12), pp. 3964–3971.

Perez-Gil, J., Cruz, A. and Casals, C. (1993) 'Solubility of hydrophobic surfactant proteins in organic solvent/water mixtures. Structural studies on SP-B and SP-C in aqueous organic solvents and lipids', *Biochim Biophys Acta*. 1993/07/01, 1168(3), pp. 261–270.

Pérez-Gil, J., Nag, K., Taneva, S. and Keough, K. M. (1992) 'Pulmonary surfactant protein SP-C causes packing rearrangements of dipalmitoylphosphatidylcholine in spread monolayers.', *Biophysical Journal*, 63(1), pp. 197–204.

Perez-Gil, J. and Weaver, T. E. (2010) 'Pulmonary surfactant pathophysiology: current models and open questions', *Physiology (Bethesda)*, 25(3), pp. 132–141. doi: 10.1152/physiol.00006.2010.

Perrin, F. (1926) 'Polarisation of Fluorescence and Mean Life of Excited Molecules', *J. Phys. Radium*, 7(12), pp. 390–401.

Plasencia, I., Baumgart, F., Andreu, D., Marsh, D. and Perez-Gil, J. (2008) 'Effect of acylation on the interaction of the N-Terminal segment of pulmonary surfactant protein SP-C with

phospholipid membranes.', *Biochimica et biophysica acta*. Netherlands, 1778(5), pp. 1274–1282. doi: 10.1016/j.bbamem.2008.02.004.

Plasencia, I., Keough, K. M. W. and Perez-Gil, J. (2005) 'Interaction of the N-terminal segment of pulmonary surfactant protein SP-C with interfacial phospholipid films.', *Biochimica et biophysica acta*. Netherlands, 1713(2), pp. 118–128. doi: 10.1016/j.bbamem.2005.06.002.

Plasencia, I., Rivas, L., Keough, K. M. W., Marsh, D. and Pérez-Gil, J. (2004) 'The N-terminal segment of pulmonary surfactant lipopeptide SP-C has intrinsic propensity to interact with and perturb phospholipid bilayers.', *The Biochemical journal*, 377(Pt 1), pp. 183–193. doi: 10.1042/BJ20030815.

Popot, J.-L. (2010) 'Amphipols, nanodiscs, and fluorinated surfactants: three nonconventional approaches to studying membrane proteins in aqueous solutions.', *Annual review of biochemistry*. United States, 79, pp. 737–775. doi: 10.1146/annurev.biochem.052208.114057.

Popot, J.-L., Althoff, T., Bagnard, D., Baneres, J.-L., Bazzacco, P., Billon-Denis, E., Catoire, L. J., Champeil, P., Charvolin, D., Cocco, M. J., Cremel, G., Dahmane, T., de la Maza, L. M., Ebel, C., Gabel, F., Giusti, F., Gohon, Y., Goormaghtigh, E., Guittet, E., Kleinschmidt, J. H., Kuhlbrandt, W., Le Bon, C., Martinez, K. L., Picard, M., Pucci, B., Sachs, J. N., Tribet, C., van Heijenoort, C., Wien, F., Zito, F. and Zoonens, M. (2011) 'Amphipols from A to Z.', *Annual review of biophysics*. United States, 40, pp. 379–408. doi: 10.1146/annurev-biophys-042910-155219.

Possmayer, F., Nag, K., Rodriguez, K., Qanbar, R. and Schurch, S. (2001) 'Surface activity in vitro: role of surfactant proteins', *Comp Biochem Physiol A Mol Integr Physiol*, 129(1), pp. 209–220.

Postis, V., Rawson, S., Mitchell, J. K., Lee, S. C., Parslow, R. A., Dafforn, T. R., Baldwin, S. A. and Muench, S. P. (2015) 'The use of SMALPs as a novel membrane protein scaffold for structure study by negative stain electron microscopy', *Biochimica et Biophysica Acta (BBA) - Biomembranes*, 1848(2), pp. 496–501. doi: https://doi.org/10.1016/j.bbamem.2014.10.018.

Poulain, F. R., Allen, L., Williams, M. C., Hamilton, R. L. and Hawgood, S. (1992) 'Effects of surfactant apolipoproteins on liposome structure: implications for tubular myelin formation.', *The American journal of physiology*. United States, 262(6 Pt 1), pp. L730-9. doi: 10.1152/ajplung.1992.262.6.L730.

Poulain, F. R., Nir, S. and Hawgood, S. (1996) 'Kinetics of phospholipid membrane fusion induced by surfactant apoproteins A and B.', *Biochimica et biophysica acta*. Netherlands, 1278(2), pp. 169–175.

Ravasio, A., Hobi, N., Bertocchi, C., Jesacher, A., Dietl, P. and Haller, T. (2011) 'Interfacial sensing by alveolar type II cells: a new concept in lung physiology?', *Am J Physiol Cell Physiol*, 300(6), pp. C1456-65. doi: 10.1152/ajpcell.00427.2010.

Ravasio, A., Olmeda, B., Bertocchi, C., Haller, T. and Perez-Gil, J. (2010) 'Lamellar bodies form solid three-dimensional films at the respiratory air-liquid interface', *J Biol Chem*, 285(36), pp. 28174–28182. doi: 10.1074/jbc.M110.106518.

Rice, W. R., Ross, G. F., Singleton, F. M., Dingle, S. and Whitsett, J. A. (1987) 'Surfactant-associated protein inhibits phospholipid secretion from type II cells', *J Appl Physiol (1985)*, 63(2), pp. 692–698.

Ritchie, T. K., Grinkova, Y. V, Bayburt, T. H., Denisov, I. G., Zolnerciks, J. K., Atkins, W. M. and Sligar, S. G. (2009) 'Chapter 11 - Reconstitution of membrane proteins in phospholipid bilayer nanodiscs.', *Methods in enzymology*. United States, 464, pp. 211–231. doi: 10.1016/S0076-6879(09)64011-8.

Robertson, B., Kobayashi, T., Ganzuka, M., Grossmann, G., Li, W. Z. and Suzuki, Y. (1991)

‘Experimental neonatal respiratory failure induced by a monoclonal antibody to the hydrophobic surfactant-associated protein SP-B.’, *Pediatric research*. United States, 30(3), pp. 239–243. doi: 10.1203/00006450-199109000-00007.

Rodriguez-Capote, K., Nag, K., Schurch, S. and Possmayer, F. (2001) ‘Surfactant protein interactions with neutral and acidic phospholipid films’, *Am J Physiol Lung Cell Mol Physiol*. 2001/06/19, 281(1), pp. L231-42.

Roldán López, N., García Álvarez, B., Pérez-Gil, J. and I., U. C. de M. F. de C. B. D. de B. y B. M. (2017) *Relaciones estructura-función de la proteína SP-C del surfactante pulmonar efectos sobre la estructura de membranas y papel del colesterol = Structure-function relationships of lung surfactant protein SP-C : effects on membrane structure and role of chole*.

Roldán, N., Aranda, E., Pérez Gil, J. and García-Álvarez, B. (2014) ‘Functional and structural characterization of pulmonary surfactant protein SP-C in nanodiscs: a nanotechnological approach’, *XIV Congress of the Spanish Biophysical Society. Alcalá de Henares, Spain*.

Roldan, N., Cruz, A., Sanz, A., Bruix, M., Pérez-Gil, J. and Garcia-Alvarez, B. (2017) ‘Delivery of Lung Surfactant SP-C Based Nanostructures to Respiratory Air-Liquid Interfacial Films’, *Biophysical Journal*. Elsevier, 112(3), p. 389a–390a. doi: 10.1016/j.bpj.2016.11.2116.

Roldan, N., Nyholm, T. K. M., Slotte, J. P., P??rez-Gil, J. and Garc??a-??lvarez, B. (2016) ‘Effect of Lung Surfactant Protein SP-C and SP-C-Promoted Membrane Fragmentation on Cholesterol Dynamics’, *Biophysical Journal*, 111(8), pp. 1703–1713. doi: 10.1016/j.bpj.2016.09.016.

Roldan, N., Pérez-Gil, J., Morrow, M. R. and García-Álvarez, B. (2017) ‘Divide & Conquer: Surfactant Protein SP-C and Cholesterol Modulate Phase Segregation in Lung Surfactant’, *Biophysical Journal*, 113(4), pp. 847–859. doi: https://doi.org/10.1016/j.bpj.2017.06.059.

Rooney, S. A. (2001) ‘Regulation of surfactant secretion’, *Comp Biochem Physiol A Mol Integr Physiol*, 129(1), pp. 233–243.

Rouser, G., Siakotos, A. N. and Fleischer, S. (1966) ‘Quantitative analysis of phospholipids by thin-layer chromatography and phosphorus analysis of spots.’, *Lipids*. United States, 1(1), pp. 85–86. doi: 10.1007/BF02668129.

Roy, J., Pondenis, H., Fan, T. M. and Das, A. (2015) ‘Direct Capture of Functional Proteins from Mammalian Plasma Membranes into Nanodiscs.’, *Biochemistry*. United States, 54(41), pp. 6299–6302. doi: 10.1021/acs.biochem.5b00954.

Runnels, L. W. and Scarlata, S. F. (1995) ‘Theory and application of fluorescence homotransfer to melittin oligomerization’, *Biophysical Journal*, 69(4), pp. 1569–1583. doi: 10.1016/S0006-3495(95)80030-5.

Ryan, M. A., Akinbi, H. T., Serrano, A. G., Perez-Gil, J., Wu, H., McCormack, F. X. and Weaver, T. E. (2006) ‘Antimicrobial activity of native and synthetic surfactant protein B peptides.’, *Journal of immunology (Baltimore, Md. : 1950)*. United States, 176(1), pp. 416–425.

Ryan, M. A., Qi, X., Serrano, A. G., Ikegami, M., Perez-Gil, J., Johansson, J. and Weaver, T. E. (2005) ‘Mapping and analysis of the lytic and fusogenic domains of surfactant protein B’, *Biochemistry*. 2005/01/19, 44(3), pp. 861–872. doi: 10.1021/bi0485575.

Sáenz, A., Cañadas, O., Bagatolli, L. A., Sánchez-Barbero, F., Johnson, M. E. and Casals, C. (2007) ‘Effect of Surfactant Protein A on the Physical Properties and Surface Activity of KL4-Surfactant’, *Biophysical Journal*, 92(2), pp. 482–492. doi: https://doi.org/10.1529/biophysj.106.090217.

Sánchez-Barbero, F., Strassner, J., García-Cañero, R., Steinhilber, W. and Casals, C. (2005) ‘Role of the degree of oligomerization in the structure and function of human surfactant protein A’, *Journal of Biological Chemistry*. ASBMB, 280(9), pp. 7659–7670.

Sanderson, R. J. and Vatter, A. E. (1977) ‘A mode of formation of tubular myelin from lamellar bodies in the lung’, *J Cell Biol*, 74(3), pp. 1027–1031.

Santos, N. C., Prieto, M. and Castanho, M. A. R. B. (1998) ‘Interaction of the Major Epitope Region of HIV Protein gp41 with Membrane Model Systems. A Fluorescence Spectroscopy Study’, *Biochemistry*. American Chemical Society, 37(24), pp. 8674–8682. doi: 10.1021/bi9803933.

Santos, N. C., Prieto, M. and Castanho, M. A. R. B. (2003) ‘Quantifying molecular partition into model systems of biomembranes: an emphasis on optical spectroscopic methods’, *Biochimica et Biophysica Acta (BBA) - Biomembranes*, 1612(2), pp. 123–135. doi: https://doi.org/10.1016/S0005-2736(03)00112-3.

Sarker, M., Jackman, D. and Booth, V. (2011) ‘Lung surfactant protein A (SP-A) interactions with model lung surfactant lipids and an SP-B fragment’, *Biochemistry*, 50(22), pp. 4867–4876. doi: 10.1021/bi200167d.

Sato, S. and Kishikawa, T. (2001) ‘Ultrastructural study of the alveolar lining and the bronchial mucus layer by block staining with oolong tea extract: the role of various surfactant materials.’, *Medical electron microscopy : official journal of the Clinical Electron Microscopy Society of Japan*. Japan, 34(2), pp. 142–151.

Schindelin, J., Arganda-Carreras, I., Frise, E., Kaynig, V., Longair, M., Pietzsch, T., Preibisch, S., Rueden, C., Saalfeld, S., Schmid, B., Tinevez, J.-Y., White, D. J., Hartenstein, V., Eliceiri, K., Tomancak, P. and Cardona, A. (2012) ‘Fiji: an open-source platform for biological-image analysis’, *Nature Methods*, 9(7), pp. 676–82. doi: 10.1038/nmeth.2019.

Schmiedl, A., Ochs, M., Muhlfeld, C., Johnen, G. and Brasch, F. (2005) ‘Distribution of surfactant proteins in type II pneumocytes of newborn, 14-day old, and adult rats: an immunoelectron microscopic and stereological study’, *Histochem Cell Biol*, 124(6), pp. 465–476. doi: 10.1007/s00418-005-0066-0.

Schoel, W. M., Schurch, S. and Goerke, J. (1994) ‘The captive bubble method for the evaluation of pulmonary surfactant: surface tension, area, and volume calculations.’, *Biochimica et biophysica acta*. Netherlands, 1200(3), pp. 281–290.

Schurch, D., Ospina, O. L., Cruz, A. and Perez-Gil, J. (2010) ‘Combined and independent action of proteins SP-B and SP-C in the surface behavior and mechanical stability of pulmonary surfactant films’, *Biophys J*. 2010/11/18, 99(10), pp. 3290–3299. doi: S0006-3495(10)01188-4 [pii]10.1016/j.bpj.2010.09.039.

Schurch, S., Bachofen, H., Goerke, J. and Possmayer, F. (1989) ‘A captive bubble method reproduces the in situ behavior of lung surfactant monolayers.’, *Journal of applied physiology (Bethesda, Md. : 1985)*. United States, 67(6), pp. 2389–2396. doi: 10.1152/jappl.1989.67.6.2389.

Schurch, S., Green, F. H. and Bachofen, H. (1998) ‘Formation and structure of surface films: captive bubble surfactometry’, *Biochim Biophys Acta*, 1408(2–3), pp. 180–202.

Schurch, S., Possmayer, F., Cheng, S. and Cockshutt, A. M. (1992) ‘Pulmonary SP-A enhances adsorption and appears to induce surface sorting of lipid extract surfactant.’, *The American journal of physiology*. United States, 263(2 Pt 1), pp. L210-8. doi: 10.1152/ajplung.1992.263.2.L210.

Schurch, S., Schurch, D., Curstedt, T. and Robertson, B. (1994) ‘Surface activity of lipid extract surfactant in relation to film area compression and collapse.’, *Journal of applied physiology (Bethesda, Md. : 1985)*. United States, 77(2), pp. 974–986. doi: 10.1152/jappl.1994.77.2.974.

Seddon, A. M., Curnow, P. and Booth, P. J. (2004) ‘Membrane proteins, lipids and detergents: Not just a soap opera’, *Biochimica et Biophysica Acta - Biomembranes*, pp. 105–117. doi: 10.1016/j.bbamem.2004.04.011.

Seminario-Vidal, L., Okada, S. F., Sesma, J. I., Kreda, S. M., Van Heusden, C. A., Zhu, Y., Jones, L. C., O'Neal, W. K., Penuela, S., Laird, D. W., Boucher, R. C. and Lazarowski, E. R. (2011) 'Rho signaling regulates pannexin 1-mediated ATP release from airway epithelia', *Journal of Biological Chemistry*, 286(30), pp. 26277–26286. doi: 10.1074/jbc.M111.260562.

Séror, C., Melki, M.-T., Subra, F., Raza, S. Q., Bras, M., Saïdi, H., Nardacci, R., Voisin, L., Paoletti, A., Law, F., Martins, I., Amendola, A., Abdul-Sater, A. A., Ciccosanti, F., Delelis, O., Niedergang, F., Thierry, S., Said-Sadier, N., Lamaze, C., Métivier, D., Estaquier, J., Fimia, G. M., Falasca, L., Casetti, R., Modjtahedi, N., Kanellopoulos, J., Mouscadet, J.-F., Ojcius, D. M., Piacentini, M., Gougeon, M.-L., Kroemer, G. and Perfettini, J.-L. (2011) 'Extracellular ATP acts on P2Y2 purinergic receptors to facilitate HIV-1 infection.', *The Journal of experimental medicine*, 208(9), pp. 1823–34. doi: 10.1084/jem.20101805.

Serrano, A. G., Cabre, E. J. and Perez-Gil, J. (2007) 'Identification of a segment in the precursor of pulmonary surfactant protein SP-B, potentially involved in pH-dependent membrane assembly of the protein', *Biochim Biophys Acta*. 2007/02/20, 1768(5), pp. 1059–1069. doi: S0005-2736(07)00005-3 [pii]10.1016/j.bbamem.2007.01.010.

Serrano, A. G. and Perez-Gil, J. (2006) 'Protein-lipid interactions and surface activity in the pulmonary surfactant system', *Chem Phys Lipids*. 2006/04/08, 141(1–2), pp. 105–118. doi: S0009-3084(06)00028-4 [pii]10.1016/j.chemphyslip.2006.02.017.

Serrano, A. G., Ryan, M., Weaver, T. E. and Perez-Gil, J. (2006) 'Critical structure-function determinants within the N-terminal region of pulmonary surfactant protein SP-B', *Biophys J*. 2005/10/11, 90(1), pp. 238–249. doi: S0006-3495(06)72206-8 [pii]10.1529/biophysj.105.073403.

Shiffer, K., Hawgood, S., Haagsman, H. P., Benson, B., Clements, J. A. and Goerke, J. (1993) 'Lung surfactant proteins, SP-B and SP-C, alter the thermodynamic properties of phospholipid membranes: a differential calorimetry study.', *Biochemistry*. United States, 32(2), pp. 590–597.

Shirahama, R., Miyazaki, Y., Okamoto, T., Inase, N. and Yoshizawa, Y. (2010) 'Proteome analysis of bronchoalveolar lavage fluid in lung fibrosis associated with systemic sclerosis.', *Allergology international : official journal of the Japanese Society of Allergology*. England, 59(4), pp. 409–415. doi: 10.2332/allergolint.10-OA-0176.

Silvius, J. R. (1992) 'Solubilization and functional reconstitution of biomembrane components.', *Annual review of biophysics and biomolecular structure*. United States, 21, pp. 323–348. doi: 10.1146/annurev.bb.21.060192.001543.

Singer, W., Frick, M., Haller, T., Bernet, S., Ritsch-Marte, M. and Dietl, P. (2003) 'Mechanical forces impeding exocytotic surfactant release revealed by optical tweezers', *Biophys J*, 84(2 Pt 1), pp. 1344–1351. doi: 10.1016/S0006-3495(03)74950-9.

Smith, P. E. S., Brender, J. R. and Ramamoorthy, A. (2009) 'The Induction of Negative Curvature as a Mechanism of Cell Toxicity by Amyloidogenic Peptides: The Case of Islet Amyloid Polypeptide', *Journal of the American Chemical Society*, 131(12), pp. 4470–4478. doi: 10.1021/ja809002a.

Stahlman, M. T., Gray, M. P., Falconieri, M. W., Whitsett, J. A. and Weaver, T. E. (2000) 'Lamellar body formation in normal and surfactant protein B-deficient fetal mice', *Lab Invest*, 80(3), pp. 395–403.

Strayer, D. S., Yang, S. and Jerng, H. H. (1993) 'Surfactant protein A-binding proteins. Characterization and structures', *Journal of Biological Chemistry*, 268(25), pp. 18679–18684.

Suzuki, Y., Fujita, Y. and Kogishi, K. (1989) 'Reconstitution of tubular myelin from synthetic lipids and proteins associated with pig pulmonary surfactant', *Am Rev Respir Dis*. 1989/07/01, 140(1), pp. 75–81.

Taeusch, H. W., Bernardino de la Serna, J., Perez-Gil, J., Alonso, C. and Zasadzinski, J. a (2005) 'Inactivation of pulmonary surfactant due to serum-inhibited adsorption and reversal by hydrophilic polymers: experimental.', *Biophysical journal*, 89(3), pp. 1769–1779. doi: 10.1529/biophysj.105.062620.

Takamoto, D. Y., Aydil, E., Zasadzinski, J. A., Ivanova, A. T., Schwartz, D. K., Yang, T. and Cremer, P. S. (2001) 'Stable ordering in Langmuir-Blodgett films.', *Science (New York, N.Y.)*. United States, 293(5533), pp. 1292–1295. doi: 10.1126/science.1060018.

Takamoto, D. Y., Lipp, M. M., von Nahmen, A., Lee, K. Y., Waring, A. J. and Zasadzinski, J. A. (2001) 'Interaction of lung surfactant proteins with anionic phospholipids.', *Biophysical journal*. United States, 81(1), pp. 153–169. doi: 10.1016/S0006-3495(01)75688-3.

Taneva, S. G. and Keough, K. M. (2000) 'Differential effects of surfactant protein A on regional organization of phospholipid monolayers containing surfactant protein B or C.', *Biophysical journal*. United States, 79(4), pp. 2010–2023. doi: 10.1016/S0006-3495(00)76449-6.

Taneva, S. and Keough, K. M. (1994a) 'Dynamic surface properties of pulmonary surfactant proteins SP-B and SP-C and their mixtures with dipalmitoylphosphatidylcholine.', *Biochemistry*. United States, 33(49), pp. 14660–14670.

Taneva, S. and Keough, K. M. (1994b) 'Pulmonary surfactant proteins SP-B and SP-C in spread monolayers at the air-water interface: I. Monolayers of pulmonary surfactant protein SP-B and phospholipids.', *Biophysical journal*. United States, 66(4), pp. 1137–1148. doi: 10.1016/S0006-3495(94)80895-1.

Taneva, S. and Keough, K. M. (1994c) 'Pulmonary surfactant proteins SP-B and SP-C in spread monolayers at the air-water interface: II. Monolayers of pulmonary surfactant protein SP-C and phospholipids.', *Biophys J.*, 66, pp. 1149–1157.

Taneva, S. and Keough, K. M. (1994d) 'Pulmonary surfactant proteins SP-B and SP-C in spread monolayers at the air-water interface: III. Proteins SP-B plus SP-C with phospholipids in spread monolayers', *Biophys J*, 66(4), pp. 1158–1166. doi: 10.1016/S0006-3495(94)80897-5.

Thompson, R. F., Walker, M., Siebert, C. A., Muench, S. P. and Ranson, N. A. (2016) 'An introduction to sample preparation and imaging by cryo-electron microscopy for structural biology', *Methods*, 100, pp. 3–15. doi: https://doi.org/10.1016/j.ymeth.2016.02.017.

Thursz, M. R. and Khamri, W. (2010) 'Chapter 35 - Host surfactant proteins in microbial recognition', in Holst, O., Brennan, P. J., Itzstein, M. von, and Moran, A. P. B. T.-M. G. (eds). San Diego: Academic Press, pp. 697–713. doi: https://doi.org/10.1016/B978-0-12-374546-0.00035-3.

Vandenbussche, G., Clercx, A., Clercx, M., Curstedt, T., Johansson, J., Jornvall, H. and Ruysschaert, J. M. (1992) 'Secondary structure and orientation of the surfactant protein SP-B in a lipid environment. A Fourier transform infrared spectroscopy study', *Biochemistry*. 1992/09/29, 31(38), pp. 9169–9176.

Vandenbussche, G., Clercx, A., Curstedt, T., Johansson, J., Jörnvall, H. and Ruysschaert, J.-M. (1992) 'Structure and orientation of the surfactant-associated protein C in a lipid bilayer', *European Journal of Biochemistry*, 203(1–2), pp. 201–209. doi: 10.1111/j.1432-1033.1992.tb19848.x.

Veatch, S. L. and Keller, S. L. (2002) 'Organization in lipid membranes containing cholesterol.', *Physical review letters*. United States, 89(26), p. 268101. doi: 10.1103/PhysRevLett.89.268101.

Velasquez, S. and Eugenin, E. A. (2014) 'Role of Pannexin-1 hemichannels and purinergic receptors in the pathogenesis of human diseases', *Frontiers in Physiology*. doi: 10.3389/fphys.2014.00096.

Venkitaraman, A. R., Hall, S. B., Whitsett, J. A. and Notter, R. H. (1990) 'Enhancement of biophysical activity of lung surfactant extracts and phospholipid-apoprotein mixtures by surfactant protein A.', *Chemistry and physics of lipids*. Ireland, 56(2–3), pp. 185–194.

Vieira, F., Kung, J. W. and Bhatti, F. (2017) 'Structure, genetics and function of the pulmonary associated surfactant proteins A and D: The extra-pulmonary role of these C type lectins', *Annals of Anatomy - Anatomischer Anzeiger*, 211, pp. 184–201. doi: https://doi.org/10.1016/j.aanat.2017.03.002.

Vorbroker, D. K., Profitt, S. A., Nogee, L. M. and Whitsett, J. A. (1995) 'Aberrant processing of surfactant protein C in hereditary SP-B deficiency.', *The American journal of physiology*. United States, 268(4 Pt 1), pp. L647-56. doi: 10.1152/ajplung.1995.268.4.L647.

Wang, L., Cai, P., Galla, H.-J., He, H., Flach, C. R. and Mendelsohn, R. (2005) 'Monolayer-multilayer transitions in a lung surfactant model: IR reflection-absorption spectroscopy and atomic force microscopy.', *European biophysics journal : EBJ*. Germany, 34(3), pp. 243–254. doi: 10.1007/s00249-004-0446-8.

Wang, P., Chintagari, N. R., Narayanaperumal, J., Ayalew, S., Hartson, S. and Liu, L. (2008) 'Proteomic analysis of lamellar bodies isolated from rat lungs.', *BMC cell biology*. England, 9, p. 34. doi: 10.1186/1471-2121-9-34.

Wang, Z., Hall, S. B. and Notter, R. H. (1996) 'Roles of different hydrophobic constituents in the adsorption of pulmonary surfactant.', *Journal of lipid research*. United States, 37(4), pp. 790–798.

Wattiez, R., Hermans, C., Bernard, A., Lesur, O. and Falmagne, P. (1999) 'Human bronchoalveolar lavage fluid: two-dimensional gel electrophoresis, amino acid microsequencing and identification of major proteins.', *Electrophoresis*. Germany, 20(7), pp. 1634–1645. doi: 10.1002/(SICI)1522-2683(19990601)20:7<1634::AID-ELPS1634>3.0.CO;2-J.

Weaver, T. E. and Conkright, J. J. (2001) 'Function of surfactant proteins B and C', *Annu Rev Physiol*, 63, pp. 555–578. doi: 10.1146/annurev.physiol.63.1.555.

Weaver, T. E., Na, C. L. and Stahlman, M. (2002) 'Biogenesis of lamellar bodies, lysosome-related organelles involved in storage and secretion of pulmonary surfactant', *Seminars in Cell and Developmental Biology*, 13(4), pp. 263–270. doi: 10.1016/S1084952102000551.

Weaver, T. E. and Whitsett, J. A. (1991) 'Function and regulation of expression of pulmonary surfactant-associated proteins.', *Biochemical Journal*, 273(Pt 2), pp. 249–264.

White, M. K. and Strayer, D. S. (2000) 'Surfactant Protein A Regulates Pulmonary Surfactant Secretion via Activation of Phosphatidylinositol 3-Kinase in Type II Alveolar Cells', *Experimental Cell Research*, 255(1), pp. 67–76. doi: 10.1006/excr.1999.4764.

Wilcox, K. C., Marunde, M. R., Das, A., Velasco, P. T., Kuhns, B. D., Marty, M. T., Jiang, H., Luan, C.-H., Sligar, S. G. and Klein, W. L. (2015) 'Nanoscale Synaptic Membrane Mimetic Allows Unbiased High Throughput Screen That Targets Binding Sites for Alzheimer's-Associated Abeta Oligomers.', *PloS one*. United States, 10(4), p. e0125263. doi: 10.1371/journal.pone.0125263.

Williams, M. C. (1977) 'Conversion of lamellar body membranes into tubular myelin in alveoli of fetal rat lungs', *J Cell Biol*, 72(2), pp. 260–277.

Wine, Y., Cohen-Hadar, N., Freeman, A. and Frolow, F. (2007) 'Elucidation of the mechanism and end products of glutaraldehyde crosslinking reaction by X-ray structure analysis.', *Biotechnology and bioengineering*. United States, 98(3), pp. 711–718. doi: 10.1002/bit.21459.

Wirtz, H. R. and Dobbs, L. G. (1990) 'Calcium mobilization and exocytosis after one mechanical stretch of lung epithelial cells', *Science*, 250(4985), pp. 1266–1269.

Wissel, H., Lehfeldt, A., Klein, P., Muller, T. and Stevens, P. A. (2001) 'Endocytosed SP-A and surfactant lipids are sorted to different organelles in rat type II pneumocytes', *Am J Physiol Lung Cell Mol Physiol*, 281(2), pp. L345-60.

Wright, J. R. (2005) 'Immunoregulatory functions of surfactant proteins', *Nat Rev Immunol*. 2005/01/05, 5(1), pp. 58–68. doi: nri1528 [pii]10.1038/nri1528.

Wright, J. R., Wager, R. E., Hawgood, S., Dobbs, L. and Clements, J. A. (1987) 'Surfactant apoprotein Mr = 26,000-36,000 enhances uptake of liposomes by type II cells.', *The Journal of biological chemistry*. United States, 262(6), pp. 2888–2894.

Wu, H., Kuzmenko, A., Wan, S., Schaffer, L., Weiss, A., Fisher, J. H., Kim, K. S. and McCormack, F. X. (2003) 'Surfactant proteins A and D inhibit the growth of Gram-negative bacteria by increasing membrane permeability.', *The Journal of clinical investigation*. United States, 111(10), pp. 1589–1602. doi: 10.1172/JCI16889.

Wustneck, R., Perez-Gil, J., Wustneck, N., Cruz, A., Fainerman, V. B. and Pison, U. (2005) 'Interfacial properties of pulmonary surfactant layers', *Adv Colloid Interface Sci*. 2005/08/27, 117(1–3), pp. 33–58. doi: S0001-8686(05)00080-1 [pii]10.1016/j.cis.2005.05.001.

Yang, L., Johansson, J., Ridsdale, R., Willander, H., Fitzen, M., Akinbi, H. T. and Weaver, T. E. (2010) 'Surfactant protein B propeptide contains a saposin-like protein domain with antimicrobial activity at low pH', *J Immunol*, 184(2), pp. 975–983. doi: 10.4049/jimmunol.0900650.

Yeow, E. K. L. and Clayton, A. H. A. (2007) 'Enumeration of Oligomerization States of Membrane Proteins in Living Cells by Homo-FRET Spectroscopy and Microscopy: Theory and Application', *Biophysical Journal*. Biophysical Society, 92(9), pp. 3098–3104. doi: 10.1529/biophysj.106.099424.

Yu, S. H. and Possmayer, F. (1998) 'Interaction of pulmonary surfactant protein A with dipalmitoylphosphatidylcholine and cholesterol at the air/water interface.', *Journal of lipid research*. United States, 39(3), pp. 555–568.

Zaltash, S., Griffiths, W. J., Beck, D., Duan, C. X., Weaver, T. E. and Johansson, J. (2001) 'Membrane activity of (Cys48Ser) lung surfactant protein B increases with dimerisation', *Biol Chem*. 2001/08/15, 382(6), pp. 933–939. doi: 10.1515/BC.2001.116.

Zaltash, S., Palmblad, M., Curstedt, T., Johansson, J. and Persson, B. (2000) 'Pulmonary surfactant protein B: a structural model and a functional analogue', *Biochim Biophys Acta*. 2000/05/29, 1466(1–2), pp. 179–186. doi: S0005-2736(00)00199-1 [pii].

Zhang, R., Sahu, I. D., Bali, A. P., Dabney-Smith, C. and Lorigan, G. A. (2017) 'Characterization of the structure of lipodisq nanoparticles in the presence of KCNE1 by dynamic light scattering and transmission electron microscopy.', *Chemistry and physics of lipids*. Ireland, 203, pp. 19–23. doi: 10.1016/j.chemphyslip.2016.12.003.

Zhang, R., Sahu, I. D., Liu, L., Osatuke, A., Comer, R. G., Dabney-Smith, C. and Lorigan, G. A. (2015) 'Characterizing the structure of lipodisq nanoparticles for membrane protein spectroscopic studies.', *Biochimica et biophysica acta*. Netherlands, 1848(1 Pt B), pp. 329–333. doi: 10.1016/j.bbamem.2014.05.008.

Zoonens, M., Giusti, F., Zito, F. and Popot, J.-L. (2007) 'Dynamics of membrane protein/amphipol association studied by Forster resonance energy transfer: implications for in vitro studies of amphipol-stabilized membrane proteins.', *Biochemistry*. United States, 46(36), pp. 10392–10404. doi: 10.1021/bi7007596.